STRESS-STRAIN-STRENGTH CHARACTERISTICS OF SATURATED SOILS

1982

MASAYOSHI SHIMIZU

STRESS-STRAIN-STRENGTH CHARACTERISTICS OF SATURATED SOILS

1982

MASAYOSHI SHIMIZU

SUMMARY

This Thesis deals with the stress-strain-strength characteristics of various kinds of saturated soils.

In the first half, a remoulded or laboratory reconstituted clay is treated and its mechanical behaviour is examined in detail by performing several types of triaxial tests: effects of the degree of overconsolidation on the dilatancy is studied; the compressibility and elastic properties when subjected to shear stress history are investigated; and the results obtained are taken into account for the development of an elasto-plastic stress-strain relationship of overconsolidated clays. The analysis of the stress ratio constant tests of the overconsolidated clay was performed by the theoretical relationship and it was ascertained that the calculated results could fairy explain the experimental ones.

The latter half of the Thesis is consacrated to experimental studies on the mechanical characteristics of various types of soils by using their undisturbed samples. Alluvial and diluvial clays and decomposed granite soils are of interest.

As to the soft alluvial clays, the estimation of undrained strength is important for the stability problems and so the correlation of unconfined compression strengths and laboratory vane shear strengths was studied. On the other hand, we often encounter the stiff overconsolidated clays such as diluvial clays. Various engineering problems are caused by their mechanical characteristics. Among them, tensile strength or creep deformation under tensile axial stress, brittle nature such

as strain softening in shearing, and delayed or secondary consolidation behaviour are studied.

Finally, the fundamental mechanical behaviour of decomposed granite soils, which cover more than 10 % of our country, are examined. The method employed here enabled us to perform a number of triaxial tests on undisturbed samples and to discuss their mechanical properties on the basis of the effective stress concept.

ACKNOWLEDGEMENT

The Author wishes to express his sincere appreciation to Professor T.Shibata of the Disaster Prevention Research Institute of Kyoto University for his supervision and encouragement throughout the course of this study. Associate Professor T.Adachi of the Institute is also gratefully acknowledged for his daily suggestion and useful discussion. The Author is indebted sincere thanks to Professor K.Akai of Kyoto University for his fundamental and advanced courses of soil mechanics and to Emiritus Professor S.Murayama of Kyoto University for his guidance to commence the research on soil mechanics.

The Author heartly thanks Technical Official H.Shimizu of the Institute for his help in performing all the experiments. Acknowledgements are also made to Messrs. K.Inoue, E.Imazato, M.Mimura, T.Tsuji, T.Shimogochi and K.Oyama for their good co-researches and to Miss Nagamune for her help of the typing of the manuscript of this dissertation.

Staffs in the Department of Civil Engineering of Tottori University are acknowledged for their hearty support on completing this dissertation.

The Author wishes to acklowledge his family for their understanding throughout the course of this study.

CONTENTS

CHAPTER 1 INTRODUCTION

1.1 OBJECTS OF THE THESIS

Soil mechanics seems to have been developed with the mission to design the soil structure or soil foundations of constructed structure of other than soils. The effort to predict the mechanical response of soils or soil structure to external agencies have been made and will have to be made.

One of the major problems in soil mechanics or soil engineering has been concerned with the stability with respect to the failure of soils or soil structures for a long time. Recently, the prediction of the mechanical behaviour not only at failure but also before the failure has been more and more required and performed. This may be partly attributed to the development of our knowledge on the mechanical properties of soils.

The most ideal analysis of the stability becomes possible by predicting effective stress paths and the deformation behaviour of soil elements within the soil structure during and after the construction work. To do so, the complete set of constitutive equations of soils are required.

An ambitious attempt of modern soil mechanics is to find mechanical properties common to as many kinds of soils as possible and to construct unified constitutive equations. The object of this study is also to perform the attempt. However, we are not yet succeeded in this attempt because there are too many kinds of soils to unify their mechanical characteristics. Consequently, we are obliged to classify soils into several kinds

by their characteristical behaviours.

Many natural deposits of clay have been overconsolidated or apparently overconsolidated during their geological history. The level of our knowledge on the mechanical characteristics of overconsolidated clays has not yet been made so high as that on normally consolidated clays. The main object of this thesis is to clarify some effects of overconsolidation to the mechanical behaviour and to construct the stress-strain equations for overconsolidated clays. Chapters 2 to 5 are consacrated to this object.

The second object of this thesis is to investigate the mechanical characteristics of undisturbed samples of soils often encountered in construction problems. In this thesis, alluvial clays, diluvial clays and a decomposed granite soil are treated.

Stiff clays such as diluvial or tertiarily deposited clays generally appear to be heavily overconsolidated. As to the engineering problems particularly associated with their mechanical characteristis, we may cite the following problems: the problem of long term stability or delayed failure of soil structure or soil foundations resulting from remarkable dilatant behaviour; the progressive failure of soil foundations or soil slopes caused by the strain softening characteristics ; and the land subsidence due to the compression of diluvial clay layers, of which importance has been rather recently recognized.

It is said that 13 % of our country is covered or consisted with granite rock masses or decomposed granite soils. Granite has played a very important role as a foundation rock mass or as

a construction material. The importance has increased and will increase more and more with incresing large scale construction problems. On the other hand, it is also the fact that we have had many damages resulted from the destruction of soil structures consisted of decomposed granite soil. It may be said that decomposed granite soils have certain injurious properties from engineering view point.

Mechanical characteristics associated with the engineering problems mentioned above must be investigated. Chapters 6 to 9 are consacrated to it.

1.2 SCOPE OF THE THESIS

In the former chapters , the experimental and theoretical studies of stress-strain behaviour of a overconsolidated clay are presented.

In Chapter 2, stress-strain behaviour of a remolded clay when overconsolidated to various degrees of overconsolidation is examined experimentally. A main purpose of this chapter is to investigate the influences of the degree of overconsolidation on the dilatancy characteristics and on relations between stress ratio and strain increment ratio.

The necessity to predict the mechanical response of soils when subjected to such vibrating forces as in earthquakes has increased. As the first stage for satisfying the necessity, it seems to be needed to clarify the stress-strain behaviour when loading direction is reversed. In Chapter 3, effects of shear stress history on the subsequent shearing deformation and isotropic

compression behaviour are investigated . Discussion is made on the efficiency of a parameter OCR defined in the usual manner as a measure for evaluating apparant overconsolidation effect caused by the stress history.

In Chapter 4 the study performed in Chapter 3 is extended to examine elastic behaviour accompanied with the unloading of shear stress. Effects of shear stress history on shear modulus and the development of the elastic domain observed in the unloading are discussed.

In Chapter 5, a method for formulating the elasto-plastic stress-strain relationships is presented.The main purpose is to show how to relate the experimental results to the theoretical formalism. Particularly, dilatancy characteristics of overconsolidated clays is taken into account in the construction of stress-strain model. Developed stress-strain relationships are applied to the analysis of the stress ratio constant tests on a overconsolidated clay.

In the latter half of the thesis, the experimental study on the mechanical behaviour of undisturbed samples of alluvial and diluvial clay deposits and a decomposed granite soil is presented.

In Chapter 6, the comparison of laboratory vane shear strength and unconfined compression strength is made on undisturbed samples from two alluvial clay layers in order to investigate the difference in these strengths due to the difference in shearing mechanism.

Chapter 7 deals with the mechanical behaviour under negative or tensile normal stress. Undisturbed diluvial clays are used. The experimental methods to determine the tensile strength of

soils are reviewed. Using the most prefarable method , the tensile strength characteristics are presented. Creep characteristics under tensile normal stress are also investigated.

In Chapter 8, results of very long term consolidation tests and conventional triaxial tests on stiff overconsolidated clays are presented. Object of the former tests is to examine so-called secondary compression and that of the latter is to clarify the elasto-plastic behaviour.

In Chapter 9, in order to investigate the fundamental mechanical characteristics of decomposed granite soil, the results of drained and undrained triaxial conventional tests on undisturbed samples are presented. Precedingly to the mechanical tests , some basic physical properties are also investigated to identify the samples used in the study.

Some conclusive remarks are summarized with the significance and future recommendation in Chapter 10.

In Appendix, some technical problems associated with the measurement of volume change in triaxial drained tests are treated. Evaporation of water in a burrete and compressibility of filter materials as side drains are examined experimentally among some problems at the measurement of volume change of cohesive soils. It is also investigated and discussed the effect of change in room temperature on the apparent volume change of a saturated soil.

CHAPTER 2 EFFECT OF OVERCONSOLIDATION ON DILATANCY OF A COHESIVE SOIL

2.1 INTRODUCTION

Many natural deposits of clay have been overconsolidated or apparently overconsolidated during their geological history (Bjerrum,1967; Soderman & Kim,1970). According to the engineering purpose, studies on the properties of such clays have been focused mainly on their strengths or some parameters at failure (Henkel,1956; Henkel,1959; Ladd & Lambe,1964; Nakase,1968). Recently, however, the importance and necessity of stress-strain behaviour of geotechnical materials have been recognized and so there have been some attempts to develop the stress-strain relationships for overconsolidated clays (Roscoe & Burland,1968; Adachi & Nishi,1976; Pender,1978; Ohmaki,1980).

This paper examines experimentally stress-strain behaviour of a remoulded clay when overconsolidated to various degrees of overconsolidation. A main object is to investigate the influences of the degree of overconsolidation on the dilatancy characteristics and on relations between stress ratio and strain increment ratio, both of which will play an important role for developing adequate stress-strain relationships for overconsolidated cohesive soils.

Volumetric strain of an ideal elastic material does not occur unless the isotropic component of stress changes. This is expressed by

$$dv = \frac{1}{K} d\sigma_m \ , \qquad \cdots\cdots\cdots\cdots\cdots\cdots (2.1)$$

where $d\sigma_m$ is a change of mean normal stress σ_m , dv is the corresponding change of volumetric strain v and K is bulk modulus. As is well known, however, particulate materials like soils rarely behave as such ideal elastic materials; volume change of real soils occurs even under the condition that effective mean normal stress is kept constant; and this phenomenon is called 'dilatancy'. In this paper, 'dilatancy' is used in this sense and defined as volume change or volumetric strain which occurs without any change of effective mean normal stress.

Shibata(1963) seems to be the first investigator on quantitative evaluation of the dilatancy for clays. He conducted conventional triaxial compression tests under constant effective mean normal stress for a normally consolidated clay and derived an important conclusion that the dilatancy of normally consolidated clays can be expressed as a linear function of stress ratio. His results have been extended by Karube & Kurihara(1966), resulting in the conclusion that the dilatancy of normally consolidated clays, when subjected to monotonically increasing shear stress, can be expressed by the following equation:

$$dv_D = D.d(\tau_{oct}/\sigma'_m), \qquad \text{.....(2.2)}$$

where dv_D is a change in volumetric strain due to dilatancy, D is a material constant called 'dilatancy coefficient' and τ_{oct} is the octahedral shear stress. Using eq.(2.2) as the expression for the dilatancy of normally consolidated clays, Ohta(1971) developed a stress-strain relationship based on the theory of plasticity. In addition, the dilatancy predicted by the Cam Clay model (Schofield & Wroth,1968) for isotropically normally consolidated

clays is the same as that by eq.(2.2).

As to the dilatancy of overconsolidated clays, the type of expression as eq.(2.2) should not be employed apriori, because there has been little test data on the dilatancy of overconsolidated clays (Parry & Amerasinghe,1973; Ohmaki,1980). In addition to this reason, we should note that the 'dilatancy coefficient' can be expected to be not constant but a function of stress ratio even for normally consolidated clays as hypothesized in the modified Cam Clay model(Roscoe & Burland,1968) or as shown by test data (Balasubramaniam & Zue-Ming,1980).

Various theories have been developed on stress-strain relationships of soils based on the theory of plasticity. On applying the plasticity theory the existence of the plastic potential is assumed whether the associated flow rule is adopted or not. When obtaining the plastic potential function, either by experiments or by theoretical considerations, it is common to express the strain increment ratio as a function of some parameters concerned with stress: e.g., the energy equations used in the Cambridge theory (Schofield & Wroth,1968; Roscoe & Burland,1968) can be regarded as such functions; Pender(1978) has hypothetically proposed an expression for plastic strain increment ratio; Vermeer (1978) has adopted the stress-dilatancy equation proposed by Rowe (1962) to express the flow rule. On the other hand, even without the introduction of the concept in the theory of plasticity, many investigations on strain increment ratio-stress ratio relations have been presented and have played important roles to understand the stress-strain behaviour of granular materials like sands (e.g., Rowe,1962; Murayama & Matsuoka,1973).

In this chapter , the state of effective stress will be expressed by the effective mean normal stress p and the deviator stress q defined as follows:

$$p = (\sigma_a + 2\sigma_r)/3; \quad \text{..... (2.3)}$$

$$q = \sigma_a - \sigma_r , \quad \text{.....(2.4)}$$

where σ_a and σ_r are axial and radial effective stresses in the triaxial test, respectively. The corresponding strain parameters will be the volumetric strain v and the shear strain ε defined as

$$v = \varepsilon_a + 2\varepsilon_r; \quad \text{.....(2.5)}$$

$$\varepsilon = \varepsilon_a - v/3. \quad \text{.....(2.6)}$$

2.2 EXPERIMENTAL PROCEDURE

2.2.1 Sample Preparation

The sample used in this study is a silty clay called Fujinomori Clay. After remoulding it with high water content two times its liquid limit for 4 days, it was one dimensionally consolidated in a consolidation cell of 25 cm in diameter under vertical pressure up to 49 kPa, and unloaded to the atmospheric pressure. It took 40 days to complete this preparation process. The physical properties of this soil are listed in Table 2.1

Trimming the consolidated sample, cylindrical specimens of 8 cm in height and 10 cm^2 in cross section were made for triaxial tests. The water content when in position in a triaxial cell was about 40 %. A filter paper having a series of strips was used around the specimen as a side drain; drainage was not allowed in the vertical direction but in the radial direction only. All the tests were performed at a constant temperature of 20 ± 0.5 °C.

2.2.2 Triaxial Tests

All the tests are isotropically consolidated drained triaxial tests, which were performed in standard GEONOR triaxial cells. Fig. 2.1 represents schematically an effective stress path employed in this study. The triaxial test process can be divided into two processes. First, specimens were isotropically consolidated up to maximum pressure p_c (=588 kPa) and isotropically unloaded to the pressure of p_c/OCR, where OCR is overconsolidation ratio. The duration for consolidation at each pressure stage was about 1 day. After this consolidation process, shear stress was applied under the condition of constant effective mean normal stress using the method of stress control. The increment of shear stress ratio q/p was held constant at 0.1; this increment was applied every day. Axial deformation and volume change were measured by a dial gauge with the minimum scale of 1/100 mm, and by a burette with that of 2/100 ml, respectively. All the tests performed are listed in Table 2.2 , where some results which will be discussed later are also given.

2.3 EXPERIMENTAL RESULTS

2.3.1 Volume Change Behaviour during Isotropic Consolidation Process

Volume change characteristics during isotropic unloading from $p=p_c$/OCR is shown in Fig. 2.2, where the ratio of the change in water content from virgin consolidated state at $p=p_c$ to the value of natural logarithm of OCR (ln OCR) is plotted against OCR on the log scale. From this figure it can be assumed that such a linear relation as

Table 2.1: Physical properties of the sample used.

G_s	L.L. (%)	P.L. (%)	P.I.	% finer than 2 μm
2.64	54.0	27.8	26.2	15

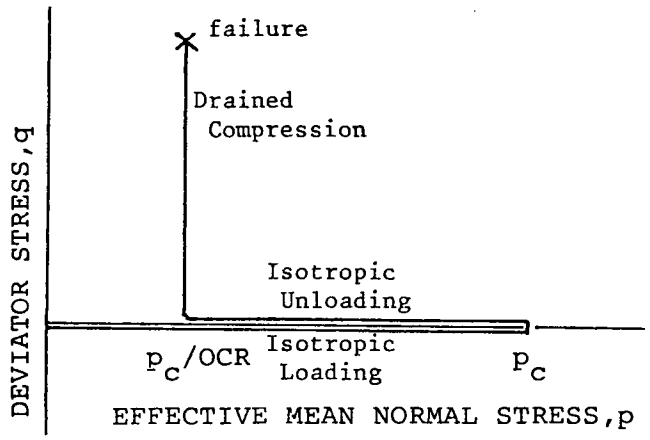

Fig.2.1: Schematic representation of the effective stress path

Table 2.2: List of tests performed and some results

Test No.	p_c(kPa)	p(kPa)	OCR	η_{DL}	μ	η_f
F302	588	588	1	-	-	1.4
F303	588	588	1	-	-	*
F304	588	392	1.5	0.4	0.9	1.4
F305	588	392	1.5	0.5	1.0	1.4
F306	588	294	2	1.1	1.2	1.5
F307	588	137	4	1.1	1.6	1.7
F308	588	137	4	1.1	1.6	1.6
F309	588	73.5	8	1.4	2.0	2.0
F310	588	73.5	8	1.4	1.8	1.8
F311	588	29.4	20	1.3	2.1	2.1
F312	588	29.4	20	1.7	2.4	2.4

* This test was stopped before failure because of leakage.

$$(w_0-w_c)/\ln n = a + b.\ln n \qquad \text{.....(2.7)}$$

exists, where n : OCR

w_0: water content at $p=p_c/n$,

w_c: water content at $p=p_c$, and

a,b: constants independent of OCR.

Differentiating eq.(2.7) isotropic swelling index κ , commonly defined as -dw/dlnp, the tangential slope of the swelling line on (w,lnp) plane, can be given by eq.(2.8):

$$\kappa = a + 2b.\ln n. \qquad \text{.....(2.8)}$$

Although it is usually assumed that the isotropic swelling lines are straight and have a constant slope, their non-linearity has been often recognized (Mesri et al.,1978; Shimizu,1978). According to Mesri et al.(1978), in which the effects of OCR and the duration of swelling on the swelling index are examined for the wide range of OCR, the swelling index generally increases with OCR, however in certain range of OCR, it levels off and even decreases slightly with OCR. It should be noted, hence, that the applicability of eq.(2.8) might be limited in a certain range of OCR. It is, however, interesting that the relationship such as eq.(2.7) may be applicable for remoulded Weald Clay (Henkel,1959) and remoulded or undisturbed St.Clair clay till (Soderman & Kim,1970) as shown in Fig.2.3.

In Fig.2.4, the swelling line approximated by eq.(2.7) is shown, as well as the virgin consolidation line, where water content is evaluated in terms of the deviation from the water content at the end of consolidation with $p=p_c$ in order to eliminate some experimental scatter in the absolute quantity of water content. It is seen that the approximated swelling line (denoted

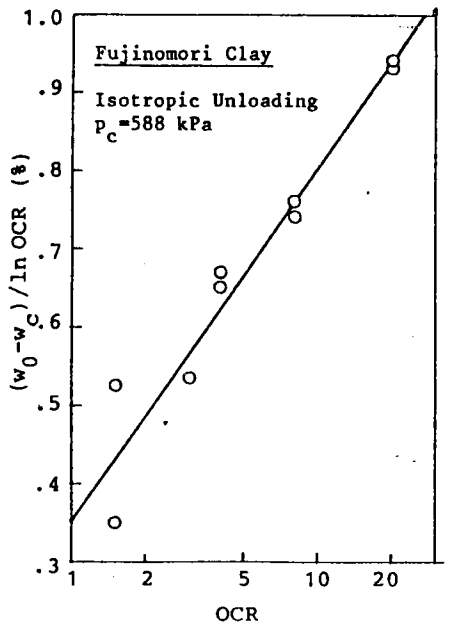

Fig.2.2: Volume change characteristics during isotropic unloading

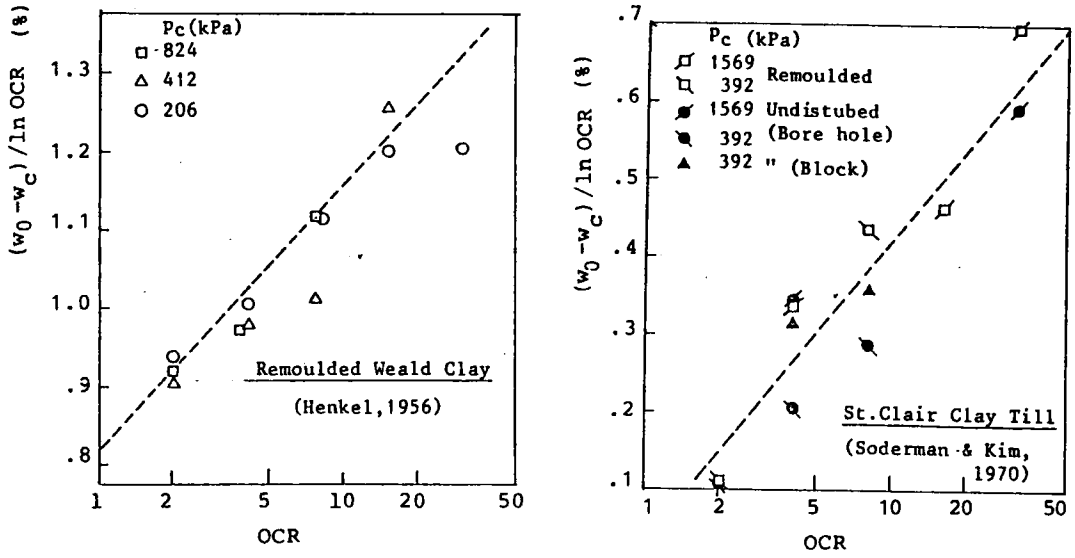

Fig.2.3: Swelling characteristics of (a) Weald Clay(Henkel,1959) and (b) St. Clair clay till (Sderman & Kim,1970)

by S.L. in the figure) is quite close to the experimental results and can well represent the non-linearity. In this figure water content at failure is also plotted. This will be discussed later.

2.3.2 Strain-Time Relations at Shear Stage

In Figs.2.5 and 2.6, volumetric strain and shear strain are shown, respectively, as a function of time elapsed after the moment of the application of an increment of shear stress at each loading stage, for Test F311 as an example. Strain is defined as the natural strain referred to the volume or the height of specimen at the start of shearing,i.e., at the end of isotropic consolidation process. From these figures it is not likely that deformation ceases completely even after 1 day for each loading stage especially at high values of stress ratio. It will be assumed, however, in the following discussion that the deformation at each loading stage ceases 1 day after the moment of load application and that strains observed after 1 day of loading are taken as strains in equilibrium corresponding to the state of stress which remains constant during each loading. Thus, time dependent behaviour of shear or volumetric strain will not be considered in this chapter

2.3.3 Stress-Strain Relations at Shear Stage

Volumetric strain and shear strain are plotted against stress ratio in Fig.2.7 and Fig.2.8 respectively. From Fig.2.7 it can be seen that such a dilatancy coefficient as used in eq.(2.2) is not constant but depends on stress ratio for each OCR. For specimens with OCR of 4, 8 or 20, negative volumetric strain occurs from the start of shear to failure; that is,

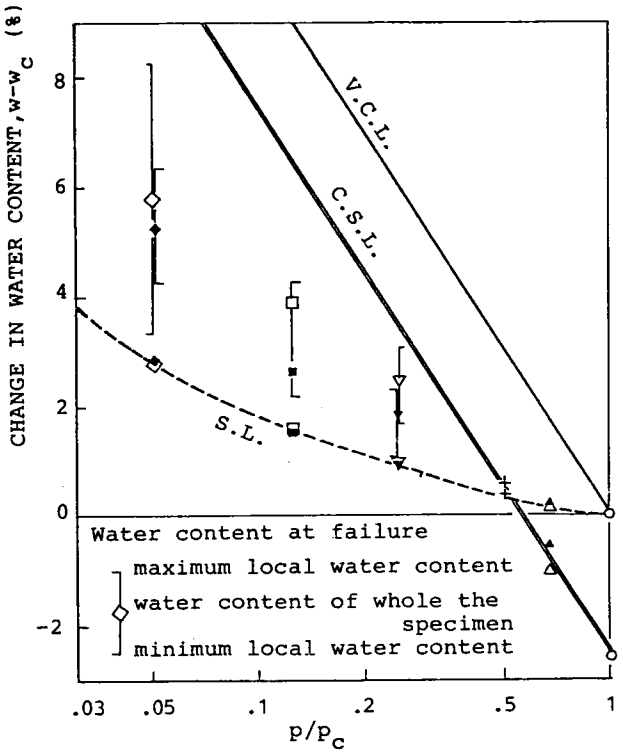

Fig.2.4: Change in water content during isotropic consolidation, rebound and at failure.

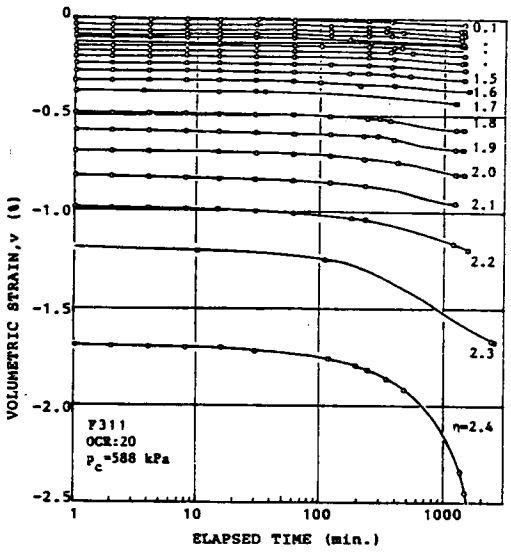

Fig.2.5: Volumetric strain vs. time (Test No.311)

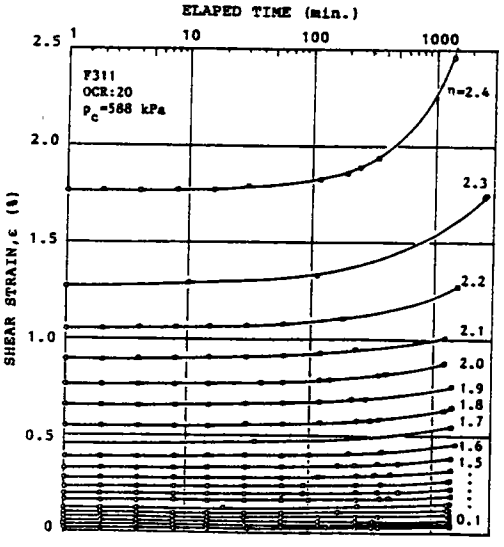

Fig.2.6: Shear strain vs. time (Test No.311)

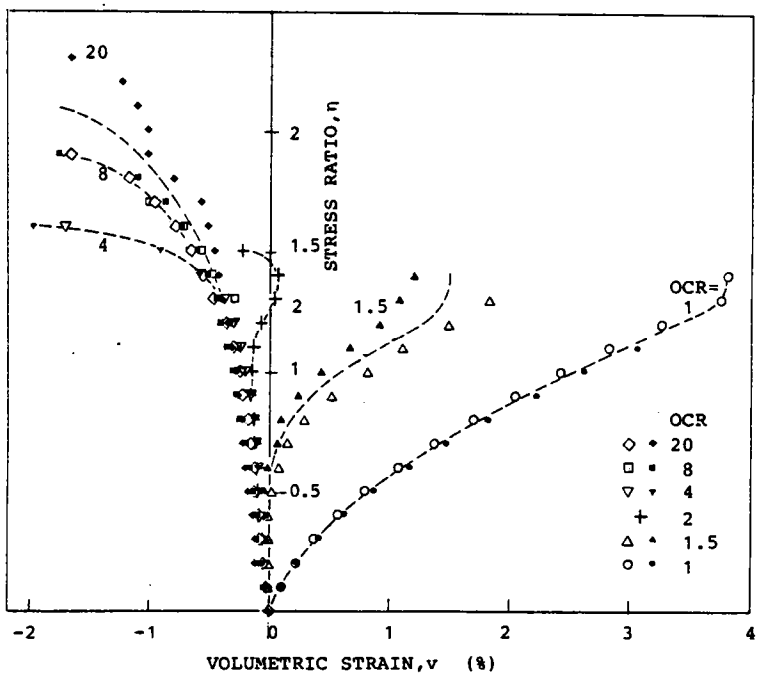

Fig.2.7: Relationships between volumetric strain and stress ratio

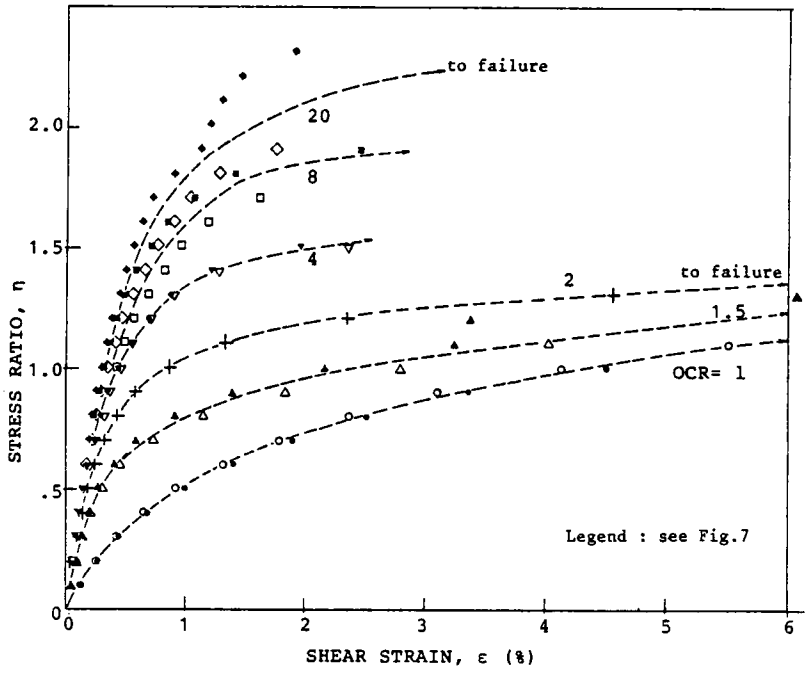

Fig.2.8: Relationships between shear strain and stress ratio.

volume expansion occurs. For OCR of 1.5 or 2, the sign of volumetric strain changes to positive from negative at a certain value of stress ratio, which seems to depend on OCR. And normally consolidated ones reveal positive volumetric strain once shear stress is applied; that is, volume contraction always occurs. These characteristics of volume change will be discussed later particularly in the light of their dependence on OCR.

2.4 DISCUSSION

2.4.1 Critical State for Overconsolidated Soils

Water content at failure evaluated in terms of the change in water content from the end of consolidation under $p=p_c$ is plotted against the normalized effective mean normal stress p/p_c in Fig.2.4 presented above. For OCRs of 1, 1.5 and 2, states at failure can be represented by a straight line being parallel to the virgin consolidation line (denoted by V.C.L.). Assuming that the failure state for normally consolidated or lightly overconsolidated specimens corresponds to the critical state as defined in the Cambridge theory, the critical state line (C.S.L.) can be expressed by the following equation:

$$w_{crit} = \Gamma - \lambda . \ln(p/p_u), \qquad \ldots\ldots\ldots\ldots (2.9)$$

where subscript 'crit' denotes the critical state, Γ is the water content at p of unit stress p_u (=100 kPa), and λ compression index for normally consolidated states (=-dw/dlnp).

As is well known, modes of failure of clays depend on the degree of overconsolidation. Normally consolidated or

lightly overconsolidated clays usually fail with the shape like a cask; heavily overconsolidated clays fail with one or two slip surfaces. It might be supposed, hence , that water content would not be uniform throughout the specimen, especially for heavily overconsolidated clays. To investigate this locality of water content, the distribution of water content at failure was measured for specimens of OCR=4, 8 or 20.

The specimens were divided to nine or ten small masses and the water content of each small mass was measured. The distribution of water content within the specimen for Test F311 is illustrated in Fig.2.9 as an example. The directions for dividing the specimen were taken so that at least one small mass could include the slip surface. As is clear in the example given in Fig.2.9, water content was relatively high for masses in the bulged portion, and the highest for one which includes the slip surface.

Maximum and minimum local water contents thus obtained and mean water content of the whole specimen are plotted in Fig.2.4. It can be seen that the maximum local water content gets near to the C.S.L. determined from the results for normally consolidated and lightly overconsolidated specimens.

The measurement of local water content was done at the moment of rupture to avoid the complete rupture of the specimen, resulting from the testing method of stress control. Since further redistribution will occur if the deformation after the rupture could be controlled to continue more slowly, local water content may be expected to be higher than measured

quantities shown in Fig.2.4. Taking into account this expected tendency of further increase in local maximum water content, it may be assumed that the critical state line for heavily overconsolidated states is the same as that for normally consolidated and lightly overconsolidated states. This is expressed by eq.(2.9)

2.4.2 Dilatancy of Overconsolidated Clay

The results shown in Fig.2.7 suggest that the volume change behaviour of overconsolidated specimens strongly depends on the degree of overconsolidation even if the normalized shear stress q/p is used. Several parameters which would serve to describe the characteristics of the volume change behaviour will be used and the variation of such parameters with the degree of overconsolidation will be investigated by using experimental results.

Fig.2.10 shows state paths on $(q/p_e, p/p_e)$ plane, where p_e is the equivalent mean normal stress defined by Hvorslev(1960) as

$$p_e = p_u . \exp\left(\frac{w_a - w}{\lambda}\right), \qquad \text{.....(2.10)}$$

where w_a is water content at the point on the V.C.L. for unit stress p_u. From this figure it appears that any stress path except those for normally consolidated specimens is fairly straight in some portion from the start of shearing. Beyond this straight portion, it begins to be curved as positive dilatant behaviour becomes more and more marked for heavily overconsolidated specimens (OCR=4, 8 or 20) and as negative dilatant behaviour for lightly overconsolidated ones (OCR=1.5

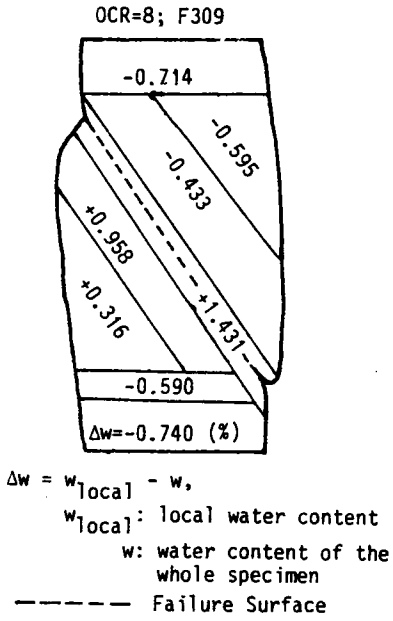

Fig.2.9: An example of the distribution of local water content.

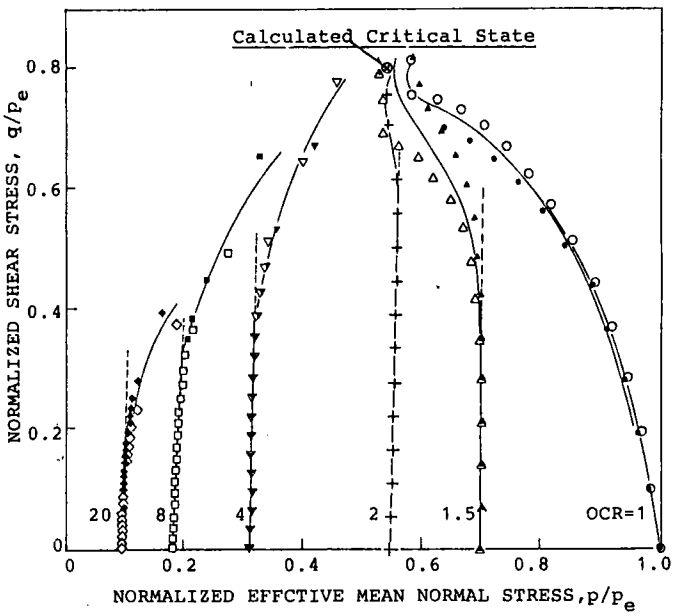

Fig.2.10: State paths on (q/p_e,p/p_e) plane

or 2). State paths for normally consolidated specimens are curved just from the beginning of shearing because of the negative dilatant behaviour. It should be noted here that the positive dilatant behaviour results in the decrease of p_e and the increase of p/p_e since p was held constant during the shearing.

From this figure it appears also that all the state paths have a tendency to arrive at a small area within which the critical state point will be located. The critical state point can be easily determined from two assumptions that the unique critical state line expressed by eq.(2.9) exists on (p,w) plane and , additionally, that the value of stress ratio at the critical state M would be constant regardless of the degree of overconsolidation. For a point at the critical state, from the definition of p_e ,

$$p_{e\ crit} = p_u . \exp\left(\frac{w_a - w_{crit}}{\lambda}\right). \qquad \ldots\ldots\ldots\ldots (2.11)$$

Substituting eq.(2.9) into the above, we obtain

$$p_{e\ crit} = p_{crit} . \exp\left(\frac{w_a - \Gamma}{\lambda}\right), \qquad \ldots\ldots\ldots\ldots (2.12)$$

and , hence, $(p/p_e)_{crit} = \exp\{(\Gamma - w_a)/\lambda\}$ and $(q/p_e)_{crit} = M.(p/p_e)_{crit}$. By using the values of w_a, Γ, λ and M the critical state point can be determined as $(p/p_e)_{crit} = 0.569$ and $(q/p_e)_{crit} = 0.797$. The values of constants mentioned above are listed in Table 2.3.

Any state path for overconsolidated specimens may be divided into two parts: straight and curved. Stress ratio corresponding to the point at which the linearity of a state path disappears and at which the state path begins to be curved will be referred to as the 'threshold of dilatancy' hereafter.

A subscript 'DL' will be used to specify the state of the threshold of dilatancy. Stress ratio at the threshold of dilatancy η_{DL} and the gradient of the linear portion of the state path as shown in Fig.2.10, D*, will be employed as parameters which characterize the volume change behaviour in the linear portion of a state path.

The variation of η_{DL} with OCR can be seen in Fig.2.11, where η_{DL} is plotted against the value of lnOCR in the log-log scale. The following relationship may be obtained between η_{DL} and OCR:

$$\eta_{DL} = M_{DL} \cdot (\ln n)^{m_{DL}} \qquad \text{.....(2.13)}$$

where M_{DL} and m_{DL} are constants: the former means the value of η_{DL} when ln n=1 or n=e (e: the base of the natural logarithm); the latter the gradient of the straight line represented in Fig. 2.11. The best fitting by means of the least square method gives 0.935 and 0.567 to M_{DL} and m_{DL} , respectively.

Fig. 2.12 shows the the variation of D* with the degree of overconsolidation. In this figure plots denoted by 'corrected' were obtained by taking into account the expansion or compression of the filter paper used as a side drain. The quantity of water expelled from or absorbed by the filter paper due to change in cell pressure was experimentally determined (Shimizu,1981). 'Non-corrected' plots were obtained directly from the results shown in Fig.2.7. From Fig.2.12 it can be seen that the inverse of D* and that of OCR can be linearly related whether or not the correction was made, resulting in the expression as follows:

w_a (%)	Γ (%)	λ ($\times 10^{-2}$)	Π
34.5	37.0	4.34	1.4

Table 2.3: List of constants for the determination of the critical state.

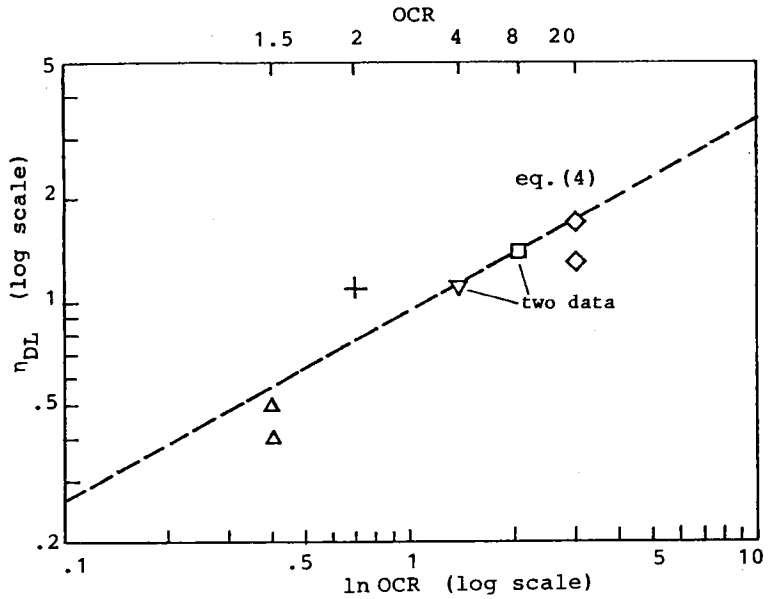

Fig.2.11: Variation of the stress ratio at the 'threshold of dilatancy' with OCR.

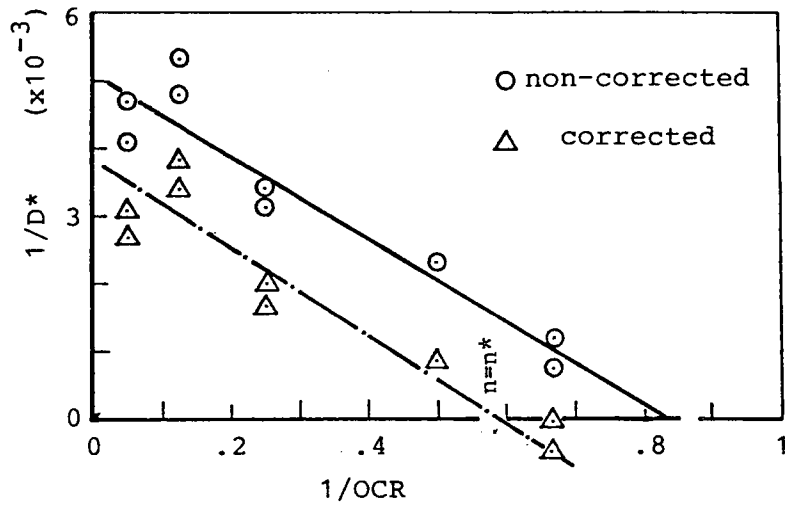

Fig.2.12: Variation of the gradient of the linear portion of state path (D*) with OCR

$$1/D^* = m^*(1/n - 1/n^*) \qquad \text{.....(2.14)}$$

The best fitting for corrected plots gives -0.065 and 1.7 to m* and n*, respectively. This equation indicates that D* is negative when OCR is smaller than n*. Hence , we assume that for a specimen with OCR smaller than n* its state path will have a linear portion with a negative value of D* in the beginning of shearing. This assumption implies that very lightly overconsolidated clay will contract just from the start of shearing as well as normally consolidated clays.

Now, we note that the dilatancy which appears at stress ratio smaller than η_{DL} is negligibly small, comparing that at stress ratio higher than η_{DL}.

2.4.3 Stress Ratio-Strain Increment Ratio Relations

The purpose of this section is to understand, experimentally, the relative influence of the degree of overconsolidation to the relationships between strain increment ratio and stress ratio. Discussions will be given being associated with the volume change behaviour shown above.

Fig.2.13 illustrates the relations between stress ratio η(=q/p) and strain increment ratio $-dv/d\varepsilon$, obtained from the p-constant tests of which results were presented above. dv and $d\varepsilon$ are volumetric and shear strain increments, respectively, corresponding to an applied stress increment.

Stress ratio- strain increment ratio relations are interesting in applying the theory of plasticity. Instantaneous strains at the application of load increment, which seem to be attributed to the elastic deformation(Casagrande &

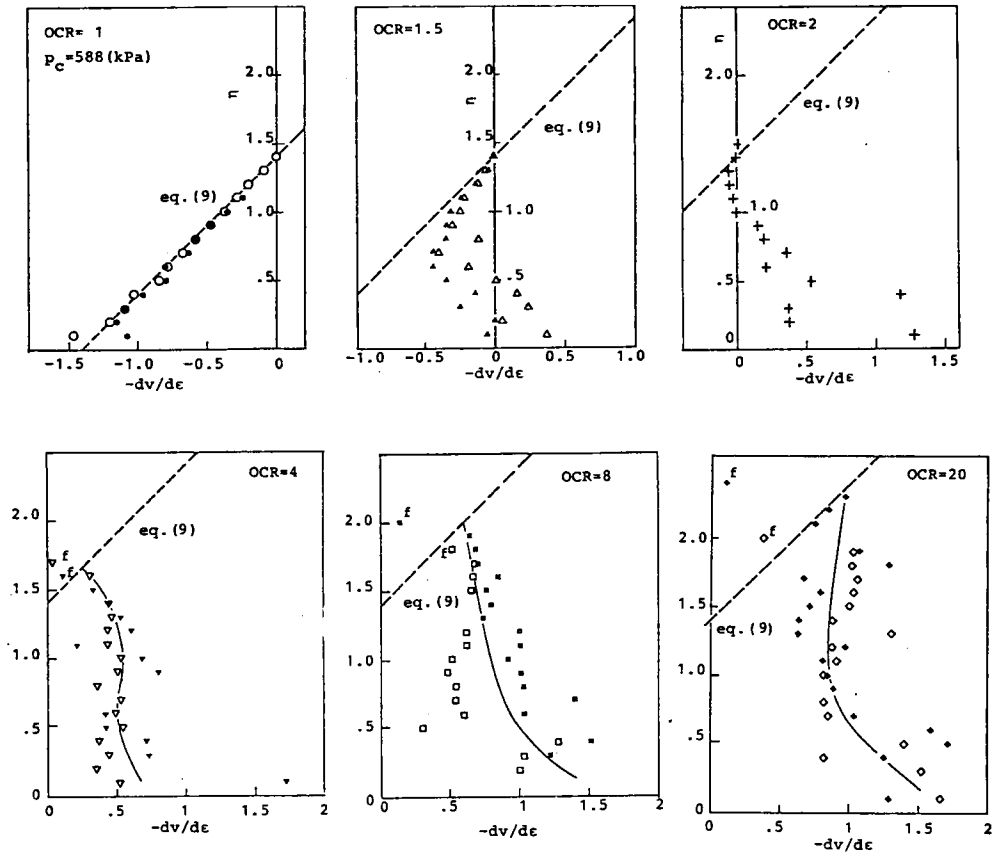

Fig.2.13: Relationships between stress ratio and strain increment ratio

Wilson,1951), were subtracted from the measured strains. Therefore, the strain increments used in Fig.2.13 may be regarded to be plastic.

This figure shows that the strain increment ratio-stress ratio relations vary with OCR. This OCR dependency will be discussed in detail.

Plots for normally consolidated specimens appear to be aligned on a straight line expressed by eq.(2.15) although for small values of η there seems to be some scatter.

$$\eta = -dv/d\varepsilon + M, \qquad \cdots\cdots\cdots\cdots\cdots\cdots (2.15)$$

where M is the value of stress ratio at $-dv/d\varepsilon=0$ or at failure. This parameter can be considered to correspond to the critical state stress ratio. Eq.(2.15) is the very energy equation in the original Cam Clay model.

Lightly overconsolidated specimens (OCR=1.5 or 2) start from states of $-dv/d\varepsilon$ positive, pass through the region within which $-dv/d\varepsilon$ is negative and reach the straight line expressed by eq.(2.15) at a certain value of η, which will be denoted by μ. Once reaching the line, they move along it and fail at $\eta=M$ with $-dv/d\varepsilon=0$.

Plots for heavily overconsolidated specimens (OCR=4,8 or 20) are always in the region of $-dv/d\varepsilon$ positive. At failure they are nearly on the straight line expressed by eq.(2.15). The stress ratio μ, defined above, hence, corresponds to stress ratio at failure for heavily overconsolidated specimens

In Fig.2.14, the variation of μ with OCR is shown. From this figure μ can be related to OCR by the expression:

$$\mu = M_\mu (\ln n)^{m_\mu}, \qquad \text{.....(2.16)}$$

where M_μ and m_μ are constants which can be determined from Fig. 2.14 M_μ represents the value of μ when ln n=1,i.e.,when n=e (e: the base of the natural logarithm). The best fitting by means of the least square method gives M_μ=1.39 and m_μ=0.428 It should be noted that the value of M_μ is almost the same as the value of M, the critical state stress ratio. From the coincidence between the values of M_μ and M, we may suppose that for OCR greater than e the sign of dilatancy due to shear is always positive.

There has been no data with which the coincidence of M_μ and M would be examined for clays other than the sample used here. However, recalling that OCR of the value of e is the boundary between 'dry' and 'wet' in the Cam Clay model, the coincidence between M and M_μ would not be strange. Accordingly, we adopt the notation M instead of M_μ. Eq.(2.16) leads to

$$\mu = M.(\ln n)^{m_\mu} \qquad \text{.....(2.17)}$$

2.4.4 State Boundary Surface

It is very intersting that, both for heavily overconsolidated specimens at stress ratio of μ and for lightly overconsolidated specimens at stress ratio greater than μ, stress ratio-strain increment ratio relations can be represented by the same equation as the energy equation in the original Cam Clay model.

According to the original Cam Clay model, eq.(2.15) is assumed to be valid for any state on the State Boundary Surface which can be derived from eq.(2.15) with a few hypotheses concerned with the concept of theory of plasticity. It will

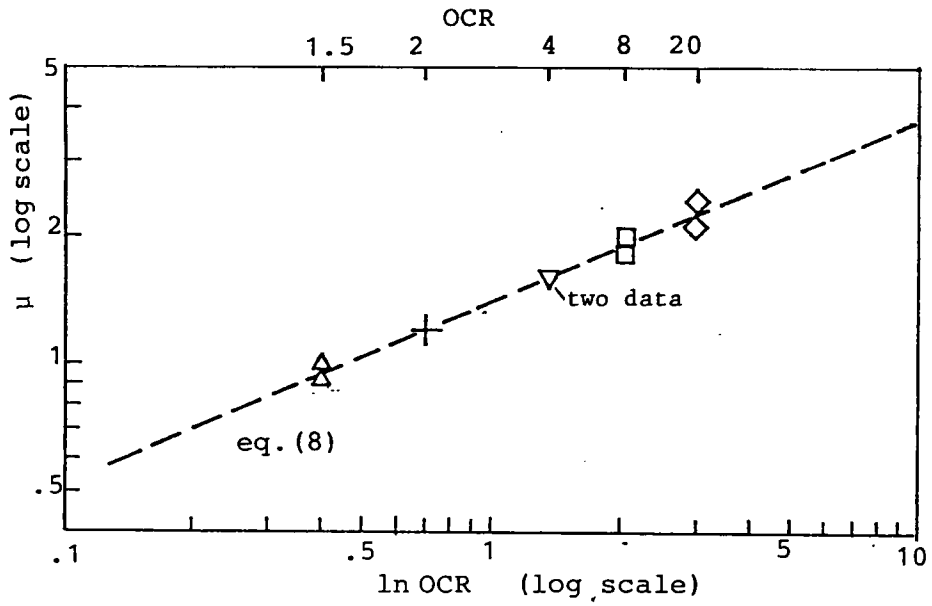

Fig.2.14: Variation of the boundary stress ratio with OCR

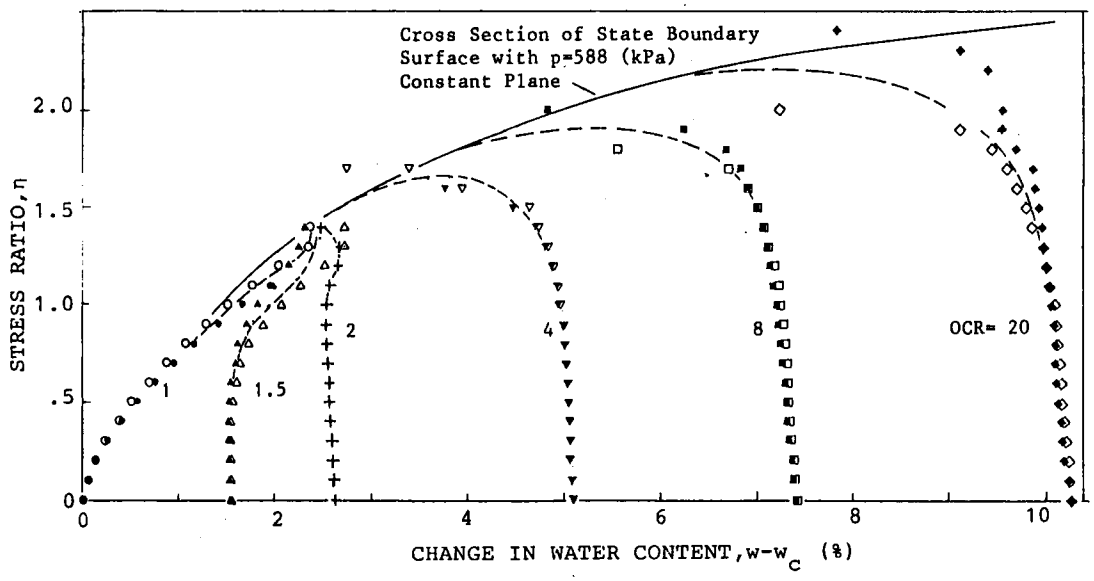

Fig.2.15: Dilatancy behaviour on the state plane with the same value of mean normal stress

not be very difficult to suppose that in (p,q,w) state space a unique boundary surface like the State Boundary Surface in the Cam Clay model exists and that on the boundary surface stress ratio-strain increment ratio relation as expressed by eq.(2.15) is valid in spite of the degree of overconsolidation although the validity is limited to a certain range of stress ratio.

In order to visualize the form of the state boundary surface, Fig.2.15 is prepared, where dilatancy behaviours are compared between specimens of various OCR but of the same value of effective mean normal stress p. Plots for a certain value of OCR were calculated by temporarily assuming that the dilatancy behaviour of a specimen consolidated to $p=p_{c0}=OCR.p_c$ and subsequently unloaded to $p=p_{c0}/OCR=p_c$ can be analogized by the behaviour of a specimen consolidated to $p=p_c$ and unloaded to $p=p_c/OCR$. The abscissa represents the change in water content referring to the water content at the point of $p=p_c$ on V.C.L..

In this figure, the envelope is considered to be a portion of the state boundary surface. It can be seen that for lightly overconsolidated specimens beyond the points corresponding to stress ratio μ defined already, the curves get near to those for OCR=1. On the other hand, plots for heavily overconsolidated specimens tend to lie on the envelope at failure,i.e., $\eta = \mu$. This means that for the states on the state boundary surface there exists a unique relation between stress ratio and strain increment ratio such as eq.(2.15),i.e., the energy equation proposed

in the original Cam Clay model may be valid even for overconsolidated specimens if their states reach the state boundary surface.

2.5 CONCLUSION

The characteristics of dilatancy, i.e., the volume change which reveals when subjected to shear stress under the condition that the effective mean normal stress is held constant, have been examined experimentally for a saturated clay soil of various OCRs.

In order to facilitate the understanding and interpretation of the results, the state paths on normalized state plane (q/p_e, p/p_e) and the relations between stress ratio and strain increment ratio were utilized. Several parameters which serve to specify the dialtancy characteristics were chosen and used.

From the behaviour of state paths on (q/p_e, p/p_e) plane (Fig.2.10) it was shown that :

i) When stress ratio is smaller than an OCR dependent value, denoted by η_{DL}, state paths are straight, and in the straight portion the variation of p/p_e, accordingly the change in water content, is negligibly small comparing to that beyond this portion

ii) The gradient of the straight portion of a state path, $D^* = d(q/p_e)/d(p/p_e)$, is positive for OCR greater than n* (n* is about 1.7 for the sample used) and it is negative for OCR smaller than n*; that is , overconsolidated specimens of OCR greater than n* dilate just from the start of shearing while those of OCR smaller than n* contract.

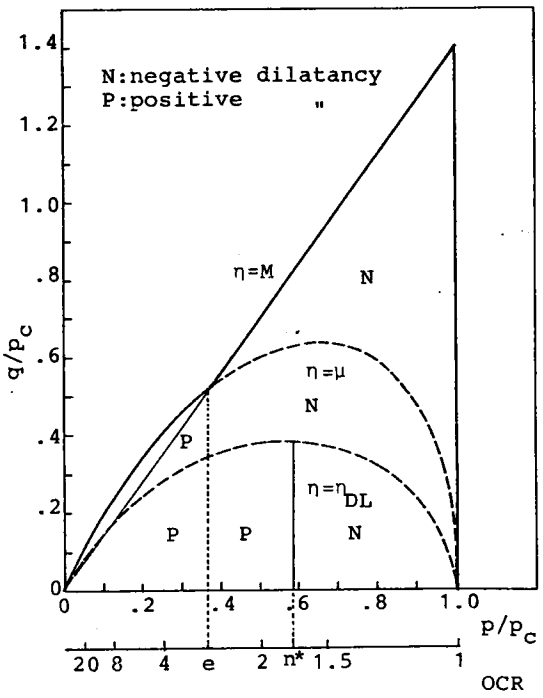

Fig.2.16: Variation of the sign of dilatancy with OCR and shear stress.

As to the relations between stress ratio and strain increment ratio, findings are summarized as follows:

i) For any degree of overconsolidation, when stress ratio reaches an OCR dependent value , denoted by μ , the relation is represented by the expression of eq.(2.15) which is the same as the energy equation assumed in the original Cam Clay model.

ii) State paths in (p,q,w) state space reach the state boundary surface at the stress ratio μ , and there seems to exist a unique relation between stress ratio and strain increment ratio on the state boundary surface as assumed in the original Cam Clay model.

iii) e(the base of the natural logarithm) is a boundary value of OCR, because for OCR greater than e the sign of strain increment ratio $-dv/d\varepsilon$ might be always positive while for OCR smaller than e it changes from positive to negative; that is, overconsolidated specimens of OCR greater than e dilate all the way from the start of shearing to filaure.

Considering both the behaviours of state paths on $(q/p_e, p/p_e)$ and the relations between stress ratio and strain increment ratio, the sign of dilatancy can be classified according to the degree of overconsolidation and the shear stress level as illustrated in Fig. 2.16 , in which shear stress q and effective mean normal stress p are both normalized by maximum normal consolidation stress p_c.

REFERENCES FOR CHAPTER 2

Adachi,T. and Nishi,K.(1976): "Constitutive equations for overconsolidated clays", Annals, Diasaster Prevention Research Institute, Kyoto Univ., No.19-B2, pp.1-13.(in Japanese)

Balasubramaniam,A.S. and Z-Ming,H.(1980): "Yielding of weathered Bangkok Clay", Soils and Foundation, JSSMFE, Vol.20, No.2, pp.1-15.

Bjerrum,L.(1967): "Engineering geology of Norwegian normally consolidated marine clays as related to settlements of buildings", Seventh Rankine Lecture, Geotechnique, Vol.17, pp.83-117.

Casagrande,A. and Wilson,S.D.(1951): "Effect of rate of loading on the strength of clays and shales at constant water content", Geotechnique, Vol.2, pp.251-263.

Henkel,D.J.(1959): "The relationships between the strength, porewater pressure, and vlume chnge characteristics of saturated clays", Géotechnique, Vol.9, pp.119-135.

Hvorselv,M.J.(1960): "Physical component of the shear strength of saturated clays", Proc. Research Conf. Shear Strength of Cohesive Soils, ASCE, pp.163-273.

Karube,D. and Kurihara,N.(1966): "Dilatancy and shear strength of saturated remoulded clays", Proc. JSCE, No.135, pp.16-24.(in Japanese)

Ladd,C.C. and Lambe,T.W.(1964): "The strength of 'undisturbed' clay determined from undrained tests", ASTM Special Tech. Pub.,No.361, pp.342-371.

Mesri,G., Ullirich,C.R. andChoi,Y.K.(1978): "The rate of swelling of over-consolidated clays subjected to unloading", Géotechnique, Vol.28, No.3, pp.281-307.

Murayama,S. and Matsuoka,H.(1973): "A microscopic study on shearing mechnics of soils", Proc. 8th ICSMFE, Vol.1, Part 2, pp.293-298.

Murthy,K.M., Sridharan,A. and Nagaraj,T.(1981): "Shear strength behaviour of overconsolidated clays", Soils and Foundations, JSSMFE, Vol.21, No.2, pp.73-82.

Nakase,A.(1968): "Effect of overconsolidation on undisturbed strength of clays", Report of the Port and Harbour Research Inst., Ministry of Transport, Japan, Vol.7, No.1, pp.4-23.

Ohmaki,s.(1980): "Strength and deformation characteristics of an O.C. clay", Proc. 3rd Int. Conf. on Numerical methods in Geomech., pp.465-474.

Ohta,H.(1971): "Analysis of deformation of soils based on the theory of

plasticity and its application to settlement of embankments", Dr. Thesis, Kyoto Univ..

Parry,R.H.G. and Amerasinghe,S.F.(1973): "Component of deformation in clays", Proc. Symposium on Plasticity and soil Mech., Cambridge, pp.108-128.

Pender,M.J.(1978): "A model for the behaviour of overconsolidated soil", Géotechnique, Vol.28, No.1, pp.1-25.

Roscoe,K.H. and Burland,J.B.(1968): "On the genaralized stress-strain behaviour of 'wet' clay", Eng. Plasticity, Cambridge Univ. Press, pp.535-609.

Rowe P.W.(1962):"The stress-dilatancy relation for static equilibrium of an assembly of particles in contact", Proc Roy. Soc. London, Series A, Vol.269, pp.500-527.

Schofield,A.N. and Wroth,C.P.(1968): Critical State Soil Mechnics, McGraw Hill.

Shibata,T.(1963): "On the volume change of normally consolidated clays", Annals, Disaster Prevention Rsearch Inst., Kyoto Univ., No.6, pp.128-134.(in Japanese)

Simizu,M.(1978): "Characteristics of dilatancy and strength of remoulded overconsolidated clay under low effective stress level", Annals, Disaster Prevention Rsearch Inst., Kyoto Univ., No.21B-2, pp.1-17.(in Japanese)

Shimizu,M.(1981): "Factors affecting the measurement of volume change of cohesive soils in drained triaxial tests", Soils and Foundations, JSSMFE, Vol.21, No.2, pp.121-128.

Soderman,L.G. and Kim,Y.D.(1970): "Effect of ground water levels on stress history of the St.Clair clay till deposit", Can. Geotech. J., Vol.7, pp.173-187.

Vermeer,P.A.(1978): "A double hardening model for sand", Géotechnique, Vol.28, No.4, pp.413-433.

CHAPTER 3 EFFECTS OF SHEAR STRESS HISTORY ON THE SHEARING AND ISOTROPIC COMPRESSION BEHAVIOUR*

3.1 INTRODUCTION

Predicting the mechanical response of soil grounds or soil structures during earthquakes is one of the most important problems concerned with soil mechanics. Comprehensive studies of mechanical behaviours of sands or clays under repeated loading are needed. In this chapter, for the first stage to achieve such an aim, mechanical behaviour of a clay when shear stress applied under the triaxial compression condition is unloaded is investigated experimentally. The effect of the stress history given in the triaxial compression condition on the deformation characteristics accompanied with the subsequent stress pathes: effective mean normal stress constant path and isotropic compression stress path, is examined.

Discussion is also made on the validity of a parameter OCR defined in the usual manner as a measure for evaluating apparent overconsolidation effect caused by the stress history.

Effective mean normal stress $p(=(\sigma_a+2\sigma_r)/3)$ and deviator stress $q(=\sigma_a-\sigma_r)$ are used as stress parameters; and corresponding strain parameters $v(=\varepsilon_a+2\varepsilon_r)$ and $\varepsilon(=2(\varepsilon_a-\varepsilon_r)/3)$ are used.

3.2 EXPERIMENTAL PROCEDURE

3.2.1 Sample and Apparatus

The sample used is a laboratory reconstituted cohesive soil called Fujinomori Clay. The method to prepare specimens for triaxial tests is similar to that described in Chapter 2.

*Shimizu(1980)

Cylindrical specimens of 10 cm^2 in cross section and 8 cm in height were used; a filter paper having a series of strips was used aound the specimen as a side drain; the drainage was not allowed in the vertical direction but in the radial direction only. The water content when in position in a triaxial cell was about 40 %. Physical properties of the sample are shown in Table 3.1 and the grain size distribution curve is shown in Fig.3.1.

Triaxial apparatus of the standard NGI type of which the loading lever had been improved to enable performance of stress controlled triaxial tests both in compression and in extension were used. The view of the loading system is shown in Photo 3.1.

3.2.1 Effective Stress Paths

All the tests performed are triaxial drained stress-controlled tests. After the isotropic consolidation up to $p=p_c/OCR$ (p_c:maximum preconsolidation stress; and OCR: overconsolidation ratio) was completed, effective stress paths shown in Fig.3.2 were given.

a) Monotonous Loading of Shear Stress (MC or ME): Stress ratio η was monotonously increased in compression (MC) or decreased in extension (ME) by increments of 0.1 from the isotropic consolidated state to the failure in compression (MC) or in extension (ME).

b) Loading-Unloading of Shear Stress (RCE): Stress ratio η was increased by increments of 0.1 and when it reached a certain value (denoted by η_R), the loading direction was reversed

Table 3.1: Physical properties of the sample used.

G_s	P.L. (%)	L.L. (%)	P.I.
2.64	27.8	54.0	26.2

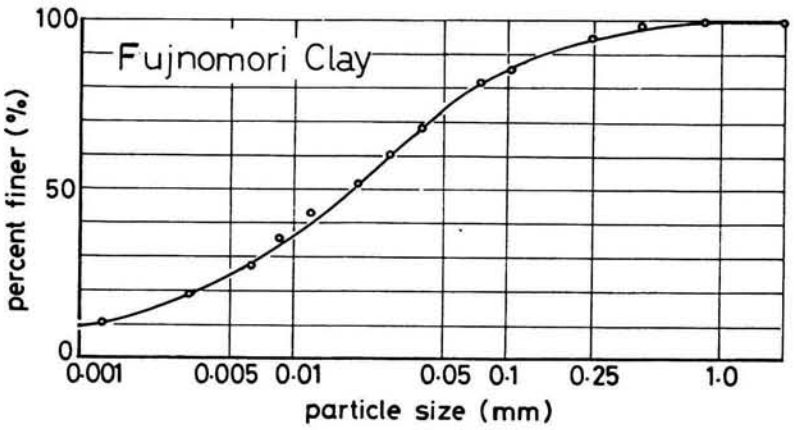

Fig.3.1: Grain size distribution curve.

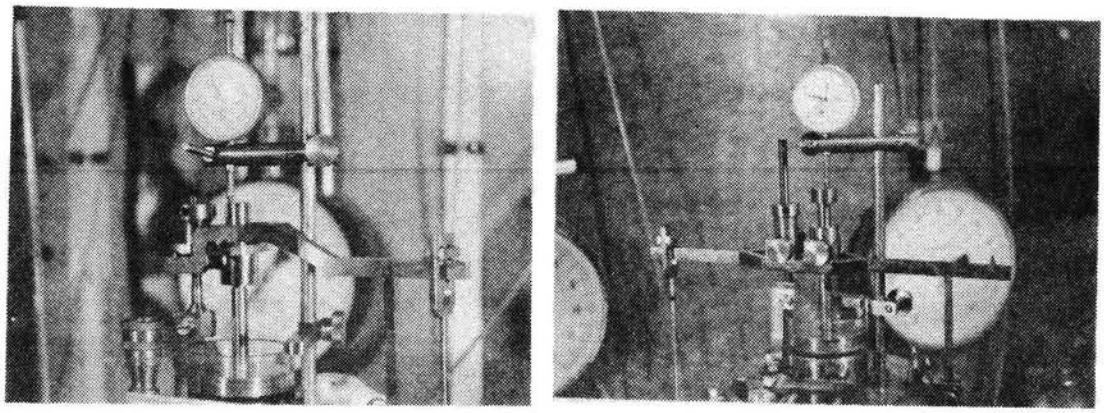

(a) (b)

Photo 3.1: Axial loading levers:

(a) Available for triaxial compression only

(b) Improved to be available for both triaxial compression and extension.

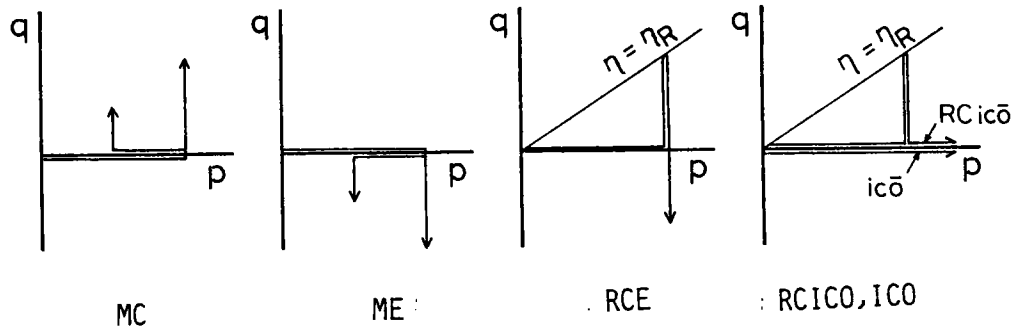

Fig.3.2: Schematic representation of stress paths used in this study.

Table 3.2: List of tests performed.

Test No.	Test Type	OCR	p (kPa)	η_R	η_f
1	MC	1	392	-	1.4
2		2	196	-	1.5
3		8	49	-	1.9
5	ME	1	392	-	-1.0
6		2	198	-	-1.1
7		2	392	-	-1.1
8		8	49	-	-1.3
9	RCE	1	392	0.4	-1.0
10		1	392	0.8	-1.0
11		1	392	1.1	-1.0
12		1	392	1.1	-1.1
13	RCICO	1	392	0.4	-
14		1	392	0.8	-
15	ICO	1	-	-	-

i.e., stress ratio η was incrementally decreased by 0.1 till the failure in extension.

Throughout these processes (MC, ME and RCE) effective mean normal stress p was kept constant.

c) Isotropic Compression after Loading-Unloading of Shear Stress (RCICO): Stress ratio η was increased by increments of 0.1 to $\eta=\eta_R$ and decreased by 0.1 as in the case of RCE, but, when the isotropic stress state ($\eta=0$) was again reached, p was increased by increments of 49 kPa without any shear stress.

d) Isotropic Compression (ICO): No shear stress was applied and the isotropic compression was performed by increasing p by increments of 49 kPa.

In Table 3.2 the list of the tests performed is given. For all the tests, loading duration under each increment of stress was approximately 1 day, it was, however, longer when the corresponding deformation had not completely ceased.

3.3 RESULTS OF EXPERIMENTS

3.3.1 Monotonous Loading Tests (MC and ME)

Stress-strain relations obtained from the monotonous loading tests are shown in Fig.3.3, representatively for ME alone. Results of MC are not shown because there seemed to be little difference in the effect of the degree of overconsolidation on the behaviour whether the stress state is in triaxial compression or in triaxial extension.

The dilatancy behaviour of a cohesive soil subjected to

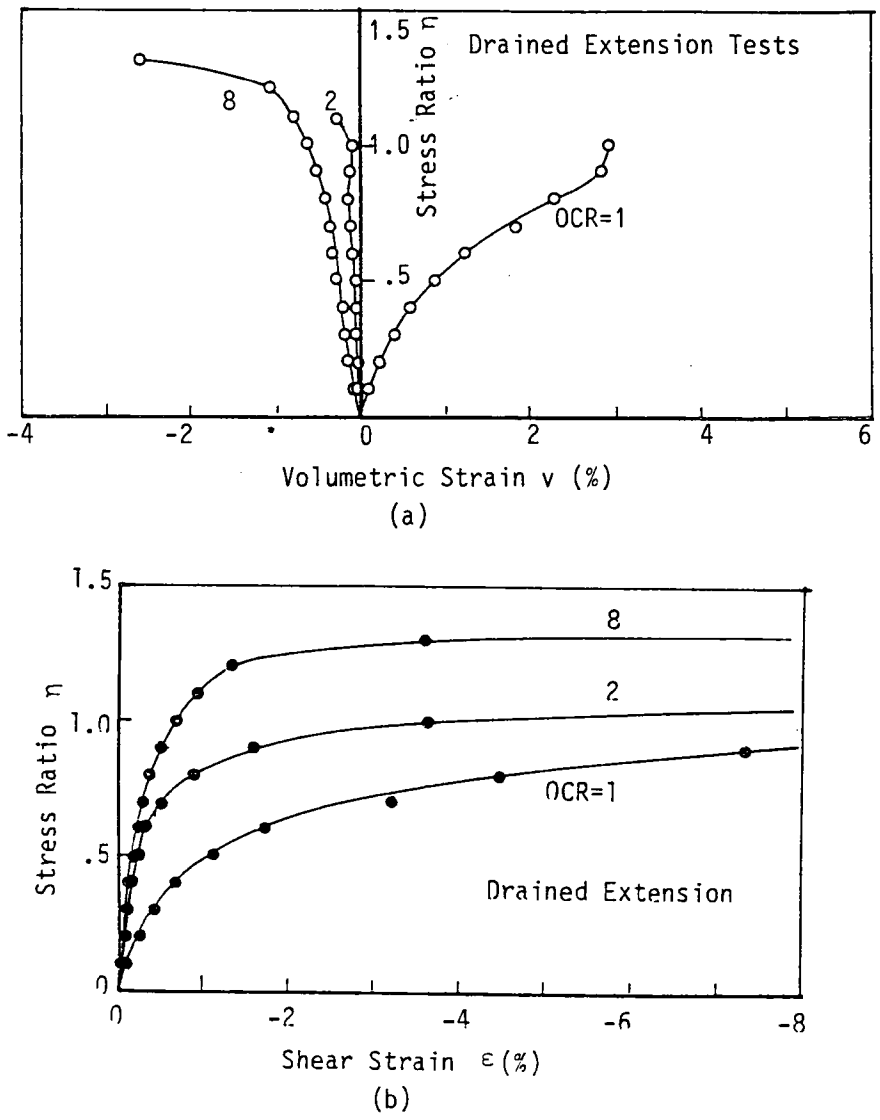

Fig.3.3: Results of monotonous loading tests(ME)
(a) Volumetric strain vs. stress ratio; and
(b) Shear strain vs. stress ratio.

various degrees of overconsolidation was already examined by performing drained triaxial compression tests of p-constant (Chapter 2). The principal feature as to the effect of overconsolidation is summarized as follows: There is a boundary value of OCR in the sense that, for OCR smaller than a certain value (1.7 was obtained for Fujinomori Clay), volume contraction occurs due to dilatancy, on the other hand, for OCR larger than the value, volume expansion occurs; the larger OCR is, the stronger the tendency for the volume to expand due to the dilatancy is. The dilatancy behaviour partly shown in Fig.3.3(a) seems to agree with the general statement above.

As for the relations between shear strain ε and stress ratio η, it can be seen from Fig.3.3(b) that, the larger OCR is, the less shear strain occurs for the same value of stress ratio.

3.3.2 Loading-Unloading Tests (RCE)

The effects of the stress history given in triaxial compression on the behaviour after the loading direction is reversed will be examined in this section.

(1) Effect of Secondary Consolidation

Effective mean normal stress p was kept constant for the tests of RCE as stated already, but even when p is constant, the phenomenon of so-called secondary or delayed consolidation is observed. Consequently, observed or measured volumetric strain may include the component of the secondary consolidation due to the hydrostatic component of stress, the proportion of which may vary between tests if the test duration differs

from test to test. The more the level of shear stress given as the stress history was, the longer the duration was required in the course of giving the stress history; for example, it took more than 33 000 minutes for Test No.11(RCE,η_R=1.1) and about 13 000 minutes for Test No.9(RCE,η_R=0.4). Thus, before examining the effect of the stress history, we must consider eliminating the influence of the time-dependent or delayed consolidation due to the hydrostatic component of stress. An attempt to eliminate such time-dependent volumetric strain will be made in the following.

Fig.3.4 shows isotropic consolidation curves for specimens No.5 and No.15, as examples, when p was increased to 392 kPa from 98 kPa. It is seen that the volumetric strain can be linearly related to the logarithm of time in the so-called secondary consolidation portion. This can be expressed as

$$dv_{sc} = \alpha\, d\ln(t/t_0), \qquad \text{.....(3.1)}$$

where v_{sc}: volumetric strain due to secondary consolidation under the isotropic stress condition,

t: elapsed time after the moment of the application of consolidation stress,

t_0: unit time(1 minute is taken) and

α: secondary compression coefficient (determined as 2.81×10^{-2} from Fig.3.4)

If it is assumed that eq.(3.1) can be applied to predict the creep component of volumetric strain due to the hydrostatic stress component even when shear stress is applied at the same time, eq.(3.1) is changed to eq.(3.2):

$$v_{sc} = \alpha.\ln\{(t_c+\Delta t)/t_c\}, \quad , \qquad \ldots\ldots\ldots\ldots (3.2)$$

where t_c: time required for the isotropic consolidation under p=392 kPa and

Δt: elapsed time after the instance of the first application of shear stress component.

In this equation v_{sc} is referred to the instance of $\Delta t=0$. Thus, the volumetric strain occurring due to the hydrostatic component of stress can be evaluated.

Relations between stress ratio η and volumetric strain v resulted from the tests of the type of RCE are shown in Fig.3.5, where the results of MC and ME for OCR=1 are also included. The volumetric strain in this figure has been obtained by subtracting v_{sc}, calculated by the use of eq.(3.2), from the measured volumetric strain. In Fig.3.5, by comparing the results of Test No.1, for which the correction of the volumetric strain is not made, with the others, it can be understood that the accumulated creep volumetric strain caused due to hydrostatic component of stress is not negligible. The volumetric strain measured under a level of shear stress may include some accumulated creep strain due to the preceding shear stress levels, it was, however, very small compared with v_{sc} and neglected.

(2) Dilatancy Behaviour

In Fig.3.5, it is natural that the relationships during loading in compression are the same for all the tests except No.1. Negative dilatancy or volume contraction occurs just from the beginning of shear. In the unloading portion, for each test of No.9, No.10, No.11 or No.12, the change in volu-

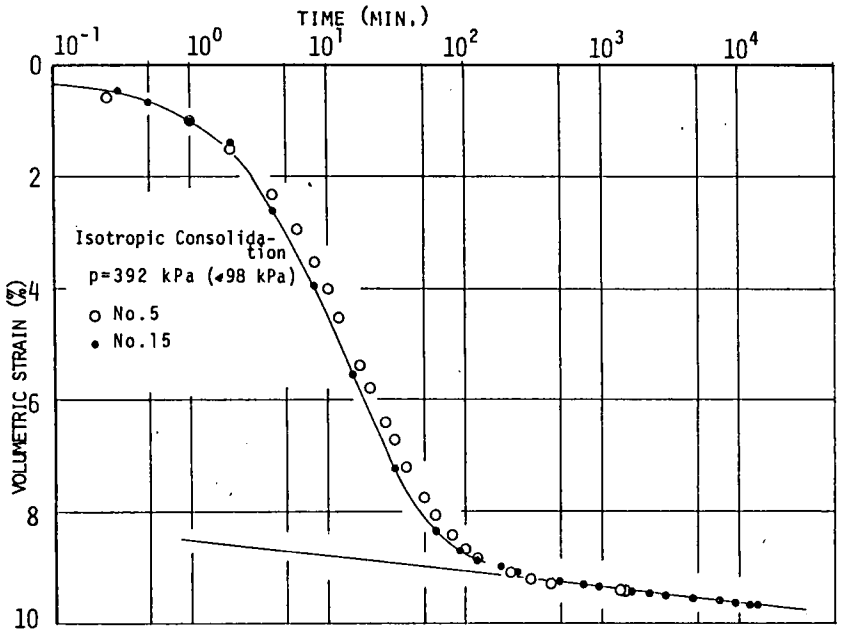

Fig.3.4: Isotropic consolidation curves under p=392 kPa.

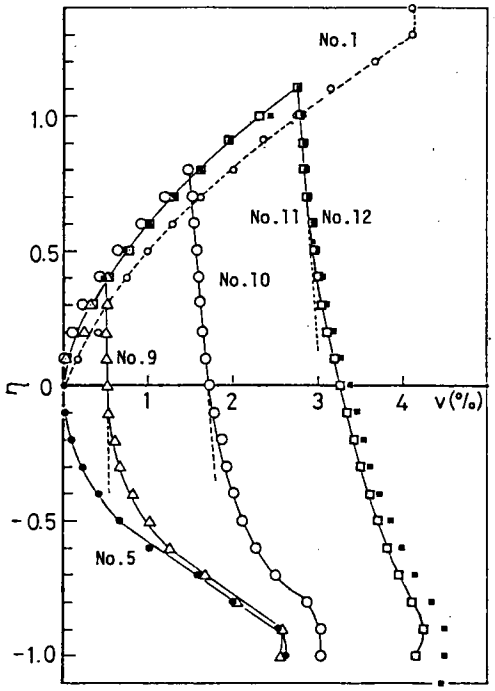

Fig.3.5: Results of MC and RCE tests; volumetric strain vs. stress ratio.

metric strain does not appear or, if any, it is negligibly small and v-η relation is linear until stress ratio reaches a certain value which seems to depend on the degree of stress history in triaxial compression. Following the linear portion, negative change in dilatancy reoccurs and, finally, failure is reached. Near the state of the failure, the change in volumetric strain is little.

The curves corresponding to the loading in triaxial compression for Tests No.9 to 12 and those of No.1 and No.5 are considered to constitute the state boundary surface (S.B.S.) described in (p,q,e or w) space (e:void ratio; and w:water content). Thus, from Fig.3.5, it can be understood that the states following the unloading in compression exist within the S.B.S. and therefore the curves in unloading portions for Tests No.9 to 12 represent the dilatancy behaviour within the S.B.S. Additionally, from the shape of the curves for No.1 and No.5, which have not experienced the unloading process,it is supposed that the shape of the S.B.S. is not symmetric with respect to the q=0 plane.

In Fig.3.5, the relationship for Test No.9(η_R=0.4) coincides with that for Test No.5(ME) at η less than about -0.6, which results in the fact that the state of No.9 reaches the S.B.S. at η=-0.6 and, subsequently, it moves on the S.B.S. in the same fashion as No.5. However, for Test No.11 (or 12, η_R=1.1), where η_R is larger than that of No.9, the curve does not join that of No.5 and failure occurs at the Dry side. In addition, the curve for No.10(η_R=0.8) is always between that for No.9 and that for No.11 from the start of unloading to the failure.

It is concluded that, when subjected to the stress history in compression greater than some level, the state following the unloading moves within the S.B.S. and failure occurs on the Dry side in the triaxial extension side. However, when the level of the stress history is relatively small, the state moves within the S.B.S. during some portion after the start of unloading and reaches the S.B.S. at a certain level of shear stress which will depend on the level of the stress history. Further it moves on the S.B.S. as if no stress history had been given.

(3) Instantaneous or Elastic Shear Strain

The sudden deformation which accompanies each increment of load can be regarded as the elastic response according to Casagrande & Wilson(1950), who state that the "instantaneous modulus of deformation calculated on the basis of the summation of the sudden deformation agreed excelently with the modulus of elasticity obtained from the dynamic method using forced vibration to produce resonance.

In Fig.3.6, the summation of the instantaneous axial strain is plotted against shear stress for several tests. The deformation measured after 6 seconds of the application of load increment was substituted for the instantaneous deformation. From this figure, it can be seen that the summation of the instantaneous axial strain is linearly related to shear stress in the whole portion of loading in compression, and that, by the susequent unloading, more than half of the strain which has occurred during loading is recovered.

In this figure, when the state of stress is changed to the extension from the compression, a discontinuous jump of the instantaneous axial strain, notable in Test No.10, is found. This jump seems to be caused by a rather inevitable defect of the mechanism of the connection between a loading ram and an end cap,i.e., the connection used is not a rigid type but an infinitely small gap is intentionally made because, if a rigid type of connection is used, the disturbance, particularly, of soft clay specimens, cannot be avoided when the loading ram is connected rigidly to the cap. The adjustment of this gap, which had been performed when the isotropic stress state was reached in the unloading process, was probably not complete.

From the reasons mentioned above, it can be said that the experimental data can be refined by the subtraction of the instantaneous deformation. In addition to that, the elastic component of the deformation can be eliminated.

In Fig.3.7, the correction of the instantaneous axial deformation is made except for Test No.1, hence, the comparison of the result of Test No.1 with those of the others can serve to estimate the order of the magnitude of the instantaneous deformation. It is understood that its proportion to the total strain is not very small.

(4) Plastic Shear Strain

In Fig.3.7, the relationships between shear strain and stress ratio are shown for tests of RCE(No.9 to 12), MC(No.1) and ME(No.5), where the shear strain has been obtained by sub-

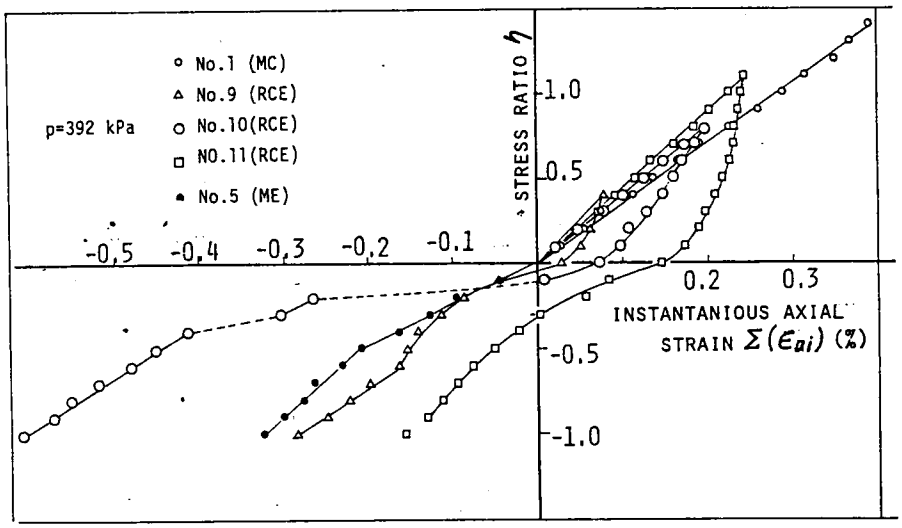

Fig.3.6: Accumulated instantaneous strain vs. stress ratio.

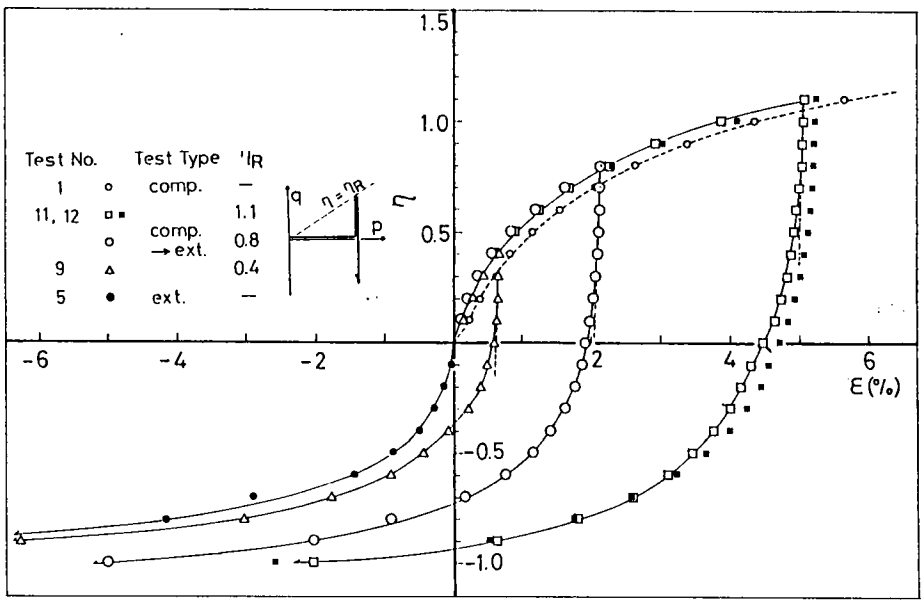

Fig.3.7: Results of MC and RCE tests; shear strain vs. stress ratio.

tracting axial deformation which suddenly occurred by the application of a load increment from the total axial deformation corresponding to the load increment. Therefore, shear strain indicated in this figure can be regarded as plastic according to the discussion above.

Also, the behaviour after unloading for tests of RCE corresponds to the state within the S.B.S. as discussed in the previous section.

In this figure it can be seen that, for each test of the type of RCE, there exists a linear relation between stress ratio η and shear strain ε in the unloading portion. In the linear portion very little change in ε occurs until η reaches a certain value. After passing the linear portion, the change in ε begins to develop with the opposite sign to that observed in the loading . Finally, it becomes infinitely large,i.e., failure is reached.

It has already been pointed out that the state for Test No.9 reached the S.B.S. when η reached the value of about -0.6. In Fig.3.7 the behaviour of Test No.9 is rather similar to that of Test No.5(ME) when η is decreased enough to be smaller than -0.6.

3.3.3 Isotropic Compression after Unloading (RCICO and ICO)

Fig.3.8 shows the results of the tests of RCICO(Test No.13 and 14) and ICO(Test No.15). In the upper part of this figure the volumatric strain or dilatancy which occurred during the loading and unloading of shear stress in triaxial compression is plotted against stress ratio; and in the lower part the

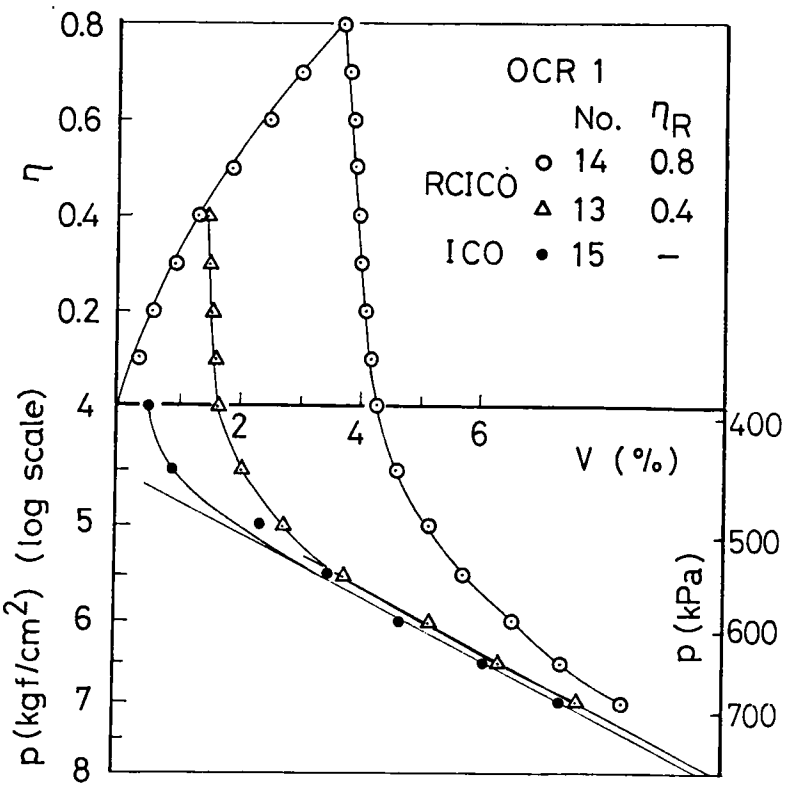

Fig.3.8: Results of RCICO and ICO tests; volumetric strain vs. stress ratio (upper part) and effective mean normal stress (lower part).

volumetric strain during the isotropic compression following the cycle is plotted against the effective mean normal stress p in the log scale.

In this figure, for tests of RCICO type the strain is referred to the state at the end of isotropic preconsolidation under p of 392 kPa. For the test of ICO(Test No.15), the volumetric strain at 392 kPa is not zero but about 0.5 %, because the duration of the isotropic consolidation under p of 392 kPa of this test was made to be equal to that during which Test No.13(RCICO) has been subjected to p of 392 kPa,i.e., to the summation of the duration required for the isotropic preconsolidation (1440 minutes) and the subsequent loading-unlloading cycle of shear stress (11 500 minutes) for Test No.13. This quantity of 0.5 % is the volumetric strain due to the time effect or secondary consolidation effect under p of 392 kPa for No.13. It might be more for No.14 because the duration in the loading-unloading cycle for the test is more than that for No.13.

The effect of the shear stress history in triaxial compression on the compressibility under isotropic stress condition can be examined in Fig.3.8. The relation between v and log p for Test No.13 and No.14(RCICO) becomes linear as well as for Test No.15, as p increases,i.e., as p reaches the value of 490 to 540 kPa for Test No.13 and 690 kPa for No.14. The straight line drawn in this figure is based on the value of compression index (C_c=0.551) obtained from the e-log p relations at the isotropic preconsolidation stage (p=196

and 392 kPa). This coincidence of three relations, two of which are for specimens with the stress history and the rest without it, indicates that, once when the state arrives again at the S.B.S. on the q=0 plane after the cycle of shear stress, the volume change behaviour on this plane is not affected by the shear history but it is represented by the unique virgin consolidation line.

In Figs.3.9 and 3.10, the volumatric strain-time relations are shown for Test No.13 and No.15, respectively. We can examine the effect of the stress history on the consolidation characteristics by comparing these two figures: there seems to be some difference in the shape of consolidation curve ; this difference results from the difference in the compressibility, particularly, at relatively small values of p; as the difference in compressibility vanishes with increasing p, also the difference in the consolidation curve vanishes. Conclusively, the consolidation characteristic is not affected by the stress history so far as the v-log p relations coincide with each other independently of whether the stress history was given or not.

3.4 OVERCONSOLIDATION INDUCED BY SHEAR STRESS HISTORY

It is common to specify the degree of overconsolidation by a parameter OCR, defined as the ratio of the maximum preconsolidation stress (p_c) to the current consolidation stress (p_a). Even when the preconsolidation stress is not artificially applied, but, for example, applied by some geological action,

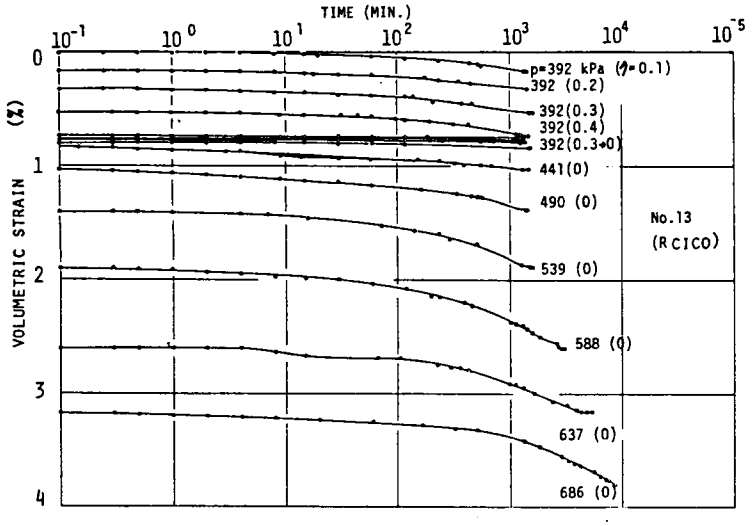

Fig.3.9: Consolidation curves of Test No.13(RCICO).

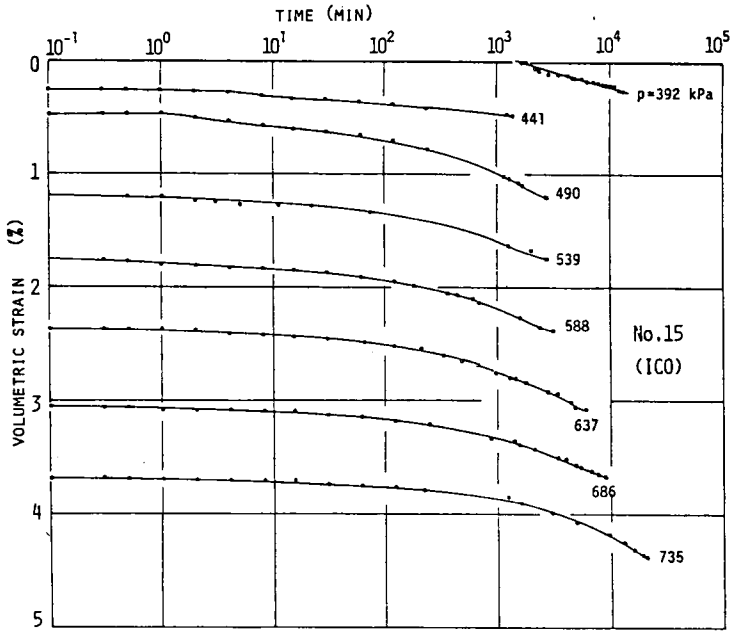

Fig.3.10: Consolidation curves of Test No.15(ICO).

it is determined as the stress at which void ratio or water content-log p curve coincides to the virgin consolidation line by performing isotropic or one dimensional consolidation tests*.

The results of the preceding section shows that the specimens having been subjected to the cycle of loading-unloading of shear stress in triaxial compression behaves like overconsolidated ones in the course of the isotropic compression after the cycle. (Fig.3.8).

Thus we will be able to define OCR as p_o/p_a, where p_o is the value of p at which the v-log p curve coincides with the virgin consolidation one and p_a is the value of p at which the cycle of shear stress was being applied. p_o could be read as 490-540 kPa for Test No.13 and 690 kPa for Test No.14, respecively, as was mentioned already.

In this section we examine, in the first, whether the Cam Clay theory(Wroth & Schofield,1968; Roscoe & Burland,1968) explain the observed behaviour in the course of the isotropic compression of specimens having been subjected to the shear stress history. Secondly, if there is any difference in shearing

---

* Here, in order to avoid confusion, the notaion of p_c is used as the real maximum preconsolidation stress, that is, maximum preconsolidation stress artificially applied to the specimen; and p_o is used as the apparent preconsolidation stress, determined or estimated from the compression behaviour. If a common terminology is used, p_o might correspond to the consolidation yielding value p_y.

behaviours between such apparent overconsolidated specimens, induced by shear stress, and the really overconsolidated specimens will be examined.

3.4.1 Cam Clay Prediction

A method to predict the apparent preconsolidation stress p_o using the Cam Clay theory is as follows:

A yield locus as the projection of the S.B.S. onto (p,q) plane is expressed by

$$\eta + M.\ln(p/p_o) = 0, \qquad \text{.....(3.3)}$$

where M is the value of η at the critical state, p_o is the value of p of the point of intersection of the current yield locus to p axis. When a specimen the stress state of which is isotropic and on the current yield locus of eq.(3.3) is sheared to $\eta=\eta_R$, the yield locus expands and passes through the new state of stress ($\eta=\eta_R$,$p=p_a$). The condition that the susequent yield locus passes the new stress state gives the equation for p_o to satisfy

$$p_o = p_a.\exp(\eta_R/M). \qquad \text{.....(3.4)}$$

When the shear stress is subsequently removed and the isotropic stress state is again reached, the expanded yield locus is not contracted. Thus the value of p_o corresponing to the isotropic stress state after the cycle of shear stress can be predicted by eq.(3.4)

The values of p_o for the case of Test No.13(η_R=0.4, p_a =392 kPa) and No.14(η_R=0.8, p_a=392 kPa) are calculated to be 522 and 694 kPa, respectively. It should be noted that those values well explain the experimental results shown in Fig.3.8.

Therefore, temporarily assuming that the yield surface of the Cam Clay Model could well predict the p_o value for the specimens used in this study, it was applied to a series of tests of RCE. The values of OCR($=p_o/p_a$) of tests RCE are listed in Table 3.3 as well as the values of real OCR(p_c/p_a) of Tests No.6 and No.7(ME) for the discussion in the following.

3.4.2 Prediction of Shearing Behaviour by Two Kinds of OCR

Here, it will be examined if the use of the parameter of OCR, determined above from the characteristics of isotropic compression, is efficient to describe shearing behaviour in triaxial extension after the cycle of loading-unloadin of shear stress in triaxial compression: in other words, if shearing behaviours of specimens with the shear stress history are compared to those of the really overconsolidated specimens employing OCR as a mesure of the degree of overconsolidation.

(1) Stress Strain Behaviour

Fig.3.11(a) and (b) show the relations between volumetric strain v and stress ratio η in the extension side for the tests listed in Table 3.3. In Fig.3.11(a),the volumetric strain is referred to the isotropic stress state after the cycle of loading-unloading of shear stress. It can be seen that, firstly, volumetric strains for all the tests of RCE are positive and their relations to stress ratio are in order of the size of the stress history or the size of OCR (p_o/p_a). This dependence on OCR is qualitatively analogous to the OCR dependence of dilatancy behaviour of a really overconsolidated soil (Chapter 2),i.e., the larger OCR(p_c/p_a) is, the less the

Table 3.3: OCR defined by the Cam Clay Model for RCE and by preconsolidation for MC and ME.

Test Type	Test No.	p	OCR	
			p_o/p_a	p_c/p_a
RCE	9	392	1.3	-
	10		1.8	-
	11,12		2.2	-
MC	1	392	-	1
ME	5	392	-	1
	6	196	-	2
	7	392	-	2

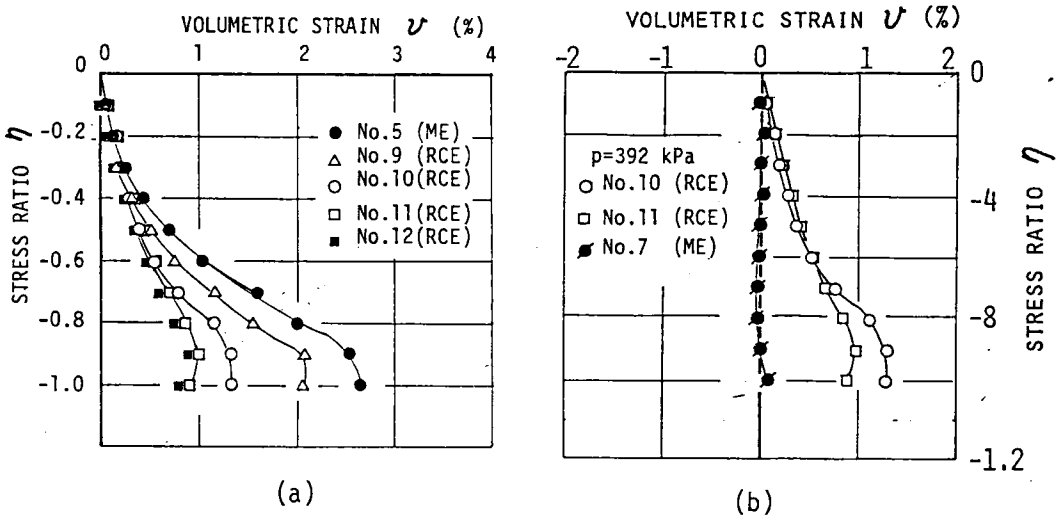

Fig.3.11: Comparison of volume change behaviour:
(a) Effect of shear induced overconsolidation; and
(b) Comparison of shear induced and real preconsolidation.

tendency for the volume to contract is.

Secondly, as to the relation for Test No.6 or No.7 (ME, p_c/p_a=2) (Fig.3.11(b)), it is apart from the relations for tests of RCE, although OCR for No.6 and No.7 is between OCR of Test No.10 (p_o/p_a=1.8) and that of No.11(2.2). This indicates that dilatancy behaviour cannot be successfully explained by the parameter of OCR, determined from the characteristics observed in the isotropic compression, but it is strongly affected by the shear stress history.

Fig.3.12 shows the plastic shear strain-stress ratio relations for the tests listed in Table 3.3. In Fig.3.12(a), a similar observation to that seen in Fig.3.11 can be made except that the OCR dependency of the shear strain behaviour is less clear than that of dilatancy behaviour shown in Fig.3.11(a). In particular, in the case when the shear stress history given in compression is large to a certain extent, it seems that the difference in shear strain behaviour in extension side vanishes. Also, in Fig.3.12(b), it can be seen that the relation for Test No.6 or No.7 (ME, p_c/p_a=2.0) is apart from the relations RCE tests.

As is clear from the discussion above, it is concluded that the stress-strain behaviour in extension side for specimens with the shear stress history in compression side cannot be explained only by the parameter of OCR; the stress-strain behaviour is strongly affected by the shear stress history.

(2) Stress Ratio-Strain Increment Ratio Relation

A similar discussion to that in the preceding paragraph

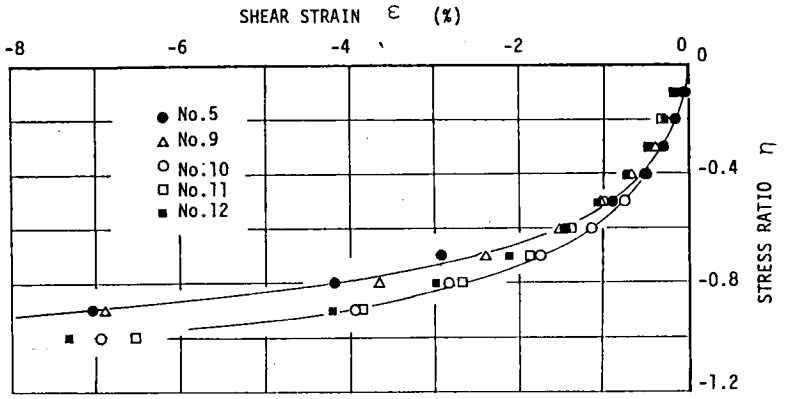

(a)

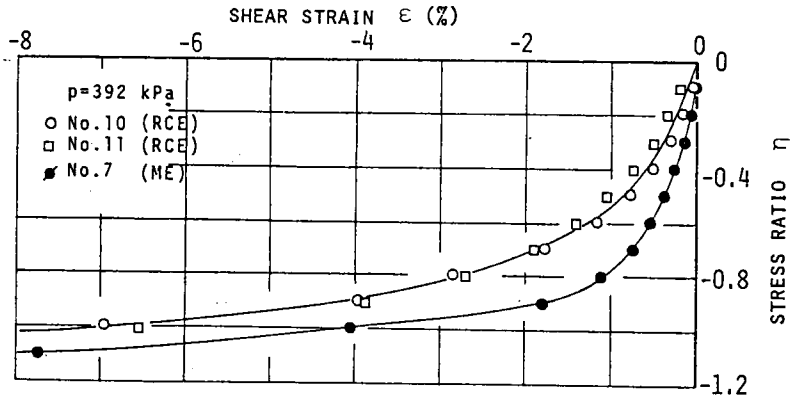

(b)

Fig.3.12: Comparison of shearing behaviour:
(a) Effect of shear induced overconsolidation; and
(b) Comparison of shear induced overconsolidation and real preconsolidation.

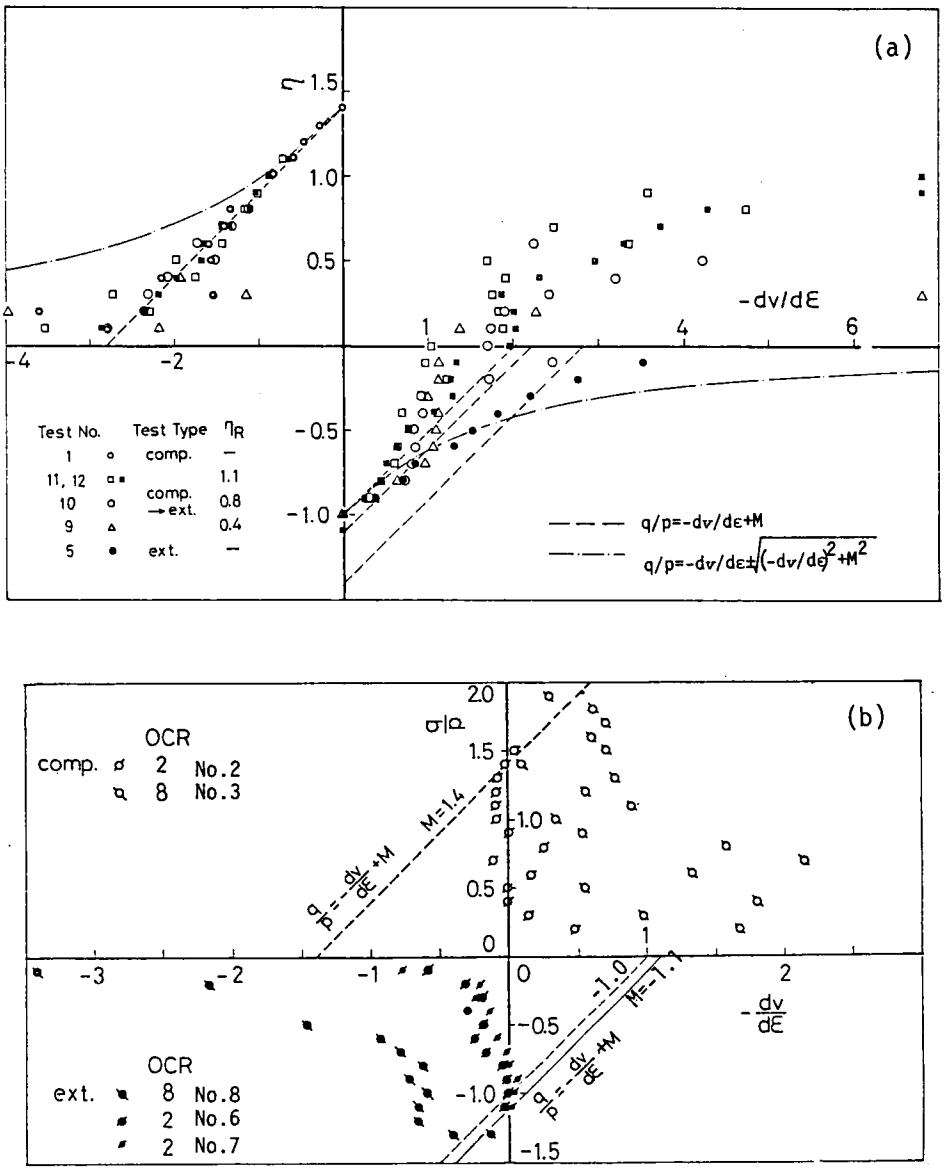

Fig.3.13: Comparison of stress ratio-strain increment ratio relations:
(a) Effects of unloading; and
(b) Effects of overconsolidation.

is made for the relations between stress ratio η and strain increment ratio $-dv/d\varepsilon$, which are shown in Fig.3.13.

In the first, limiting the consideration to the relations for RCE and No.5(ME,OCR=1), it appears from Fig.3.13(a) that their plots exist in the range of positive strain increment ratio ($-dv/d\varepsilon>0$). As the shearing in extension procedes to a certain extent, the relations become to be in order of the size of the history of shear stress in compression. These observations are considered to correspond to the results already shown in Fig.3.5 or 3.11, where the change in volumetric strain was negative except the point near the failure. The higher the degree of the history is, the less the volume contractivity is.

Secondly, comparing the relations of Tests No.6 and No.7 with those for RCE(Fig.3.13(b)), the latters are apart from the formers, as has been pointed out with respect to the stress-strain relations,i.e., plots for Test No.6 and No.7 are always in the range of negative strain increment ratio ($-dv/d\varepsilon<0$) but those for RCE are not. This discrepancy results in the conclusion, which is quite similar to that derived for the stress-strain relations, that stress ratio-strain increnent ratio relations of specimens with the shear stress history cannot be explained by the relations of specimens subjected to the monotonous loading in extension even if the values of OCR are the same for these two.

3.5 CONCLUSIONS

Effects of shear stress history on the subsequent shearing deformation and isotropic compression behaviours were investigated. Shear stress history was given as the cycle of loading-unloading of shear stress in the triaxial compression. Subsequent shearing was performed in the triaxial extension.

Some main results are summarized as follows:

1) Dilatancy behaviour in triaxial extension after the stress history is affected by the degree of shear stress history, while corresponding shear deformation behaviour is not so fairly affected by it, partcularly when the degree of the history shear stress is relatively low .

2) When stress ratio given as the history is low, the state of the specimen reaches the state boundary surface (S.B.S.) in extension. Once the state reaches the S.B.S., both shear deformation and dilatancy behaviour become similar to those of specimens without history.

3) When the specimens having been subjected to the stress history is isotropically compressed, they behaves like overconsolidated specimens. The stress at which the v-log p relation coincides with the virgin consolidation curve can be well predicted by the Cam Clay theory.

4) The applicability of the parameter OCR defined on the basis of the isotropic comression behaviour for explaining the shering behaviour was examined. OCR for specimens with the shear stress history was determined by the Cam Clay theory. As the results, shearing behaviour and dilatancy characteristics could not predicted by the parameter OCR.

REFERENCES FOR CHAPTER 3

Karube,D. and Kurihara,N.(1966): "On the dilatancy and shearing strength remoulded clays", Proc. JSCE, No.135,pp.16-24. (in Japanese)

Roscoe,K.H. and Burland,J.B.(1968): "On the generalized stress-strain behaviour of 'wet' clay", Eng. Plasticity, Cambridge Univ. Press, pp.535-609.

Shimizu,M.(1979): "Dilatancy characteristics and stress-strain behaviour of a clay in N.C. and O.C. state", Annals, Disaster Prevention Research of a clay in N.C. and O.C. state", Annals, Disaster Prevention Reseach Inst., Kyoto Univ.,Vol.22, No.B-2. pp.85-105. (in Japanese)

Shimizu,M.(1980): "Effects of shear stress history on stress-strain behaviour in triaxial extension and isotropic compression of clay", Annals, Disaster prevention Research Inst., Kyoto Univ.,Vol.23, No.B-2, pp.73-86. (in Japanese)

Schofield,A.N. and Wroth,C.P.(1968): Critical State Soil Mechnics, McGraw Hill.

CHAPTER 4 ELASTIC BEHAVIOUR OF A SATURATED CLAY DURING UNLOADING OF SHEAR STRESS

4.1 INTRODUCTION

The necessity to predict the mechanical response of soils when subjected to such vibrating forces as in earthquakes has increased. At the same time it is necessary to clarify the stress-strain behaviour when the direction of the stress is reversed.

Generally , if it is assumed that the whole component of strain which recovers when the stress having been applied is removed is elastic, experimental results would not be well explained. We have to consider that the recoverable component of strain should include some plastic component. Such behaviour is regarded to be attributed to the property of materials which shows the so-called Bauschinger's effects (Hill,1950).

There have been many attempts to describe stress-strain behaviours of soils based on the theory of elasto-plasticty. However, such a Bauschinger's effect will be taken into account if kinematic hardening model is adopted for the soil concerned. In facts, a few studies in which kinematic hardening model is taken into account have been presented (Prévost,1977; Mroz et al., 1978).

In this chapter, the study performed in Chapter 3 will be reexamined and extended by adding further experiments. In the preceding chapter, it was pointed out that we could observe elastic behaviour when shear stress was gradually decreased, i.e., unloading was done, under the triaxial stress condition.

In this chapter, the range over which elastic behaviour might be observed will be examined. And effects of shear stress history on shear modulus will be also discussed. All the experiments were performed in the axisymmetric stress condition and the sample is assumed to be fully saturated.

4.2 EXPERIMENTAL PROCEDURE

4.2.1 Sample

The sample used is a silty clay called Fujinomori Clay. The powered sample was mixed with water at water content of about two times its liquid limit and fully remoulded; after the remoulding, it was preconsolidated up to vertical pressure of 49 kPa and rebounded to the atmospheric pressure in a large one dimensional consolidation cell. Thus prepared sample was trimmed to be triaxial specimens of 8 cm in height and 3.56 cm in diameter. The detail of the method to prepare the specimens was already described in Chapter 2.

Water content in position in a triaxial cell was about 40 %. Liquid limit is 54.0 %; plastic limit 27.8 %; plasticity index 26.2, clay content in weight (<2μm) 15 %; and specific gravity of soil grain 2.64.

4.2.2 Apparatus

Drained and undrained conventional triaxial tests were performed. The apparatus for the drained tests are the same to those described in Chapter 3. Those for undrained tests are also NGI type triaxial apparatus, but they have been improved so that it can be allowed that the channel for drainage and back pressure is completely independent of the channel for measurement of pore-

water pressure. Pore-water pressure was measured at the center of the lower end of specimen by means of a pressure transducer.

4.2.3 Triaxial Tests

(1) Drained Tests

Effective stress path is schematically represented in Fig.4.1 . Prior to the shear tests all the specimens were normally consolidated by hydrostatic stress up to p_c (p_c: maximum preconsolidation stress) and then rebounded to p_c/OCR (OCR: overconsolidation ratio). p_c of 588 or 392 kPa and OCR of 1, 2 or 8 were chosen. Following the preconsolidation, shear stress was applied in triaxial compression so that the increment of stress ratio η(=q/p, where q is deviator stress; p is effective mean normal stress) was 0.1. When the stress ratio reached a prescribed value (denoted by η_R), it was decreased by 0.1 until the failure in triaxial extension state appeared. The procedure above is the same to that performed in the preceding chapter except that it was only normally consolidated specimens that shear stress was unloaded.

(2) Undrained Tests

All the specimens were isotropically consolidated, firstly under p=98 kPa without any back pressure, and, secondly, consolidated up to a prescribed pressure with the back pressure of 196 kPa. The maximum preconsolidation stress was 392, 196 or 98 kPa. Porewater pressure coefficient B (Skempton,1956) was measured after the first stage preconsolidation. The B value of nearly 1 was attained for all the specimens.

Following the preconsolidation, shear stress was applied, by strain control, in triaxial compression. When the effective stress ratio reached a prescribed value (denoted by η_R as well as for drained tests), the direction of axial deformation was reversed. The specimens except one were made to fail in triaxial extension. For the one, the repetitive shear stress was applied in triaxial compression only.

Very small rate of axial deformation, as for undrained tests, of 3.24×10^{-4} %/min was chosen, because it was considered that, if the rate had been relatively large, the detail of the stress strain relation might have been missed since the large change in deviator stress corresponding to a small change in the axial deformation was expected after the reverse of shear direction according to previous experiences.

In the case when the connection between the loading ram and a cap must be rigid as in strain-controlled undrained tests, specimens have the possibility to be disturbed more or less at the moment of the connection. To avoid this disturbance, the following process was employed: after the isotropic consolidation prior to the shear test was completed, the loading ram was detouched from the cap and connected to the load cell; the triaxial cell was raised with the prescribed or controlled speed and, when some deviator stress was developed after the loading ram was touched to the cap, the loading ram was connected to the cap.

4.3 EXPERIMENTAL RESULTS

In the preceding chapter (Chapter 2), it was observed

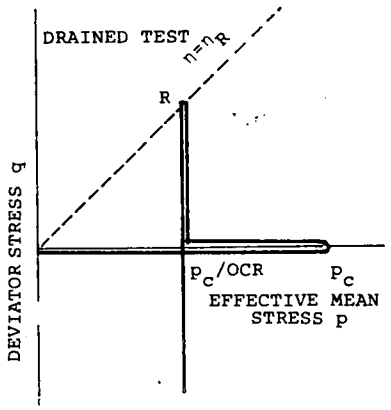

Fig.4.1: Schematic diagram of effective stress path for drained tests.

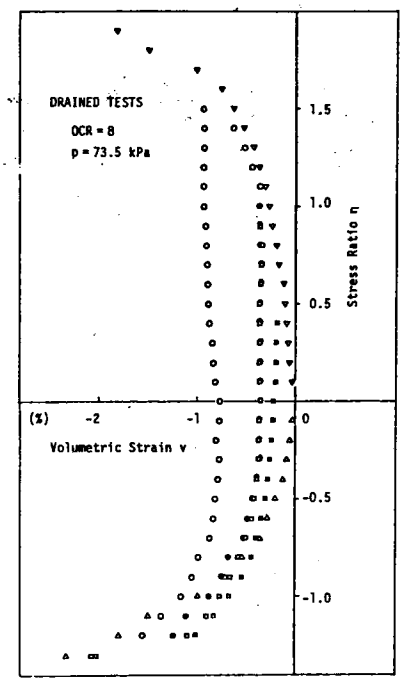

Fig.4.2: Relations between volumetric strain v and stress ratio form drained tests

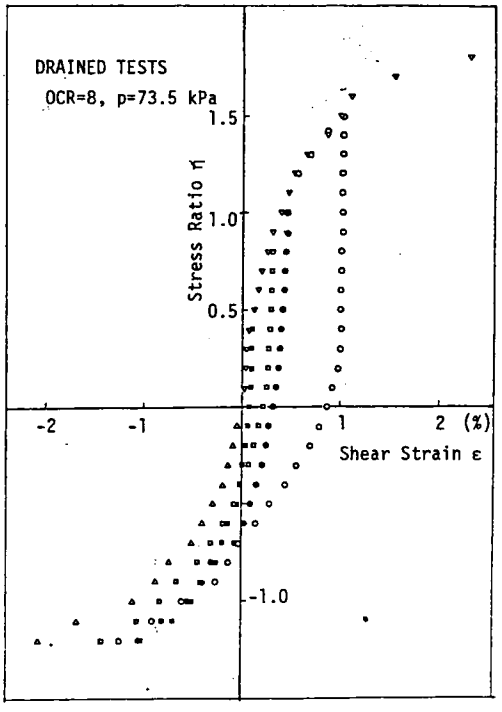

Fig.4.3: Relations between shear strain and stress ratio from drained tests.

that, when normally consolidated specimens were subjected to the unloading of shear stress after its loading in triaxial compression state of stress, there existed a linear portions in η-v relation and in η-ε relation, respectively, and that in the linear portion the change in v did not nearly occur as well as the change in ε.

Here the results of drained tests for OCR other than 1 and undrained tests will be investigated with respect to the existence of such linear portions in η-v and q-ε relations.

4.3.1 Drained Tests

(1) Dilatancy Behaviour

Fig.4.2 shows the relations between η and v, resulted from drained tests for OCR=8. v is the volumetric strain due to dilatancy since effective mean normal stress p was held constant during these tests. It can be seen that negative volumetric strain or positive dilatancy develops as stress ratio is increased, but after the unloading, the change in v is negligibly small and the η-v relation is linear until η reaches a certain value.

(2) Shear Strain Behaviour

In Fig.4.3 the relations between η and ε resulted from the same tests to those shown in Fig.4.2 are presented, where a similar discussion to that in the above is possible: the relations are non-linear in the loading part, but they are linear and the change in ε is negligibly small in a certain range of the unloading part; passing the linear portion, they begins to be curved.

Shear strain in this figure was calculated by subtracting instantaneous axial strain which accompanied each increment of shear stress from the measured total axial strain increment correponding to the stress increment. Thus obtained shear strain can be regarded as plastic strain, as mentioned in Chapter 3 and therefore it can be said that specimens behaves as an elastic material in the linear portion in Fig.4.3, in the sense that plastic shear strain does not occur there.

4.3.2 Undrained Tests

All the undrained tests were performed for normally consolidated state (OCR=1) with varying consolidation stress p_c. The case of p_c=196 kPa will be presented since the principal feature of results shown in the following is common to other cases (p_c=392 and 98 kPa).

(1) Effectaive Stress Paths

Fig.4.4 shows the effective stress paths, where the paths for loading of shear stress in triaxial compression are represented by the path of the case of η_R=1.1. In this figure, as shear stress increses to the unloading point, positive excess pore-water pressure develops due to negative dilatancy and effective mean normal stress p decreases. This agrees with well known undrained behaviours of normally consolidated clays.

Each effective stress path during the unloading stage can be divided into two portions: one is linear portion which appears just from the beginning of the unloading; another is a curved

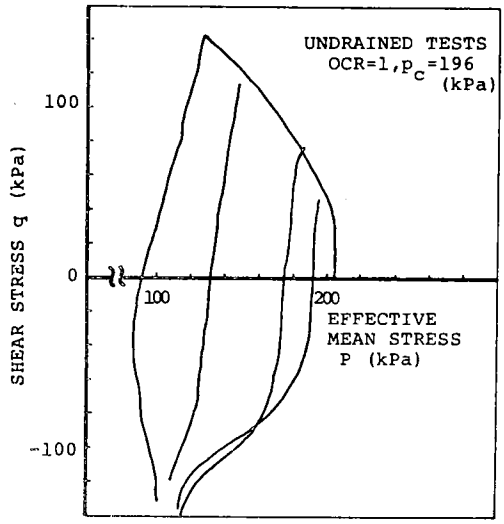

Fig.4.4: Effective stress paths obtained from undrained tests.

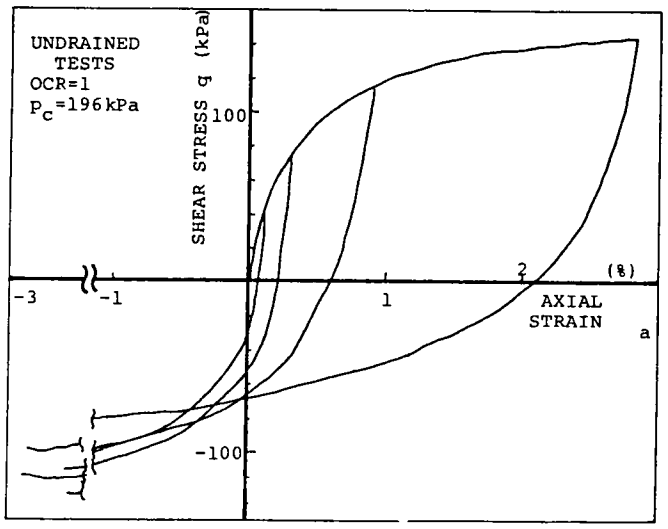

Fig.4.5: Relations between shear stress q and shear strain ε obtained from undrained tests.

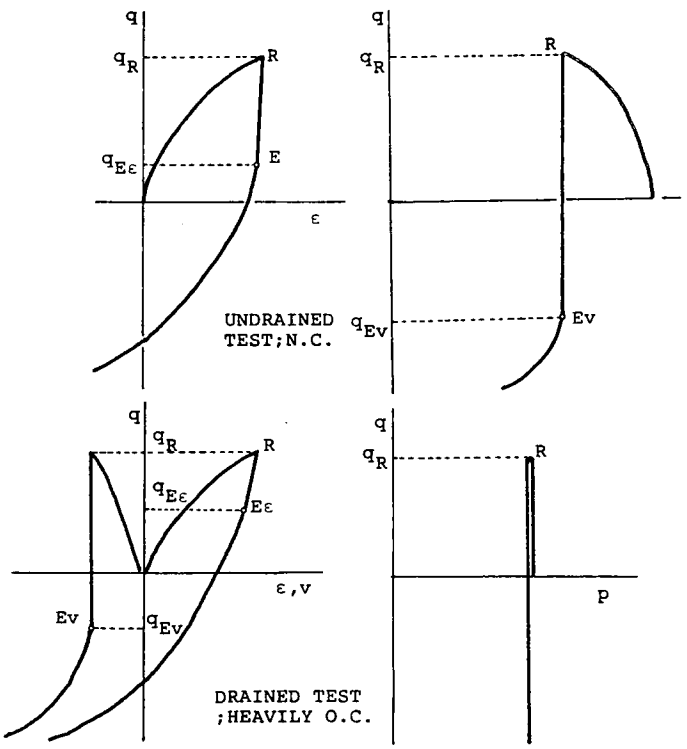

Fig.4.6: Schematic representation of characteristics observed in unloading stage.

portion which follows the linear portion and continues to the failure state.

In the cases when stress ratio at which the unloading begins, η_R, is relatively small (η_R=0.2 and 0.4), the change in p is negligibly small in the linear portion for each test, and according to further unloading two stress paths coincide. The portion where these two stress paths coincide is expected to coincide to the stress path of a test sheared monotonously in extension side, which was not performed for the case of p_c=196 kPa.

In the cases when η_R is relatively large (η_R=0.8, 1.1), p continues to decrease even in the linear portion during the unloading stage. After this portion, in the case of η_R=0.8, p further decreases to fail and, in another case of η_R=1.1, p increases to fail.

Furthermore, it can be seen that states at failure in terms of effective stress are independent of η_R.

It was shown above that the effective stress paths had different shapes which depend on η_R. But, because, in the linear portion which appears after the unloading, the change in p is much smaller than before and after this portion, it can be said that in this portion the dilatancy does not occur or, if it occurs, it is substantially negligible.

(2) Shear Stress- Shear Strain Relations

Fig.4.5 shows the relations between shear stress and shear starin, which correspond to the effective stress paths shown in Fig.4.4. The relations from the start of shearing to the

beginning of the unloading are represented by the relation for η_R=1.1.

Each of these relationships appears to be non-linear from the start of shearing in triaxial compression, and it becomes linear over a certain range once the loading direction is reversed. With further unloading, it becomes again non-linear, i.e., shear strain further develops and the failure is reached. It seems that the length and gradient of the linear portion is small when η_R is large and v.v.

4.3.3 Summary of the Results

Among the results mentioned above with respect to the behaviour observed when shear stress is gradually removed or the loading direction is reversed, it is common to all types of test condition, i.e., whether it is drained or undrained test and whether it is for normally consolidated or overconsolidated state, that:

(a) when shear stress is incrementally removed, q-ε relation is linear over a certain range, and

(b) when shear stress is incrementally removed, dilatancy does not occur over a certain range, i.e., in drained tests with constant p, volumetric strain v does not nearly occur; and in undrained tests the change in effective mean normal stress p is relatively small.

The characteristics (a) and (b) are schematically represented in Fig.4.5. As shown in this figure, the state where the characteristics (a) vanishes in the unloading part is denoted by E_ε, and that of (b) is denoted by E_v.

The characteristics (a) can be specified by the following equation:

$$d\varepsilon = \frac{1}{G'} dq \qquad \text{----------(4.1)}$$

provided that G′ is constant. On the other hand, the characteristics (b) may be specified by the following equation:

$$dv = \frac{1}{K'} dp \qquad \text{----------(4.2)}$$

, because, if dv=0 (undrained tests), then dp=0, and if dp=0 (drained tests with constant p), then dv=0. Here, it should be noted that it is not necessary for K′ to be constant. In addition, if both characteristics (a) and (b) are observed at the same time, characteristics (a) is constrained by the condition resulting from (b) that p is constant therefore, G′ is not necessarily constant. A value of G′ in eq.(1) is one corresponding to the current value of p but G′ can vary with p.

If mechanical behaviour of a material can be specified by eqs.(4.1) and(4.2), the material will be identical to the homogeneous elastic material. Generally, the constitutive equations of the elastic material are represented by:

$$d\varepsilon_{\alpha\alpha} = \frac{1}{3K} d\sigma_{\beta\beta}, \qquad \text{----------(4.3)}$$

$$de_{ij} = \frac{1}{2G} dt_{ij} \qquad \text{----------(4.4)}$$

where ε_{ij} and σ_{ij}: strain tensor and effective stress tensor, respectively,

e_{ij} and t_{ij}: deviatoric components of ε_{ij} and σ_{ij}, respectively,

K: bulk modulus, and

G: shear modulus.

In the case of the axisymmetric condition of stress, eqs.(4.3) and (4.4) are changed to:

$$dv = \frac{1}{K}\, dp \qquad \text{----------(4.3')}$$

$$d\varepsilon = \frac{1}{3G}\, dq \qquad \text{----------(4.4')}$$

The discussion above that the behaviour of a clay when shear stress is gradually removed, i.e., the loading direction is reversed, is identical to that of an elastic material is valid only if the characteristics (a) and (b) are observed at the same time, at least, in a certain range of the states in termes of stress and strain. The simultaneity of these two characteristics is examined in Figs.4.7(a)and(b) which show the variations of q_R-q_{E_ε} or q_R-q_{E_v} with η_R for drained tests and for undrained tests, respectively. In Fig.4.7(a) it can be seen that, for each value of OCR, (q_R-q_{E_v}) is always larger than (q_R-q_{E_ε}). Fig.4.7(b) also shows that (q_R-q_{E_v}) is larger than (q_R-q_{E_ε}) if the same consolidation stress is considered.consequently, from these figures, it can be said that dv=0 in drained tests with constant p or dp=0 in undrained tests, i.e., dilatancy does not occur so long as the linearity of the relation between q and ε is observed. In other words, characteristics (b) is observed so long as characteristics (a) is observed.

Thus, it is concluded that, in the linear portion of q-ε relation observed after the reverse of loading direction, the soil behaves as an elastic material of which the constitutive equations are given by eqs.(4.3') and (4.4') or, more generally, eqs.(4.3) and (4.4).

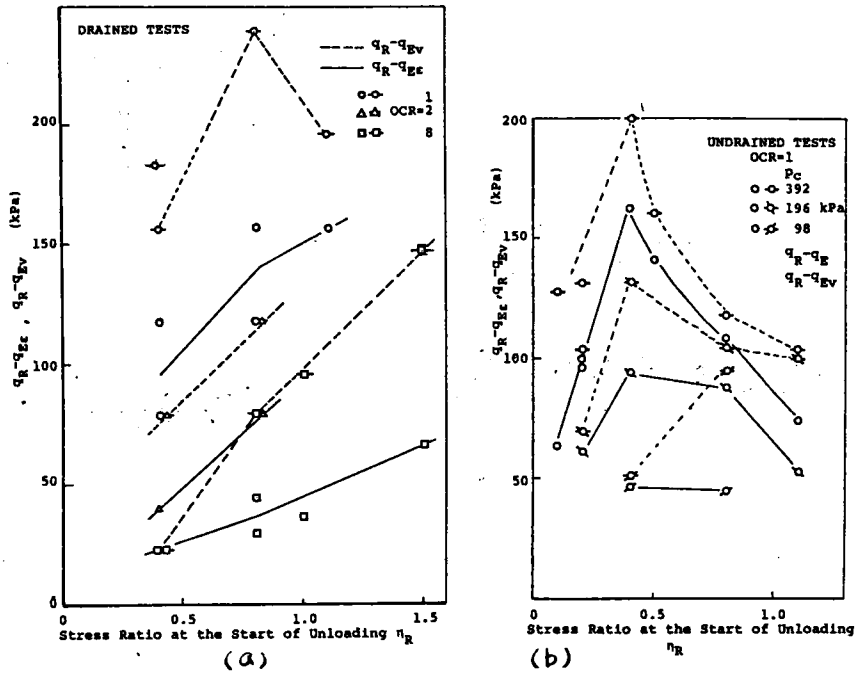

Fig.4.7: Comparison between two kinds of elastic regions: elastic regions defined based on the characteristic either of no dilatancy or of linearity in q-ε : (a) Results of drained tests; and (b) Results of undrained tests.

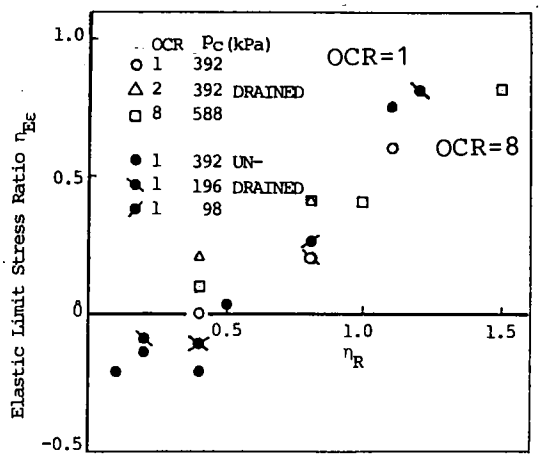

Fig.4.8: Elastic limit stress ratio vs. stress ratio at the start of unloading η_R

4.4 EFFECTS OF SHEAR STRESS HISTORY ON THE SIZE OF ELASTIC RANGE

In this section, the variation of the size of the elastic range with the degree of shear history will be examined. To do so, it is important to choose parameters for evaluating the degree of the shear history and the size of the elastic range.

4.4.1 Elastic Range Based on the linearity of q-ε Relation

In Fig.4.7 already presented, two parameters of η_R and (q_R-q_E) were chosen. These parameters, however, are not very useful for the object of this section because the relations between these two depend on both the type of test and the condition of consolidation prior to the shearing, as discussed above. In Fig.4.8, stress ratio at which the linearity of q-ε relation vanishes, η_E, is plotted against stress ratio η_R. Limiting the discussion to the case of OCR=1, the relation between these parameters seems to be represented by one curve, as shown in the figure, in spite of the difference in the drainage condition (drained or undrained). For OCR other than 1, there seems to be other relations. As the reason why the η_R-η_E relations depend on OCR, we can adduce that, even if specimens with various OCR are subjected to the same value of shear stress as the stress history, change in the internal structure corresponding to the stress ratio varies with OCR.

It is reasonable that the portion of a stress path corresponding to the linear part of q-ε relation observed after

the reverse of the loading direction will be called 'elastic range'. Fig.4.7 shows that the size of the elastic range varies with the degrees of the shear history even if both the consolidation history prior to the shearing and the types of test are common. The relation between the elastic range and the degree of the shear history, if which is evaluated by the stress ratio η_R, differs according to both the consolidation history and the types of test.

The soil structure at the start of unloading of shear stress differs according to the degrees of the shear history even when the consolidation history and the types of test are common. On the other hand, the way in which the internal structure changes due to the shearing differs according to the consolidation conditions and to the types of test.

By considering that the effects of shear stress history can be attributed to the change in internal structure of soils, shear strain which has occurred till the beginning of the unloading is taken as a parameter representing the quantity of the history. On the other hand, the quantity defined in the following equation is taken as a parameter representing the size of the elastic range.

$$\Theta = \tan 2\theta = (\eta_R - \eta_{E\varepsilon})/(1+\eta_R \cdot \eta_{E\varepsilon}) \qquad (4.5)$$

The angle θ is half of the angle between the lines $\eta=\eta_R$ and $\eta=\eta_{E\varepsilon}$, as shown in Fig.4.9.

Fig.4.10 shows the relations between Θ and ε_R. It appears from this figure that the parameter Θ would be related uniquely to the another parameter ε_R. This implies that the degree

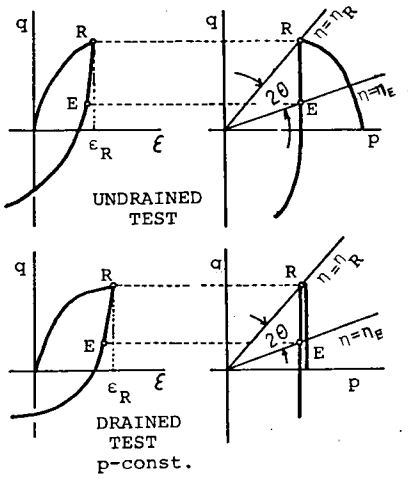

Fig.4.9: Parameter Θ vs. shearing history ε_R.

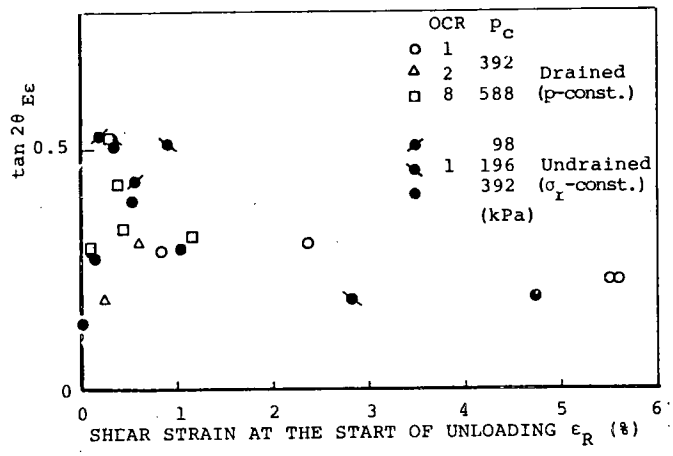

Fig.4.10: Definition of a parameter Θ (=tan2θ).

of change in the internal structure during shear deformation might be evaluated to some extent by the shear strain parameter ε_R. However, if the initial internal structure is different, the internal structure at the unloading will not be the same for all the specimens even when they have been subjected to the same shear strain ε_R. Accordingly, such relations as shown in Fig.4.10 might not be substantial.

4.4.2 'Elastic Range' based on the Dilatancy Characteristics

In Fig.4.11, the threshold value of stress ratio η_{Ev} is plotted against stress ratio at the beginning of unloading η_R. It is seen that the characteristics of the relations are completely different between the case of OCR=1 or2 and the case of OCR=8, while the relations , shown in Fig.4.8, between η_R and $\eta_{E\varepsilon}$ was little dependent on OCR.

Firstly, the case of OCR=1 will be considered. The relations of η_R and η_{Ev} seems to be independent of both the drainage condition and the consolidation stress. This can be explained by the well known facts that dilatancy would be expressed uniquely by stress ratio in spite of the difference in the consolidation stress (Shibata,1963; Karube & Kurihara,1966) and that shear strain is also expressed uniquely by stress ratio. When normally consolidated clay specimens are subjected to a certain same value of stress ratio in spite of the drainage condition (drained or undrained), shear strain or dilatancy is common to all the specimens and the degree of the change in internal structure due to the shearing would be also the same for all the specimens.

Secondly, in the case of OCR=8, η_{Ev} varies nearly linearly with increasing degree of shear stress history η_R. Elastic range where no dilatancy occurs after the unloading is larger for heavily overconsolidated specimens comparing with normally or lightly overconsolidated specimens even with high value of history stress ratio η_R. It is supposed that the concept of isotropic hadening is more applicable for hevily overconsolidated specimens than for normally consolidated or lightly overconsolidated specimens. In other words, yield locus extends isotropically by isotropic preconsolidation by té manner for yield locus to extend is not isotropic with resoect to the hardening accompanied with shearing in the nomally consolidated state.

4.4.3 Dilatancy Behaviour in (p,q,w) Space during Unloading

In Fig.4.11 we saw already that there would be a unique relation between η_{Ev} and η_R in spite of the consolidation stress or drainage conditions for OCR=1. We consider this fact in three dimensinal space (p,q,w), where w is water content.

Provided that the state of the soil may be defined in the (p,q,w) space, the concept of the State Boundary Surface (S.B.S.) has been introduced (Wroth & Schofield,1968; Roscoe & Burland, 1968). S.B.S. is the boundary surface outside of which the state of the soil can not exist. Following three assumptions (i to iii) enables that three dimensional surface S.B.S. can be expressed in terms of two parameters, p/p_e and q/p_e, i.e., on the (p/p_e, q/p_e) plane, where p_e is the equivalent consolidation stress of Hvorslev.

i: State path along which the state of isotropically normally

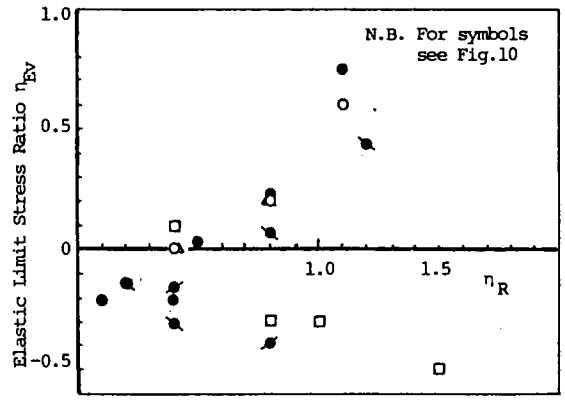

Fig.4.11: Elastic limit stress ratio η_{Ev} vs. η_R.

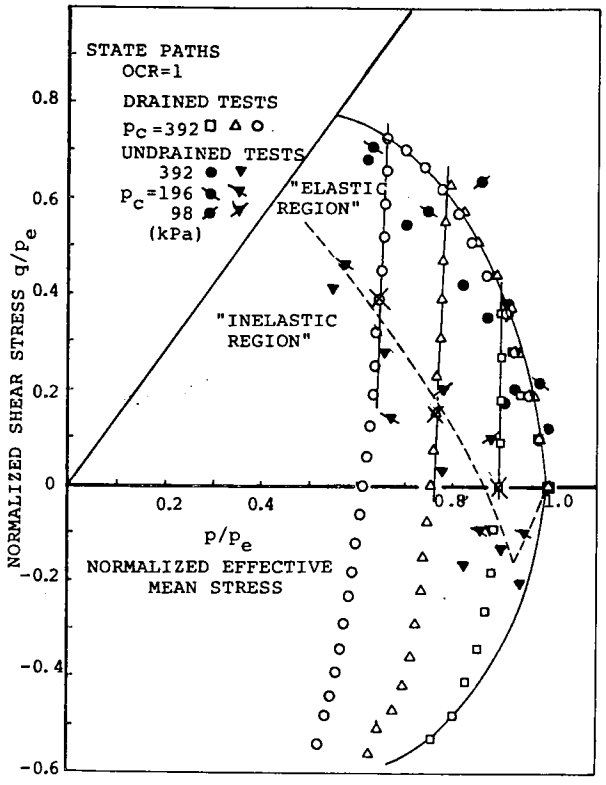

Fig.4.12: State paths on normalized stress plane (p/p_e,q/p_e) of both drained and undrained tests for OCR=1.

consolidated clay moves when subjected to undarined shear constitutes the S.B.S. in (p, q, w) space with varying consolidation pressure or water content.

ii: Effective stress paths projected on (p,q) plane of undrained state paths are similar each other with respect to the origin of the (p,q) coordinate plane.

iii: Virgin consolidation line is determined uniquely for a given soil, and its w-log p relation is linear.

Further, if it is assumed that state paths for p constant drained tests on normally consolidated clays are on the S.B.S., state paths for normally consolidated specimens can be expressed as a curve on the $(p/p_e, q/p_e)$ plane.

Thus, in Fig.4.12, the results of p-constant tests and consolidated undrained tests are shown on the $(p/p_e, q/p_e)$ plane. In order to avoid the complication, state paths for undrained tests are represented by two representative point: the point at the unloading (o,●,◐) and that of threshold point of dilatancy during unloading (▽,▼,◑). State paths for initial loading do not completely coincide for both drained and undrained tests, however, they may be regarded to be on a curve in spite of drainage condition. This implies that four assumptions mentioned above would be reasonable.

As to behaviours after unloading, state paths for p-constant drained tests begin to be off parallel to the axis of q/p_e at certain points (denoted by the symbole x). It appears that these points agrees well with elastic limit points determined from results of undrained tests.

It is concluded from discussions above that, when some shear stress history is given on the S.B.S., unique domain in (p,q,w) space where little dilatancy occurs is made and that the boundary of this domain is unique independently of consolidation pressure or drainage condition applied during the process of stress history.

4.5 EFFECTS OF SHEAR STRESS HISTORY ON ELASTIC SHEAR MODULUS G

4.5.1 Single Reverse of Shearing Direction

It was observed that no or little dilatancy occurs while q-ε relation is linear during unloading process. This implies that elastic shear modulus G can be determined as the slope of the linear portion. From eq.(4.4'),

$$G = \frac{\Delta q}{3\Delta \varepsilon} \qquad \text{.....(4.5)}$$

In this section, effects of shear stress history on G will be examined.

In Fig. 4.13, non-dimensinalized shear modulus $\bar{G}$ (=G/p) is plotted against history stress ratio η_R for p-constant drained tests. For a given OCR, $\bar{G}$ seems to be constant and independent of η_R. Consequently, it may be said that G is independent of shear stress history at least for p-constant drained tests.

As for the undrained tests, shear modulus G is plotted against η_R in Fig.4.14. It can be seen from this figure that G decreases with increasing η_R. Taking into account the fact, obtained from p-constant tests, that G would be constant; G does not change when subjected to shear stress history so far

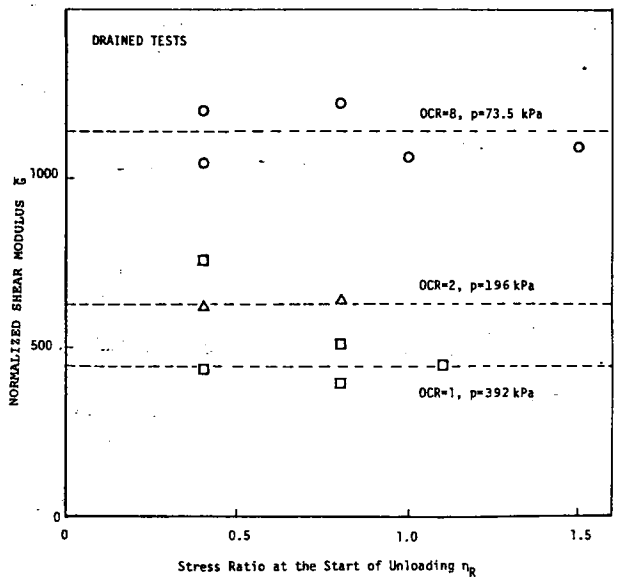

Fig.4.13: Normalized shear modulus $\bar{G}$ vs. stress ratio history η_R (p-constant drained tests).

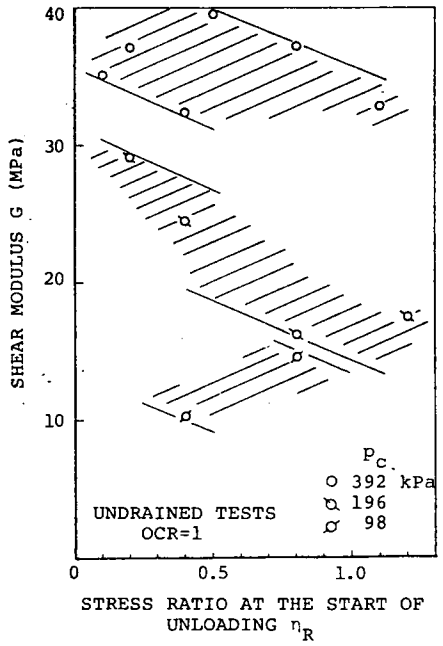

Fig.4.14: Shear modulus G vs. stress ratio history η_R. (undrained tests)

as p does not change, however, when p decreases as in the case of undrained tests on normally consolidated clays, G also decreases.

Consider further the dependency of G on p. Fig.4.15 shows the relations of G and p which have been obtained from results shown in Figs.4.13 and 4.14 and those of othere tests. In this figure, for undrained tests in which p could not be constant even just after the unloading, the value of p at the beginning of unloading is taken as the value of p during unloading. Plots denoted by the same symboles corresponds to tests in which consolidation history and drainage condition are the same and only degree of shear stress history differs from each other.

Followings are derived from Fig.4.15:

Firstly, we consider the case of undrained tests for OCR=1.

- For a given condition of consolidation and drainage, as p decreases with increasing shearhistory, G also decreases;
- Limiting to the tests in which consolidation history is not diffrerent but initial water content at the preparation of the sample is different, G is larger when water content is relatively low than when water content is high;
- For tests in which specimens were prepared in the same consolidation batch, relations between G and p may be expressed by a unique line in spite of the difference in consolidation stress or water content. This implies that the variation of G caused by the difference in consolidation stress is equivalent to the variation of G with decreasing p due to undrained shear stress history or due to the difference in consolidation stress.

Secondly, we consider the results of drained tests:

- the decrease in p accompanied with the overconsolidation or rebound is followed by the decrease in G, and the way in which G decreases with decreasing p is similar to that in undrained tests.

Summarizing the discussions above, we can conclude that G decreases not due to shear stress history but due to decrease in p.

4.5.2 Repeated Loading Test

Discussions in the preceding have been based on the results of various tests in which the reverse of shearing direction was single. For one specimen, the repetition of loading and unloading was performed and the relation of G and p was examined.

The sample used in this test is the same to that of ● and ◥ in Fig.4.15 and has the same consolidation history to that of ●.

Fig.4.16(a) shows stress- strain relation, and Fig.4.16(b) shows the corresponding effective stress path. In these figures, to avoid the complication, loading part of each cycle is not shown. Further, in Fig.4.17, shear modulus G determined as the slope of unloading part of each cycle shown in Fig.4.16(a) is plotted against p at the beginning of unloading corresponding to the cycle.

From Fig.4.17, it can be seen that:

- G decreases with the repetition of loading-unloading;
- G-p relation of Fig.4.17 is almost the same to that of the same sample shown in Fig.4.15. This leads to the conclusion that G decreases if p decreases whether shear stress history

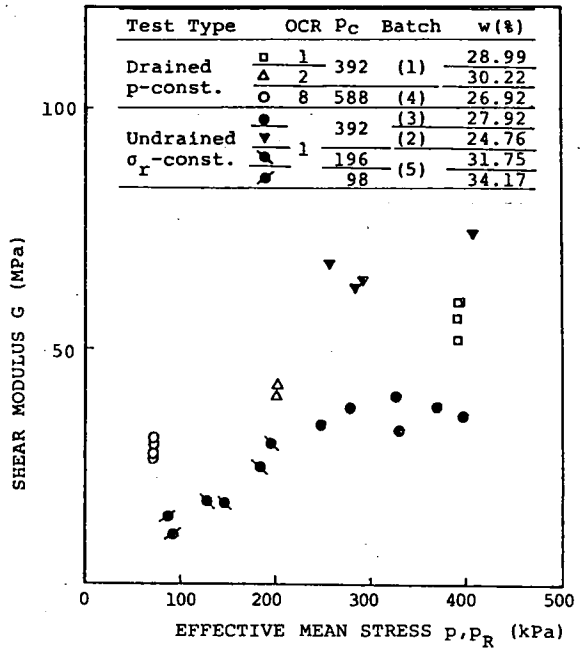

Fig.4.15: Shear modulus G vs. effective mean normal stress p.

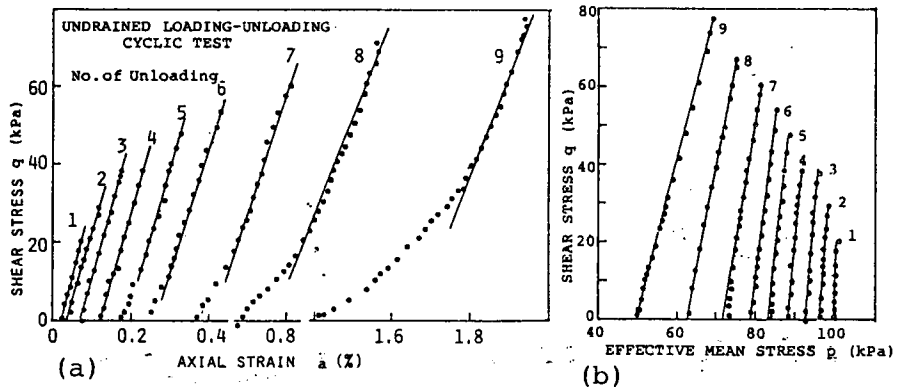

Fig.4.16: Results of the one way repeated loading test
(a) Stress-strain relation during unloading; and
(b) Effective stress paths during unloading.

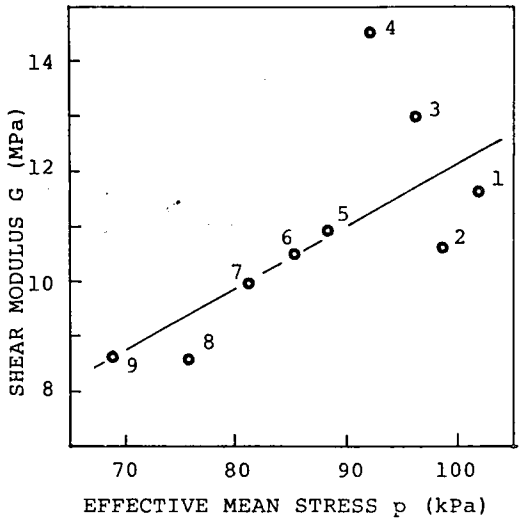

Fig.4.17: Variation of G with effective mean normal stress p in the one way repeated loading test.

is given contineously or discretely with unloading process; namely, that the relation of G and p is independent of the way in which p decreases.

4.6 CONCLUSIONS

It was observed that, when shear stress was applied and removed, the cohesive soils behaves elastically. The variations of elastic domains determined on the stress plane and of the elastic shear modulus with shear stress history having given before before the unloading process were examined. Main conclusions are summarized as follows:

1) No or little dilatancy occurs while the linearity is observed between q and ε after the unloading. Consequently, we can define elastic range as the linear portion of $q\sim\varepsilon$ relation.

2) A parameter θ(eq.(4.5)) which is a function of stress ratio at the beginning of unloading η_R and stress ratio at which q-ε linearity disappears during unloading $\eta_{R\varepsilon}$ to describe the elastic range after the unloading, and another parameter ε_R which is shear strain at the beginning of the unloading were chosen to examine the effects of shear stress history on the elastic range. As the results, a unique relation between these two parameters was found in dependently of the drainage condition or consolidation history (Fig.4.9).

3) Shear stress history given on the S.B.S. makes a certain domain in which elastic behaviour can be observed after the unloading (Fig.4.12).

4) Elastic shear modulus G was determined as the slope of the linear portion of q-ε relation and the effects of shear stress history was examined. As the results, it was shown that G was not affected by shear stress history but by change in effective mean normal stress p. Further, the G-p relation is uniquely determined in spite of consolidation stress for a given sample.

Values of G determined by the use of the method employed in this study should be compared with those determined by dynamic testing method(Ishihara,1976).

REFERENCES FOR CHAPTER 4

Hill,R.(1950): The Mathematical Theory of Plasticity, Oxford Univ. Press.

Prevost,J-H.(1977): "Mathematical modelling of monotonic and cyclic undrained clay behaviour", Int. J. Numerical and Analytical Methods in Geomechanics, Vol.1, pp.195-216.

Mroz,Z. et al.(1978): "An anisotropic hardening model for soils and its application to cyclicloading", Int. J. Numerical and Analytical Methods in Geomechanics. Vol.2, pp.203-221.

Shimizu,M.(1980): "Effects of shear stress history on stress-strain behaviours in "triaxial extension" and isotropic compression of clay", Annals, Disaster Prevention Reseach Inst., Kyoto Univ.,Vol.23, No.B-2, pp.73-86. (in Japanese)

Fung,Y.G.(1965): Foundations of Solid Mechanics, Prentice Hall. Inc.

Karube,D. and Kurihara,N.(1966): "Dilatancy and shear strength of remoulded clays", Proc., JSCE, No.135, pp.16-24.(in Japanese)

Wroth,P. and Schofield,A.N.(1968): "On the generalized stress-strain behaviour of 'wet clay'", Eng. Plasticity, Cambridge Univ. Press, pp.539-609.

Ishihara,K.(1976): Foundations of Soil Dynamics, Kajima Press.(in Japanese)

CHAPTER 5 MODELLING OF STRESS-STRAIN RELATIONSHIPS OF OVERCONSOLIDATED CLAYS BASED ON PLASTICITY THEORY

5.1 INTRODUCTION

In Chapters 2,3 and 4 , attempts to clarify the mechanical responses of normally consolidated or overconsolidated clays when being given some particular external agencies of stress were made. However, a main object to have performed such rather particular experiments lies in expecting to formulate general constitutive equations which will enable to describe mechanical responses when subjected to more general external agencies.

Soil mechanics seems to have developed with the mission to predict the mechanical response of soils or soil structures. Such response had been imposed to be replaced by the phenomenon of so-called failure for a long time. However, recently, the practical requirement to predict the mechanical behaviour before the failure has been more and more recognized. This may be partly attributed to the rapid development of means for analysis. In facts, many theoretical and experimental relationships of stress-strain behaviours have been proposed.

In this chapter, a method for formulating an elasto-plastic stress-strain relationship will be presented. The main purpose is to show how to relate the experimental results to the theoretical formalization. Particularly, dilatancy characteristics of overconsolidated clays, which have been difficult to be considered in the construction of the theory, will be emphasized.

5.2 GENERAL FORMULATION OF STRESS-STRAIN RELATIONS OF ELASTO-PLASTIC MATERIALS

The formulation of stress strain relations based on the plasticity theory is developed in this section.

5.2.1 Yield Functions

(1) Yield Surface

Consider that the state of a plastic material can be defined by a set of (σ_{ij}, ξ_{Σ}), where ξ_{Σ}(Σ=1,2,...N) are parameters being determined by history of plastic defomation and σ_{ij} is stress tensor. We assume that the yield function F exists :

$$F = F(\sigma_{ij}, \xi_{\Sigma}) \qquad \text{.....(5.1)}$$

For a given set of ξ_{Σ}(Σ=1,2,..N), the relation:

$$F(\sigma_{ij}, \xi_{\Sigma}) = 0 \qquad \text{.....(5.2)}$$

constitutes the boundary between elastic and plastic domains in the stress space (σ_{ij}). The curved surface of eq.(5.2) are called yield surface. Here, we define the sign of the function F so that the plastic domain and elastic domain correspond to the condition of F=0 and F<0, respectively (see Fig.5.1).

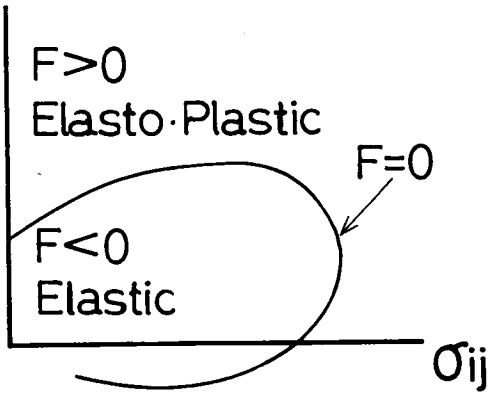

Fig.5.1: Elastic and elasto-plastic domains defined in stress space

(2) Criterion of Loading

When the state of stress is on the current yield surface,i.e., when eq.(5.2) is satisfied, the criterion to determine whether plastic deformation occurs or not can be defined according to the condition of subsequent change in stress.

Considering that the plastic deformation always accompanies the change in ξ_Σ,the condition for no plastic deformation to occur is given by $d\xi_\Sigma=0$ for all Σ. In this case, the change of the yield surface due to the change in stress is expressed by

$$dF\big|_{d\xi_\Sigma=0} = \frac{\partial F}{\partial \sigma_{ij}} d\sigma_{ij} \qquad \cdots\cdots\cdots\cdots\cdots (5.3)$$

The condition above can be divided into two cases:

$$\frac{\partial F}{\partial \sigma_{ij}} d\sigma_{ij} < 0 \qquad \cdots\cdots\cdots\cdots\cdots (5.4)$$

$$\frac{\partial F}{\partial \sigma_{ij}} d\sigma_{ij} = 0 \qquad \cdots\cdots\cdots\cdots\cdots (5.5)$$

The condition of eq.(5.4) is called unloading and eq.(5.5) is called neutral loading. And the case of $dF\big|_{d\xi_\Sigma=0} > 0$ is not possible by the definition of F=0.

Further , when plastic deformation occurs due to the change in stress $d\sigma_{ij}$, at least one of ξ_Σ(Σ=1,2,..N) must change and the state of stress moves onto a subsequent yield surface:

$$F(\sigma_{ij}+d\sigma_{ij},\ \xi_\Sigma+d\xi_\Sigma) = 0 \qquad \cdots\cdots\cdots\cdots\cdots (5.6)$$

From eqs.(5.2) and (5.6),

$$dF = \frac{\partial F}{\partial \sigma_{ij}} d\sigma_{ij} + \frac{\partial F}{\partial \xi_\Sigma} d\xi_\Sigma = 0 \qquad \cdots\cdots\cdots\cdots\cdots (5.7)$$

must be satisfied. If the change in stress such that

$$\frac{\partial F}{\partial \sigma_{ij}} d\sigma_{ij} > 0 \qquad \text{..... (5.8a)}$$

is given, then

$$\frac{\partial F}{\partial \xi_\Sigma} d\xi_\Sigma = -\frac{\partial F}{\partial \sigma_{ij}} d\sigma_{ij} < 0 \qquad \text{..... (5.8b)}$$

And the opposite condition such as

$$\frac{\partial F}{\partial \sigma_{ij}} d\sigma_{ij} < 0 \quad \text{and} \quad \frac{\partial F}{\partial \xi_\Sigma} d\xi_\Sigma > 0 \qquad \text{..... (5.9)}$$

is also possible. Eqs. (5.8) and (5.9) define the plastic hardening and plastic softening materials, respectively.

The criterion on the plastic loading can be summarized as follows:

i) $F = 0$ and $dF\big|_{d\xi_\Sigma = 0} > 0$ ----------impossible

ii) $F = 0$ and $dF\big|_{d\xi_\Sigma = 0} < 0$ ----------unloading

iii) $F = 0$ and $dF\big|_{d\xi_\Sigma = 0} = 0$ ----------neutral loading

iv) $F = 0$ and $dF\big|_{d\xi_\Sigma \neq 0} = 0$

$\frac{\partial F}{\partial \sigma_{ij}} d\sigma_{ij} > 0$ and $\frac{\partial F}{\partial \xi_\Sigma} d\xi_\Sigma < 0$: hardening

$\frac{\partial F}{\partial \sigma_{ij}} d\sigma_{ij} < 0$ and $\frac{\partial F}{\partial \xi_\Sigma} d\xi_\Sigma > 0$: softening

} ----loading

5.2.2 Plastic Strain Increment

The plastic deformation occurs only when at least one of loading parameters ξ_Σ changes. The simplest expression for this condition is given (Kitagawa,1979) as

$$d\varepsilon^P_{ij} = h_{ij\Sigma}({}^{\sigma}kl, {}^{\xi}\Sigma) d\xi_\Sigma \qquad \text{.....(5.10)}$$

where $d\varepsilon^P_{ij}$ is plastic strain increment tensor.

The direction of the change in ξ_Σ may be assumed to be determined by the current state $(\sigma_{ij}, \xi_\Sigma)$, i.e.,

$$d\xi_\Sigma = r.Z_\Sigma(\sigma_{ij},\xi_\Gamma) \qquad \text{.....(5.11)}$$

As eq.(5.7) must be satisfied for the loading condition, putting eq.(5.11) into eq.(5.7), we obtain

$$\frac{\partial F}{\partial \sigma_{ij}} d\sigma_{ij} = - \frac{\partial F}{\partial \xi_\Sigma} r.Z_\Sigma \qquad \text{.....(5.12)}$$

or

$$r = - \frac{1}{Z_\Gamma \frac{\partial F}{\partial \xi_\Gamma}} \frac{\partial F}{\partial \sigma_{ij}} d\sigma ij \qquad \text{.....(5.13)}$$

Consequently,

$$d\xi_\Sigma = - \frac{Z_\Sigma}{Z_\Gamma \frac{\partial F}{\partial \xi_\Gamma}} \frac{\partial F}{\partial \sigma_{ij}} d\sigma_{ij} \qquad \text{.....(5.14)}$$

Thus, the change of loading parameters has been related to the change of stress.

Finally, the plastic strain increment $d\varepsilon^P_{ij}$ can be also related to the stress increment:

$$d\varepsilon^P_{ij} = f_{ij}(\sigma_{mn},\xi_\Sigma)\frac{\partial F}{\partial \sigma_{kl}} d\sigma_{kl} \qquad \text{.....(5.15)}$$

$$\text{with } f_{ij} = - \frac{h_{ij\Sigma} Z_\Sigma}{Z_\Gamma \partial F/\partial \xi_\Gamma}$$

In the case of N=1, it is not necessary to assume eq. (5.11) because eq.(5.14) is equivalent to eq.(5.7) And therefore, eq. (5.15) becomes

$$d\varepsilon^P_{ij} = f_{ij}(\sigma_{mn},\xi)\frac{\partial F}{\partial \sigma_{kl}} d\sigma_{kl} \qquad \text{.....(5.15')}$$

$$\text{with } f_{ij} = -\frac{h_{ij}}{\frac{\partial F}{\partial \xi}}$$

We assume the existence of the plastic potential $g(\sigma_{mn},\xi_\Sigma)$. The tensor function f_{ij} in eq.(5.15) or eq.(5.15') can be expressed as

$$f_{ij} = H(\sigma_{kl},\xi_\Sigma)\frac{\partial g(\sigma_{mn},\xi_\Sigma)}{\partial \sigma_{ij}} \qquad \text{.....(5.16)}$$

Eqs.(5.15) and (5.16) shows that the principal axes of the plastic strain increment tensor coincide with the principal axes of stress tensor. Thus, so called 'co-axiality' has been assumed. Plastic strain increment tensor can be expressed , using the plastic potential g, as:

$$d\varepsilon_{ij}^{P} = H \frac{\partial g}{\partial \sigma_{ij}} \frac{\partial F}{\partial \sigma_{kl}} d\sigma_{kl} \qquad \text{.....(5.17)}$$

If the loading condition is satisfied by the change of stress, the sign of H can be restricted by the loading criterion as follows:

For both plastic hardening and plastic softening materials,

$$H \frac{\partial g}{\partial \sigma_{ij}} d\sigma_{ij} > 0 \qquad \text{.....(5.18)}$$

is derived because $(\partial F/\partial \sigma_{kl}).d\sigma_{kl} > 0$ and $d\sigma_{ij} d\varepsilon_{ij}^{P} > 0$ for plastic hardening and $(\partial F/\partial \sigma_{kl}).d\sigma_{kl} < 0$ and $d\sigma_{ij} d\varepsilon_{ij}^{P} < 0$. for plastic softenig. If the associated flow rule is assumed, the sign of H is restricted as follows:

$$\begin{aligned} &H > 0 \text{ for hardenig material, and} \\ &H < 0 \text{ for softenig material} \end{aligned} \qquad \text{.....(5.19)}$$

5.2.3 Elasto-Plastic Strain Increment (Fung,1965)

Stress-starin relationships for an isotropic elastic material is given by

$$\varepsilon_{ij}^{E} = \frac{1+\nu}{E} \sigma_{ij} - \frac{\nu}{E} \sigma_{\alpha\alpha} \delta_{ij} \qquad \text{.....(5.20)}$$

where E and ν are elastic constants: E is Young's modulus and ν is Poisson's ratio. The incremental stress-strain relationships are derived from these as

$$d\varepsilon_{ij}^{E} = \frac{1+\nu}{E} d\sigma_{ij} - \frac{\nu}{E} d\sigma_{\alpha\alpha} \delta_{ij} \qquad \text{.....(5.21)}$$

The elastic constants are related to shear modulud G and bulk modulus K by the relation:

$$\nu = \frac{3K-2G}{2(3K+G)} \quad , \quad E = \frac{9KG}{3K+G} \qquad \text{.....(5.22)}$$

Complete relationships for elasto-plastic strain increment are

$$d\varepsilon_{ij} = d\varepsilon_{ij}^{E} + d\varepsilon_{ij}^{P}$$

$d\varepsilon_{ij}^{P}$ was already presented by eq.(5.17).

5.3 ELASTO-PLASTIC STRESS-STRAIN RELATIONS FOR OVERCONSOLIDATED CLAYS

5.3.1 General Remarks

(1) Axisymmetric Stress Condition

Assuming that the plastic characteristics of the material considered is isotropic, yield function F depends only on the invariants (with respect to the rotation of the coordinate) of stress, strain and strain history (Fung,1965). In the preceding section the plastic strain and plastic strain history have been included in loading parameters ξ_{Σ} (Σ=1,2,.,N).

It is expected to develop the constitutive equations of the remoulded clay,used in Chapter 2 to 4, from the experimental results. Experiments were restricted to the conventional triaxial tests in which the stress is axisymmetric (Fig.5.2). Under such a condition of stress, three invariants of stress are not independent each other. Hence, we assume a yield function and a plastic potential function of the following form:

$$F = F(I_1, J_2, \xi_{\Sigma})$$

$$g = g(I_1, J_2, \xi_{\Sigma}), \qquad \text{.....(5,23)}$$

where I_1 is the 1st invariant of effective stress and J_2 is the 2nd invariant of deviatric stress tensor:

$$I_1 = \sigma_{\alpha\alpha} \qquad J_2 = \frac{1}{2} s_{ij} s_{ij} \quad \text{with } s_{ij} = \sigma_{ij} - \frac{1}{3}\sigma_{\alpha\alpha}\delta_{ij} \quad \ldots(5.24)$$

In this case, the general equation for plastic strain increment is expressed as

$$d\varepsilon_{ij}^{P} = H \frac{\partial g}{\partial \sigma_{ij}} \frac{\partial F}{\partial \sigma_{kl}} d\sigma_{kl} \qquad \ldots\ldots\ldots\ldots(5.17bis)$$

where

$$H = H(I_1, J_2, \xi_\Sigma) \; ; \; g = g(I_1, J_2, \xi_\Sigma) \; ; \qquad \ldots\ldots\ldots(5.25)$$

$$\left.\begin{aligned} \frac{\partial g}{\partial \sigma_{ij}} &= \left(\frac{\partial g}{\partial I_1}\delta_{ij} + \frac{\partial g}{\partial J_2} s_{ij}\right) \text{ ;and} \\ \frac{\partial F}{\partial \sigma_{kl}} d\sigma_{kl} &= \frac{\partial F}{\partial I_1} dI_1 + \frac{\partial F}{\partial J_2} dJ_2 \end{aligned}\right\} \ldots\ldots\ldots\ldots(5.26)$$

Let coordinate axes (X_1, X_2, X_3) coincide with the direction of the principal axes of stress and X_1 coincide with the symmetric axis of stress (see Fig.5.2).

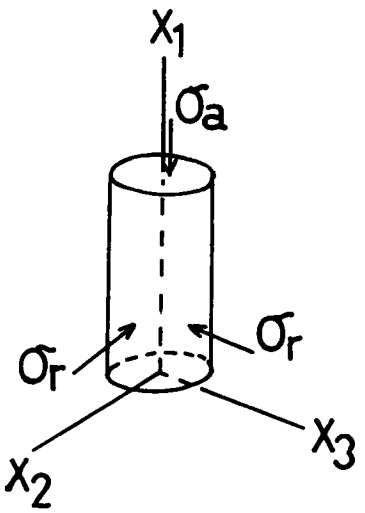

Fig.5.2: Spatial coordinate axes and conventional triaxial test condition

(2) Loading Parameters

Loading parameters must be functions of some variables which can reflect the internal structure of the material. Many quantities might be taken as such variables. It is supposed that the internal structure would yield the proper plastic deformation characteristics, hence, we evaluate the internal structure by the plastic strain tensor. Since we have assumed the isotropy of the plastic characteristics, loading parameters are also assumed to be functions of the invariant(s) of plastic strain tensor . The first invariant of the plastic strain tensor (i.e., the plastic component of the volumetric strain) is chosen as such a variable.

Volume change of soils occurs due to the change in deviatoric component of stress (dilatancy) as well as due to the change in isotropic component of stress (,which will be called the "consolidation" in the narrow sense). The former can be evaluated by performing p-constant tests (p:effective mean normal stress), as shown in Chapter 2 to 4; the latter should be, in principle, examined by tests in which deviatoric component of stress is held constant (J_2-constant tests). However it is easily supposed that, if J_2-constant tests are performed with non zero J_2, the results of the tests will include the effect of dilatancy because, as shown in Chapter 2, dilatancy characteristics strongly depend on the degree of overconsolidation and consequently on the current level of effective mean normal stress. And therefore, we consider that the volume change due to "consolidation" should be evaluated

by performing isotropic consolidation tests.

Two loading variables are assumed: one is the volumetric strain due to dilatancy(v_D); and another is the plastic volumetric strain resulted from the isotropic consolidation tests(v_{co}). Further we assume the following relation between loading parameters and loading variables:

$$\xi_s = \xi_s(v_D, v_{co}) \ ; \ \xi_c = \xi_c(v_{co}) \quad \text{.....(5.27)}$$

Note that we have not used a loading variable corresponding to the deviatoric component of plastic strain. This is because the distorsional plastic deformation and its history are considered to be reflected to the volumetric strain due to dilatancy.

(3) Separated Yield Functions

It was shown in Chapter 2 that the dilatancy behaviour was affected by both the degree of overconsolidation and the level of deviatoric stress. Consequently, v_D is a function of both I_1 and J_2. On the other hand, v_{co} is a function of only I_1. From eq.(5.27), ξ_s is considered to be related to I_1 and J_2 while ξ_c to only I_1.Thus, the relation between the loading parameter and stress invariants is different between two loading parameters, and therefore we choose two corresponding yield functions:

$$F_s = F_s(I_1, J_2, \xi_s)$$
$$F_c = F_c(I_1, \xi_c) \quad \text{.....(5.28)}$$

Further, as to the plastic potential function, following forms similar to those for F_s and F_c are assumed:

$$g_s = g_s(I_1, J_2, \xi_s);$$
$$g_c = g_c(I_1, \xi_c) \qquad \text{.....(5.29)}$$

From eqs.(5.17) and (5.25), we can derive the general form of plastic strain increments:

$$d\varepsilon_{ij}^P = d\varepsilon_{ijs}^P + d\varepsilon_{ijc}^P \qquad \text{.....(5,30a)}$$

where

$$d\varepsilon_{ijs}^P = C_s . H_s . \frac{\partial g_s}{\partial \sigma_{ij}} \frac{\partial F_s}{\partial \sigma_{kl}} d\sigma_{kl}, \quad d\varepsilon_{ijc}^P = C_c . H_c . \frac{\partial g_c}{\partial \sigma_{ij}} \frac{\partial F_c}{\partial \sigma_{kl}} d\sigma_{kl} \qquad \text{.(5.30b)}$$

C_s and C_c become 1 or 0 according to the plastic loading condition for each yield function. If the loading condition (see sec.5.2.1(2)) is satisfied, C_s (or C_c) is 1, and otherwise 0.

In the following, two strain parameters $v(=\varepsilon_{\alpha\alpha})$ and $\varepsilon(=e_{11})$, which were used in the analysis of the experimental results, will be used and therefore it is convenient to derive equations for their increments. Using eqs.(5.28) to (5.30),

$$dv_s^P = d\varepsilon_{\alpha\alpha s}^P = C_s . H_s . 3 \frac{\partial g_s}{\partial I_1} \left(\frac{\partial F_s}{\partial I_1} dI_1 + \frac{\partial F_s}{\partial J_2} dJ_2 \right) \qquad \text{(5.31a)}$$

$$d\varepsilon_s^P = de_{11s}^P = C_s . H_s . \frac{\partial g_s}{\partial J_2} s_{11} . \left(\frac{\partial F_s}{\partial I_1} dI_1 + \frac{\partial F_s}{\partial J_2} dJ_2 \right)$$

$$dv_c^P = C_c . H_c . 3 \frac{\partial g_c}{\partial I_1} \frac{\partial F_c}{\partial I_1} dI_1 \qquad \text{(5.31b)}$$

$$d\varepsilon_c^P = 0$$

(4) Procedure for Determination of Yielding, Plastic Potential and Hardening Functions

When obtaining concrete stress-strain relations based on

the theory of plasticity, as is clear from eqs.(5.31a) and (5.31b), we must determine such functions as F_s, g_s, H_s; and F_c, g_c,H_c in certain ways. A few remarks on the determination of these functions will be given.

Only eq.(5.31a) is treated as an example. Functions H_s and $\partial g_s/\partial I_1$ are functions of the state (I_1,J_2,ξ_s) and not of the state path, while $(\partial F_s/\partial I_1)dI_1+(\partial F_s/\partial J_2)dJ_2$ is dependent on the state path and the current state.

As to the determination of the function g_s, plastic strain increment ratio $dv_s^P/d\varepsilon_s^P$ can be used. In fact, from eq.(5.31a),

$$\frac{dv_s^P}{d\varepsilon_s^P}=3\frac{(\partial g_s/\partial I_1)}{(\partial g_s/\partial J_2)s_{11}} \qquad \text{.....(5.32)}$$

The right hand side of this equation does not depend on the stress path, but depends only on the state. Hence, if the plastic strain increment ratio is examined experimentally along a properly chosen stress path and expressed by the stress, we can obtain the functional form of g_s.

The yield function must be determined so that the yielding condition (F_s=0) gives a boundary in the stress space, inside which the soil considered is elastic and on which considerable plastic deformation occurs (see Fig.5.1). Thus the yielding function is determined by considering the facts observed in certain tests performed.

The hardening (or softening) function will be determined by the following way:
If a functional relationship between either dv_s^P or $d\varepsilon_s^P$ and changes in stress invariants is determined experimentally, we can determine the form of H_s because $g_s$and F_s might have been

known by the way mentioned above. We will use the experimentally obtained relation between $(dv_s^P)_{dI_1=0} \equiv dv_D$ and dJ_2 for the determination of H_s.

5.3.2 Modelling of Plastic Shearing Behaviour

(1) Initial Yield Surface

For a material which has not been subjected to any plastic shear deformation, initial yield locus may be regarded as one of the inherent mechanical properties.

Almost all the types of granular materials behave as positive or negative dialtant materials. This is one of the major difference from the behaviour of ideal elastic materials. From the view point that such a difference from the behaviour of linear elastic materials may be regarded as characteristics of plastic materials, dilatant behaviour is taken as the most representative plastic behaviou of soils amongst others.

In Chapter 2, we dealt with the volume change behaviour due to dilatancy for an overconsolidated clay and it was pointed out that there was a threshold value of stress ratio, denoted by η_{DL}, which is a function of OCR. When stress ratio $\eta(=q/p$, where $q=\sqrt{3J_2}$, $p=I_1/3)$ is lower than η_{DL}, volume change due to dilatancy is negligibly small, and on the other hand, when η becomes larger than η_{DL}, it can not be no longer neglected. And it was also shown that the relations between shear strain and shear stress for overconsolidated specimens were linear in the beginnig of shearing (see Fig.2.8).

We assume that the volume change due to dilatancy v_D, which has been chosen as a loading variable, does not occur

unless stress ratio η reaches η_{DL}; i.e., the stress point of $\eta=\eta_{DL}$ on the constant effective mean normal stress path is taken as the initial yield point of overconsolidated specimens. For various values of $p=p_c/OCR$, where p_c is the maximum preconsolidation stress, corresponding values of η_{DL} can be determined by the following expression:

$$\left.\begin{aligned}&\eta = \eta_{DL}\\ &\text{with } \eta_{DL} = M_{DL}.\left(\ln\frac{p_c}{p}\right)^{m_{DL}} \qquad (2.13)\text{bis}\end{aligned}\right\} \quad \cdots\cdots (5.33)$$

For a given value of p_c, eq. (5.33) gives an initial yield locus for states on the same swelling line expressed by eq. (2.7) :

$$w-w_c = (a + b.\ln\frac{p_c}{p}).\ln\frac{p_c}{p} \qquad (2.7)\text{bis} \quad \cdots\cdots (5.34)$$

Eliminating p_c from eqs. (5.33) and (5.34), we obtain the following relation between w, q and p:

$$q = p.M_{DL}.\left(-S+\sqrt{(S^2-T)}-\ln p\right)^{m_{DL}} \quad \cdots\cdots\cdots (5.35)$$

where $S = (a-\lambda-2b.\ln p)/2b$

$$T = \{w-w_a+a.\ln p+b.(\ln p)^2\}/b$$

Eq. (5.35) gives the cross sections with p=constant of initial yield surface in (p,q,w) space. In Fig. 5.3 two representative cross sections, which correspond to p_c=constant and p=constant, are schematically shown.

Eq. (5.33) can be expressed in terms of stress invariants:

$$F_i \equiv \sqrt{3J_2} - \frac{I_1}{3}M_{DL}.\left(\ln\frac{3p_c}{I_1}\right)^{m_{DL}} = 0 \quad \cdots\cdots\cdots (5.36)$$

Thus defined initial yield function F_i satisfies the condition that the elastic or non-plastic domain is given by $F_i<0$. Since the initial yield locus of eq. (5.36) was determined from the results of p-constant tests, it corresponds to the yield function F_s, one of separated yield functions. Namely,

$$F_{si} = F_i \quad \cdots\cdots\cdots\cdots (5.37)$$

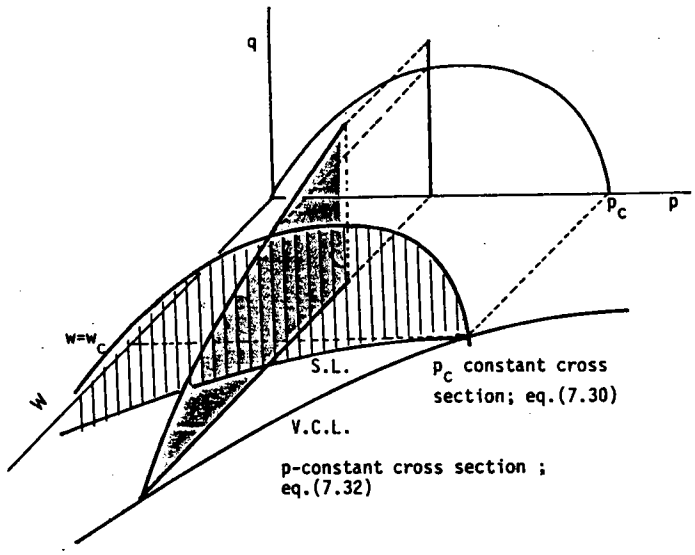

Fig.5.3: Initial yield surface in (p,q,w) space.

(2) Shearing Yield Function

Isotropic hardening or softening is assumed here. Taking account of eq.(5.37), the following form of the shearing yield functions is assumed:

$$F_s = \sqrt{3J_2} - \frac{I_1}{3} M_{DL} \cdot \left(\ln \frac{\xi_s}{I_1/3}\right)^{m_{DL}} \qquad \cdots\cdots\cdots\cdots (5.38)$$

where M_{DL} and m_{DL} are constant; ξ_s is a loading parameter as a function of v_D and v_{co}. Partial derivatives included in the right hand side of eq(5.31a) become as follows:

$$\frac{\partial F_s}{\partial I_1} = \frac{1}{3} M_{DL} \cdot \left(\ln \frac{\xi_s}{I_1/3}\right)^{m_{DL}-1} \cdot \left(m_{DL} - \ln \frac{\xi_s}{I_1/3}\right)$$

$$\cdots\cdots\cdots\cdots (5.39)$$

$$\frac{\partial F_s}{\partial J_2} = \frac{3}{2\sqrt{3J_2}}$$

It is examined here whether the flow rule associated with the shearing yield locus can be available or not to the experimental results obtained in Chapter 2. Strain increment ratio derived from the flow rule associated with such an isotropic hardening or softening type of yield locus as eq.(5.38) is expected to be a function of only stress ratio and not dependent on OCR. In fact, from eq.(5.32) with the condition of $g_s=F_s$, we can derive an expression of strain increment ratio as a function of only stress ratio as follows:

$$\frac{dv_s^P}{d\varepsilon_s^P} = M_{DL} \cdot m_{DL} \cdot \left(\frac{\eta}{M_{DL}}\right)^{\left(\frac{m_{DL}-1}{m_{DL}}\right)} - \eta \qquad \text{.....(5.40)}$$

According to the experimental results shown in Fig.2.13 (Chapter 2), starin increment ratio clearly depends on OCR for a given stress ratio. For example, at $\eta=1.0$, which is the value larger than η_{DL} for OCR of 4, 8 or 20, strain increment ratio is not constant for OCR of 4, 8 or 20.

In consequence, we may not adopt the assumption of the associated flow rule at least for such a shearing yield function as eq.(5.38).

(3) Shearing Plastic Potential

It was explained that eq.(5.32) was not dependent on the choice of the stress path. Using this fact, we determine the plastic potential function g_s from the experiments performed along p-constant stress paths.

We use the experimental fact, obtained in Chapter 2, that, when and after stress ratio η arrives at $\eta=\mu$ during p-constant test, the relation of stress ratio - strain increment ratio is expressed as

$$-\left.\frac{dv_s^P}{d\varepsilon_s^P}\right|_{dI_1=0} = \eta - M \quad \text{at } \eta = \mu, \qquad (2.15)\text{bis} \quad \cdots\cdots\cdots\cdots (5.41)$$

where μ is a function of current OCR defined as p_c/p such that

$$\mu = M.(\ln\frac{p_c}{p})^{m_\mu} \qquad (2.17)\text{bis} \quad \cdots\cdots\cdots\cdots (5.42)$$

Combining eq.(5.41) and eq.(5.42), we obtain the following equation for the shearing plastic strain increment ratio:

$$-\left.\frac{dv_s^P}{d\varepsilon_s^P}\right|_{dI_1=0} = M.\{(\ln\frac{p_c}{p})^{m_\mu} - 1\} \qquad \cdots\cdots\cdots\cdots (5.43)$$

We recall here that, when η is less than μ for a given value of OCR, the variation of strain increment ratio with stress ratio is relatively small, as is shown in Fig.2.13. Thus, it will be reasonable to assume that strain increment ratio is constant for each OCR and the constant value is described as the value at $\eta=\mu$. Consequently, the differential equation for an equi-potential curve on (p,q) plane is given by

$$\frac{dq}{dp} = M.\{(\ln\frac{p_c}{p})^{m_\mu} - 1\} \qquad \cdots\cdots\cdots\cdots (5.44)$$

The integral of this equation leads to :

$$g_s = q - M.\left[(-p_c).\{\sum_{i=1}^{\infty}\frac{(\ln\frac{p_c}{p})^{m_\mu+i}}{\prod_{k=1}^{i}(m_\mu+k)}\} - p\right] - C = 0 \qquad \cdots\cdots\cdots\cdots (5.45)$$

where g_s is shearing plastic potential function, and C is integration constant. C would be determined by an initial condition, but for the current purpose, the determination of C is not necessary, because our interest is focused to derive the

following partial derivatives:

$$\frac{\partial g_s}{\partial I_1} = -\frac{M}{3}\{(\ln \frac{p_c}{I_1/3})^{m_\mu - 1}\}$$

$$\frac{\partial g_s}{\partial J_2} = \frac{3}{2\sqrt{3J_2}} \qquad \text{for } \eta<\mu \quad \ldots\ldots\ldots\ldots (5.46)$$

As pointed out in Chapter 2 , μ has the following meanings:

i) after η reaches to μ, the state of the specimen is on the state boundary surface;

ii) when current OCR, defined by p_c/p , is less than e (=base of the natural logarithm), η can become greater than μ, while, when the current OCR is larger than e, peak shear stress is reached at $\eta=\mu$; and

iii) in spite of OCR, the stress ratio- strain increment ratio on the state boundary surface is expressed by the relation of eq. (5.41) .

And therefore we can derive the following equations from eq. (5.41) for $\eta \geq \mu$ in the case of OCR<e or for the post peak in the case of OCR>e.

$$\frac{\partial g_s}{\partial I_1} = \frac{1}{I_1/3}\cdot(M - \frac{\sqrt{3J_2}}{I_1/3})$$

$$\frac{\partial g_s}{\partial J_2} = \frac{1}{I_1/3}\cdot\frac{3}{2\sqrt{3J_2}} \qquad (\text{for } \eta\geq\mu,\ \text{OCR}<e;\ \text{or for post peak, OCR}>e) \quad \ldots\ldots\ldots\ldots (5.47)$$

(4) Hardening or Softening Function : H_s

As was already pointed out, at 5.3.4 (2), the hardening or softening function H_s in eq. (5.31a) is a function of the state (I_1, J_2, ξ_s). This leads to that we can determine the function

H_s by a certain experiment along a properly chosen stress path. We use the results of p-constant tests mentioned in Chapter 2. Change in v_D can be related to the change in J_2 as follows:

$$dv_s^P\Big|_{dI_1=0} = dv_D = f_D . dJ_2 \qquad \cdots\cdots\cdots\cdots (5.48)$$

where f_D is a function of the current state, being called "dilatancy function":

$$f_{D(N)} = \frac{A_s M^2}{M-\eta} \cdot \frac{1}{(I_1/3)} \cdot \frac{3}{2\sqrt{3J_2}}$$

$$f_{D(P)} = \frac{G_s}{1+w.G_s \sqrt{3J_2} - [2.A.\{(\frac{p}{p_e})_{crit} - (\frac{p}{p_e})\} - B]p} \cdot \frac{\lambda}{} \cdot \frac{1}{\frac{2\sqrt{3J_2}}{3}}$$

(see Appendix 5A.2)

$\cdots\cdots\cdots\cdots (5.49)$

$f_{D(N)}$ corresponds to negative dilatancy which occurs when the current OCR ($=p_c/p$) is less than e , while $f_{D(P)}$ corresponds to positive dilatancy which occurs when OCR is larger than e. A_s is a constant parameter to describe the shear stress- strain relationships for normally consolidated specimens: M is the critical state stress ratio; G_s is specific gravity of soil grains; A and B are parameters to describe the dilatant behaviour on $(p/p_e, q/p_e)$ plane, which are functions of OCR . (The derivation of these dilatancy functions can be developed with mathematical expressions for the dilatancy behaviour given in sec.5A.2.)

By comparing eq. (5.48)' with eq. (5.31a), H_s can be determined as

$$H_s = \frac{f_D}{3\frac{\partial g_s}{\partial I_1} \cdot \frac{\partial F_s}{\partial J_2}} \qquad \cdots\cdots\cdots\cdots (5.50)$$

because $dI_1=0$ in eq. (5.31a). The partial derivatives $\partial F_s/\partial J_2$ and $\partial g_s/\partial I_1$ are given by eqs. (5.39) and (5.47) or (5.48) respectively.

5.3.3 Plastic Consolidation Characteristics

We have assumed such expression for the consolidation yield function as given by eq. (5.28). The simplest forms for F_c and g_c which satisfy eq. (5.28) are given as

$$F_c = g_c = \frac{I_1}{3} - \xi_c$$

and $$\xi_c = p_a \qquad \text{..... (5.51)}$$

where p_a is the current value of $I_1/3$ and the equation above indicates that any change in I_1 accompanies the change in plastic volumetric strain v_c^p.

For the determination of H_c, we can use the results from J_2=constant tests. Since it has been assumed that no plastic shear strain e_{ijc}^p is caused due to any change in I_1, we can utilize the results of isotropic consolidation, rebound and recompression tests ($J_2=0$). In this case, as explained in sec.5A.1, following relation is derived:

$$dv_c^p = f_c . dI_1 \qquad \text{.....(5.52)}$$

where

$$f_c = -\frac{1}{1+w.G_s} . \chi . (\kappa - \kappa_s) \frac{1}{I_1}$$

with $\chi=1$ when $dI_1>0$,

$\chi=-1$ when $dI_1<0$; and

$\kappa = \lambda$ for $\eta \geq \mu$,

$\kappa = \kappa_{rc}$ for $\eta < \mu$.

In this equation, λ, κ_s and κ_{rc} are normal compression index,

swelling index and recompression index, respectively. Comparison of eq. (5.52) and eq. (5.31b) gives the expression for H_c as:

$$H_c = 3.f_c \qquad \text{.....(5.53)}$$

5.4 ANALYSIS OF STRESS RATIO CONSTANT TESTS

5.4.1 Experimental procedure

Drained triaxial compression tests were performed along the stress paths shown in Fig.5.4. The sample used is Fujinomori Clay. Specimens were consolidated to the maximum preconsolidation stress p_c of 392 kPa and rebounded to $p_o=p_c/OCR$ of 46.6 kPa (OCR= 8.42). Incremental shear stress was applied with the constant value of $p=p_o$ until the stress ratio reached a prescribed value of 1.2, 0.8 or 0.4; both increments of p and q was applied so that stress ratio was kept constant at $\eta=\eta_0$.

5.4.2 Calculation Procedure

Fig.5.5 illustrates the stress path and some points at which stress-strain relation changes: IS denotes the p-constant portion in which all the plastic strain components do not change; SF denotes the stress ratio constant portion. In SY, plastic shearing strains do not change, but plastic consolidation component changes because $F_c=0$ and $dI_1 \neq 0$. Point B is the intersection with $\eta=\mu$ curve; plastic potential function g_s is different between YB and BF. If p_Y is smaller than p_E (E: the point at which current OCR is equal to e (the base of the natural logarithm), dilatancy function f_D must be $f_{D(P)}$ for YE and $f_{D(N)}$ after E.

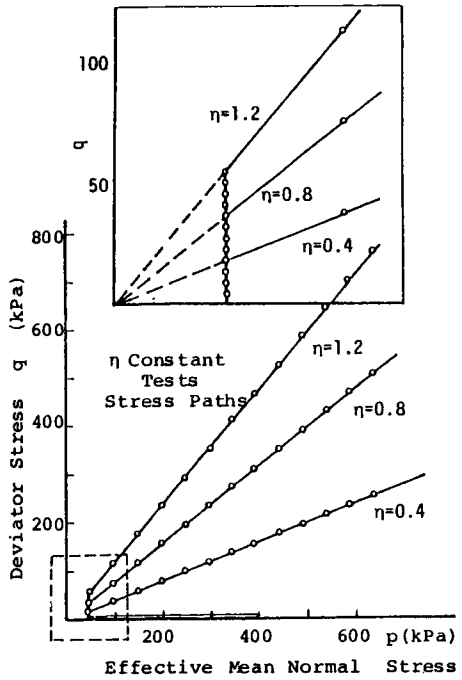

Fig.5.4: Stress paths of stress ratio constant tests.

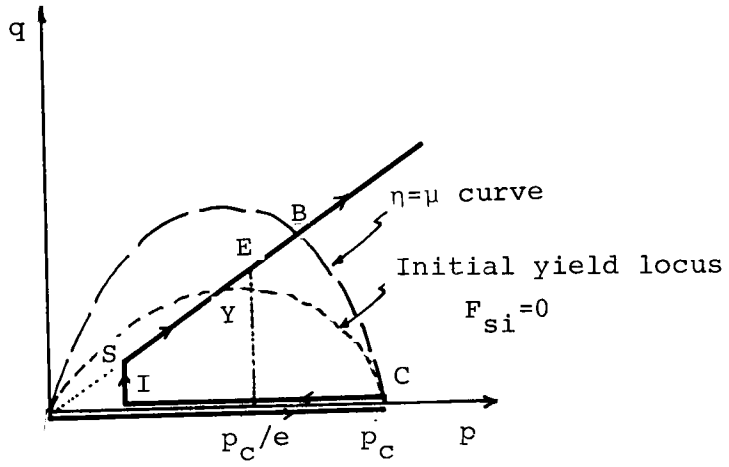

Fig.5.5: Stress path and some characteristical points in the theory.

Values of the constants used in the analysis is listed in Table 5.1. All the values were estimated from the results obtained in Chapters 2 to 4.

Table 5.1: List of the constants used in the calculation

λ	0.0434	(1) isotropic compression, rebound and recompression
a	0.00439	
b	0.00159	
c	0.00346	
d	0.00500	
w_a	0.345	
M	1.4	(2) critical state
Γ	0.320	
M_{DL}	0.935	(3) initial shearing yield locus
m_{DL}	0.567	
m_μ	0.428	(4) state boundary surface
A_s	0.0123	(5) negative dilatancy function
G_0	15000 (kPa)	(6) elastic shear modulus: $G=G_0\sqrt{p/p_0}$ with p_0=100 kPa.

5.4.3 Comparison of Experimental and Calculated Stress-Strain Curves

The relations between v and p are shown in Figs.5.6(a) and (b). It can be seen from the comparison of these figures that the calculated strain is larger than the experimental one; that this tendency is empfasized for η=1.2; and that calculated volumetric strain decreases from Y to E for η=1.2 because of the exagerated effect of positive dilatancy.

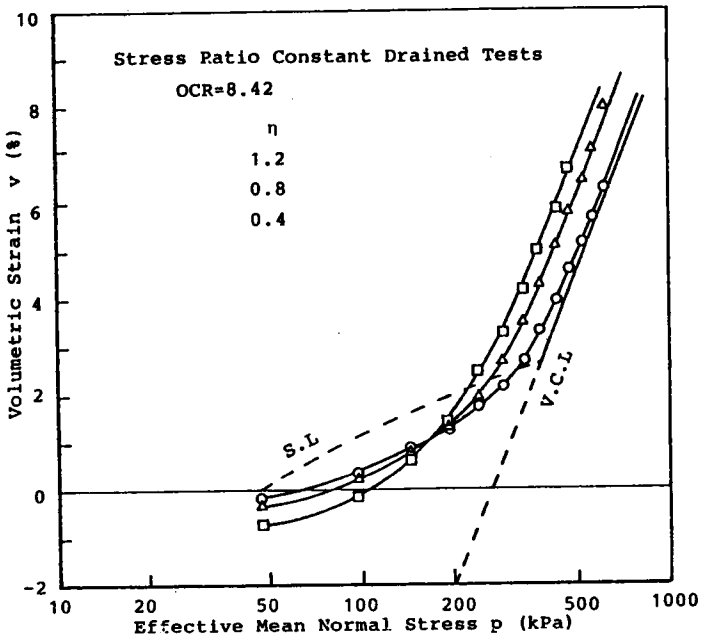

(a)

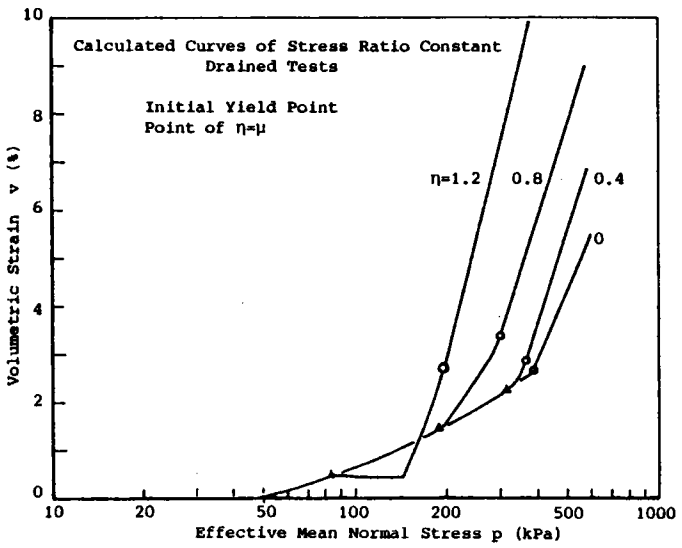

(b)

Fig.5.6: Relations between volumetric strain and effective mean normal stress by
(a) experiments; and
(b) calculations.

Figs.5.7 (a) and (b) show the relations of ε and p. From these figures, it is seen that the calculated shear strain is comparable with the experimental one except for η=1.2. Too large shear strain for η=1.2 seems to be attributed to the fact that the value of 1.2 is near to the critical state stress ratio.

We can summarize the observations above:
When the constant value of stress ratio is so large as the critical stress ratio, calculated strains tend to be overestimated. However, in the case when η is not so large, the reasonable strains are calculated by the theory.

5.5 CONCLUSIONS

Theoretical formulation of stress-strain relatioships based on the theory of plasticity was given. The experimental results obtained in the study of Chapter 2 to 4 were taken into account in the construction of the concrete equations.

The stress-strain relationships developed in this chapter is characterized by :

i) the plastic deformation of soils was assumed to consist of two types of deformation mechanism: one is shearing and another is isotropic compression; two loading variables v_D and v_{co} were chosen and each of them was related to the increment of stress invariants so that $dv_D=f_D dJ_2$ and $dv_{co}=f_c dI_1$, respectively.

ii) two loading parameters $\xi_s=\xi_s(v_D,v_{co})$ and $\xi_c=\xi_c(v_{co})$ were incorporated in the yielding functions F_s and F_c, respectively.

iii) initial yield locus of $F_s=0$ was determined as a boundary curve within which no dilatancy occurs, while outside which

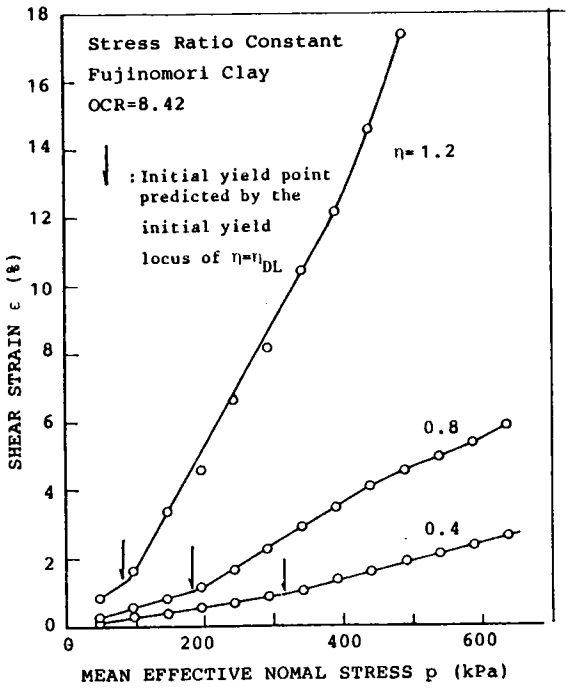

(a)

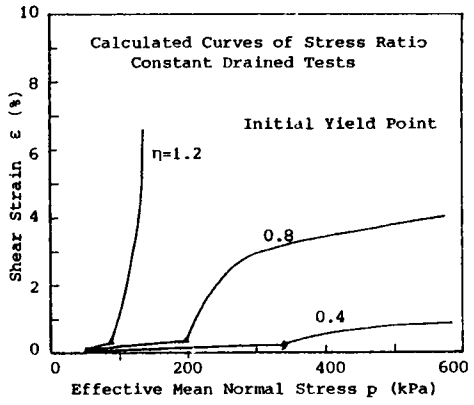

(b)

Fig.5.7: Relations between shear strain and effective mean normal stress by
(a) experiments; and
(b) calculations.

dilatancy is considerable;

iv) the hardening or softening function H_s was determined from the experimental expression of dilatancy .

v) plastic hardening condition associated with consolidation yield function F_c is always satisfied and associated flow rule was assumed.

vi) non-associated flow rule was assumed with respect to the plastic shearing strain dv_s^P and $d\varepsilon_s^P$ from the experimentak results.

The calculated curves of stress-strain was compared with the experimental results for stress ratio constant tests. The strain was estimated reasonably in the case when the stress ratio was not so high, but overestimated in the case when the stress ratio was so high.

REFERENCES FOR CHAPTER 5

Fung,Y.C.(1965): Foundation of Solid Mechanics, Prentice-Hall,

Kitagawa,K.(1979):Foundation of the Theory of Plasticity,

Nikkan Kogyo Press. (in Japanese)

APPENDIX FOR CHAPTER 5

5A.1 Volume Change under All Round Stress

In order to evaluate non-linearity of w-logp relations during isotropic swelling or rebound and isotropic recompression, it was assumed that swelling index κ_s and recompression index κ_{rc} vary linearly with $\ln(p_c/p)$, as shown in Fig.5A.1.

It was verified that the swelling index κ_s (=-dw/dlnp) could be related non linearly to lnp as

$$\kappa_s = a + 2.b.(\ln n) \qquad \text{.....(5A.1)}$$

where n is OCR defined as p_c/p (p_c: maximum preconsolidation stress) and a and b are constants.

As to the recompression index κ_{rc}, the following equation was proposed and its validity was examined experimentally:

$$\kappa_{rc} = -\frac{\bar{k}\lambda - a}{\ln N}(\ln n) + \bar{k}\lambda \qquad \text{.....(5A.2)}$$

where N is the maximum preconsolidation ratio. Denoting the consolidation stress at the beginning of the recompression by p_o, N is defined as $N=p_c/p_o$. $\bar{k}$ is a function of N. Because the validity of eq.(5A.1) was shown in Chapter 2 (Fig.2.2 and Fig.2.3(a) and (b)), here only eq.(5A.2) is examined.

In Fig.5A.2, the results of isotropic compression, rebound and recompression tests are shown. The data in this figure are used to determine the relation between κ_{rc} and n or that between $\bar{k}$ and N.

Integrating eq.(5A.2) with $w=w_o$ at $p=p_o$, we obtain the following relation:

$$\frac{w-w_o}{\ln(p/p_o)} = \frac{\bar{k}\lambda - a}{2\ln N}(\ln n) - \frac{\bar{k}\lambda + a}{2} \qquad \text{.....(5A.3)}$$

Fig.5A.3 shows the relations between $(w-w_o)/\ln(p/p_o)$ and n in the log scale. It is clear from this figure, linear relations depending on N exist. From the relation below:

$$-\frac{\bar{k}\lambda+a}{2} = \frac{w-w_o}{\ln(p/p_o)}\Bigg|_{n=1,} \qquad \text{.....(5A.4)}$$

the value of $\bar{k}$ can be determined as a function of N. Fig.5A.3 also shows the variation of $-(\bar{k}\lambda+a)/2$ with N, resulting in the expression

$$\bar{k} = -\frac{1}{\lambda}(c.\ln N + d), \qquad \text{.....(5A.5)}$$

where c and d are constants for all N.

We can summarize the isotropic consolidation, rebound and recompression behaviour by the following equations:

$$dw|_{q=0} = \begin{cases} -\lambda.d\ln p : dp>0 \text{ for normally consolidated state} \\ -\kappa_{rc}.d\ln p : dp>0 \text{ for overconsolidated state} \\ -\kappa_s.d\ln p : dp<0 \text{ for both normally and overconsolidated state} \end{cases} \qquad \text{.....(5A.6)}$$

Values of constants of the sample used in the study of Chapter 2 are listed in Table 5A.1.

Table 5A.1: Values or constans describing the isotropic compression, rebound and recompression

w_a	λ	a	b	c	d
0.345	4.34×10^{-2}	4.39×10^{-3}	1.59×10^{-3}	3.46×10^{-3}	5.00×10^{-3}

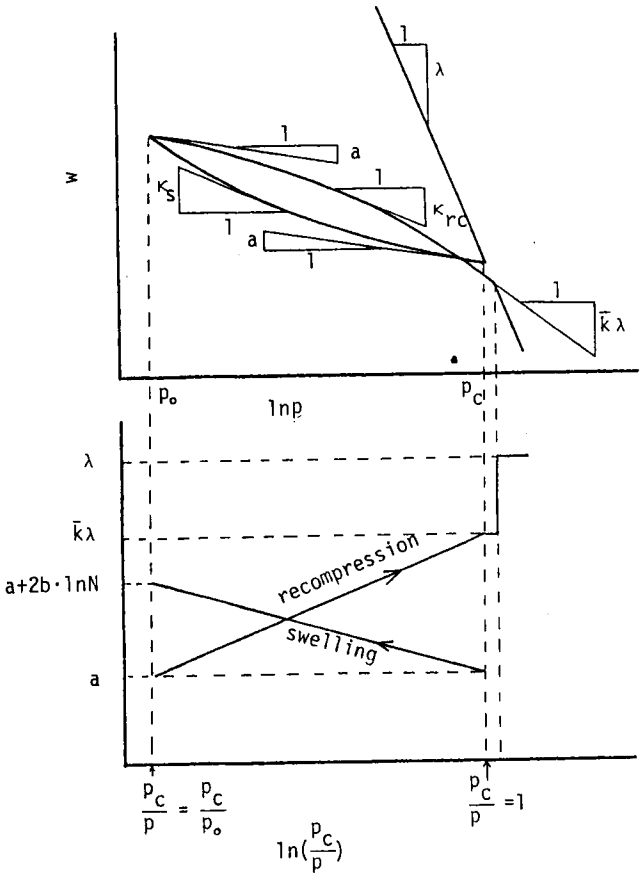

Fig.5A.1: Hypothesis on the variations of swelling index with effective mean normal stress

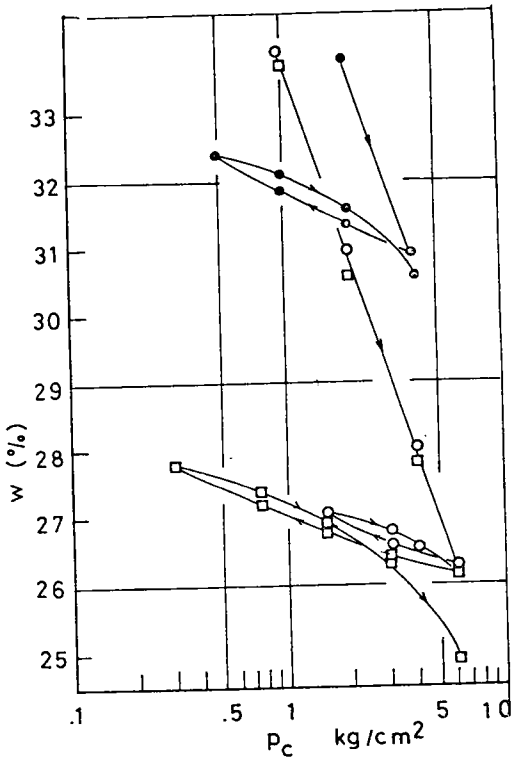

Fig.5A.2: Water content vs. log of p; isotropic compression, rebound and recompression tests.

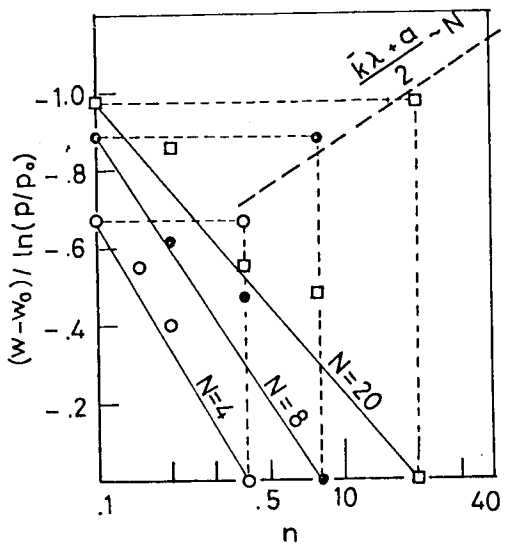

Fig.5A.3: $(w-w_o)/\ln(p/p_o)$ vs. OCR and $(\bar{k}\lambda+a)/2$ vs. N.

5A.2 Dilatancy Functions

(1) Positive Dilatancy Function

We give a mathematical expression to the state paths on the $(q/p_e, p/p_e)$ plane shown in Fig.2.10(Chapter 2). For each path corresponding to a certain value of OCR, following conditions are assumed (see Fig.5A.4):

i) Each path must pass through the point of the critical state $((q/p_e)_{crit}, (p/p_e)_{crit})$;

ii) Each path must pass through the point of threshold of dilatancy $((q/p_e)_{DL}, (p/p_e)_{DL})$;

iii) Each path osculates with such a straight line as

$$q/p_e = \mu.(p/p_e) \qquad \text{.....(5A.7)}$$

This condition implies that stress ratio becomes maximum at $\eta=\mu$ (μ gives the maximum stress ratio for heavily over-consolidated specimens, Chapter 2).

iv) Each path can be expressed by a parabora.

Considering both the assumptions i) and iv), we can assume the function of the form in the following:

$$Y_{crit} - Y = A.(X_{crit} - X)^2 + B.(X_{crit} - X) \qquad \text{.....(5A.8)}$$

with $Y=q/p_e$ and $X=p/p_e$

The values of X_{crit} and Y_{crit} were given in Chapter 2. In Fig. 5A.5, the relations between Y_{crit}-Y and X_{crit}-X, resulted from the experimental data in the study of Chapter 2, are shown. As can be seen in this figure, eq.(5A.8) assumed in the above may agree fairly with the experimental data.

From the assumptions ii) and iii), we obtain the following expressions for the coefficient B:

$$B = \mu - 2.(L + \sqrt{L.N}) \qquad \text{.....(5A.9)}$$

with $L=(\mu.X_{crit}-Y_{crit})/(X_{crit}-X_{DL})$; and

$$N=(Y_{crit}-Y_{DL})/(X_{crit}-X_{DL})$$

A is also determined as follows:

$$A = \frac{(B - \mu)^2}{4.(\mu.X_{crit}-Y_{crit})} \qquad \text{.....(5A.10)}$$

In the equation above, μ, X_{DL} and Y_{DL} are functions of OCR. Recalling the results obtained in Chapter 2 that the volume change can be neglected at η smaller than η_{DL}, we can approximate X_{DL} by

$$X_{DL} = (p/p_e)_{DL} \cong (p/p_e)_0, \qquad \text{.....(5A.11)}$$

where the subscript o denotes the state at the beginning of the shearing. By using the equation for isotropic swelling line, eq.(2.7) or (2.8), we can derive the following expression:

$$(p/p_e)_o = \frac{1}{n} \exp\{\frac{(a + b.\ln n).\ln n}{\lambda}\} \qquad \text{.....(5A.12)}$$

Further, Y_{DL} is determined as $Y_{DL}=\eta_{DL}.X_{DL}$ and η_{DL} is given by eq.(2.13). Additionally,μ is given by eq.(2.17). The constants included in eqs.(2.13) and (2.17) were given in Chapter 2.

The differential form of eq.(5A.12) is obtained by considering that each curve on the state plane or each equation derived in the above corresponds to a certain value of OCR and consequently p, and that A and B and p are regarded as constants. Finally the following equation has been obtained:

$$dw = - \frac{\lambda}{\eta - \{2.A.\{(p/p_e)_{crit}-(p/p_e)\} + B\}} dq \qquad \text{....(5A.13)}$$

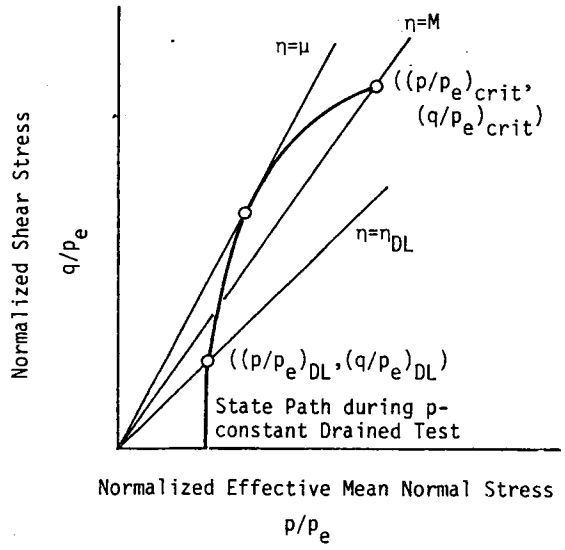

Fig.5A.4: Schematic representation of a state path on the $(q/p_e, p/p_e)$ plane

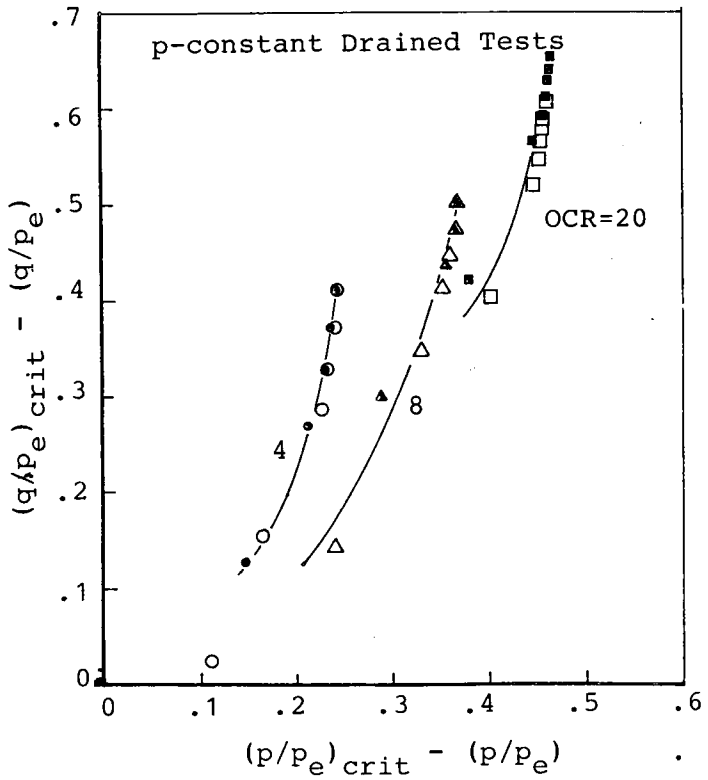

Fig.5A.5: State paths (from experimental data of Chapter 2)

(2) Negative Dilatancy

It can be seen from Fig.2.7 that, in the range of stress ratio over which positive change in volumetric strain ,i.e., negative change in dilatancy occurs, the tangent of the η-v curve has the slope dependent only on the value of η. Considering this characteristic, we may use the relation of η-v for normally consolidated state.

Stress strain behaviour for a normally consolidated state during p constant shear test can be specified by the following characteristics:

i) Stress ratio - strain increment ratio relation is given by the following equation (see Fig.2.13):

$$-\frac{dv}{d\varepsilon} = \eta - M \qquad \text{.....(5A.14)}$$

ii) Relations between shear strain ε and stress ratio η may be given by

$$\eta = \frac{\varepsilon}{A_s + B_s.\varepsilon} \quad \text{or} \quad \frac{\varepsilon}{\eta} = A_s + B_s.\varepsilon \qquad \text{.....(5A.15)}$$

in spite of the difference in p. One example which indicates the availability of the equation above is shown in Fig.5A.7. Differential form of this equation becomes

$$d\varepsilon = \frac{A_s}{(1 - \eta/M)^2}\, d\eta, \qquad \text{.....(5A.16)}$$

where it is considered that $d\eta/d\varepsilon=0$ at $\eta=M$. From eqs(5A.14) and (5A.16), we obtain the following expression for dilatancy volume change of normally consolidated state:

$$dv_D = \frac{A_s.M^2}{M - \eta}.\frac{1}{p}.\, dq \qquad \text{.....(5A.17)}$$

This equation indicates that $dv_D/d\eta$ is a function of only stress ratio when p is constant

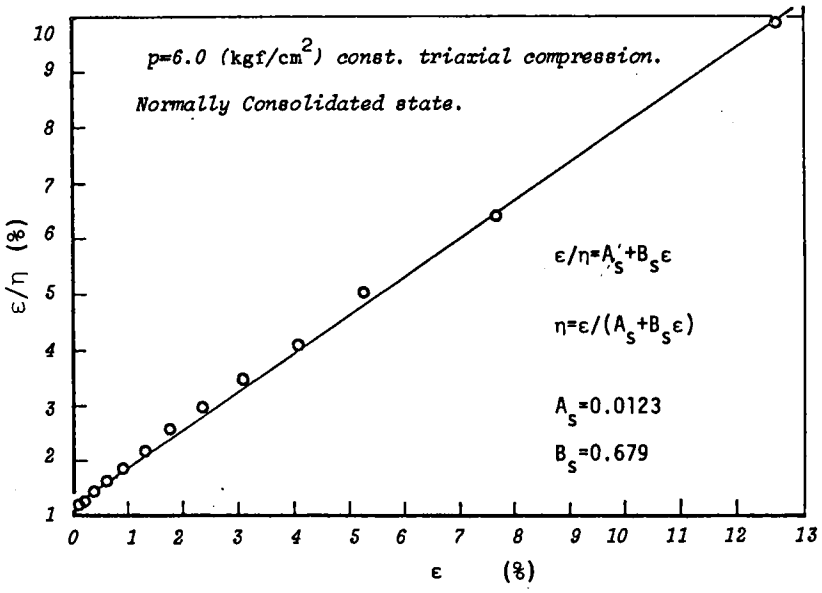

Fig.5A.6: ε/η vs. ε; p-const. drained test of normally consolidated clay

CHAPTER 6 COMPARISON OF UNCONFINED COMPRESSION STRENGTH AND LABORATORY VANE SHEAR STRENGTH

6.1 INTRODUCTION

Attempts to compare unconfined or undrained triaxial compression strength and in-situ vane shear strengths have been made by many researchers. Since the unconfined or undrained triaxial compression strengths could have included more or less some effects of the disturbance caused by sampling, the comparison is essentially difficult, and an established conclusion has not been obtained. The comparison should be made by considering the difference in strength due to the difference in the shearing mechanism between the laboratory undrained and in-situ vane shear tests.

Unconfined compression strengths and laboratory vane shear strengths were compared. Both can be considered to include the effects of sampling disturbance, and the difference in strength between them, if any, would have been caused by the difference in shearing mechanism.

6.2 SAMPLES AND TEST PROCEDURE

Two undisturbed alluvial cohesive soils were used. One had been from Naruo, Nishinomiya City, Hyogo Prefecture and another from Tsuruga, Miyazu City. Each bored sample had the cylindrical shape of 7.5 cm in diameter and about 10 cm in height. An unconfined compression test was performed for one bored sample, while two laboratory vane shear tests were conducted for one bored sample. Specimens for unconfined compression tests were 3.56 cm

(*) Shimizu & Shibata (1980)

in diameter and about 8 cm in height. The rate of axial deformation was controlled to be 1 %/min. Laboratory vane shear tests were conducted by using a special apparatus, shown in Photo 6.1, made so that vane blade (2cm in height and 1 cm in width) is fixed and specimen can be rotated.

The shape of specimen for the vane test is as shown in Fig.6.1. The container within which the specimen had been placed was fixed to rotating table. The rotation of the table was operated by hand. The measurement of the torque was done by measuring the angle of rotation of the spring which is fixed to the vane rod.

This apparatus was made originally so that the very soft clay could be tested, and so the rigidity of the spring for the measurement of the torque is not very high enough to completely fix the vane rod, particularly for not very soft soils. In consequence, for the control of the angular velocity of rotation, the angle of rotation of both the vane rod and the rotating table must be controlled. Because it was impossible to control the angular velocity of the vane rod, only the angular velocity of the table was held constant. The angular velocities of the table of 1°/sec and 2°/sec were employed. Therefore, true angular velocity during shear was not constant but variable, dependently on the deformability of the specimen; higher was the angular velocity of the table, higher was the true angular velocity for a given specimen.

Vane rod was inserted into the specimen so that its depth would be equal to the height of the blade (2 cm) in order that

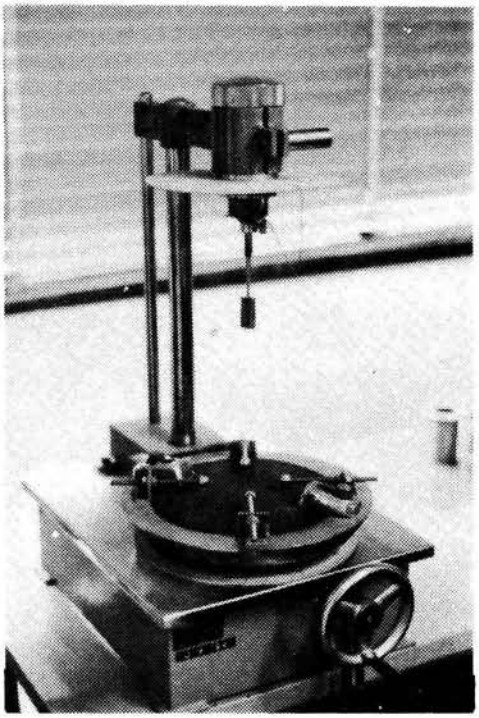

Photo 6.1: Laboratory vane shear test apparatus

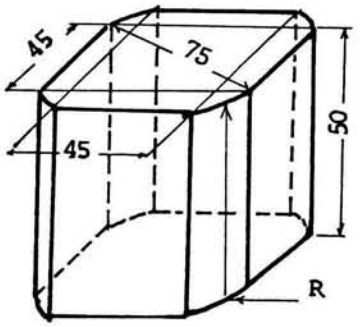

unit: mm

Fig.6.1: Dimension of the specimen for laboratory vane shear test.

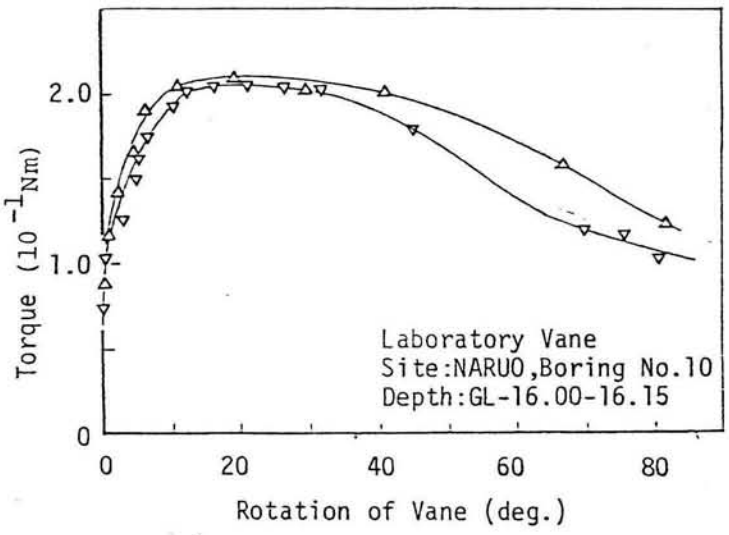

Fig.6.2: Example of relations between measured torque and rotating angle.

the occurrence of the friction between the vane rod and the surrounding soil could be avoided. In this case, the vane shear strength S_v is obtained by the following equation, by assuming that the shear resistance on shearing plane is uniformely distributed,

$$S_v = \frac{M}{\frac{13}{12}\pi D^3} \tag{6.1}$$

where M is the measured maximum torque D is the width of the blade.

One of the relations between torque and rotating angle is shown in Fig. 6.2

6.3 RESULTS

6.3.1 Sample from Naruo

Samples bored at eleven points were tested. Representative results, Boring No.10, are presented in Fig. 6.3. Soil profiles other than No.10 are about the same to that of No.10, however the depth and the thickness of the clay layer from which samples were mainly bored are varied a little between points.

As is clear from Fig. 6.3, the numbers of test were not many enough to compare the unconfined compression strength and the vane shear strength along the depth. And so, the comparison between the two was made by choosing a pair of the two which satisfies the following condition :

① they are from the same boring point

② the difference in sampling depth is less than 1 m

③ the conservation of the sample is good

④ the difference in water content at testing is less than 5 %

⑤ soil classification based on the grain size distribution is the same for them, and

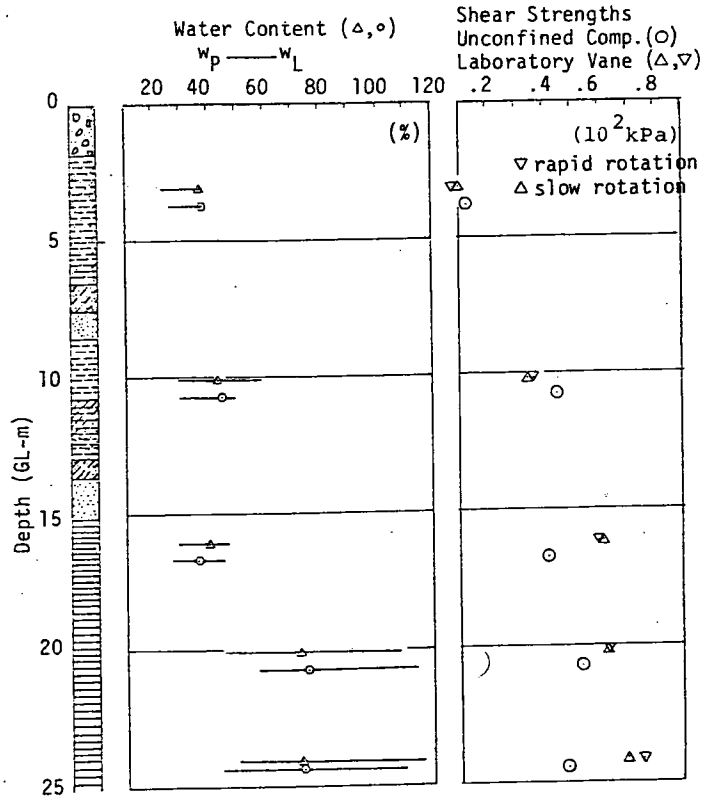

Fig.6.3: Soil profile and vertical variations of $q_u/2$ and s_v (Naruo Boring No.10)

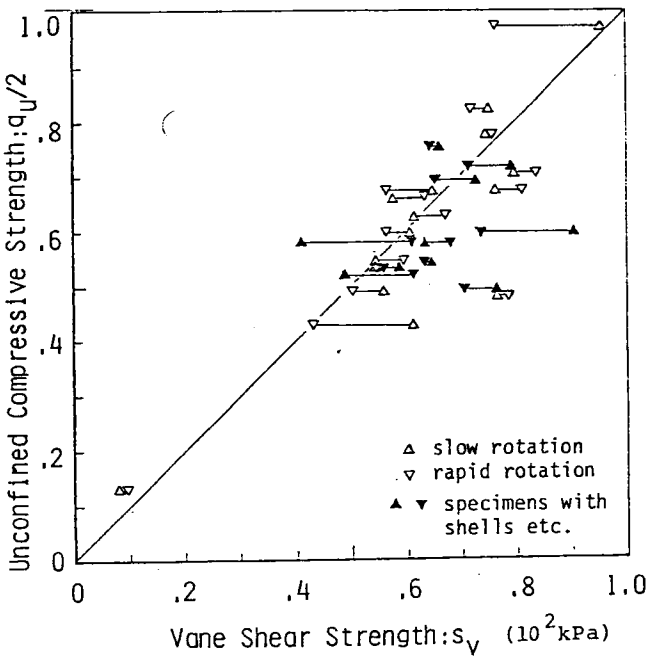

Fig.6.4: Comparison of $q_u/2$ and s_v (Naruo)

⑥ consistency limits are the same for them

According to the conditions above, a pair in the depth of 10 to 11 m in Fig.6.3 must be extruded for the comparison because of the loss of condition ⑥.

Similar examinations were made also for results of the samples other than Boring No.10. In Fig. 6.4 , test results for all boring points are shown . Unconfined compression strength $q_u/2$ is compared with vane shear strength S_v. It is seen in Fig. 6.4 that the correlation is not poor but the tedency of $S_v=q_u/2$ is found as a whole, however, that, in more detail, $q_u/2>S_v$ is seen when $q_u/2$ is relatively large and $q_u/2<S_v$ when $q_u/2$ is relatively small.

Further, in Fig.6.4, the effect of the rate of rotating angle is not markedly seen and therefore the avarage value between the quick test (2 %/min) and the slow test (1 %/min) will be used for discussion in the following.

6.3.2 Sample from Miyazu City

Samples from four point of boring were used. The soil profile was almost the same between them. All the test data are gathered in Fig.6.5. As a whole, a tendency of $q_u/2<s_v$ is found.

6.4 CONSIDERATIONS

According to Bjerrum & Simons(1960), c_u/p-P.I. relations based on in-situ vane shear tests are different from similar relations based on undrained triaxial tests, particularly in the range of low P.I. If the data for such low P.I. include the data

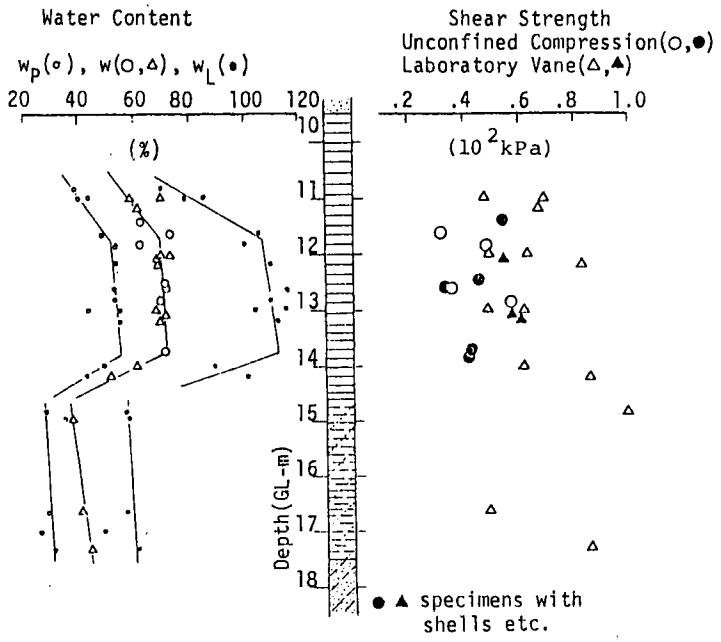

Fig.6.5: Soil profile and vertical variations of $q_u/2$ and S_v (Miyazu).

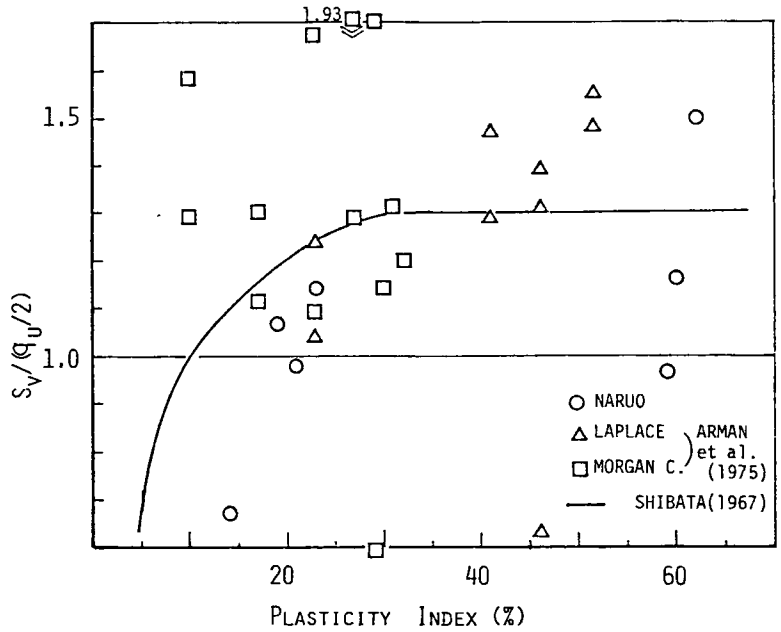

Fig.6.6: $S_v/(q_u/2)$ vs. P.I.

of a wide range of p (consolidation stress), the general tendency of the difference mentioned above would be valid even in the case when p is relatively high. Noting that the disturbance of samples due to sampling should be less in high p than in low p, the difference in c_u/p in the range of low P.I. can be considered essential despite the degree of the sampling disturbance.

From such a view point, $S_v/(q_u/2)$ is compared with P.I., in Fig. 6.6 , where the results for samples of Boring No.9, 10 and 11(Naruo) of which consistency limits were measured are shown.

Additionally, the results by Arman et al(1975) and Shibata (1967) are also plotted. The tendency of $S_v/(q_u/2)>1$ can be seen when P.I. is relatively large, but it is not the case when P.I. is relatively small. For extremely small P.I., S_v can be smaller than $q_u/2$ This indicates that the difference in strength due to the difference in the shearing mechanism will reveal for poorly plastic soils.

6.5 CONCLUSIONS

The comparison between the laboratory vane shear strength and the unconfined compression strength was made on two undisturbed alluvial clays. The correlation of thses two strength was found to be fairy good. The tendency so that the vane strength becomes larger than the unconfined strength was seen. The difference in these strengths might be attributed to the difference in the shearing mechanism. It was pointed out that the possibility that the difference in strength due to the difference in shearing mechanism depends on the type of soils,i.e., the ratio of these two strengths was examined in terms of the plas-

ticity index, larger the vane strength compared with the unconfined strength.

REFERENCES FOR CHAPTER 6

Arman,A. et al.(1975): "Study of the vane shear", Proc., Conf. on In-situ Measurement of Soil Properties, ASCE, Vol.1, pp.93-120.

Bjerrum,L. and Simons,N.E.(1960): "Comparison of shear strength characteristics of normally consolidated clays", proc., Research Conf. on Shear Strength of Cohesive Soils, ASCE, pp.711-726.

Shibata,T.(1967): "Study of the vane shear strength of clays", Proc., JSCE, No.138, pp.39-48.(in Japanese)

Shimizu,M. and Shibata,T.(1980): "Comprison of unconfined compression strength and laboratory vane shear strength on undisturbed alluvial clays", Proc. Symp. Vane Shear Tests, JSSMFE, Osaka, Japan, pp.67-70.(in Japanese)

CHAPTER 7 TENSILE STRENGTHS OF COHESIVE SOILS

7.1 INTRODUCTION

The necessity of studies on the behaviour of soils under low effective stress including tensile or negative normal stress has been recognized for both engineering and physical problems concerning with soils. Failures of such soil structures as natural or artificial soil slopes (Eden & Mitchel,1970; Conlon, 1966) and earth dams (Eisenstein et al.,1972; Narita,1976; Leonards & Narrain,1963; Lee & Shen,1969) etc are often initiated by the propagation of tensile crack caused by tensile stress in the soil structure.

The evaluation and determination of the tensile strength as well as the cohesive component mobilized in shearing (Conlon, 1966; Iyer,1975) are enabled by examining the strength envelop in the range of low effective stress. Studies on the mechanical behaviour of clays under low effective stresses at failure have been very few, due mostly to experimental difficulties.

In this chapter, methods for measuring tensile strengths of soils are reviwed and discussed; and results from the most preferable method, the triaxial extension test using bone-shaped specimens, are presented.

7.2 METHODS FOR MEASUREMENT OF TENSILE STRENGTH OF SOILS

7.2.1 Previous Studies

Some methods have been proposed and used for measuring tensile strenfth of soils.

Direct tensile tests have been performed by many researchers (Hasegawa & Ikeuchi,1962 and 1964; Ingles & Fridman,1963; Helenelund,1967; Hasegawa & Ikeuchi,1970; Ito et al.,1974; Kajitani et al.,1975; Ohne et al.,1976). In this method, it is difficult to apply the tensile load to the soil specimen. Various devices to grip the specimen were proposed:

In the studies by Hasegawa et al. tension was applied through two small thin steel plates buried in the egg-shaped enlarged ends of the specimen being laid horizontally and the tensile load was also applied horizontally. According to Suklie & Drnovsek(1964), it is in the soil mechanics laboratory of the University of Ljubljiana(Yugoslavia) that the tensile tests for soils were firstly made using horizontally laid specimens of a rectangular profile with expanded heads. Helenelund(1967) applied the tensile load through plates buried vertically in a relatively large specimen box filled with a fibrous peat. In the study by Ito et al.(1974), the end of a specimen was gripped by the gum rubber in which compressed air was applied. In Kajitani et al.(1975), many pins were inserted into the upper and lower parts of a specimen through small holes in metal boxes which cover both ends of the specimen.

As indirect tests, bending tests (Ingles & Fridman,1963; Ajaz & Parry,1975a, 1975b,1975c; Ajaz,1980), hollow cylinder test (Suklje & Drnovsek,1964) and diametral compression test (so called Brazilian test, Ingles & Fridman,1963; Narrain & Rowat, 1970; Mellor & Hawkes,1971; Ito et al.,1974; Eisenstein, 1972) have been often used for soils.

In the Brazilian test, the material tested must be assumed to be ideally elastic to obtain the theoretical stress solution or tensile strength (Akazawa,1943). And in this test, the stress state is not unidimensional but bidimensional. These shortcomings have received considerable attention in the fields of concrete testing , rock mechanics and ceramic technology. Nevertheless, the use of this method is recommended provided certain improvements are considered (Mellor & Hawkes,1971). Such improvement as the use of curved loading platen or the use of ring specimens is efficient for rocks (Awaji & Saito,1978; Coleback,1966). However, for soils which behave as inelastic materials, the substantial assumption of the ideal elasticity may not be allowed. Krishnayya & Eisenstein(1974) used the Brazilian test for compacted till. To overcome the shortcomings of this method, they examined the difference in elastic moduli for compression and tension and also evaluated the strain component due to compressive stress. Nevertheless, the substantial shortcoming of the necessity of assuming ideal elasticity was not avoided.

According to Ajaz & Parry(1975a), "amongst the indirect type of tension tests the bending test is unique in that both extreme fibre compressive and tensile stresses can be obtained from the applied bending moment and observed strains by a differential method of analysis not based on any preferred stress-strain law." The Cambridge radiograph technique using an embeded grid of lead shot was used for monitering the displacement field within soil beam specimen.

In a series of studies by Ajaz et al, the pore-pressure distribution is not mesured and so the effective stress-strain relation can not be obtained. In the Author's opinion, it is the most important to evaluate the effective stresses in any soil mechanics problems.

Bishop & Garga(1969) proposed a method by which the informations with respect to the effective stresses can be obtained. Iyer(1975) adopted this method and examined strength behaviour of undisturbed sensitive clay, Leda Clay, in low effective stress level. Kazama et al.(1976) and Ramiah et al.(1977) also used this method to investigate the tensile strength characteristics of compacted soils.

The efficiency of this method should be recognized, but at the same time the limitation must be noted. The detail and the discussion of the limitation of this method will be given in the following.

7.2.2 Principle of Triaxial Extension Tests Using Bone-Shaped Specimens (Method by Bishop & Garga,1969)

The range of stress realized in the conventional triaxial test for specimens with cylidrical form is limited as shown in Fig.7.1. In the conventional triaxial compression test ($\sigma_1 = \sigma_a \geqq \sigma_2 = \sigma_3 = \sigma_r$, where $\sigma_1, \sigma_2, \sigma_2$ are the maximal, intermediate and minimal effective principal stresses,respectively and σ_a and σ_r are axial and radial stresses in the conventional triaxial test, respectively), the condition of $\sigma_r = 0$ is reached before the condition of $\sigma_a = 0$ is reached, while in the extension test

($\sigma_1=\sigma_2=\sigma_r \geqq \sigma_3=\sigma_a$) $\sigma_a=0$ is reached before $\sigma_r=0$. Namely,

$$\sigma_3 = \sigma_r \geqq 0 \quad \text{(in the triaxial compression)}$$
$$\sigma_3 = \sigma_a \geqq 0 \quad \text{(in the triaxial extension)} \qquad \text{.....(7.1)}$$

For the determination of the real cohesion component of shear resistance or the tensile strength, as the intercept of Mohr's circle of stress with the axis of shear or normal stress, the state of stress such that

$$\sigma_1>0 \text{ and } \sigma_3<0 \qquad \text{.....(7.2)}$$

must be realized. However, from eq.(7.1) it is clear that neither compression nor extension test cannot give such a condition. It will be shown that, if we use bone-shaped specimens in the triaxial extension test, it is possible to realize the condition of eq.(7.2).

Considering the equilibrium of forces acting on the shaded portion between the upper end plane and an arbitrary horizontal plane in Fig.7.2, average normal stress on the arbitrary plane σ can be given as follows:

$$\sigma = \frac{1}{r}(\sigma_E - \sigma_r) + \sigma_r \qquad \text{.....(7.3)}$$
$$\text{with } r=A/A_E$$

where σ_E is the normal stress on the upper (or lower) end plane, and A and A_E are cross sectional areas of the arbitrary plane and the end plane.

The variations of r and consequently σ along the axial direction are schematically shown in Fig.7.2. The possible minimum value of σ is obtained from the general limiting condition in extension test (: $\sigma_E \geqq 0$) as

$$\sigma \geqq \sigma_r\left(1 - \frac{1}{r_0}\right) = \sigma_0 \qquad \text{.....(7.4)}$$

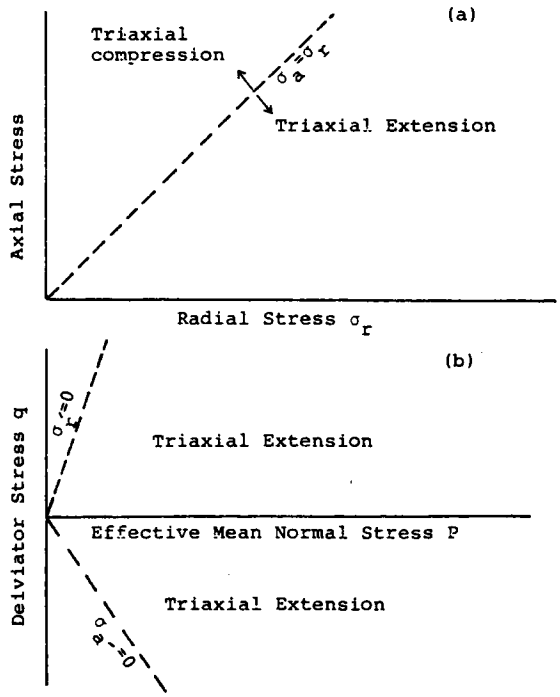

Fig.7.1 Possible range of stress in conventional triaxial test with cylindrical specimen.

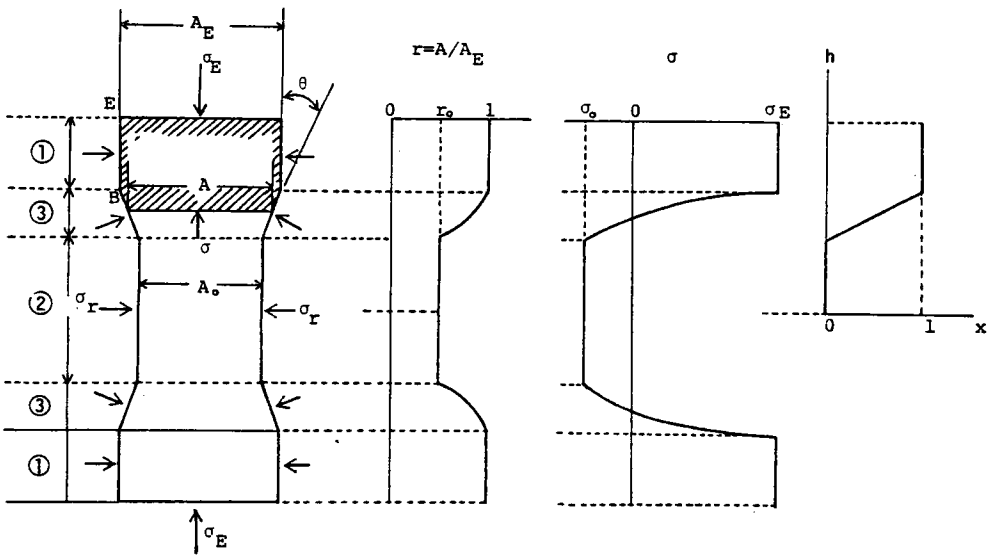

Fig.7.2 Stresses acting on a bone-shaped specimen and variations of area ratio r and average normal stress σ on an arbitrary plane.

where r_0 is the value of r at the narrow portion. This equation shows that σ_0 can be negative, i.e., σ_0 can be tensile normal stress when r_0 is smaller than 1, and also that, if r_0 is known, σ_0 of negative value can be evaluated.

7.3 EXPERIMENTS

7.3.1 Samples Used

A remoulded clay called Fujinomori Clay and two kinds of undisturbed diluvial clays, called in this chapter OT Clay and ON Clay, were used. The undisturbed clays were obtained by boring at certain sites in Osaka Prefecture. The method for preparation of the remoulded sample is the same as that described in Chapter 2. Their consistency limits are given in Table 7.1.

A special tool, shown in Photo 7.1, was used to trim the samples to be bone-shaped specimens. Representative dimensions of both cylindrical specimens and bone-shaped specimens are shown in Fig.7.3.

Every specimen was, firstly, isotropically consolidated up to a pressure prescribed consolidation stress. For the remoulded sample, the consolidation stress was removed so that a prescribed value of OCR was obtained. For undisturbed samples, the rebound was not done because they had been probably overconsolidated by the geological action. Indeed, by performing oedmeter tests on these samples, maximum preconsolidation stresses were estimated as shown in Table 7.1.

7.3.2 Experimental Procedure

Table 7.1 Consistency limits of samples used.

Samples		Consistency			Preconsolidation stress
Name	Type	P.L.	L.L.	P.I.	p_c (kPa)
Fujinomori Clay	Remoulded	26	48	22	-
Osaka Taisho Clay (OT)	Undisturbed Dilluvial	31	83	52	510*
Osaka Nanko Clay (ON)	Undisturbed Dilluvial	41	128	87	206*

N.B. * Determined from oedometer test.

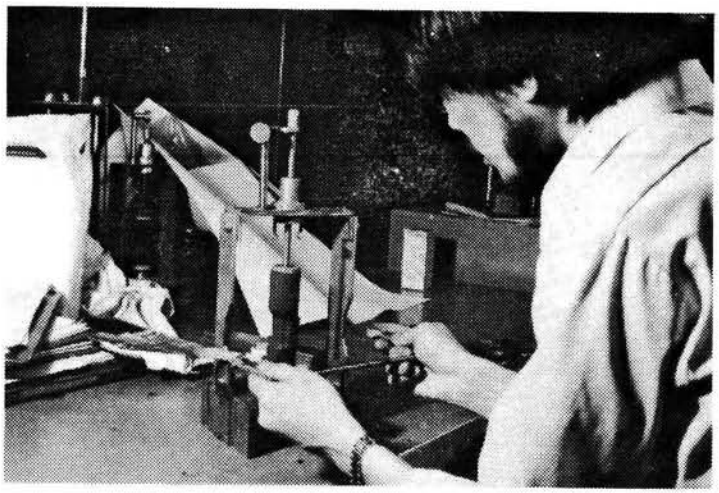

Photo 7.1 Special tool for preparation of bone-shaped specimen.

Four main series of tests were conducted:

Series 1 : Triaxial extension tests were carried out using both bone-shaped specimens and cylindrical specimens of the remoulded sample. The resulted stress-strain behaviours were compared to examine fundamental characteristics of the triaxial extension test by the use of bone-shaped specimens;

Series 2 : The effects of the confining stress and the degree of the overconsolidation on the tensile strength were investigated. The remoulded sample was mainly used; and

Series 3 : Two undisturbed samples were used to estimate tensile strengths of cohesive soils in the field.

For three series above, strain-controlled drained tests were performed except one test in series 2, which was performed under undrained condition to investigate the effect of the drainage condition on the effective stress state at failure.

Series 4 : After the completion of preconsolidation, prescribed deviator stress was applied under the drained condition. Creep deformation under negative or tensile normal stress as well as positive or compressive stress was examined. For this purpose the remoulded sample was used.

The rate of axial deformation of 0.008 %/min was ordinarily employed for the remoulded sample, and it was 0.0008 %/min for undisturbed samples.

7.4 FUNDAMENTAL INVESTIGATION OF THE TRIAXIAL EXTENSION TEST FOR BONE-SHAPED SPECIMENS

7.4.1 Method for Correction of Strain Non-Uniformity

Problems accompanied with the mechanism of the triaxial extension test of bone-shaped specimens are presented and examined in this section. A method for correcting the strain non-uniformity, which is one of the most important probles, will be proposed and the efficiency of the method will be demonstrated.

(1) Non-Uniformity of the Strains

A result from one of triaxial extension tests using bone-shaped specimens is presented in Fig.7.4. Variations of axial stress in the narrow portion σ_0 and two deviator stresses $\sigma_r-\sigma_E$ and $\sigma_r-\sigma_0$ and volumetric strain in the whole specimen v with axial strain ε_a are shown. The uniformity of strains was assumed in this figure. They were calculated as follows:

$$v = -\ln(V_t/V_{t0}); \text{ and } \varepsilon_a = -\ln(H_t/H_{t0}) \quad \text{.....(7.5)}$$

where V_t and H_t denote the total volume and total height of the specimen,respectively, and V_{t0} and H_{t0} are the initial values of V_t and H_t ,respectively.

This figure shows that there exist two values of axial stress corresponding to one value of axial strain. This means that stress-strain relationship varies from part to part within the specimen. This discrepancy with the principle of mechanics has resulted from the assumption of the uniformity of strains. Consequently, the assumption is not proper and a method for correcting the non-uniformity must be considered.

We may assume that there would exist a limited zone in which the strain is uniform although the strain cannot be uniform over the whole specimen. Further, we assume that it is uniform

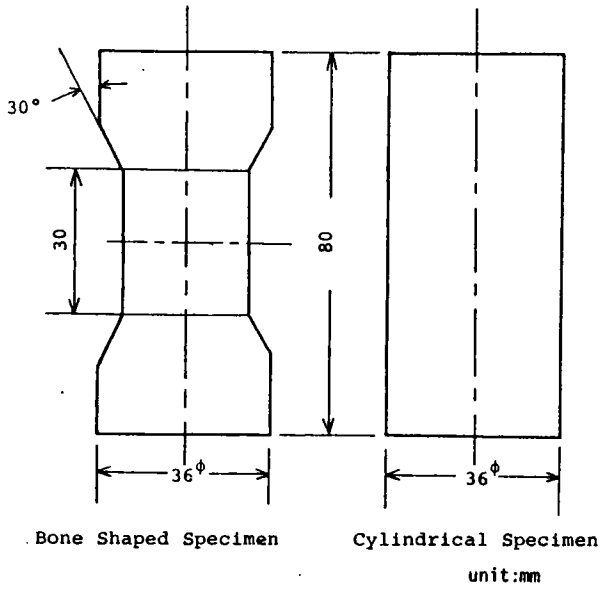

Fig.7.3 Typical dimensions of a bone-shaped specimen and a cylindrical specimen.

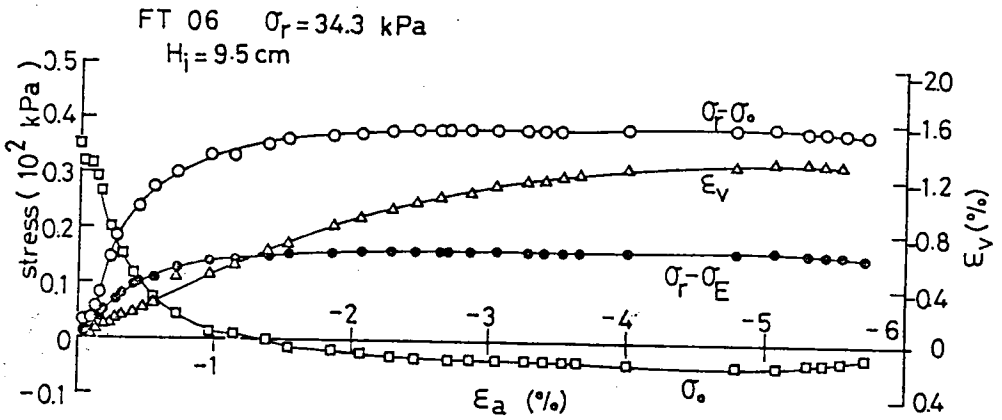

Fig.7.4 Representative results of a triaxial extension test by the use of a bone-shaped specimen.

entirely in the thick part and in the narrow part, and that over in the intermediate part (denoted ③ in Fig.7.2) it is not uniform.

The change in the height and the volume of the whole specimen ($\Delta H_t, \Delta V_t$) may be divided into three components: one is resulted from the change of the thick part ($\Delta H_1, \Delta V_1$); one is resulted from the change of the narrow part ($\Delta H_2, \Delta V_2$); and the rest is the change of the intermediate part ($\Delta H_3, \Delta V_3$). We obtain the following equation for the change in the height of the specimen.

$$\begin{aligned} \Delta H_t &= \Delta H_1 + \Delta H_2 + \Delta H_3 \\ &= -\left(H_{10}\varepsilon_{a1} + H_{20}\varepsilon_{a2} + \int_0^{H_{30}} \varepsilon_{a3} dh \right), \end{aligned} \qquad \cdots\cdots\cdots (7.6)$$

where the subscript 0 denotes the reference state and h is a variable concerned with longitudinal distance as shown in Fig.7.2. An analogous equation is derived for the volume change. In the following discussion, when obtaining equations for the volume change, H and ε_a may be replaced by V and v, respectively.

(2) Assumption on the strain in the intermediate part

Following three cases will be considered with respect to the evaluation of ε_{a2} so that the problem might be simplified:

Case A: Strain in the intermediate part is assumed to be uniform and equal to that in the thick part,i.e.,

$$\varepsilon_{a3} = \varepsilon_{a1} \qquad \cdots\cdots\cdots\cdots\cdots (7.7a)$$

Case B: Strain in the intermediate part is assumed to be uniform and equal to that in the narrow part,i.e.,

$$\varepsilon_{a3} = \varepsilon_{a2} \qquad \cdots\cdots\cdots\cdots\cdots (7.7b)$$

Case C: Strain in the intermediate part is assumed to be linearly related to the strains in the thick part and narrow part,i.e.,

$$\varepsilon_{a3} = (\varepsilon_{a1} - \varepsilon_{a2}).x + \varepsilon_{a2} \quad \text{.....(7.7c)}$$

where x is a function of h as shown in Fig.7.2.

For each case above, ε_{a2} can be derived as follows:

$$\varepsilon_{a2} = \begin{cases} -\{\Delta H_t + (H_{10}+H_{30}).\varepsilon_{a1}\}/H_{20} & \text{for Case A.....(7.8a)} \\ -(\Delta H_t + H_{10}.\varepsilon_{a1})/(H_{20}+H_{30}) & \text{for Case B.....(7.8b)} \\ -\{(2H_{10}+H_{30}^2.\tan\theta).\varepsilon_{a1}+2\Delta H_t\}/\{2(H_{20}+H_{30})-H_{30}^2.\tan\theta\} & \text{for Case C.....(7.8c)} \end{cases}$$

where θ is the angle between the longitudinal axis and the surface of the intermediate part. Among the quantities in the right side of these equations, ΔH_t can be measured by the use of a dial gauge; H_{10}, H_{20} and H_{30} are the heights at the reference state, namely, at the end of the isotropic consolidation stage prior to shearing and they can be obtained by the reasonable assumption that the strain during the isotropic consolidation stage is isotropic; and ε_{a1} is unknown.

Equations (7.8a) to (7.8c) imply that, if we know the axial strain in the thick part ε_{a1} in any way, we can evaluate the axial strain in the narrow part ε_{a2} The strain in the intermediate part ε_{a3} can be evaluated by the use of eq.(7.7) in each case.

(3) Estimation of the axial strain in the thick part

If the thick part of a bone-shaped specimen is considered to be a part of a conventional cylindrical specimen, the stress-strain relations of the cylindrical specimen under the same

stress condition and having the same diameter as those of the bone-shaped specimen will represent the stress-strain relations of the thick part so far as the range of stress induced in the thick part is not beyond the range of stress mobilized in the cylindrical specimen.

From the equlibrium of forces on the portion between E and B of the bone-shaped specimen (see Fig.7.2), the following relation is obtained:

$$T/A_{E0} = (\sigma_r-\sigma_E).(1-v_1)/(1-\varepsilon_{a1}) \quad \ldots\ldots(7.9)$$

where T is the force giving the deviator stress, A_{E0} is the cross sectional area of the end plane at the beginning of shearing and subscript 1 denotes the quantities in the thick part. A similar equation is obtained for the cylindrical specimen:

$$T/A_{E0} = (\sigma_r-\sigma_a).(1-v)/(1-\varepsilon_a) \quad \ldots\ldots(7.10)$$

Eqs.(7.9) and (7.10) imply that, when the state of stress and strain within the thick part of the bone-shaped specimen is equivalent to that within the cylindrical specimen, the value of the quantity T/A_{E0} must be common to both tests. In consequence, if we perform the test using the cylindrical specimen and the test using the bone-shaped specimen under the same condition of stress history and the rate of deformation etc., we can evaluate the strain within the thick part of the bone shaped specimen using T/A_{E0} as ameasure of the stress-strain state.

(4) Application of the method proposed and the results

Three cases were applied to a test with a bone-shaped specimen. Another test with a cylindrical specimen in which the

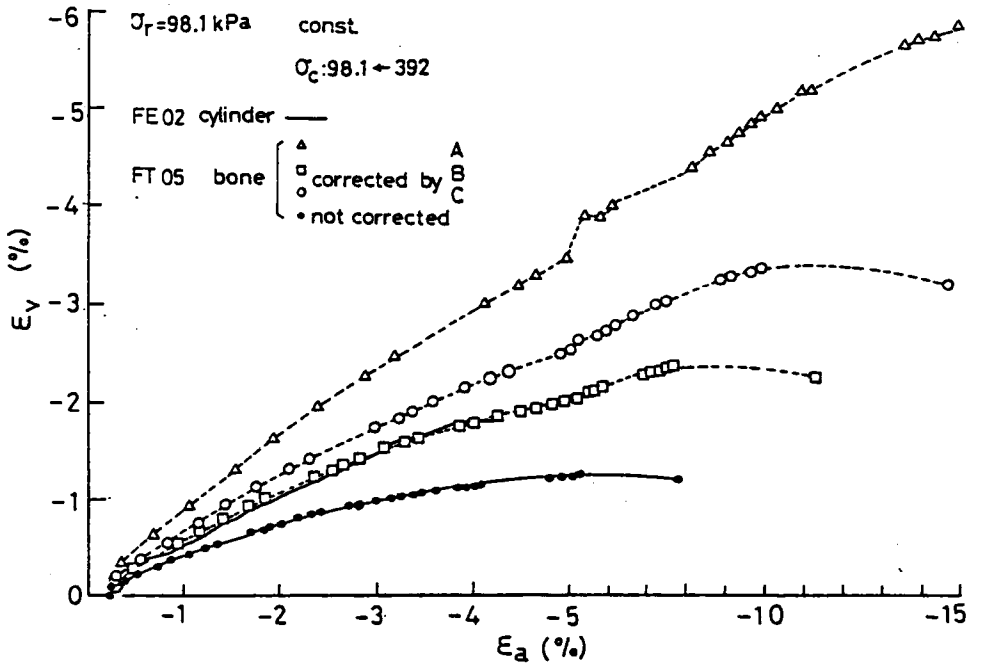

Fig.7.5 Corrected relations between volumetric strain and axial strain for the narrow part.

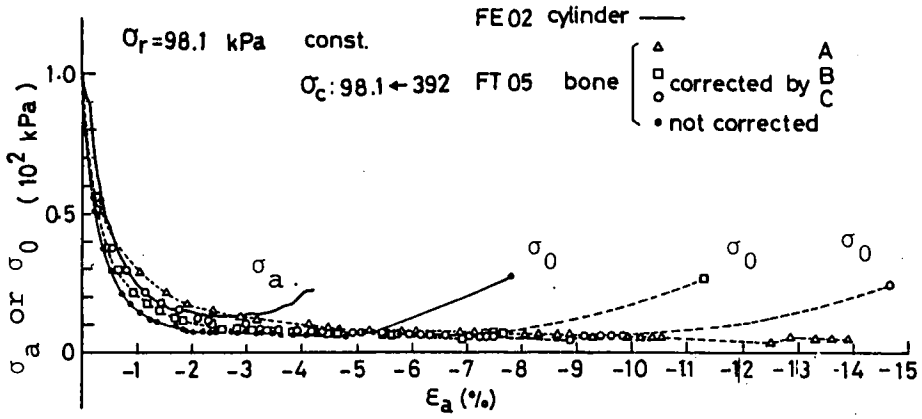

Fig.7.6 Corrected relations between axial normal stress σ_0 and axial strain ε_a

stress condition,i.e., the state of σ_a (or σ_E) and σ_r , was set to be the same as that in the former test was performed to evaluate the strain in the thick part of the bone-shaped specimen ε_{a1} and v_1.

Relations between volumetric strain v and axial strain ε_a in the narrow part are shown in Fig.7.5. A thick solid curve in this figure corresponds to the test with the cylindrical specimen. It can be seen that the tendency of the variation of v with ε_a is explained in the case B better than in other cases.

Fig.7.6 shows the relations between axial normal stress σ_0 and the axial strain ε_{a2} in the narrow part. From this figure, it seems that σ_0 at failure,i.e., at the state of minimal value of σ_0 , is not nearly affected by cases in the assumption.

We examine to which extent the proposed method for correction can evaluate the non-uniformity of strain. Fig.7.7 shows the distribution of measured water content in a specimen at the end of the test. From the figure the difference in volumetric strain between in the thick part and in the narrow part can be eatimated. The measured value of the difference in v is compared with tha calculated values using the proposed method for correction in Fig.7.8. It can be seen that by either the case B or C the measured value is well explained.

From the discussion above it is concluded that according to the assumed cases different stress-strain relations are obtained, but the value of axial stress at failur is not fairly dependent on the assumed cases and that among three cases

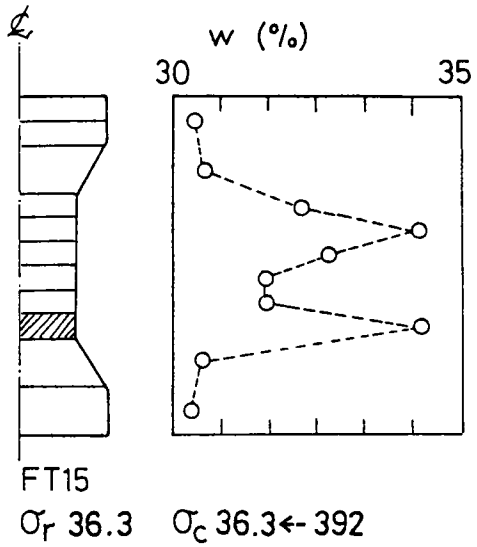

Fig.7.7 Distribution of water content at the end of the test.

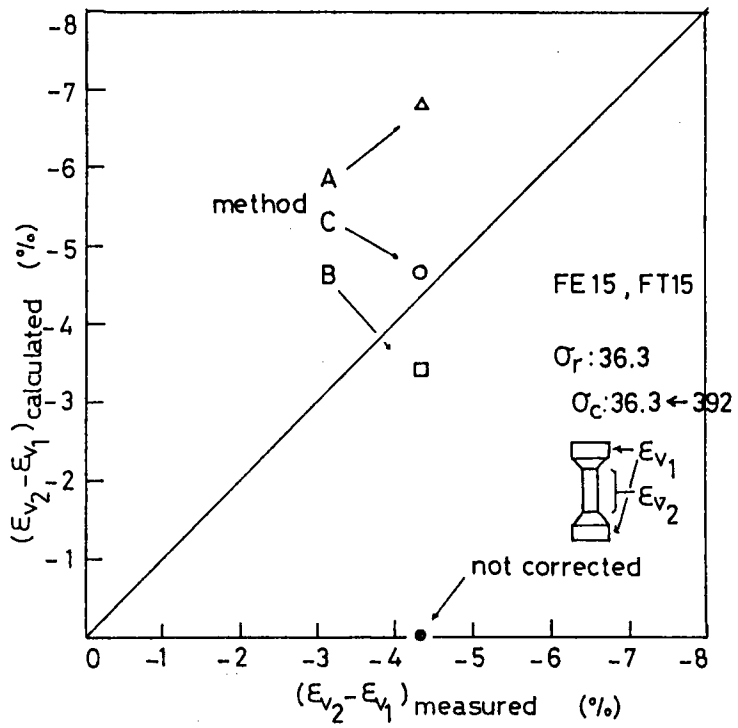

Fig.7.8 Difference in water content in the narrow part and in the thick part; comparison of the experimental and calculated results.

assumed, the case B seems to be the best.

7.4.2 Effect of the Rate of Deformation

Generally, even under the drained condition, excess porewater pressure is not dissipated and so applied total stress can not be regarded as effective stress unless the rate of deformation is enough slow. In order to examine the effect of the rate of deformation on the tensile strength, two tests were performed: one is a very slow drained test of which the deformation rate is about one-tenth the ordinary rate; and another one is an undrained test which might be considered identical to a very fast test in which the drainage is not allowed.

Fig.7.9 shows the effective stress paths of these tests. There is marked difference in the effective stress path. By analogy from the difference between these two, it is supposed that if we perform such a fast test, the dissipation of excess porewater pressure is not completely allowed; the tensile or shear strength will be overestimated; and also that the axial stress mobolized in the fast test will not be eventually tensile, but may be compressive. In the case examined here, the apparent "tensile" strength in the undrained test is about 7 times the drained tensile strength.

7.4.3 Effect of the Shape of Specimen

In order to investigate the effect of the difference in the shape of specimen on the extensional shear or tensile strength , both tests by the use of a cylindrical specimen and

by the use of bone-shaped specimen were performed for a certain condition of stress history.

Fig.7.10 shows the results of such tests, where non-corrected values of stress at failure are plotted because, as was concluded in the preceding section, the values of stress at failure is nearly independent of the cases in the assumption for correcting the strain non-uniformity or of whether the correction is made or not. It can be seen from this figure that strengths obtained when bone shaped specimens are used tend to be larger than those when the cylindrical specimens are used. As this reason, we can cite the difference in the rate of axial loading between two cases. Even if the axial strain rate is common in two cases, the increasing rate of tensinal loading in the narrow part of the bone-shaped specimen is always larger than in the case of the cylindrical specimen. This is easily understood because the condition such that:

$$| \sigma_0 - \sigma_r | > | \sigma_E - \sigma_r | \qquad \cdots\cdots\cdots\cdots\cdots\cdots (7.11)$$

is always valid during the test of the bone-shaped specimen. Consequently, as is supposed from the discussion on the effect of the rate of deformation, strengths measured by the use of the bone-shaped specimen can be probably overestimated.

7.4.4 Modes of Failure

In fig.7.11, several views of specimens at failure are sketched. Both the tests No.FT04 and No.FE04 have the same stress history but the shape of specimen is different from each other. The bone-shaped specimen seems to have failed in tension,

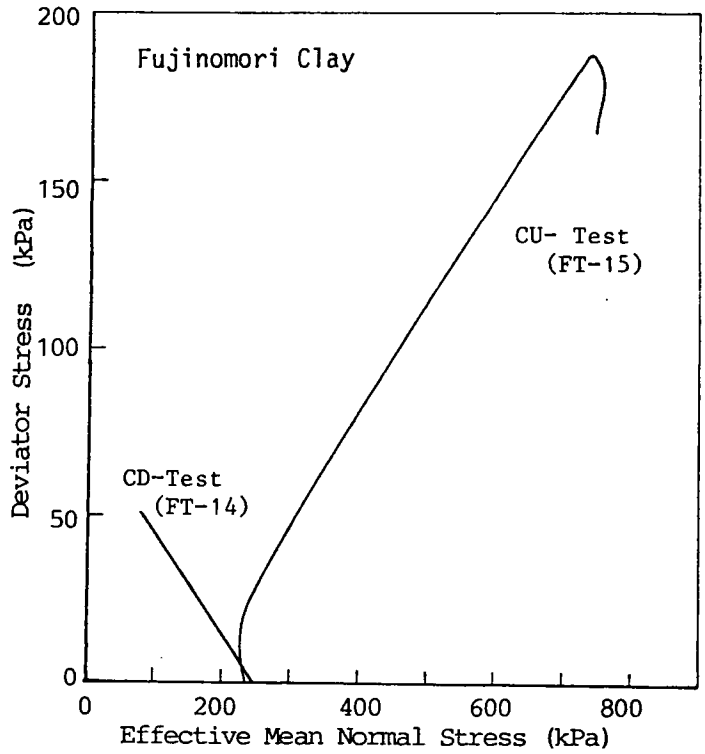

Fig.7.9 Comparison of effective stress paths for undrained and drained tests.

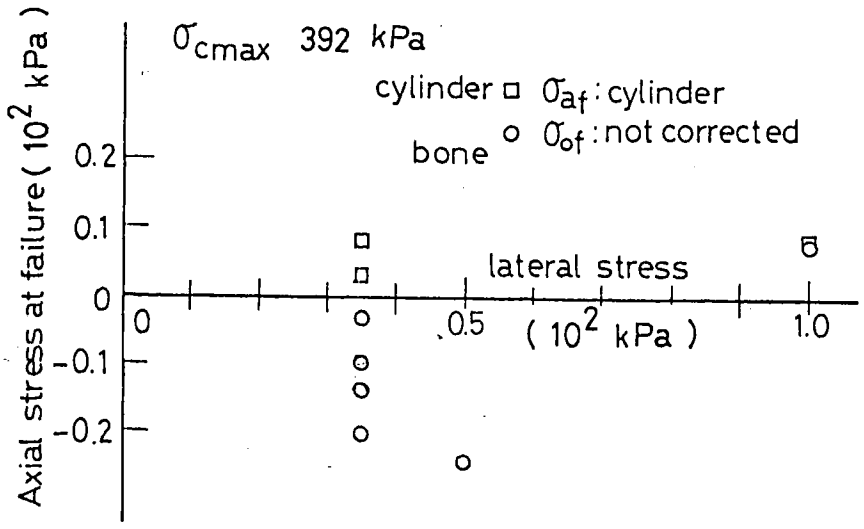

Fig.7.10 Effects of the shape of specimen on the strength

but the cylindrical specimen failed by shear. The mode of failure may be possibly dependent on the type of the shape of specimen.

Iyer(1975) has given an interesting observation on the tensile failure of remoulded soils. According to him, the angle of the failure plane can be 90° from the direction of axial stress even for some cases in which axial stress is not negative. From this reason, he explains that: in the low confining stress, local or micro-scopic negative stress can cause the initiation of the micro-fissure and the microfissure grows to be the tensile rupture plane; on the other hand when the confining stress is relatively high, the occurrence of such microfissure may be prevented and the frictional behaviour is observed. This interpretation seems to be valid for remoulded soils because they have not high tensile strengths.

Thus, judgement whether the mode of failure is tensile or not will be made by observing the inclination of failure plane.

7.5 TENSILE STRENGTH OF COHESIVE SOILS

7.5.1 Remoulded Clays

A series of tests were performed to examine the effect of the confining stress and the degree of overconsolidation on the tensile strength of remoulded clays.

In Fig.7.12, Mohr's circles of stress at failure are shown. They had been consolidated at the maximum all round pressure

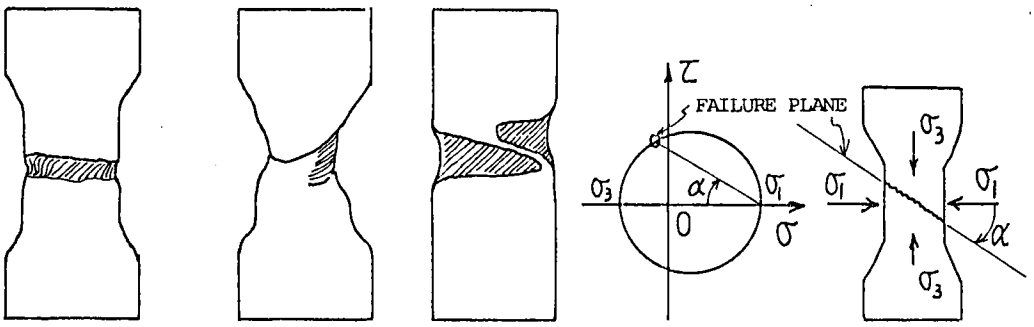

FT 04
σ_{cmax}= 329
σ_r= 34.3
σ_{0f}=-9.12

FT 05
σ_{cmax}=329
σ_r= 98.1
σ_{0f}=8.04

FE 04
σ_{cmax}=329
σ_r=34.3
σ_f= 7.85

Fig.7.11 Modes of failure

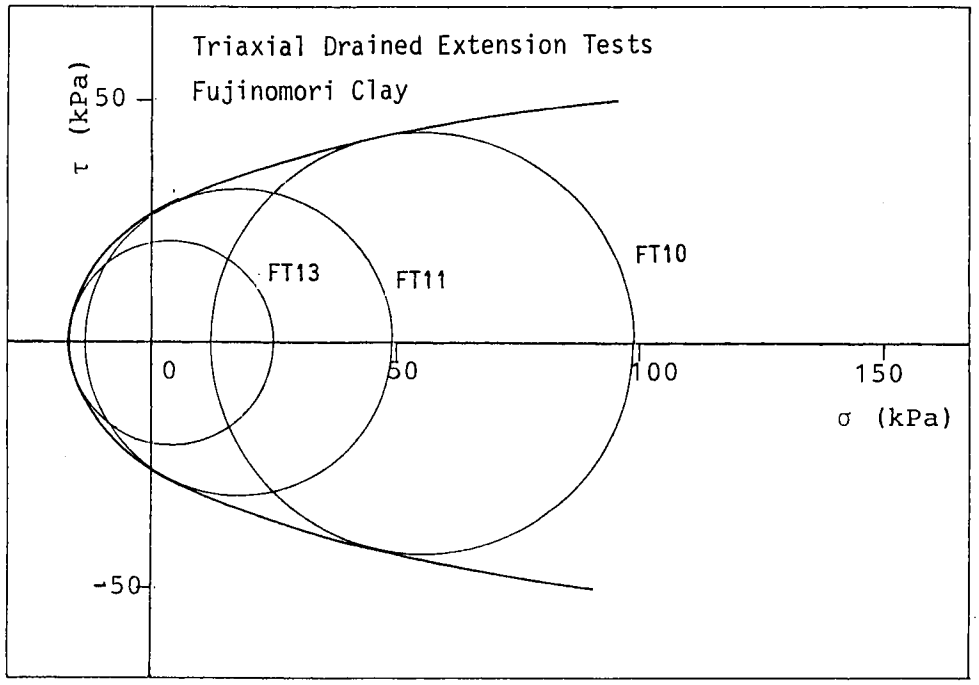

Fig.7.12 Mohr's circles of stress at failure

of σ'_{cmax}=981 kPa and subjected to the rebound to prescribed values of stress: σ'_{cmax}/OCR. From this figure we can examine the shape of the failure envelope at low confining stresses. From the observation that the mode of failure for test No.Ft.10 and FT11 was by shear and that for Test No.FT13 was tensile. The failure envelope was drawn so that it passed through points of $\tau \neq 0$ for the former tests and the point of $\tau=0$ for the last.

Fig.7.13 shows the state of stress at failure in terms of σ'_{0f} vs. σ'_r. In this figure the results of another series of tests in which σ'_{cmax} was 329 kPa are also shown. It had been expected that the tensile strength should be higher for the case of higher σ'_{cmax}, but, so far as the limited data as shown in this figure are concerned with, it is difficult to say so.

The shape of the failure envelope appears to be like that of cohesive material: i.e., in the range of σ'_r lower than about 50 kPa the variation of σ'_{of} with σ'_r is relatively small. On the other hand, in the higher level of σ'_r , the type of the failure envelope appears to become frictional. This appearance coincides with the observation of the failed specimens which was mentioned in the preceding section.

Tensile strength is plotted against the value of OCR in Fig.7.14. The value of σ'_r during extension test is common to all the tests while maximum preconsolidation stress is varied. It is difficult to derive a definite conclusion with respect to the effect of OCR on the tensile strength from such limited data. However, if we venture to derive a tendency , it appears that σ'_{0f} is rather constant and independent of OCR. This is

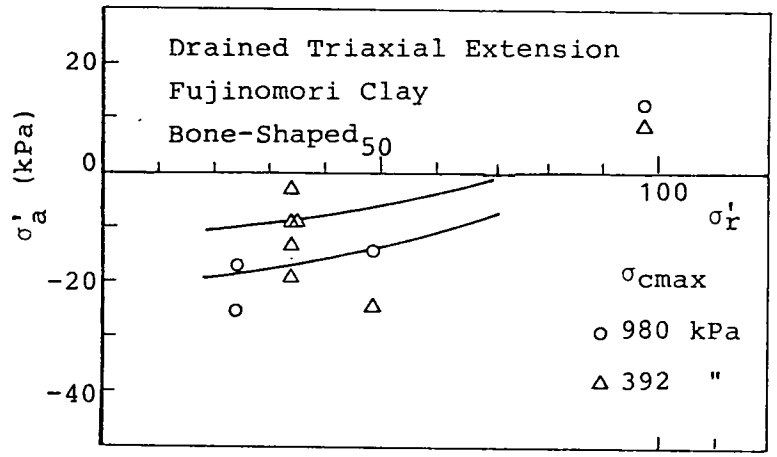

Fig.7.13 Failure envelopes for the remoulded sample

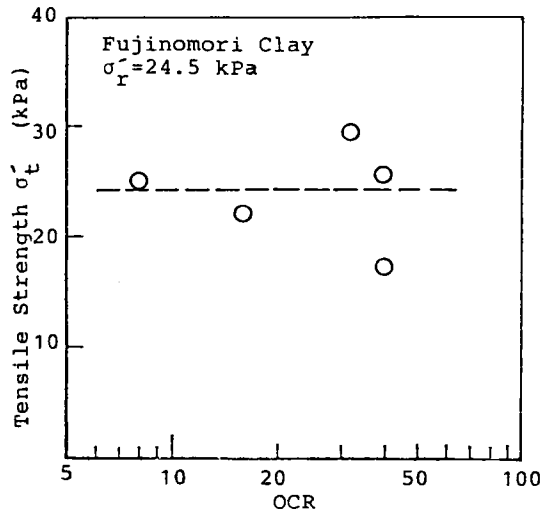

Fig.7.14 Tensile strength vs. OCR (remoulded sample)

not very irrelevant discussion because all the tests were performed under very low confining stresses and the type of failure was cohesive as was pointed out in the above.

7.5.2 Undisturbed Clays

A series of extension tests using bone-shaped specimens were performed for two undisturbed diluvial clays: ON Clay and OT Clay. For OT Clay the resulted stress-strain relationships are shown in Figs.7.15 and 7.16; for ON Clay in Figs.7.17 and 7.18.

For the relations between σ'_{0f} and ε_a shown in Figs.7.15 and 7.17, strains which develop before failure occurs for both samples are appreciably less than those for remoulded Fujinomori Clay(see Fig.7.4). This probably reflects the brittle nature of the cementation bonds between clay particles or between the aggregates of clay particles.

All the specimens tested failed at a plane perpendicular to the tensile axial stress, hence, the minimal value of the axial stress, σ'_{0f}, gives tensile strength σ_t.In Fig.7.19, the tensile strength σ_t is plotted against the confining stress σ'_r. In this figure, for comparison, the result for Blue London Clay (Bishop & Garga,1969) are also shown.

It is apparent from Fig.7.19 that these undisturbed clays can withstand substantial tensile stresses, and that the tensile strength for each sample is almost independent of the confining stress in the range examined as in the case for remoulded sample. This was also pointed out by Bishop & Garga(1969).

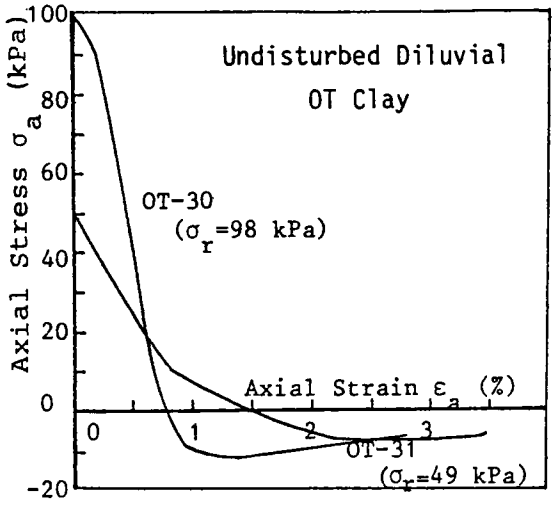

Fig.7.15 Axial stress vs. axial strain (undisturbed OT clay)

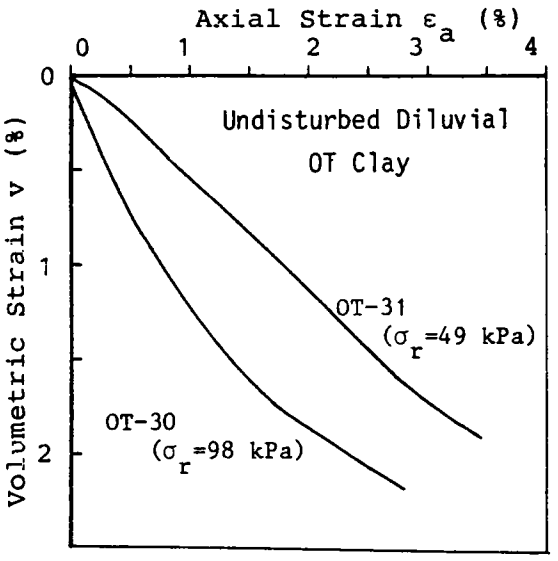

Fig.7.16 Volumetric strain vs. axial strain (undisturbed OT clay)

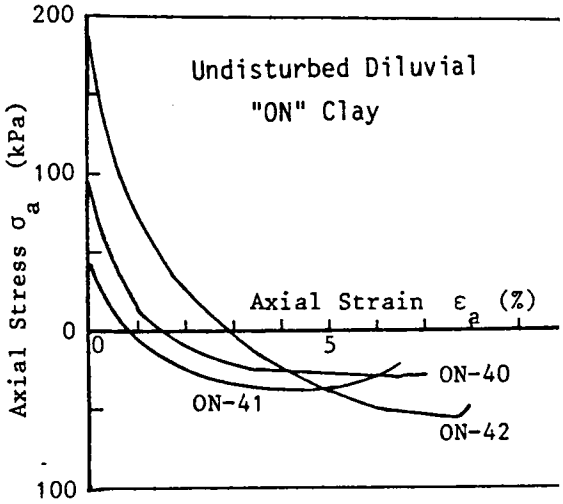

Fig.7.17 Axial stress vs. axial strain (undisturbed ON clay)

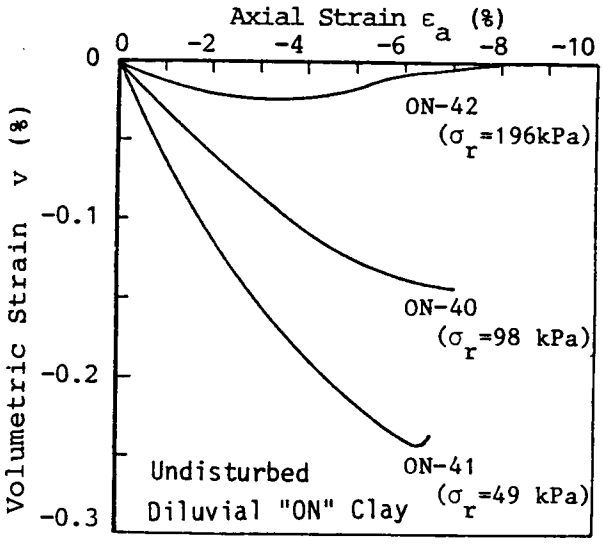

Fig.7.18 Volumetric strain vs. axial strain (undisturbed ON clay)

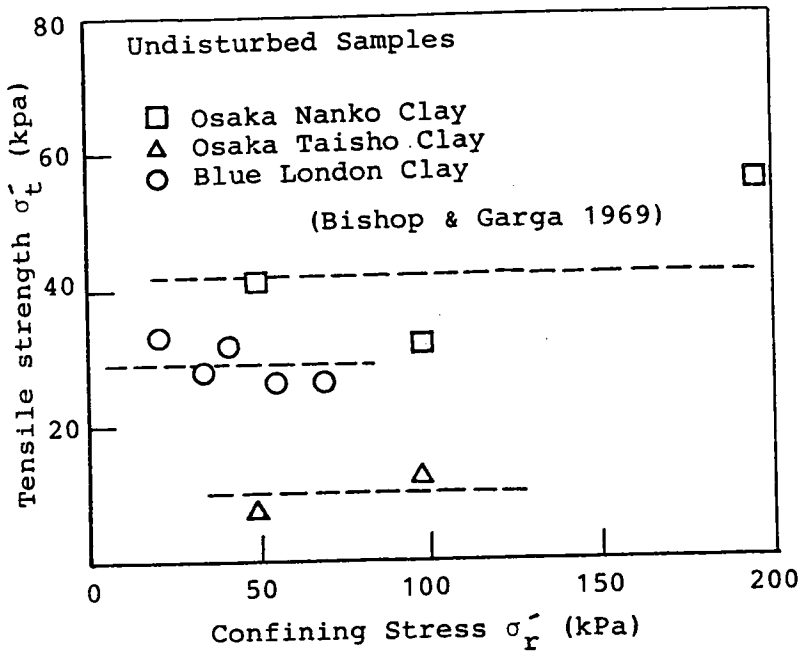

Fig.7.19 Tensile strengths vs. effective confining stress for undisturbed clays

The tensile strength lies in the range of 8 to 13 kPa for OT Clay and 32 to 56 kPa for ON Clay, and the tensile strength of London Clay lies between them. The difference in plasticity index (P.I.) between these three undisturbed clays should be noticed when explaining the difference in the tensile strength. P.I. for ON Clay of which the tensile strength is the highest of these three is 87 %; this is much higher than others, 51 % for OT Clay and 46 % for London Clay. More data for other undisturbed clays are required to derive a definite conclusion with respect to the dependency of the tensile strength on P.I..

The level of the tensile strength of the remoulded sample seems to be comparative to those of undisturbed clays. The tensile strength of the remoulded clay seems too high if it is accepted that the cementation bonds of undisturbed clays would have been destroyed by remoulding them. As was described in sec.7.3.2, the rate of axial deformation for the remoulded clay was about ten times that for undisturbed clays. It appears that the discussion given in sec.7.4.2 may be applied to explain such high tensile strength for the remoulded sample.

7.6 CREEP CHARACTERISTICS UNDER TENSILE NORMAL STRESS

Creep characteristics under low effective stresses ,including negative or tensile stresses, are treated.

7.6.1 Transient Creep

After the completion of preconsolidation stage, prescribed deviator stress was applied under the drained condition. σ'_{cmax} was 785 kPa and confining stress σ'_r during the creep test was

24.5 kPa. The deviator stress q was varied from specimen to specimen. Cylindrical specimens were not used, but bone-shaped specimens were tested.

Axial strain ε_a and volumetric strain v are plotted against the logarithm of the elapsed time t in Figs.7.20 and 7.21, respectively. The correction of the non-uniformity of strains is not made in these figures. Creep rupture was observed for four specimens; their levels of creep stress were all higher than others.

The variations of the absolute values of the rates of strain , $|\dot{\varepsilon}_a|$ and $|\dot{v}|$, with the elapsed time are shown in Figs.7.22 and 7.23, respectively, in the form of log-log plot. Denoting the strains at sequential times t_i and t_{i+1} $(t_{i+1}>t_i)$ by ε_i and ε_{i+1},respectively, the strain rate at time t_{i+1}, $\dot{\varepsilon}_{t=t_{i+1}}$, was defined as $(\varepsilon_{i+1}-\varepsilon_i)/(t_{i+1}-t_i)$.

It can be seen from Figs.7.22 and 7.23 that, for specimens without creep rupture, each of curves may be divided into two stages: the initially observed stage may be called "quasi-steady state" in the sense that the change in $\log|\dot{\varepsilon}_a|$ or $\log|\dot{v}|$ is fairly less than in the following stage; the second is the transient stage. Specimens which ruptured at relatively early time ($t \leq$ 300 min) enters into the steady stage immediately after the "quasi-steady stage" without experiencing the transient stage and fail.

The creep behaviour in the "quasi-steady state" is explained in Fig.7.24. The effective stress state at onset of the creep stress might lie on the effective stress path of undrained test.

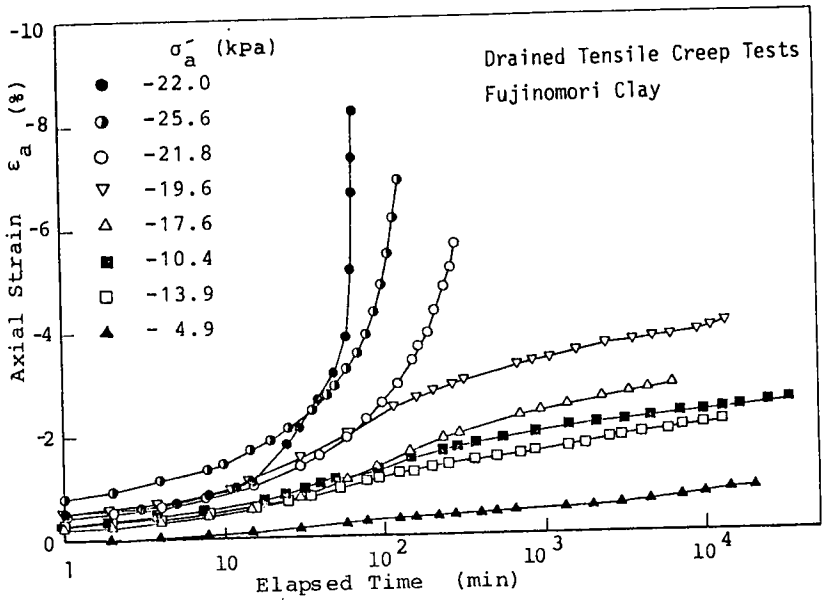

Fig.7.20 Variations of axial strain with time during creep tests

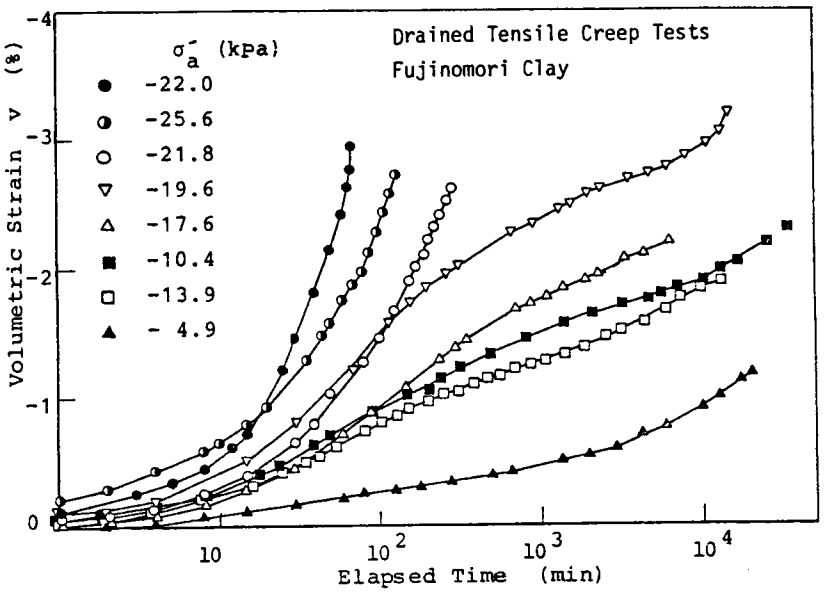

Fig.7.21 Variations of volumetric strain with time during creep tests

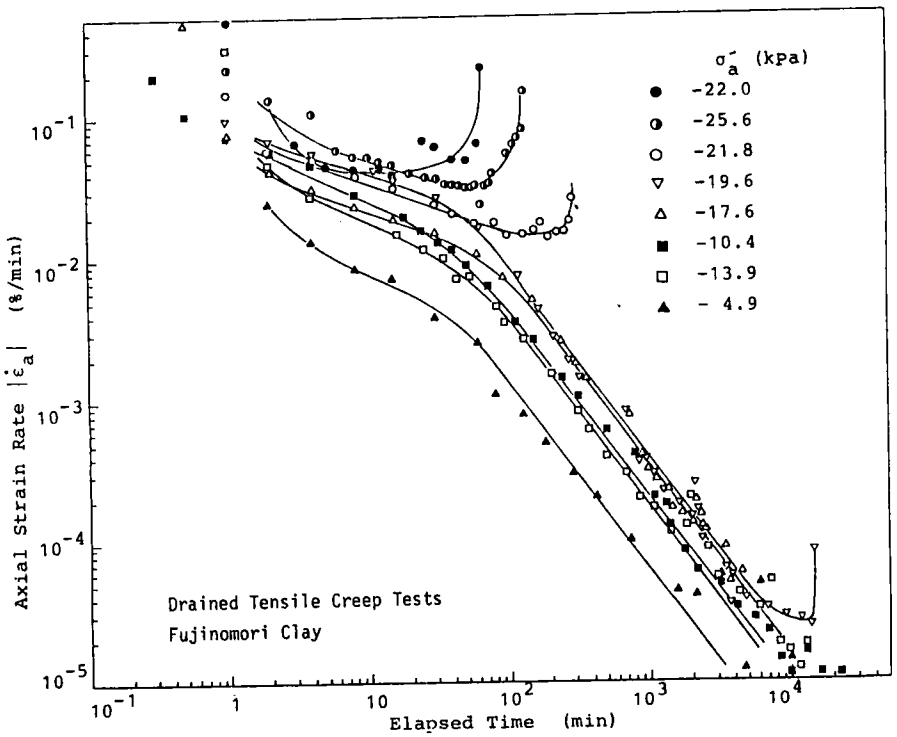

Fig.7.22 Axial strain rate vs. log t

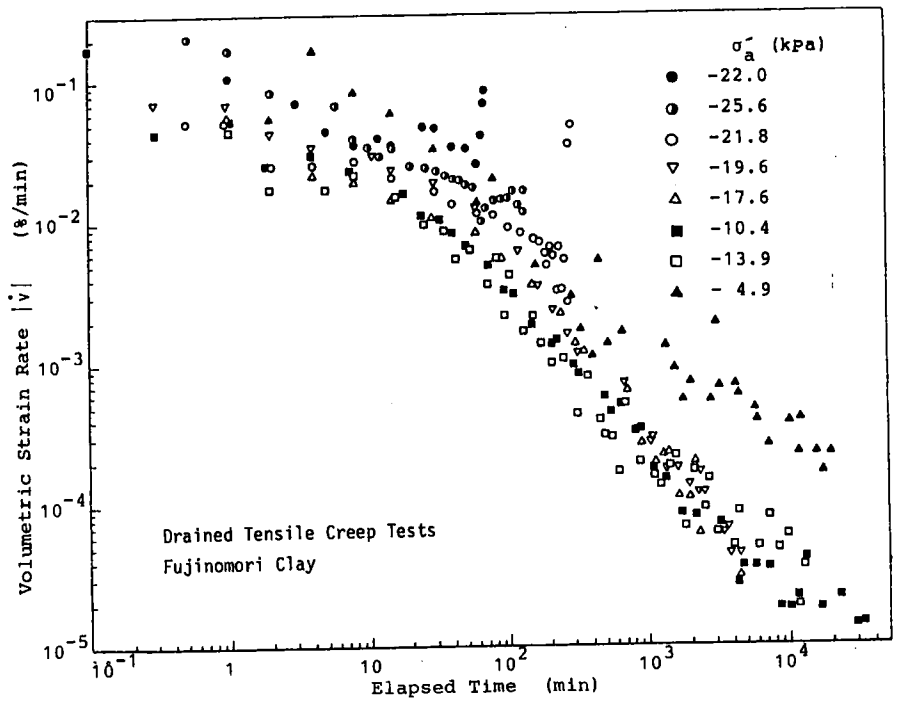

Fig.7.23 Volumetric strain rate vs. log t

The state of stress moves along the line of q=constant with time; the effective mean normal stress p is gradually decreased with time; the decrease of p with time results in the increase of stress ratio $\eta=q/p$; the increase of η cancels the damping tendency of creep deformation; and therefore the totally observed rate of strain is less during this "quasi-steady state" than the second transient state. The decrease in p with time causes also the volume expansion by which the damping tendency of creep volume change is resisted (see Fig.7.23)

In the second transient stage, the relations for all the specimens are expressed by straight lines which have a certain slope. This is expressed by

$$\log|\dot{\varepsilon}_a| = B + m.\log(t/t_0) \qquad \text{.....(7.12)}$$

where t_0 is a reference time, B is the value of $\log|\dot{\varepsilon}_a|$ at $t=t_0$ and m is the slope of the straight lines. m is independent of the creep intensity, but B is probanly a function of the creep intensity. In fact, the value of B extrapolated from the curves in Fig.7.22 is plotted against σ_a in Fig.7.25. From the figure, B may be considered proportional to σ_a, resulting in

$$B = \alpha.\sigma_a + A'. \qquad \text{.....(7.13)}$$

Combining eqs.(7.12) and (7.13), we obtain the following three parameters equation:

$$|\dot{\varepsilon}_a| = A.e^{\alpha|\sigma_a|}.(t/t_0)^m \qquad \text{.....(7.14)}$$

Alternatively, we can displace ε_a and σ_a by ε and q,respectively, since similar results to those discussed in the above was also obtained for the rate of shear strain $\dot{\varepsilon}$ and shear

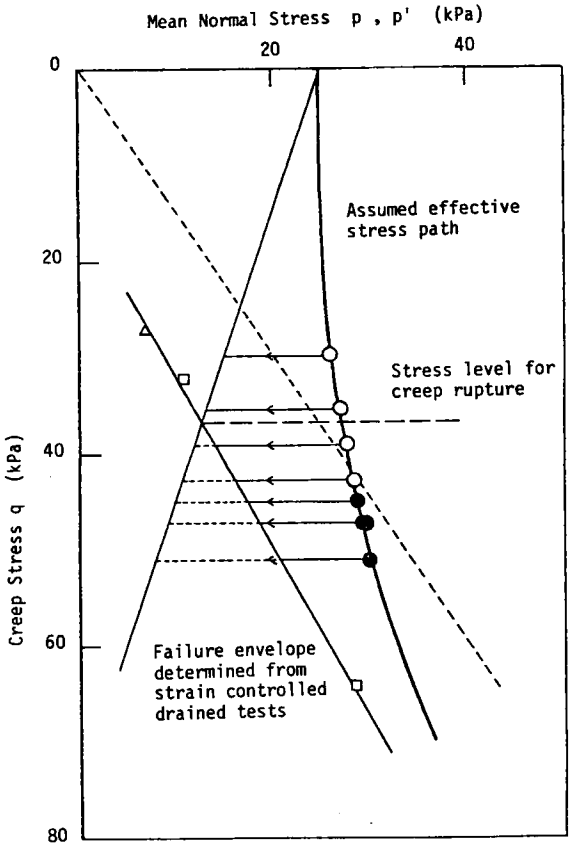

Fig.7.24
Interpretation of drained tensile creep tests

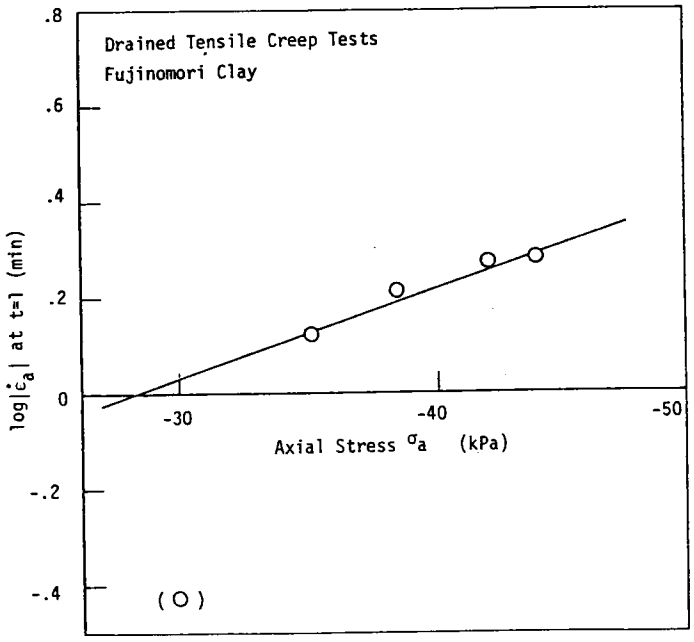

Fig.7.25
Variation of the coefficient B with creep intensity

stress q (Fig.7.26), thus we obtain

$$|\dot{\varepsilon}| = A.e^{\alpha|q|}(t/t_0)^m \qquad \text{.....(7.15)}$$

This equation is quite the same as the creep equation derived by Mitchell(1976). Various kinds of soils and test types were considered, however, the test data were only concerned with drained or undrained compression condition.

Here, it is interesting that the Mitchell's equation can be extended to the creep deformation during transient stage under tensile normal stress.

It should be noted, as pointed out by Mitchell(1976), that this equation is only phenomenological equation and it does not imply anything about the mechanism underlying the deformation process. In other words, the creep deformation phenomenon under tensile normal stress can be expressed as in the case of compressive stress, although the deformation mechanism will probably differ from that under the compressivs stress.

7.6.2 Creep Rupture

Saito & Uezawa(1961) found an experimental relationship between minimum strain rate $\dot{\varepsilon}_s$ and the time to creep rupture t_f by conducting undrained triaxial or unconfined compression tests on undisturbed silty, clayey and loam soils:

$$t_f.\dot{\varepsilon}_s = \text{constant.} \qquad \text{.....(7.16)}$$

Sekiguchi(1971) also found the following relation performing undrained triaxial creep tests on an undisturbed alluvial clay.

$$t_*.\dot{\varepsilon}_s = \text{constant,} \qquad \text{.....(7.17)}$$

where t_* is t_s, t_a or t_f (t_s is the time when the minimum strain

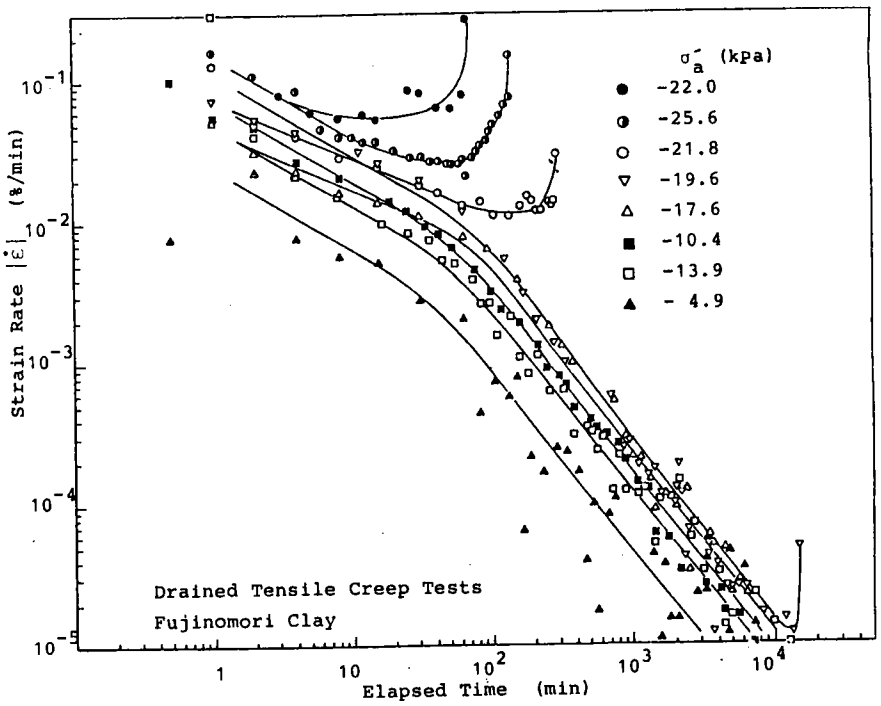

Fig.7.26 Shaer strain rate vs. log t

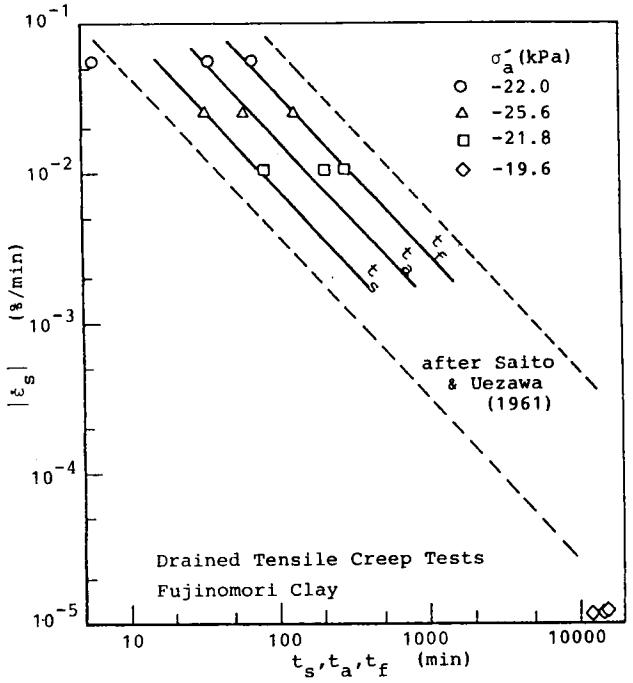

Fig.7.27
Minimum shear strain rate vs. t_s, t_a and t_f

rate appears; t_a is the time when accelerated creep begins; and t_f is the time of the creep rupture). Mitchell(1976) used such a type of equation as eq.(7.16) as the possible principle relating the creep rupture to the time of it and presented an equation for the estimation of the constant included in eq.(7.16).

From Figs.7.22 and 7.26, it can be seen that the log of the minimum strain rate would be related to the log of the time to creep rupture. In fact, Fig.7.27 shows that the relations between $|\dot{\varepsilon}_s|$ and t_f are such as eq.(7.16). In this figure, the relations proposed by Sekiguchi(1972) are also plotted. It is interesting that the empirical equation such as eq.(7.16) or (7.17) is also applicable for the creep rupture under tensile normal stress.

As was pointed out by Saito & Uezawa(1961), creep phenomena which accompany some cracks on the surface of soil slope are frequently observed. Taking into account that such cracks would have been caused by any tensile normal stress, the observation in Fig.7.27 is of practical importance when predicting the time to creep rupture under tensile normal stress.

7.7 CONCLUSION

For the purpose to clarify the strength and creep characteristics of clays under very low stress level including tensile nomal stress, drained triaxial extension tests using bone-shaped specimens were performed. The conclusions are summarized as follows:

i) The method for the measurement of tensile strengths of clays

proposed by Bishop & Garga(1969) is available for both undisturbed stiff clays and remoulded overconsolidated clays, although this method has some limitations.

ii) The most important shortcoming of this method is that strain and stress is not uniform within the bone-shaped specimen. However, to correct the direct or measured strains or stresses is possible, and it is particularly important that strength can be determined almost uniquely for a given soil with or without the correction of the strain non-uniformity.

iii) For both undisturbed and remoulded overconsolidated clays, tensile strengths do not depend on the confining stress, which indicates that the tensile strength of soil will be regarded as one of the mechanical properties of the soil.

iv) The effect of the rate of deformation was examined by performing an undrained test and a very slow drained test both of which have the same consolidation history. The result was used for the interpretation of the difference in tensile strength due to the difference in the shape of the specimen, and the creep behaviour during the transient creep stage.

v) Even under tensile normal stress, the empirical creep equation proposed by Mitchell(1976) is available for the trainsient creep stage.

vi) The prediction of creep rupture by equations by Saito & Uezawa(1961) or Sekiguchi(1972) is also applicable for tensile creep tests.

References for Chapter 7

Akazawa,T.(1943): "Method for determing internal stress by the compression of concrete", J.JSCE, Vol.29, No.11, pp.777-783.(in Japanese)

Ajaz,A. and Parry,R.H.G.(1975à):"Stress-strain behaviour of two compcted clays in tension and compression", Geotechnique, Vol.25, No.3, pp.495-512.

Ajaz,A. and Parry,R.H.G.(1975b): "Brazilian tensile test for soils: Discussion", Can. Geotech. J., Vol.12, pp.542-544.

Ajaz,A. and Parry,R.H.G.(1975c): "Analysis of bending stress in soil beams", Geotechnique, Vol.25, No.3, pp.586-591.

Ajaz,A. and Parry,R.H.G.(1976): "Bending test for compacted clays", Proc., ASCE, Vol.102, GT9, pp.929-943.

Ajaz,A.(1980): "Time-dependent behaviour of compacted clays in tension and compression", Geotechnique, Vol.30, pp.67-76.

Awaji,H. and Sato,S.(1978): "Failure condition under two dimensional stress and prediction of tensile strength", Materials, Proc., JSTM, Vol.27, No.295, pp345-355.(in Japanese)

Bishop,A.W. and Garga,V.K.(1969): "Drained tension tests on London Clay", Geotechnique, Vol.19, pp.309-313.

Colback,P.S.B.(1966): "An analysis of cracking in earth dams", Proc. Symp. Appl. Finite Element Method in Geotech. Eng., U.S. Waterw. Exp. Stn., Vicksburg, miss., pp.431-456.

Hasegawa,H. and Ikeuchi,M.(1962): "Uniaxial tensile test for disturbed soils", Proc. 17th National Conf., JSCE. Vol.III, pp.33-34.(in Japanese)

Hasegawa,H. and Ikeuchi,M.(1964): "On the tensile strength test of disturbed soils", IUTAM Symp., Grenoble, pp.405-412.

Hasegawa,H. and Utsuki,A.(1970): "Tensile strength of sandy clays", Proc. 25 National Conf., JSCE, Vol.iii, pp175-176.(in Japanese)

Helenelund,K.V.(1967): "Vane tests and tension tests in fibrous peat", Proc. Geotech. Conf., Oslo, Vol.1, pp.199-203.

Ingles,O.G. and Fridman,S.(1963): "An examination of some methods for strength measurement in soils", Proc. 4th Australia-New Zealand Conf. SMFE, Adelaide, pp.213-219.

Ito,M et al.(1974): "Method of tensile test for soils", Proc. 29th National Conf., JSCE, Vol.III, pp.210-212.(in Japanese)

Iyer,T.S.R.(1975): "The behaviour of Drammen plastic clay under low effective stresses", Can. Geotech. J., Vol.12, pp.70-83.

Kajitani,M. and Zaiki,K.(1975): "On the measurement of tensile strength for soil", Proc. 10th National Conf., JSSMFE, pp.261-264.(in Japanese)

Kazama,H. et al.(1976): "Characteristics in compression and tension of compacted soils", Proc. 31st National Conf., JSCE, Vol.III, pp.133-134.(in Japanese)

Krishnayya,A.V.G. and Eisenstein,Z.(1974): "Brazilian tensile test for soils", Can. Geotech. J., Vol.11, pp.632-642.

Lee,K.L. and Shen,C.K.(1969): "Horizontal movement related to subsidence", J. Soil Mech. Found. Div., ASCE, Vol.95, SM1, pp.139-166.

Leonards,G.A. and Narain,J.(1963): "Flexibility of clay and cracking of earth dams", J. Soil Mech. Found. Div., ASCE, Vol.89, SM2, pp.47-98.

Mellor,M. and Hawks,I.(1971): "Measurement of tensile strength by diametral compression of discs and annuli", Eng. Geol., Vol.5, No.3, pp.173-225.

Mitchell,J.K.(1976): Fundamentals of Soil Behaviour, John Wiley & Sons,Inc..

Narain,J. and Rawat,P.C.(1970): "Tensile strength of compacted soils", J. Soil Mech. Found. Div., ASCE, Vol.96,SM6, pp.2185-2190.

Narita,K.(1976): On the Mechnism of Crack Generation in Fill-Type Dams, Doctorial Thesis submitted to Tokyo Institute of Technology.(in Japanese)

Ohne,Y et al.(1976): "A tensile test of soils", Proc. 11th National Conf. SMFE, JSSMFE, pp.303-306.(in Japanese)

Ramiah,B.K. et al.(1977): "Some studies on the tensile strength of soils", Proc. 5th South-East Asian Conf. on Soil ENG., Bangkok, Thailand, pp. 327-337.

Saito,M. and Uezawa,T. (1961): "Failure of clays due to creep", Proc. 5th Int. Conf. SMFE, pp.315-318.

Sekiguchi,H.(1972): "Mechanical characteristics of clays subjected to various stress history", Graduation Thesis, Kyoto University, Faculty of Eng..

Suklje,L. and Drnovsek,J.(1964): "Investigation of the tensile deformability of soils using hollow cylinders", Proc. 6th Int. Conf. SMFE, pp368-372.

CHAPTER 8 SHEAR AND CONSOLIDATION CHARACTERISTICS OF STIFF OVERCONSOLIDATED CLAYS

8.1 INTRODUCTION

Terzaghi(1936) classified natural clays into the following three types:

i) Stiff fissured clay

ii) Stiff intact clay

iii) Soft intact clay

This chapter deals with the shearing behaviour and one dimensional compression behaviour of stiff intact or fissured clays.

Such stiff clays as diluvial or tertiary deposited clays generally appear to be heavily overconsolidated. As to the engineering problems particularly associated with their mechanical characteristics, we may cite following problems :

i) the problem of long term stability or delayed failure of soil structures or soil foundations resulting from remarkable dilatant behaviour (Terzaghi,1936; Skempton,1964 and 1970; Peck,1967);

ii) the progressive failure of soil foundations or soil slopes caused by the strain softening characteristics (Bjerrum,1967; Bishop,1967; Lo,1972; Palmer & Rice,1973. Rice,1973); and

iii) the land subsidence due to the compression of diluvial clay layer, of which importance has been rather recently recognized (Murayama et al.,1981).

Object of this chapter is to investigate mechanical characteristics associated with the engineering problems cited

above by performing conventional triaxial tests and oedometer tests on undisturbed diluvial clays. Firstly, stress-strain-pore water pressure behaviour in triaxial test is examined and its elasto-plastic properties are discussed. Strain softening behaviour is also discussed. Secondly, the results of a considerably long term one dimensional consolidation test is presented and so-called secondary compression behaviour is investigated. Also, the results of repeated loading tests are presented and the effect of the repetition of loading- unloading is examined.

8.2 ELASTO-PLASTIC BEHAVIOUR OF A STIFF OVERCONSOLIDATED CLAY*

8.2.1 Previous Studies

Mechanical characteristics of undisturbed London Clay concerned with particular engineering problems have been rigorously investigated by many reserchers (Ward et al., 1959; Bishop et al.,1965; Ward et al.,1965; Hooper & Butler,1966). Major interests were mainly focussed to their shear strengths. Because of its brittle nature, there exists a marked difference in peak shear strength and residual strength accompanied with large deformation. The determination of shear strength parameters for stability design has become problem. Quantitative evaluation of the strain softening behaviour which appears on such stiff clays as, e.g., London Clay seems to have been firstly made by Bishop(1967): he proposed an index called "Brittleness Index I_B" to express the degree of strain softening, and recommended to take it into account when performing stability analysis of

* partly reported by Shimizu(1980 a) and (1980 b)

slopes constituted of brittle soils.

Values of I_B determined from conventional consolidation undrained tests (CIU) and consolidation drained tests (CD) on samples of a layer Ma3 in Osaka Diluvial Formation was measured as 30 % for CIU and 40~56 % for CD tests, respectively (Murayama & Shimizu,1974). Bâzant(1976) and Prévost & Hoëg(1975) gave certain expressions when developing or constituting the stress-strain relationships for strain-softening material.

Strain-softening materials can be generally classified as "instable materials" in the sense that they are not satisfied with the "stable" condition of the hypothesis by Drucker(1959). Even when an instable material is treated, associated flow rule or normality condition was assumed by Palmer et al.(1967) and Prévost & Höeg(1975).

Certain conditions are required for rigidity of testing machine when performing such shear tests as triaxial compression tests on instable or strain softening materials (e.g. Sture & Ko, 1978).

Because of the vague definition of I_B, it has a substantial shortcoming that it depends on the choice of effective stress path during shear tests. The stress path dependency of I_B was examined by Law(1981).

More substantial appoach to the strain softening should be made based on the deformation behaviour, i.e., stress-strain formulation should be done. Stress-strain curves for strain softening materials are not one-to-one corresponding. Consequently, in order to formulate the relations between stress

and strain, it is necessary to give an experimental or hypothetical equation which represents the non one-to-one corresponding property

Attempts to develop the finite element method for boundary value problems associated with strain-softening soils have been made by Hoëg(1972), Pariseau(1972), Nayak(1972) and Desai(1974). Pressuremeter in strain-softening soil was analyzed by Prêvost & Hoëg(1975). It should be noted that their analysis would be applicable to only plastically incompressive soils under the undrained condition.

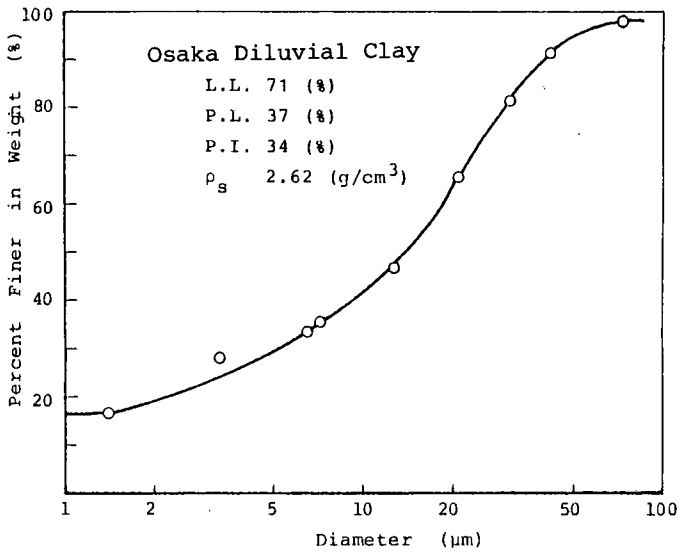

Fig.8.1: Physical properties and grain size distribution curve.

8.2.2 Experiments

(1) Sample Used

The sample used is undisturbed diluvial clay from Tondabayashi City, Osaka Prefecture. Block samples were taken and trimmed to be triaxial specimens of 10 cm^2 in cross section and about 8 cm in height. In Fig.8.1, consistency limits and grain size distribution curve are shown.

(2) Experimental Procedure

Isotropic consolidation and undrained triaxial compression tests (CIU) were performed. Two series of triaxial tests were conducted : one is consisted of monotonous loading test to investigate the fundamental behaviour; and another includes unloading-reloading cycle(s) and or stress relaxation-reloading cycle(s) during the shearing stage to investigate the visco-elastic or elasto-plastic behaviour.

8.2.3 Experimental Results and Discussion

(1) Monotonous Loading Tests

Figs.8.2 and 8.3 show the results of CIU tests. It appears that; each stress-strain curve is linear over a wide range of shear stress from the beginning of shear (Fig.8.2); as the shear stress mobilized q gets near to the peak, the linearity disappears; once the peak shear resistance is mobilized, the shear resistance decreases to a certain level; the decrease in shear stress stops at the strain level of about 1.5~2.0 % of axial strain and almost constant shear resistance is obtained at such relatively small strain as 4 %.

As to effective stress paths (Fig.8.3), for all tests except

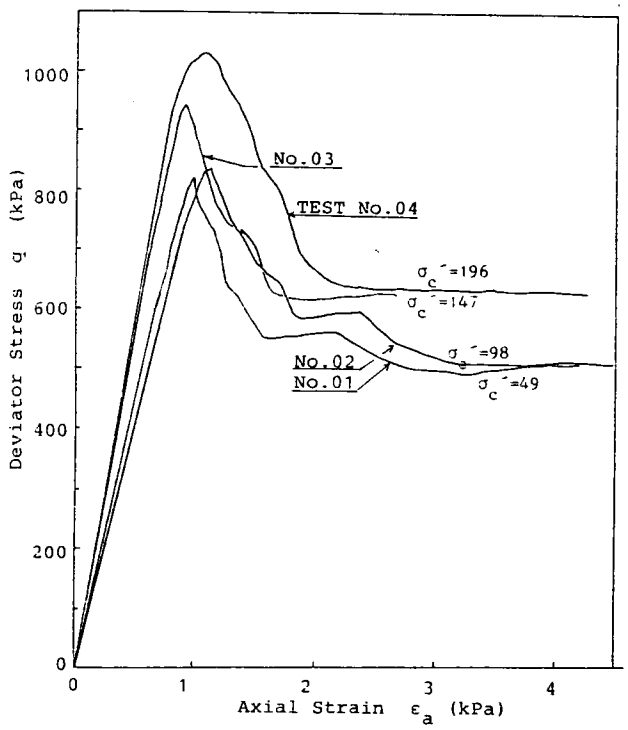

Fig.8.2: Deviator stress vs. axial strain (CU tests)

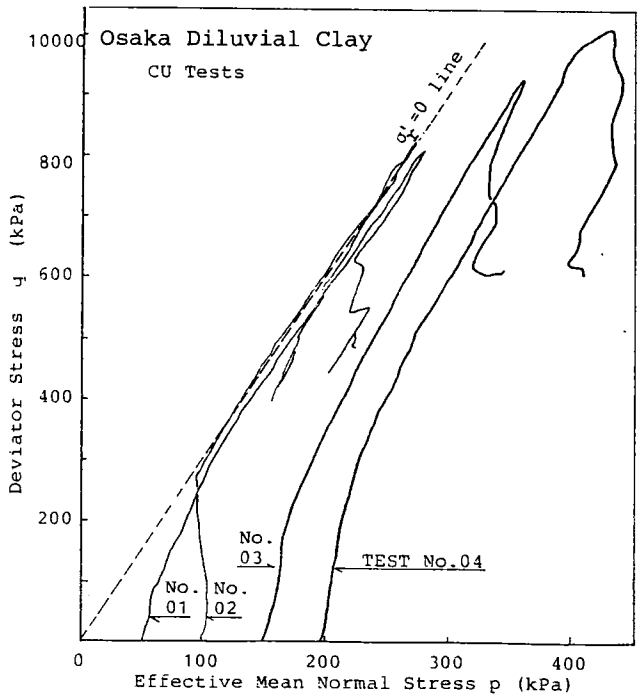

Fig.8.3: Effective stress paths (CU tests)

Test No.02 effective mean normal stress p never decreases before the peak is reached for the range examined of consolidation stress. Because of some fissures within the specimen for Test No.02, p decreases or negative dilatant behaviour appears, however, it is supposed that the decrease in p does not mean the negative dilatancy but it reflects the disturbance which might occurred when preparing the specimen.

Further, it is supposed from Fig.8.3 that the complete undrained condition is not satisfied for Test No.01 and No.02. Their effective stress paths coincide with the line of $\sigma_Y'=0$ because the tendency for pore water pressure to become superior to the confining stress is continued from a certain level of shear stress. The line of $\sigma_r'=0$ gives the limit of the range of stress. This indicates that triaxial compression tests are not available for determining shear strengths of stiff clays under relatively low effective confining stress.

(2) Unloading-Reloading and Relaxation-Reloading

In Figs.8.4 and 8.5, the results of the second series of tests are shown. General behaviours mentioned above are also observed for this series of tests; the linearity in each stress-strain curve and that in each effective stress path can be seen and the end points of the linearity are denoted by symbols and , respectively. From Fig.8.5, it is seen that the linearity of effective stress path disappears prior to that of stress-strain for relatively high effective confining stress. In the linear portion of effective streee path, change in effective mean normal

stress is almost zero. This means that dilatancy occurs before the linear property of stress-strain relationship disappears. For low effective confining stress level, the difference between two points is not very clear.

We compare behaviours during unloading-reloading cycles given before and after the peak shear stress. It is observed that, by the post peak unloading-reloading cycle, shear stress just before unloading can not be reattained while prepeak unloading-reloading cycle accompanies the continuous strain hardening. This means that something which would serve to cause strain-softening has happened during unloading-reloading cycle. This agrees phenomenologically with the strain-softening due to cyclic loading. The value of peak shear stress would not have been lowered even when the unloading-reloading cycle is given before the peak.

Relaxation was also performed after or before the peak for Test No.15 or No.10, respectively. The effective stress path for Test No.10 after the relaxation is not shown in Fig.8.5 to avoid the compliquation.

For Test No.15, it is observed that the stress recovered after the reloading following the relaxation is higher than that before the relaxation. On the other hand, for Test No.10 the stress becomes also higher after the relaxation-reloading cycle than before it. Consequently, for both cases, the increase in shear stress after the relaxation can be attributed to the time hardening effect or the thixotropic effect.

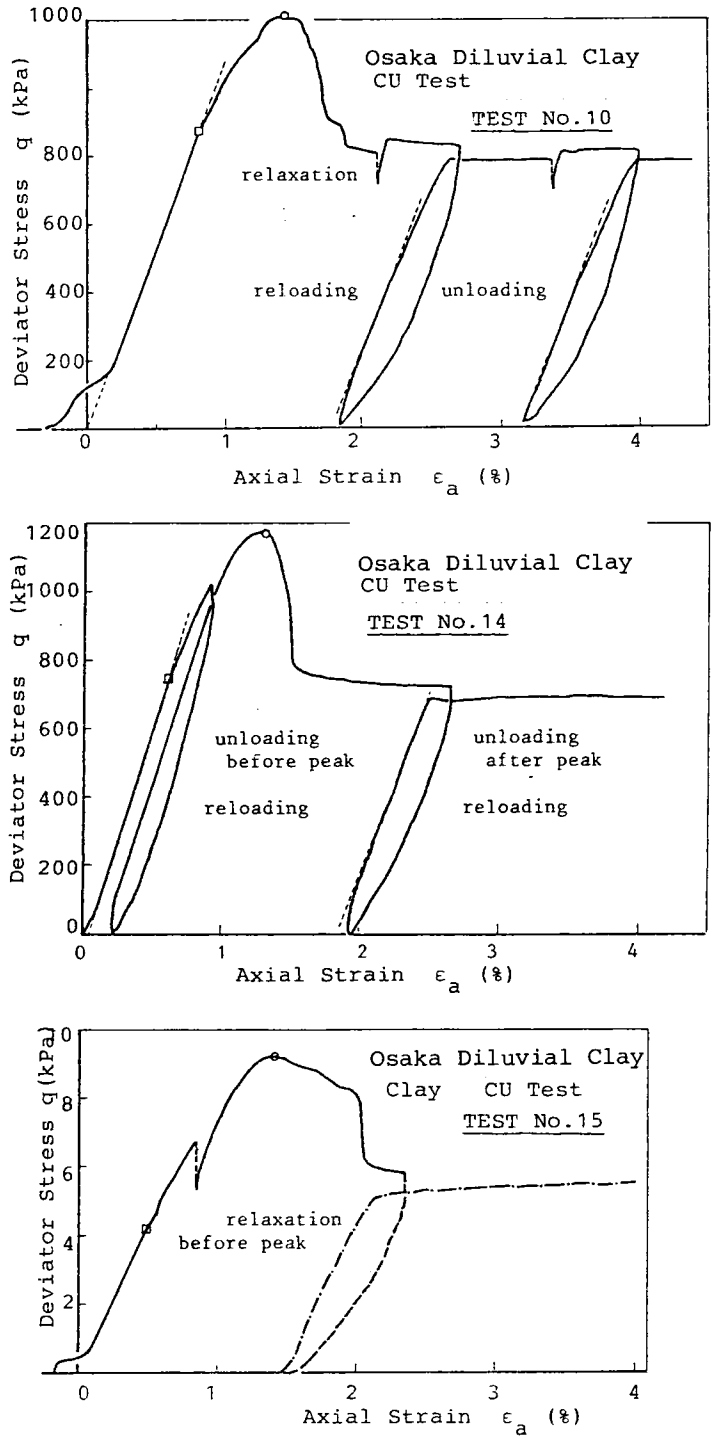

Fig.8.4: Stress-strain curves (Unloading-Reloading and/or Relaxation-reloading Tests)

(3) Excess Pore-Water Pressure

The degree of dilatancy can be considered reflected in the pore-water pressure behaviour. A relation between excess pore-water pressure Δu and change in total mean normal stress $\Delta\sigma_m$ is represented in Fig.8.6, for Test No.15. It is seen from this figure that; the ratio of $d(\Delta u)/d(\Delta\sigma m)$ is measured as 0.94 in the beginning of shear; the ratio is 1 during relaxation (1→2), which means that the relaxation process is elastic or non=dilatant process; the ratio is less in the unloading process (4→5) than in the reloading process, which indicates that dilatant tendency continues slightly even when unloading has been begun although this tendency disappears during reloading.

(4) Yield Locus and Failure Envelope

Elastic behaviour was observed in the beginning of shear, i.e., the linearity of stress-strain curve or that of effective stress path was observed. Thus we can determine the elastic limit or initial yield locus. In Fig.8.7, stress ratio $\eta(=q/p)$ and effective mean normal stress p at the point where the linearities are disappears (point denoted by the symbol or Δ in Figs.8.4 and 8.5) are plotted. The state at the peak is also plotted. Linear relation is obtained for each state. This indicates that, for both initial yield locus and failure envelope, the following expression is applicable:

$$\frac{q}{p} = M \ln\left(\frac{p_o}{p}\right) \qquad \text{----------(8.1)}$$

where M is the slope of the line and p_o is the value of p corresponding to the fictitious point of $\eta=0$. It is clear from

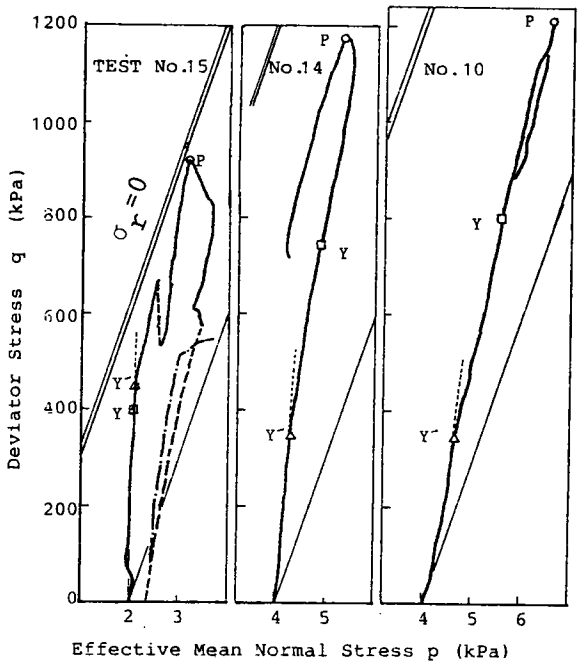

Fig.8.5: Effective stress paths (corresponding to Fig.8.4)

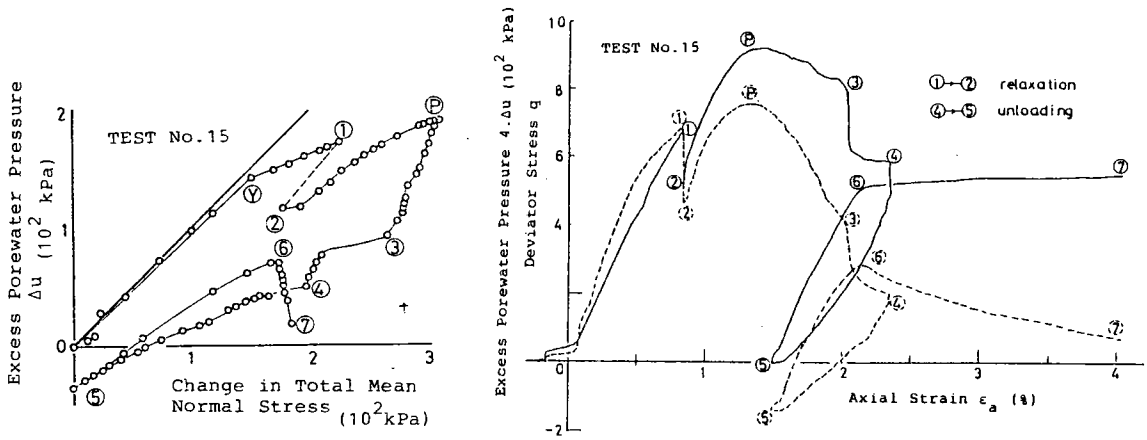

Fig.8.6: Typical porewater pressure behaviour

(a) Stress-strain-porewater pressure relation

(b) Excess porewater pressure vs. change in total mean normal stress

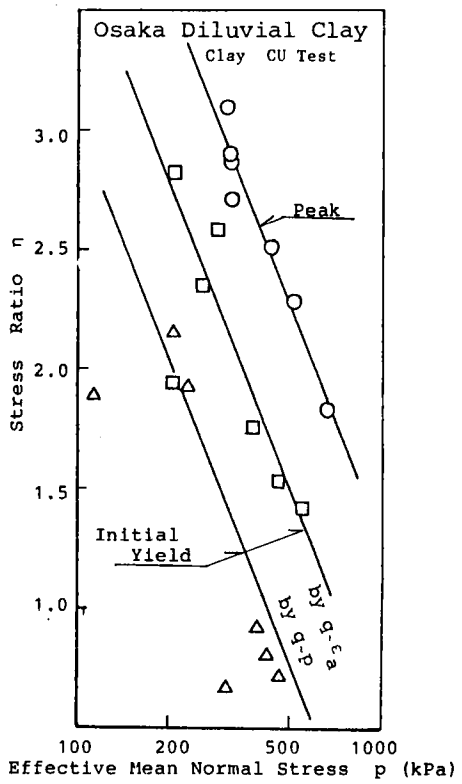

Fig.8.7: Initial yield locus and failure envelope

Fig.8.7 that M is constant and independent of the states, while p_o varies. It is interesting that eq.(8.1) is the same to the evergy equation proposed in the original Cambridge theory.

Discussions above are based on the limited data, and therefor we can not extend them more generally. Only the phenomena have been clarified.

8.3 LONG TERM CONSOLIDATION CHARACTERISTICS

8.3.1 General Remark

The compression of clays gradually or time-dependently develops. One major reason of the delayed compression is, as is well known, due to the required time for dissipation of pore-water pressure. But, we know that there exists so-called secondary compression phenomenon. Even after the dissipation of excess pore water pressure is completed, time dependent compression occurs. Any flow of pore water should always accompony the gradient of the potential of pore water within the clay layer or within the clay specimen, hence, strictly speaking, the process of dissipation of pore water pressure has not been completed after the primary consolidation. In this sense, the term of secondary compression is not proper but the term secondary consolidation would be better (Aboshi & Matsuda,1981).

Up to the time, the secondary consolidation or compression (the latter will be used according to the common usage) has been concerned with the soft alluvial clays. However, very big construction projects have increased and the interests of soil engineers should be also directed to stiff clays. The settlement of stiff clay layer is as well important for the design of bearing capacity as for the prevention or prediction of land subsidence.

Bjerrum proposed the concept of delayed compression by which only normally consolidated clays could be apparently into the overconsolidated state. Akai & Sano(1981) presented data on the

long term consolidation of Osaka upper diluvial clay (Ma12) and derived a conclusion that the clay had not been subjected to effective overburden superior to the present effective overburden, but it appeared be overconsolidated because of the delayed compression.

Aboshi & Matsuda(1981) presented the results of a very long time duration oedometer test and derived a conclusion that the coefficient of secondary compression C_α seemed to decrease after a long elapsed time.

8.3.2 Very Long-Term Consolidation Test

(1) Sample and Experimental Procedure

The sample used for the test mentioned below is the same to that used for shearing tests of which results were already presented in Sec.8.2 (see Fig.8.1). An oedometer test was performed. Prior to the long term consolidation, compression-unloading-reloading cycles were given. e~log p relation obtained from this process is shown in Fig.8.8. Creep tests was performed at vertical pressure of 941 kPa. which was attained before the end of second unloading-reloading cycle. This value of vertical pressure is within the overconsolidation as shown in Fig.8.8. The room temparature for this test was held constant at 20±0.5°C except that a few times at which it increased at most by about 8°C because of sudden trouble of the air-conditionning system. Thus, the discussion below will be based on the assumption that the effect of change in room temparature is not included in the results.

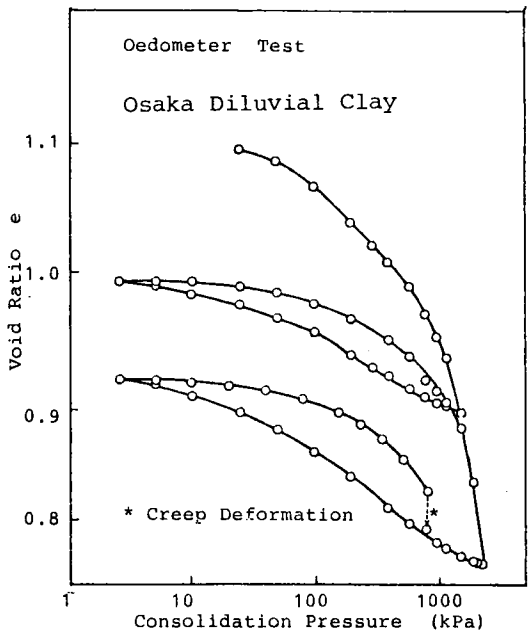

Fig.8.8: Void ratio vs. log of vertical consolidation stress (prior to the creep test)

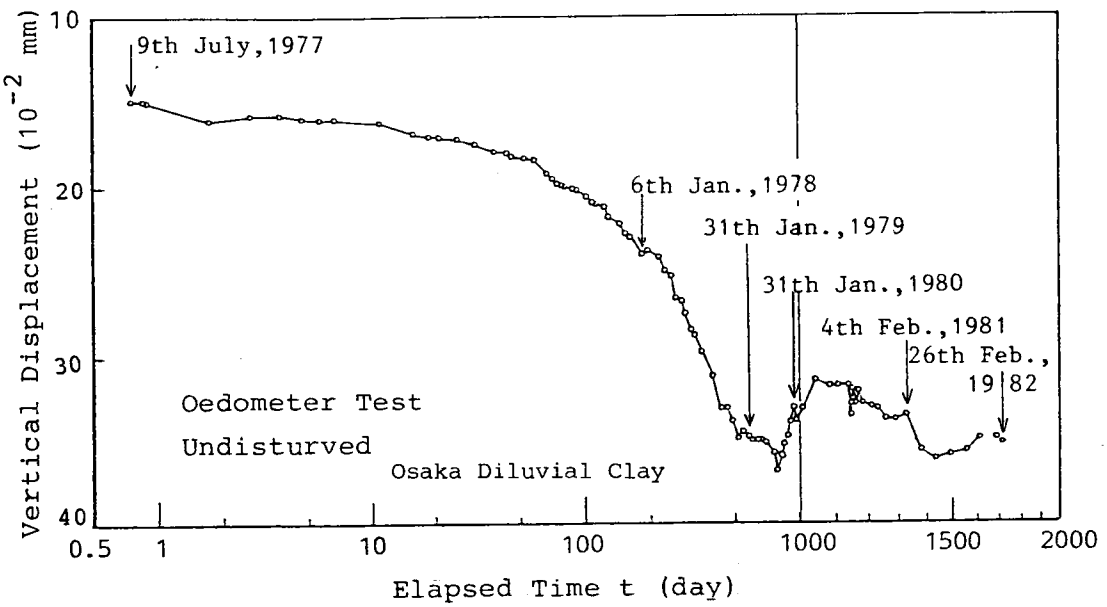

Fig.8.9: Settlement-time relation during the creep test.

(2) Experimental Results

The variation of vertical displacement ρ with time t is shown in Fig.8.9. Data from 0.5 day to 1700 days after the load application are shown. From this figure, the linearity of ρ~log t relation is observed in the range of t less than about 25 days (3.6×10^4 minutes), but passing the linear portion, the relation becomes curved and coefficient of secondary compression (the tangent of the curve) increases with increasing log t. This observation does not agree with the data by Aboshi & Matsuda(1981), as mentioned in the preceding (8.3.1). The rate of the decrease in the settlement rate ($d\rho$/dlog t) becomes rather suddenly smaller or null at about t=500 days. After t=500 days, small fluctuation is observed. Any periodity can not be derived in the fluctuation.

From the observations mentioned above, we can derive the following possible questions :

i) Does the behaviour after 500 days mean the end of secondary compression?

ii) What does the fluctuation mean? If it is not essential, it means probably the loss of accuracy of measurement. If it shows physically or mechanically substantial feature, what is it?

iii) Sould we consider some chemical agency, e.g., effects of change in chemical component of pore water supplied to prevent the desiccation or chemical agency itself between pore water and soil grains ?

We can answer to the question (ii) that there should not have been the loss of accuracy of the measurement because, in the same laboratory, other triaxial tests were performed and there was not

any trouble in the measurement. However, one reason for the fluctuation is cited as follows : as stated already, a few trouble of the air-conditionning system occurred suddenly, and at each time of the trouble, the system was checked, and eventually the controlled temperature was reset. Only slight difference in temperature, e.g., ±0.2 to 0.5°C may affect the compressibility.(see Appendix).

For the third question, the possibility of the effects of chemical agency of pore water may possibly exist, but our degree of knowledge on it is too low to give any comment on this effect.

Finally, the possibility of the existence of the end of secondary compression should be available because, if there were not the end, the secondary compression would continue infinitely long and, as the results, the void ratio of the clay would have become zero. In the field, all the geotechnical materials have certainly finite void ratio. The void ratio which correspond to the applied effective stress may exist.

8.3.3 Repeated Loading Tests

(1) Sample

The sample used is from Senshu Region, Osaka Prefecture. This sample had been called OKS No.2*. The detail of the soil profile is shown elsewhere (Murayama et al.,1981). The depth of the sample used for the experiments is 95.8 to 96.8 meters below the ground surface. Preconsolidation vertical pressure determined by oedometer tests was varied from 1470 to 1960 kPa for the sample of the depth between 90~100 m. Plasticity index of this clay is about 75 %.

(2) Experimental Procedure

Fig.8.10 shows relations between vertical displacement ρ and verical consolidation stress p for these tests. In Table 8.1, the condition of tests is shown. Test No.1 and No.2 are repeated loading tests where, consolidating up to prescribed value of p_1 the increment $\Delta p=p_u-p_1$ was applied and unloaded. This cycle of loading-unloading was repeated about 80 times. Under a given p, consolidation duration was 24 hours. Test No.3 is creep test. This was performed to examine the effect of repetition of loading-unloading to the compressibility.

---

* The sampling was performed under the direction of "Research Committee of Land Subsidence in Dilluvial Clay Layer in Senshu Region" organized in Kansai Branch of JSSMFE.

Table 8.1: Upper and lower consolidation stresses

Tests	Type	Upper Consolidation Pressure p_u (kPa)	Lower Consolidation Pressure p_l (kPa)
No.1	Repeated Loading	1412	1255
No.2	"	1098	785
No.3	Creep	(1255)	(1255)

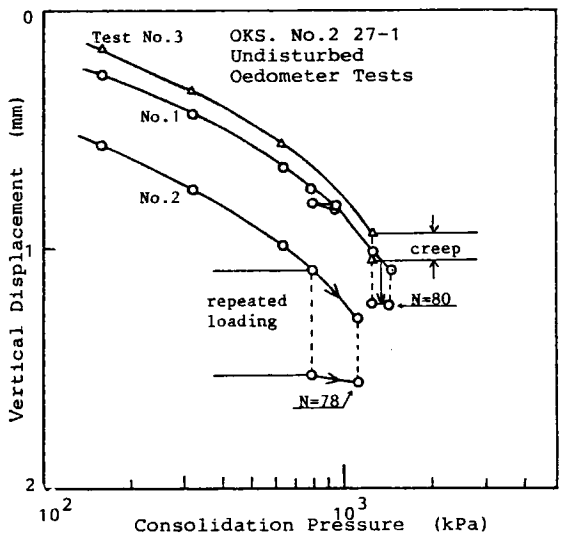

Fig.8.10: Vertical settlement vs. log of vertical consolidation stress (prior to and at the end of the repeated loading tests and the creep test).

(3) Results and Discussion

It is seen from Fig.8.10 that specimens have similar compressibility before the repetition or creep was performed.

In Fig.8.11, the comparison of the compressibility during the cycle of loading-unloading between Test No.1 and No.2 is shown. Marked difference in behaviour can not be seen although only initial settlement accompanied with the first cycle is different from each other. For both tests, it is observed that the vertical displacement ρ is related linearly to the number of cycle N in the range of N larger than about 20.

The effect of the repeated loading to the compressibility was examined by Yagi(1981). He compared the compressibility between a creep test under $p=p_u$ and repeated loading tests under $p=p_u$ and $p=p_u-\Delta p$. According to him, the compressibility becomes large in the case of load increment Δp larger than a certain value, and in this case the total settlement was more than that of the creep test.

In Fig.8.12, variations of ρ with time elapsed from the first application of the p_1 is compared between the repeated loading test (No.1) and the creep test (No.3). So far as this figure is concerned with, effects of repetition of loading-unloading will not be noticed. Further, the variation curve is linear in the beginning range of t but becomes curved from $t=5\times10^4$ minutes for both types of test. In consequence, we can conclude that, for the clay used, the effect of the repetition is not clear but the continuous settlement is caused by the secondary compression effect.

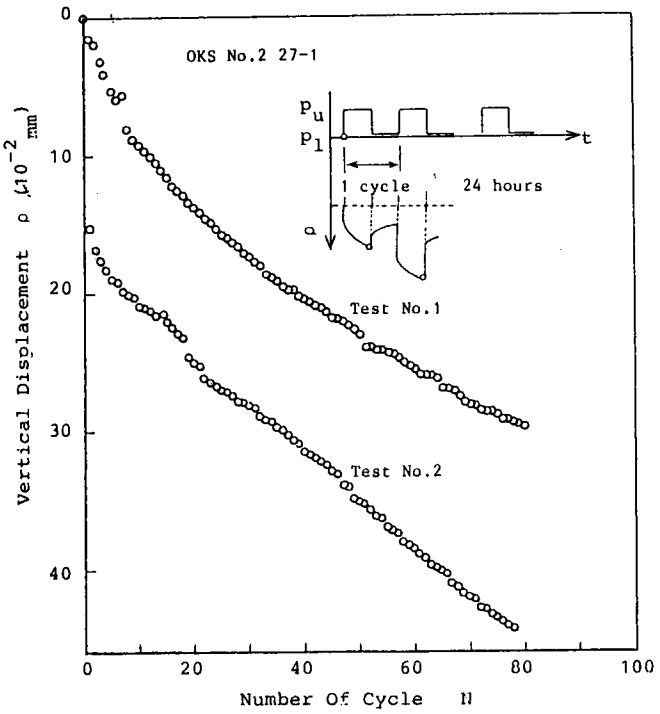

Fig.8.11: Comparison of two repeated loading tests.

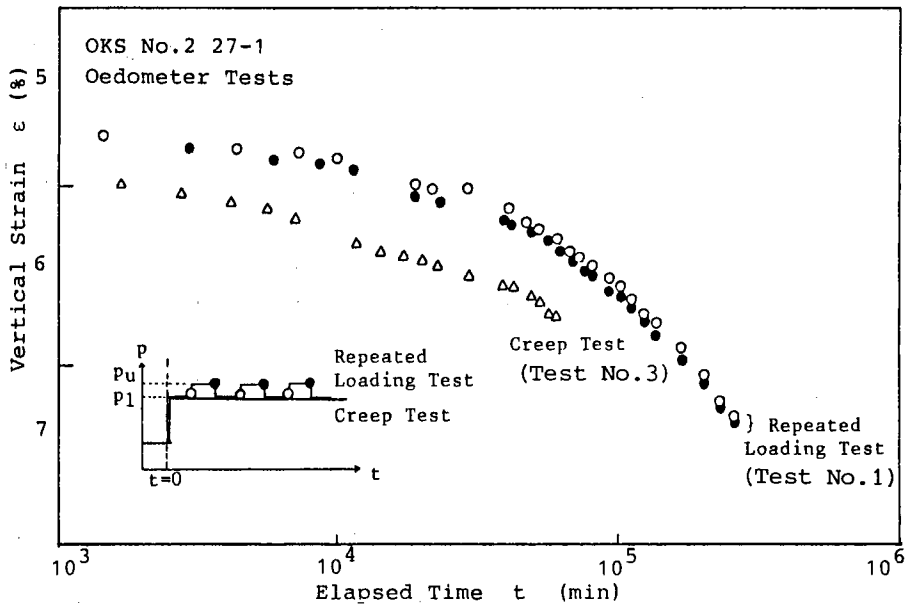

Fig.8.12: Comparison of a creep test and a repeated loading test.

8.4 CONCLUSIONS

Conventional triaxial tests and oedometer tests were performed on stiff diluvial clays. Main conclusive remarks in this chapter are given as follows :

i) For a stiff overconsolidated undisturved clay, of which stress-strain relations are remarkably strain-softening, the tendency of strain softening is continued during unloading-reloading cycle of shear stress after the peak. When the stress relaxation-reloading was done, the recovered shear stress became larger than the value before the relaxation for a given strain. This was supposed due to the time hardening effect.

ii) Secondary compression of a stiff overconsolidated clay ceasees after very long time duration. According to the oedometer test performed, about 500 days was required for the end of the secondary compression.

iii) For a clay used, effects of repeated loading were not clearly noticed, the continuous settlement under repeated loading will be attributed to the effect of secondary or creep compression.

REFERENCES FOR CHAPTER 8

Aboshi,H. and Matsuda,H.(1981): "Secondary compression of clays and its effect on settlement analysis",Tsuch To Kiso, J., JSSMFE, Vol.29, No.3, pp.19-24.(in Japanese)

Akai,K. and Sano,I.(1981): "Long-term consolidation of Osaka upper diluvial clay", Tsuchi To Kiso, J., JSSMFE, Vol.29, No.3, pp.43-47.(in Japanese)

Basant,Z.P.(1976): "Instability, ductility and size effect in strain-softening concrete", Proc. ASCE, Vol.102, EM2, pp.331-344.

Bishop,A.W., Webb,D.L. and Lewin,P.I.(1965): "Undisturbed samples from Ashford Common Shaft: strength -effective stress relationships", Géotechnique, Vol.15, pp.1-31.

Bishop,A.W.(1967): "Progressive failure with reference to the mechanism causing it", Proc. Geotech. Conf., Oslo, Vol.2, pp.142-150.

Bjerrum,L.(1967): "Progressive failure in slopes of overconsolidated plastic clay and clay shales", J. Soil Mech. Found. Div.,ASCE, Vol.93, SM5, pp.3-49.

Drucker,D.C.(1959): "A definition of stable in plastic meterial", J. Applied Mech., Trans. ASME, March, pp.101-106.

Hõeg,K.(1972): "Finite element analysis of strain-softening clay", J. Soil Mech. Found. Div., ASCE, Vol.98, pp.43-58.

Hooper,J.A. and Butler,F.G.(1966): "Some numerical results concerning the shear strength of London Clay", Géotechnique, Vol.16, pp.282-304.

Law,K.T.(1981): "Effect of stress path geometry on soil brittleness", Géotechnique, Vol.31, No.2, pp.279-287.

Lo,K.Y.(1972): "An approch to the problem of progressive failure", Can. Geotech. J., Vol.9, pp.407-429.

Murayama,S et al.(1981): "Research on the land subsidence in diluvial clay layer in Senshu Region, Osaka", Osaka Prefectural Authorities and Kansai Branch of JSSMFE.

Murayama,S. and Shimizu,M.(1974): "A few mechanical properties of Osaka Diluvial Clays", Proc., 9th National Conf. Soil Mech. Found. Eng., pp.263-266.(in Japanese)

Nayak,G.C. and Zienkiewicz,O.C.(1972): "Elasto-plastic stress analysis. A generalization for various constitutive relations including strain-softening', Int. J. Numerical Method in Eng.,Vol.5, pp.113-135.

Palmer,A.C., Maier,G. and Drucker,D.C.(1967): "Normality relation and convexity of yield surfaces for unstable materials on structural elements", J. Appl. Mech., Trans. ASME, pp.464-470.

Palmer,A.C. and Rice,J.R.(1973): "The growth of slip-surfaces in the progressive failure of overconsolidated clay", Proc. Roy. Soc., London, Series A, Vol.332, pp.527-548.

Pariseau,W.G.(1972): "Elasto-plastic analysis of pit slope stability", Proc. Application of the FEM in Geotech. Eng., Vicksburg, Miss., Vol.1, pp.349-383.

Peck,R.B.(1967): "Stability of natural slopes", J. Soil Mech. Found. Div., ASCE, Vol.93, SM4, pp.403-417.

Prévost,J.-H. and Höeg,K.(1975): "Analysis of pressuremeter in strain-softening soil", J. Geotech. Eng. Div., ASCE, GT8, pp.717-732.

Prévost,J.-H. and Höeg,K.(1975): "Soil mechnics and plasticity analysis of strain-softening", Géotechnique, Vol.25, No.2, pp.279-287.

Rice,J.R.(1973): "The initiation and growth of shear bands", Proc. Symp. Role of the Plasticity in Soil Mech., pp.263-274

Shimizu,M.(1980a): "Consideration on strain softening behaviour of a stiff overconsolidated clay", Proc. Annual Regional Conf., Kansai Branch,JSCE, pp.III.3.1-2.(in Japanese)

Shimizu,M.(1980b): "Elastoplastic behaviour of a stiff overconsolidated clay-strain-sftening behaviour-", 35th Annual National Cog., JSCE, Vol.3, pp.89-90.(in Japanese)

Skempton,A.W.(1964): "Long-term stability of clay slopes", Géotechnique, Vol.14, pp.77-101.

Skempton,A.W.(1970): "First-time slides in overconsolidated clay", Géotechnique, Vol.20, No.3, pp.320-324.

Sture,S. and Ko.H-T.(1978): "Strain-softening of brittle geologic materials", Int. J. Numerical andAnalytical Methods in Geomech., Vol.2, pp.237-253.

Terzaghi,K.(1936): "Stability of slopes of natural clay", Proc. 1st ICSMFE, Vol.1, pp.161-165.

Ward,W.H., Marsland,A. and Samuels,S.G.(1965): "Properties of the London Clay at the Ashford Common Shaft: in-situ and undrained strength test", Géotechnique, Vol.15, pp.321-344.

Yagi,N.(1981): "Characteristics of compressibility of soil",Research on Land Subsidence in Diluvial Clay Layer in Senshu Region, Osaka Prefectural Authorities and Kansai Branch of JSSMFE, pp.155-163.

CHAPTER 9 MECHANICAL BEHAVIOUR OF UNDISTURBED SAMPLES OF DECOMPOSED GRANITE SOILS

9.1 INTRODUCTION

9.1.1 Object

It is said that 13 % of the area of our country is covered or consisted with granite rock mass or decomposed granite soils (JSSMFE,1979). Granite has played a very important role as a foundation rock mass or as a construction material. The importance has increased and will increase more and more with increasing large scale construction problems.

On the other hand, it is also the fact that we have had many damages resulted from the destruction of soil structures consisted of decomposed granite soil. It may be said that decomposed granite soils have certain injurious properties from the engineering view point.

Studies on the physical and mechanical characteristics of decomposed granite soils have developed recently. Thier historical aspects and the present stage are presented in detail,e.g.in JSSMFE(1979).

In the field of soil mechanics, decomposed granite soils are usually treated as one of special soils although the engineering use of them is not rare but very usual. As one of the reasons, we can cite the difficulty of sampling and testing their undisturbed samples. One of the special , if we are allowed to say so, characteristics different from other sedimentary rocks or soils may be the susceptibility to the destruction of their original internal

structure or fabric. Such problems as structure or fabric must be concerned with the weathering.

To investigate the mechanism or the cause of weathering is of course important, however, for soil engineers who must usually encounter the weathered state resulted from the process of weathering , it is more important and indispensable to investigate the mechanical or physical properties of the weathered soil, and also to relate them to the degree of weathering. If we succeed in relating these two, the generalization of the results obtained for a certain problem will be possible. From such a view point, many attempts have been made.

The main object of this chapter is to investigate the fundamantal mechanical characteristics of decomposed granite soil in order to not only find the particularity, if any, of the characteristics but also to compare them with the findings previously obtained for other types of soils in the field of soil mechanics. Consequently, the triaxial tests, through which effective stress states can be known, were mainly performed for examinig the fundamental behaviour of certain undisturbed samples.

9.1.2 Brief Review of Previous Studies

Various physical quantities have been used as measures for evaluating the degree of weathering. Aoyama et al.(1977) has compared the vertical variation of ignition loss, X-ray diffraction frequency and porosity and showed that the variation of these three parameters corresponded well each other. Matsuo & Nishida (1968) has proposed the use of specific gravity of feldspar as the measure of weathering. Further, they pointed out that the apparent

specific gravity of soil grains, measured for samples with non-saturated voids rested within soil grains, can be also a good measure(Nishida & Matsuo,1970)

Grain size distribution of a decomposed granite soil depends on methods employed for the measurement because of the crushing of soil grains. However, it is generally said that most of decomposed granite soils have well graded distribution.

As to the mechanical characteristics of undisturbed samples, Shono et al.(1975) has derived a conclusion that there was clear correlation between the angle of internal friction ϕ_D and the degree of weathering. Onodera et al.(1976) and Nishida & Aoyama (1981) have conducted direct shear tests for undisturbed samples.

Permeability is considered one of mechanical characteristics and at the same time it can be regarded as a direct measure of weathering. Generally, it may be expected that more is dry density of sample , less is the permeability. This was verified by Aboshi et al.(1976) and Shono et al.(1976). However, there would be opposite cases. If the degree of weathering is extremely high enough to increase the proportion of clay fraction, permeability would decrease because of the chemical interaction between porewater and clay minerals. In this sense, to know the permeability of the sample used in a study can lead to understand its internal structures.

9.2 SAMPLES

9.2.1 Description of the Site and Geology

The site for sampling is about 20 km in the south-west.

from Takamatsu City (see Fig.9.1). The elevation of the site is about 280 m from the sea level. Sampling was done at four points, denoted by A, B, C and D as shown in Fig.9.2, at the foot of an slope surface exposed by cutting. Distance between sampling points was about 20 m. The depth of the overburden before the cutting were 0, 5, 10 and 15 m at points A, B, C and D, respectively. According to the geological map, the geology of this region is grano-diorite or biotite granite (Fig.9.1).

9.2.2 Method for Sampling

As stated above, the sampling was performed at four points. The sampling method for Sample A differs from others. Since Sample A was surface soil subjected to heavily weathering, a pipe made of vinyl chloride, 14 cm in inner diameter and 3 mm thick, was directly forced into the subsoil by hammer tapping and pulled out. The upper and lower ends of the sample in the pipe were sealed with plaster de Paris.

Samples B, C and D appeared gravel to sand like and were susceptible to be easily disturbed. They are called Oni-Masa and distinguished from such a heavily weathered soil as Sample A which is called Nan-Masa.

The ground surface exposed by cutting was further cut away about 30 cm thick and the intact surface was exposed. Blocks of about 15x15x30(cm) were made by scraping with a knife edge. Each block was covered with a pipe of vinil chlorite or a rectangular hollow pipe of wood. The liquid of plaster de Paris was poured onto the both ends of the block sample.

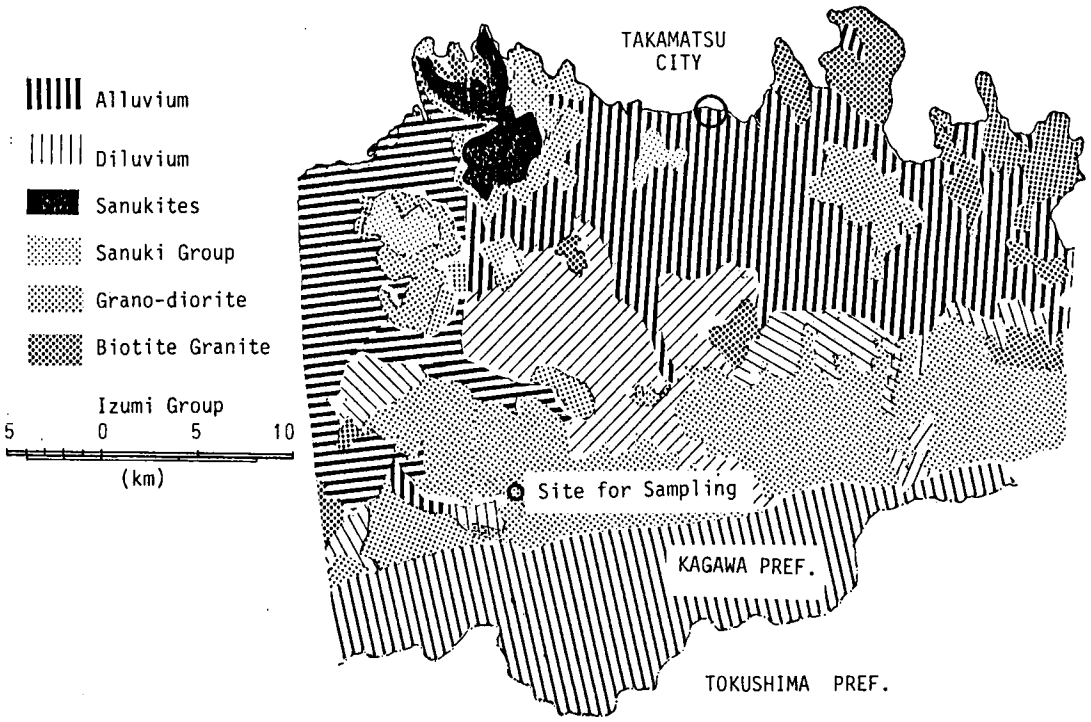

Fig.9.1: Geological condition of the site for sampling.

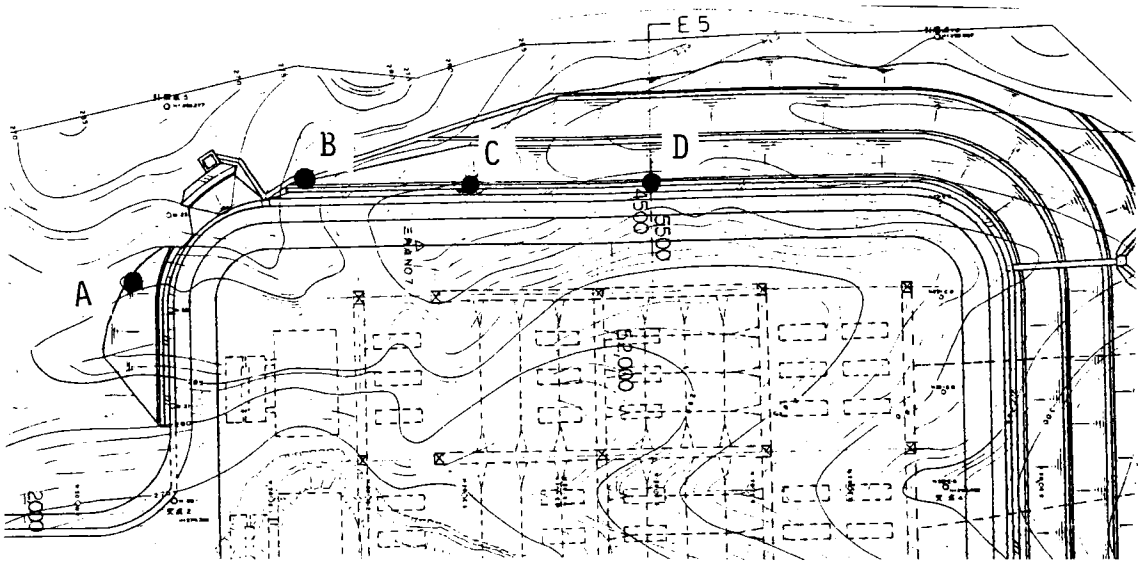

Fig.9.2: Field for sampling.

The operation was performed very carefully, otherwise grains or fragments of the block sample were fallen and the sample would be completely disturbed. The blocks scraped and those covered with tubes of vinil chlorite are shown in Photos 9.1 and 9.2, respectively.

9.2.3 Presentation of Specimens for Triaxial Tests

Sample A was trimmed with a wire saw to be cylindrical specimens of about 3.5 cm in diameter and 8 cm in height for triaxial tests.

For samples other than A, firstly, the whole block sample in the frame was subjected to the application of vacum in water, so that the degree of saturation was raised to more than 90 %. Each saturated block was let freeze in a refrigerator and the freezing was further developed with dry ice. The freezed block was cut with a disk cutter to be triaxial specimens with square cross section of 4x4 (cm) and 10 cm in Height.

A representative specimen for the triaxial test of Sample C is shown in Photo 9.3 and the cut surface of Samples B and C are shown in Photo 9.4(a) and (b). It is observed from Photos 9.4(a) and (b) that there are some joint like discontinuities in Sample B while for Sample C there is no. In Sample D, the discontinuity was not observed. This difference in the internal structure seems to reflect some difference in the degree of weathering. Particularly, the fact that Sample B has some mineralogically discontinuous appearance while C and D have no such an appearance will result in some difference in mechanical behaviour between them as will be shown and

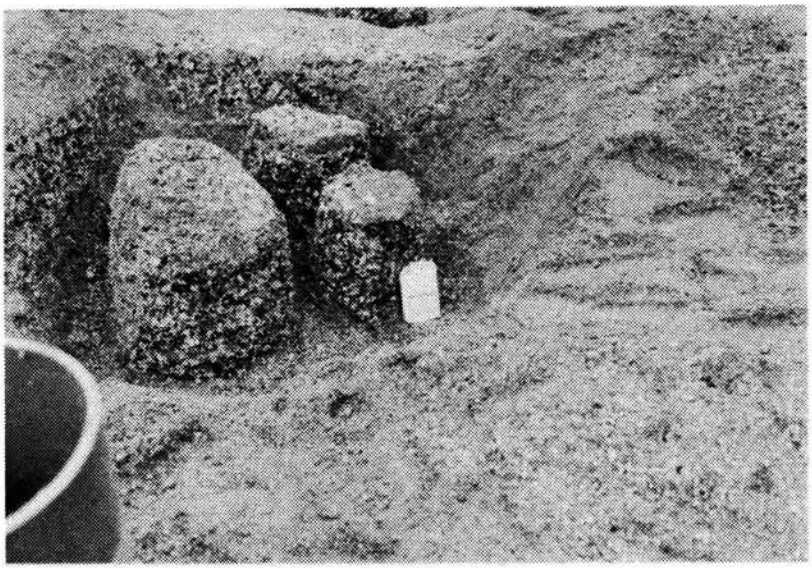

Photo 9.1: Scraped block samples.

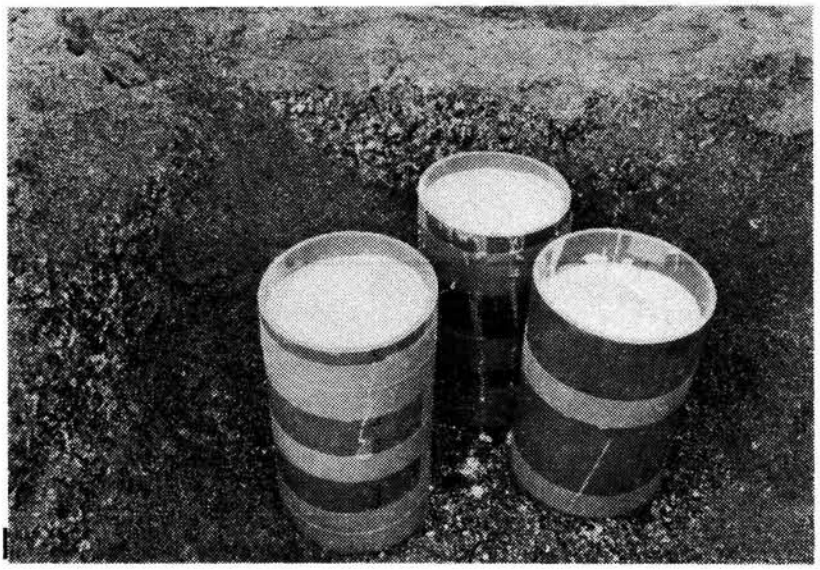

Photo 9.2 Block sample covered with a tube of vinyl chloride

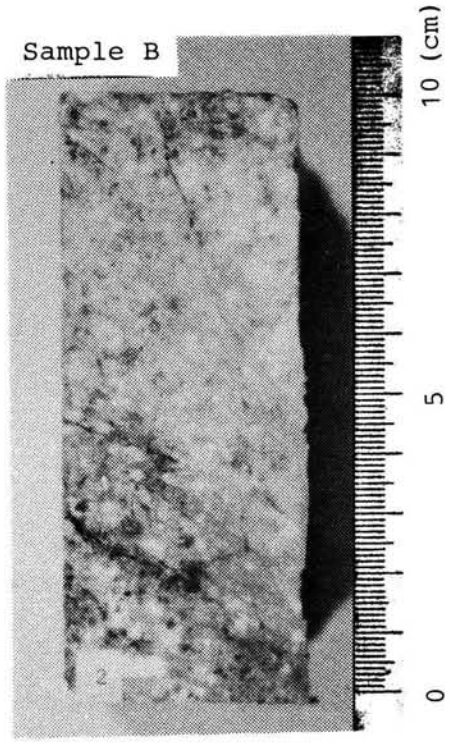

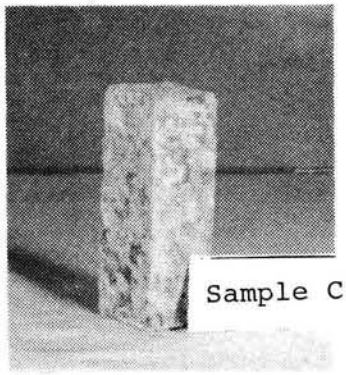

Photo 9.3: Representative specime for the triaxial test of Sample B (left) and Sample C (above).

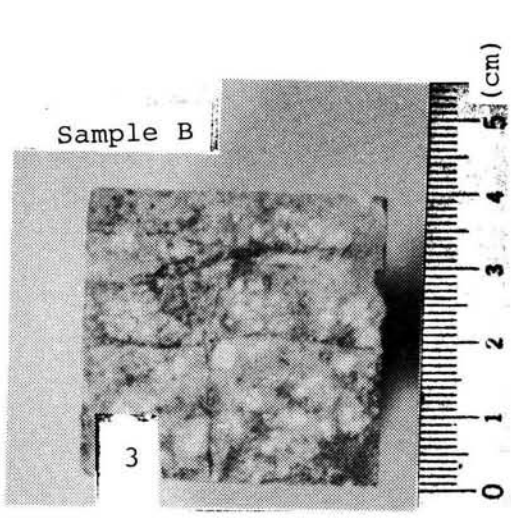

(a)

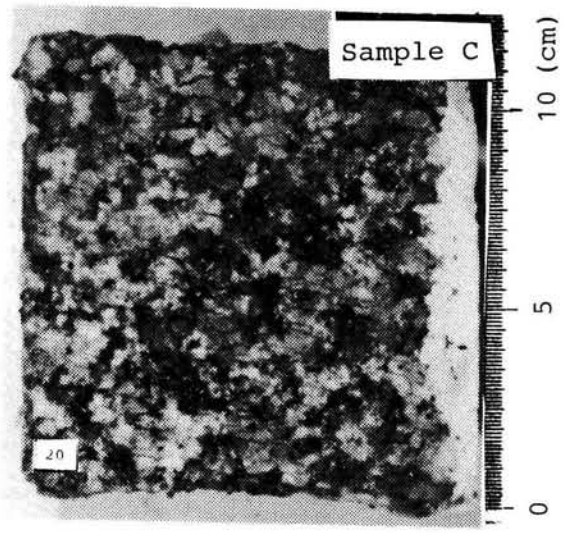

(b)

Photo 9.4: Internal structure of samples:
(a) Sample B; and
(b) Sample C.

discussed in detail later.

9.3 PHYSICAL PROPERTIES OF SAMPLES USED

Generally, as is well known, soils classified into decomposed granite have many types according to the original rocks, the degree of weathering or geological history etc. In consequence, it is necessary and indispensable to clarify the identity of the sample used. To do so, various types of physical properties of the samples used were examined.

9.3.1 Grain Size Distribution

In general, the characteristics of grain size distribution is one of major factors controlling the mechanical properties of soils. Nevertheless, for decomposed granite soils, definite method for measuring the grain size distribution is not yet established at present, because the composite grains are susceptible to be crushed by various external or artificial agencies. As the results, the grain size distribution differs between procedures adopted. In this study, with the object of knowing even approximately a tendency of the grain size distribution, measurement was performed as follows:

The sample not subjected to any control of grain size was watered through 74 μm sieve. This procedure of watering seems to serve to release the cementation at contacts, particularly, of fine grains. Grains which remained in the 74 μm sieve was further sieved, while for grains which had passed through it, sedimentation analysis was performed. As is clear from the procedure, any artificial crushing of soil grains

was not made.

The grain size distributions for Samples A, B and C are shown in Fig.9.3. It is seen from this figure that all the specimens examined are well graded and that they have the same value of uniformity coefficient D_{60}/D_{10}.

Lumb(1965) and Nishida(1963) have pointed out that the value of uniformity coefficient increases with increasing degree of weathering, but for samples used in this study is not the case.

9.3.2 Specific Gravity

Specific gravity of soil grains for decomposed granite soil is difficult to be defined as well as the grain size distribution. Specific gravity, particularly apparant specific gravity of soil grains can be taken as the measure of the degree of weathering (Matsuo & Nishida,1968). Here, two types of specific gravity were measured: one is that defined as the specific gravity A, G_{sA}, and anther the specific gravity B, G_{sB}, in "Method for Testing Soils"(JSSMFE,1974). As is shown in Table 9.1,G_{sA} was less than G_{sB} for all the samples used and it is the largest for Sample A. G_{sA} for Sample B was considerably larger than that for Sample C or D. This leads to that Sample A is the most strongly weathered between four samples and Sample B is secondly highly weathered. The degree of weathering for Samples C and D are not very distinguishable.

9.3.3 Initial Void Ratio

Initial void ratio of specimens for triaxial tests was determined by

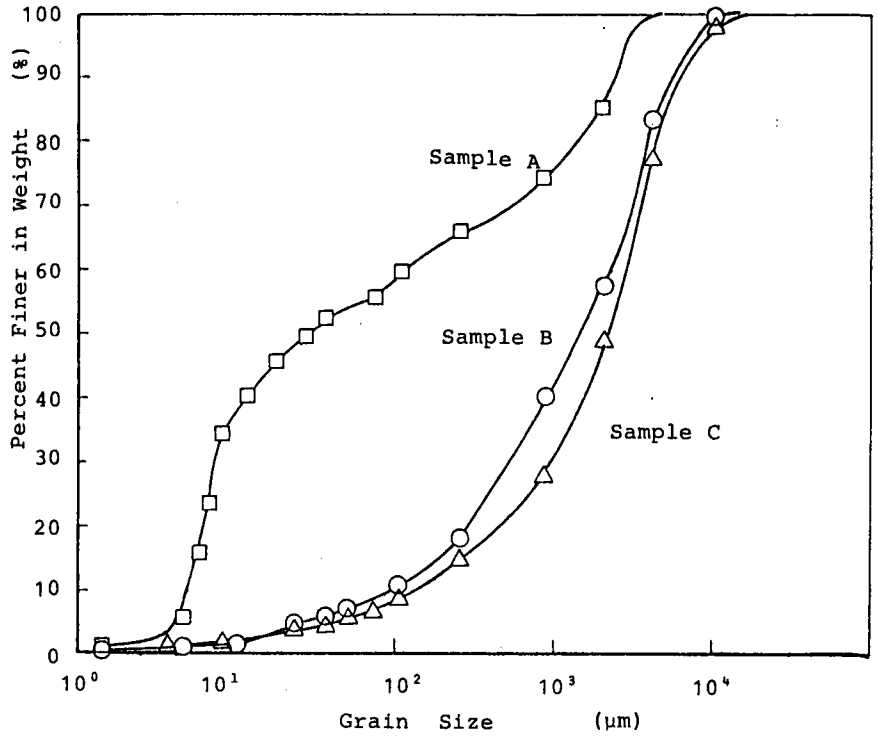

Fig.9.3: Grain size distributions.

Table 9.1: Physical properties of samples.

Sample Name			A	B	C	D
Sampling Depth (GL-m)			0	5	10	15
Mineral Composition (%)	quartz		-	53.10	48.45	-
	feldspar		-	22.08	22.84	-
	colored minerals		-	24.82	28.71	-
Specific Weight (g/cm^3)		A	2.635	2.585	2.599	-
		B	2.638	2.640	2.681	-
Initial Void Ratio	average		1.070	0.515	0.387	0.399
	standard deviation		0.0748	0.0351	0.0245	0.0132
Grain Size Distribution	D_{10} (μm)		5	135	100	-
	D_{60} (μm)		115	2850	2200	-
	D_{60}/D_{10}		23	21	22	-

$$e_i = \frac{V_t - W_s/(G_{sB}\gamma_w)}{W_s/(G_{sB}\gamma_w)}$$

where γ_w is the weight of water per unit volume at 20°C,

W_s is the weight of the dried specimen, and

V_t is the total volume of the freezed specimen.

The specific gravity of soil grains at the temperature lower than 0°C was not measured and so the equation above is only approximate,i.e., the thermal volume change of soil grains is neglected.

The average value of e_i and its standard deviation are listed in Table 9.1. e_i is the largest for Sample A. Comparing the values of e_i between Samples B, C and D, e_i for B is the largest than others. This agrees with the results concerning with the specific gravity.

9.3.4 Mineral Compostion

Decomposed granite soil is composed of primary minerals such as feldspar, quartz and colored minerals. The composition of these minerals was examined according to the method defined in "Method for Testing Soils"(JSSMFE,1974). For the separation of colored minerals, the method of megnetic separation was adopted. And the heavy liquid separation method was used for the determination of the composition ratio between quartz and feldspar. The results are given in Table 9.1. The compositions for Sample B and C lie in the range for a decomposed granite soil from Mt.Ikoma, which was used in the study by Matsuo & Nishida (1968).

9.4 PROCEDURE AND RESULTS OF MECHANICAL TESTS

9.4.1 Outline of Experimental Procedure

All the tests described here are concerned with undisturbed samples. The list of the tests is given in Table 9.2.

For Sample A, two kinds of tests were performed: oedometer tests and consolidation undrained triaxial compression tests. For the former tests, the consolidation ring was easily forced into the sample although some fibrous fragments of roots of plants were included in. For CU tests, after the isotropic consolidation for 24 hours, during which the primary consolidation was completed, shear stress was applied under the undrained condition. The rate of axial strain was 0.02 %/min. Back pressure of 196 kPa was applied since the isotropic consolidation stage.

For Samples B, C, and D, isotropic compression (CI) and consolidation drained (CD) or undrained (CU) triaxial compression tests were performed. CD and CU were by the strain control; the rate of axial strain for CD was determined as 0.007 %/min based on the consolidation characteristics, which had been examined in the preconsolidation stage prior to applying shear stress; the method for determination of the rate of axial strain was according to Bishop & Henkel(1964). For CU tests, the rate of axial strain of 0.05 %/min was adopted. Back pressure of 490 kPa was applied for CU tests.

Further, permeability tests were performed on Sample C. The specimen of 4x4 (cm) in the rectangular cross section and 4 cm in height was set up in a mold of circular cross section. The pore between the specimen and the mold was filled with

Table 9.2: List of mechanical tests.

		Sample(s)
Permeability Tests		C
Oedometer Tests		A
Triaxial Tests	Drained	B, C
	Consolidation Undrained	A, B, D

parafin, of which the permeability can be considered null. The saturation of the specimen was again increased by the use of vacum. Method of varying water head was adopted. Permeabilities in two directions, vertical and horizontal, were measured to examine the anisotropy with respect to the permeability.

9.4.2 Experimental Results

(1) Oedometer Tests for Sample A

In Fig.9.4 relations of void ratio vs. log of consolidation pressure are shown. It can be seen from the figure that the virgin compression curve has not a clear turning point and , hence, that the determination of the preconsolidation stress is not easy. Considering that Sample A is the soil near the ground surface, the loss of the turning point of the virgin compression curve can be understood. During the cycle of unloading and reloading, the behaviour is elastic or recoverable as in the case of sedimentary clays.

From the results shown in Fig.9.4, we can determine the compressibility: the compression index C_c, swelling index C_s and recompression index C_r, which are given in Table 9.3. These values are not far from the general values for sedimentary

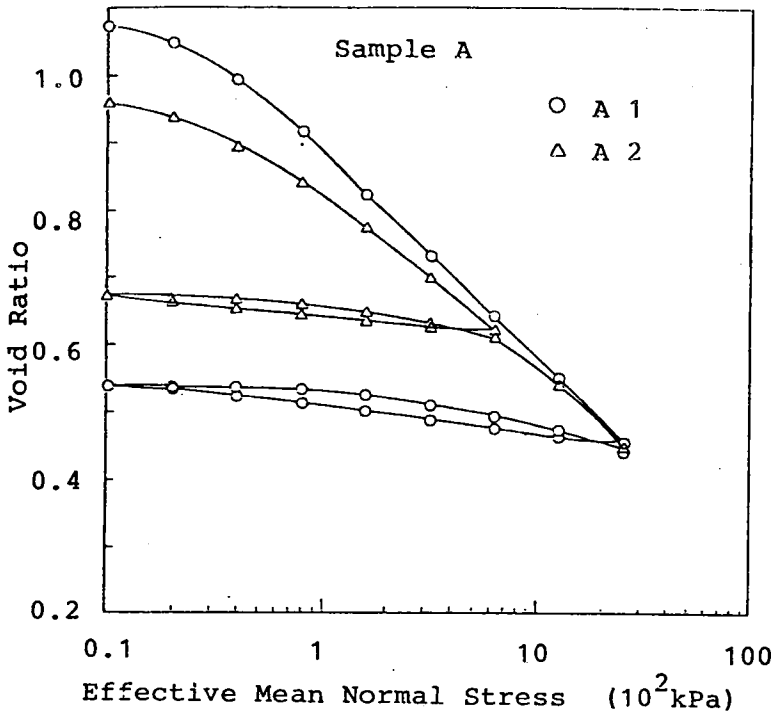

Fig.9.4: Void ratio vs. logarithm of consolidation stress
(Oedmeter tests on Sample A)

Table 9.3: One dimensional compressibility of Sample A.

Sample Name	Initial Voidratio	Degree of Satulation	C_c	C_r	C_s
A 1	1.100	85.65%	0.34	0.044	0.031
A 2	1.020	96.81%	0.31	0.032	0.028

clays.

(2) CU Tests on Sample A

In Figs.9.5 and 9.6, the relations between shear stress q and axial strain ε_a and the effective stress paths from CU tests are shown, respectively. Both figures show that the behaviour during undrained shear depends on the confining stress. In particular, the shape of the effective stress paths

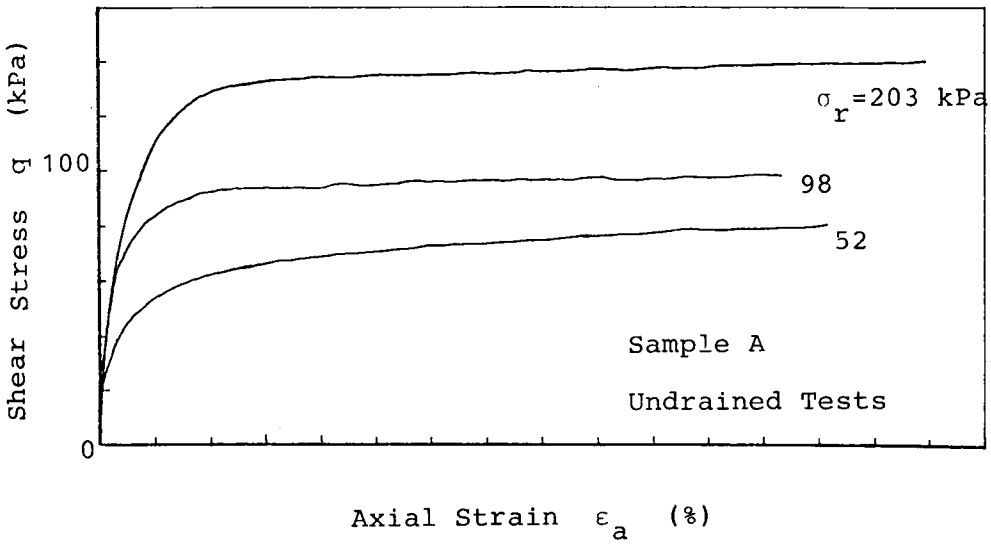

Fig.9.5: Shear stress vs. axial strain (CU tests on Sample A).

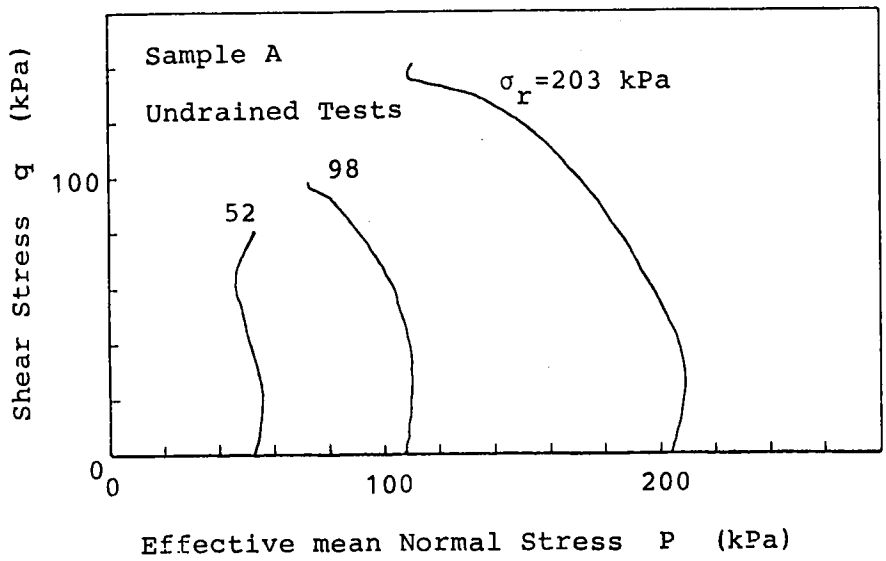

Fig.9.6: Effective stress paths (CU tests on Sample A)

is like that of overconsolidated clays under low effective confining stress and like that under high confining stress. It is concluded that the particular deviation from the general behaviour observed on sedimentary clays can not be found.

Strength parameters in terms of effective stress are determined as internal angle of friction $\phi'=29.1°$, and the apparent cohesion $c'=8.8$ kPa.

(3) Permeability Tests on Sample C

Darcy's law was found to be satisfied and the permeability coefficient k was calculated and plotted against dry density ρ_D of the specimen in Fig.9.7. It can be seen from this figure that the variation of k with ρ_D is very small, as is not the

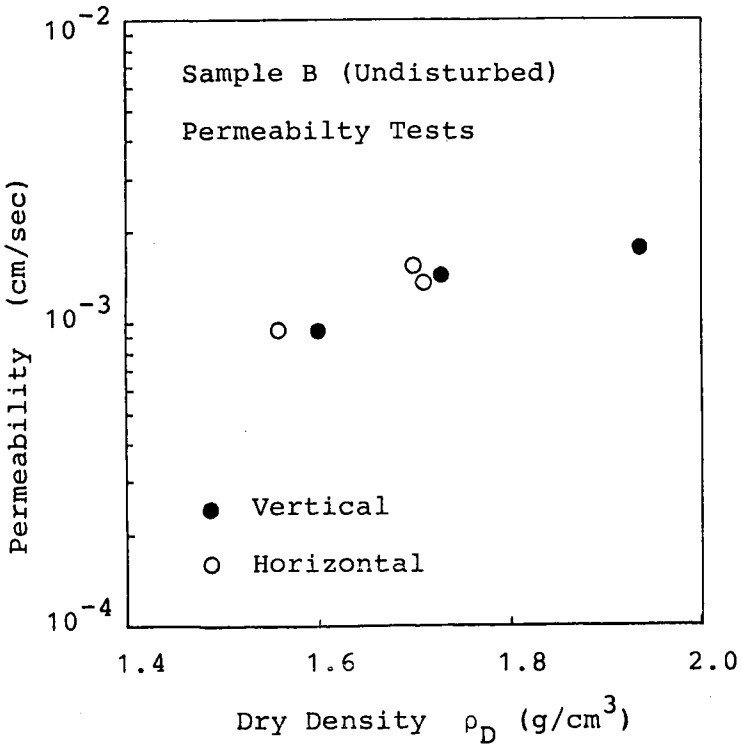

Fig.9.7: Permeability coefficient vs. dry density.

cases of previous studies (e.g.,Aboshi et al,1976), and that there is no difference in k between the vertical and horizontal directions, i.e., the anisotropy with respect to permeability is not found for this soil.

The order of values obtained here are comparable to that for undisturbed Myosin Masa, the sample used in Shono et al.(1975) and Aboshi et al.(1976).

(4) Drained Triaxial Tests

In Fig.9.8(a) and (b), the variations of shear stress $q(=\sigma_a-\sigma_r$; deviator stress) with axial strain ε_a for Samples C and B are shown respectively. It is clear that $q-\varepsilon_a$ relations are dependent on the confining stress σ_r. For Sample C, at relatively high confining stress, the stress-strain is a type of strain hardening and softening, but with decrease of σ_r the degree of the softening tendency decreases. This is very comparable with the behaviour of the densed Toyoura Sand (Miura & Yamanouchi, 1971).

The strain at the peak of q is not dependent on σ_r but almost constant of about 9 %. However, this is not the case for Sample B (Fig.9.8(b)), i.e., except Test No.B37, all the relations have not the peak of shear stress in the range of strain examined here. The difference in the behaviour seems to result from the difference in the initial structure, as already mentioned (sec.9.2.3). Such a difference in mechanical behaviour due to the difference in the internal structure will be sometimes pointed out later.

In spite of the level of σ_r, $q-\varepsilon_a$relation is linear in

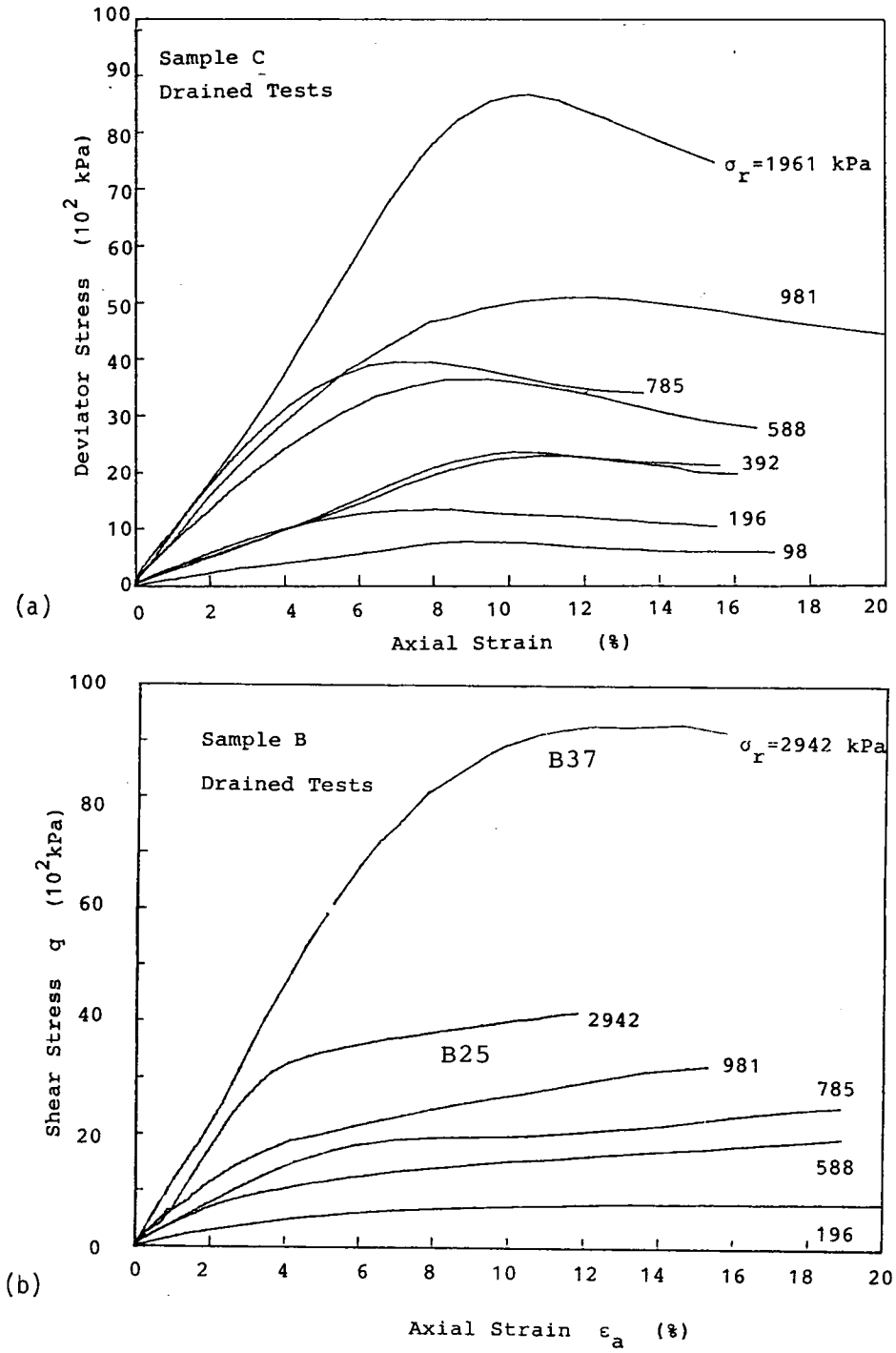

Fig.9.8: Shear stress vs. axial strain (Drained triaxial tests):
(a) Sample C
(b) Sample B

the beginning of shearing. Beyond a certain level of shear stress, which seems to be dependent on σ_r, the relation begins curved. This linearity will be utilized to evaluate the elastic shear modulus G later.

In Figs.9.9(a) and (b), the relations between volumetric strain v and axial strain ε_a are presented for Sample B and C. There would be the dependency of the relations on σ_r although it is not very clear. As the outline of these behaviours, we might say that the volume contraction occurs in the beginning of the shear; that its development is less with relatively low confining stress; and that even volume expansion occurs from a certain level of ε_a. On the other hand, for Sample B, such a marked tendency of the volume expansion is not found.

The loss of the clearness with respect to the volume change behaviour seems to have the origin that the initial void ratio e_i is not constant even for the same sample, but it is varied from specimen to specimen as will be seen in Fig. 9.16. The detail of the volume change behaviour will be given later with the addition of the discussion on the dilatancy.

(5) Undrained Tests (CU) on Samples B and D

Stress-strain relations resulted from CU tests are shown in Fig.9.11(a) and (b). As is shown in Fig.9.11(a) and (b), q-ε_a relations for both samples are not smooth. Sample B has not the peak stress but q continues to increase with increasing ε_a, as is the case of drained tests for the sample. On the other hand, for Sample D, the peak shear stress is reached and its peak value is maintained for relatively long range

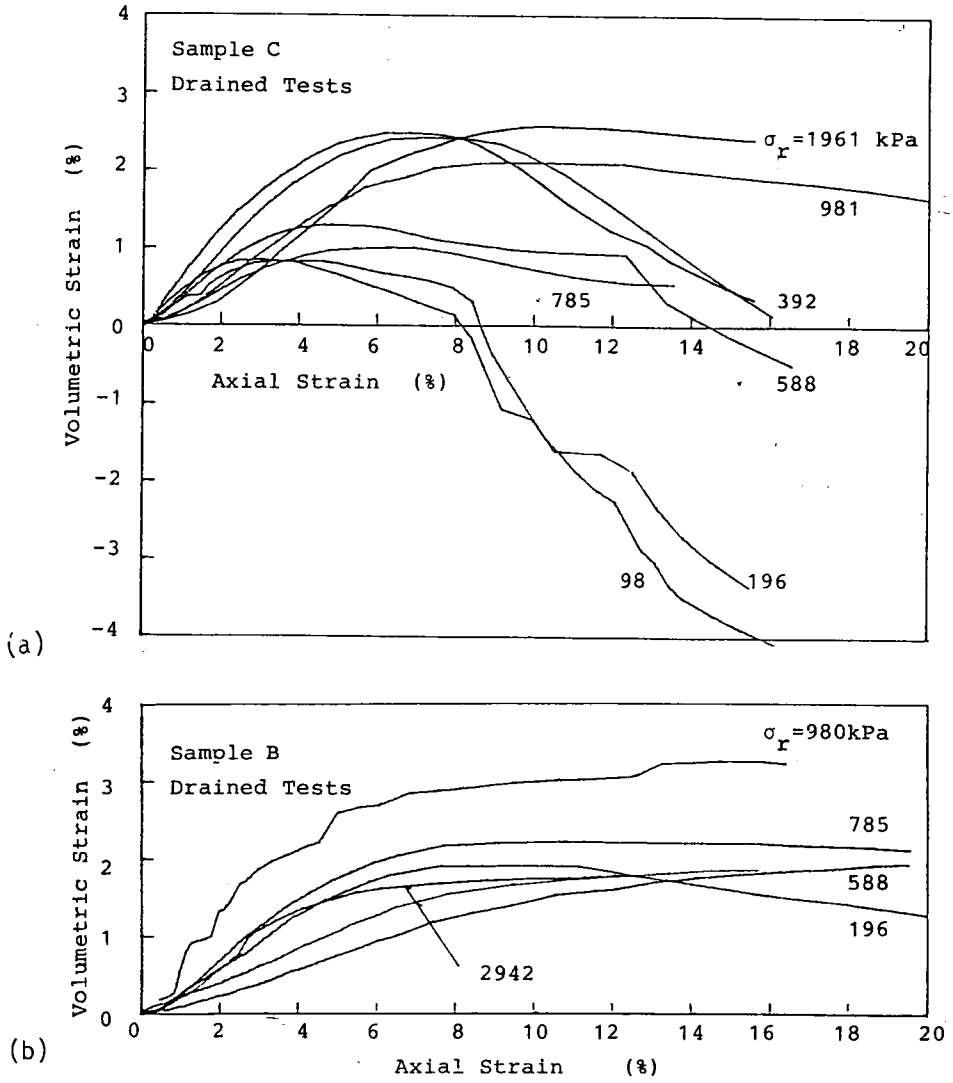

Fig.9.9: Volumetric strain vs. axial strain (Drained triaxial tests)
(a) Sample C
(b) Sample B

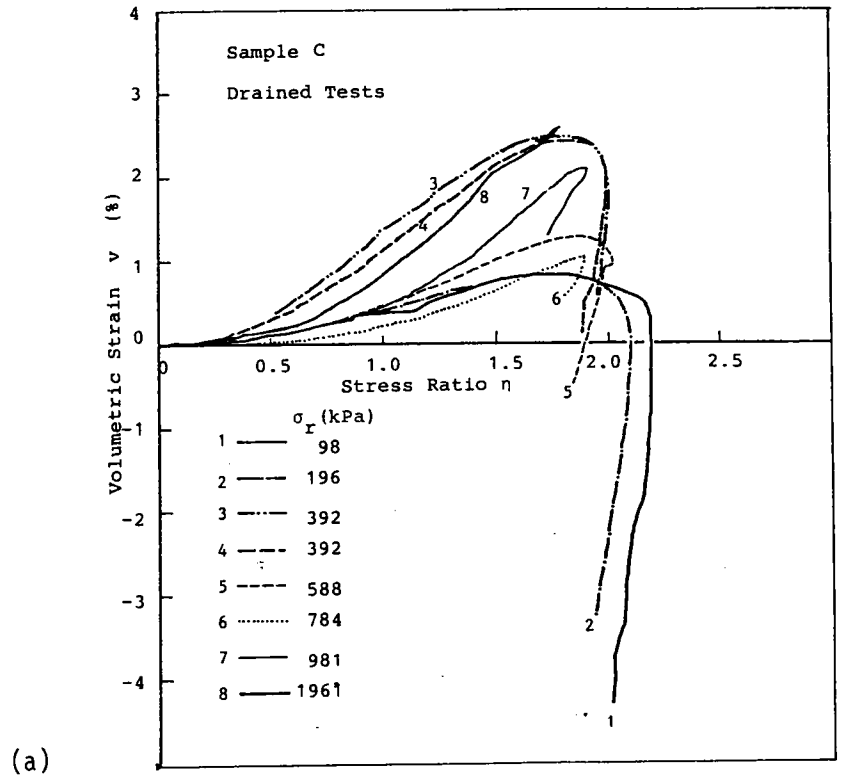

(a)

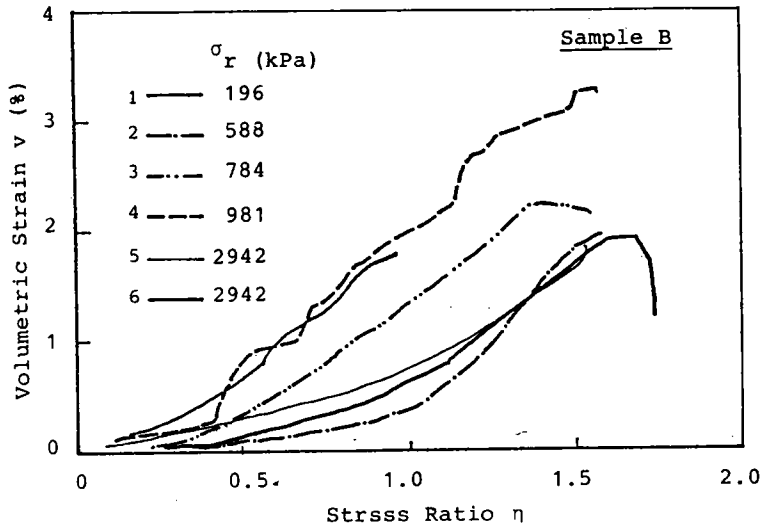

(b)

Fig.9.10: Volumetric strain vs. stress ratio (Drained tests).
(a) Sample C
(b) Sample B

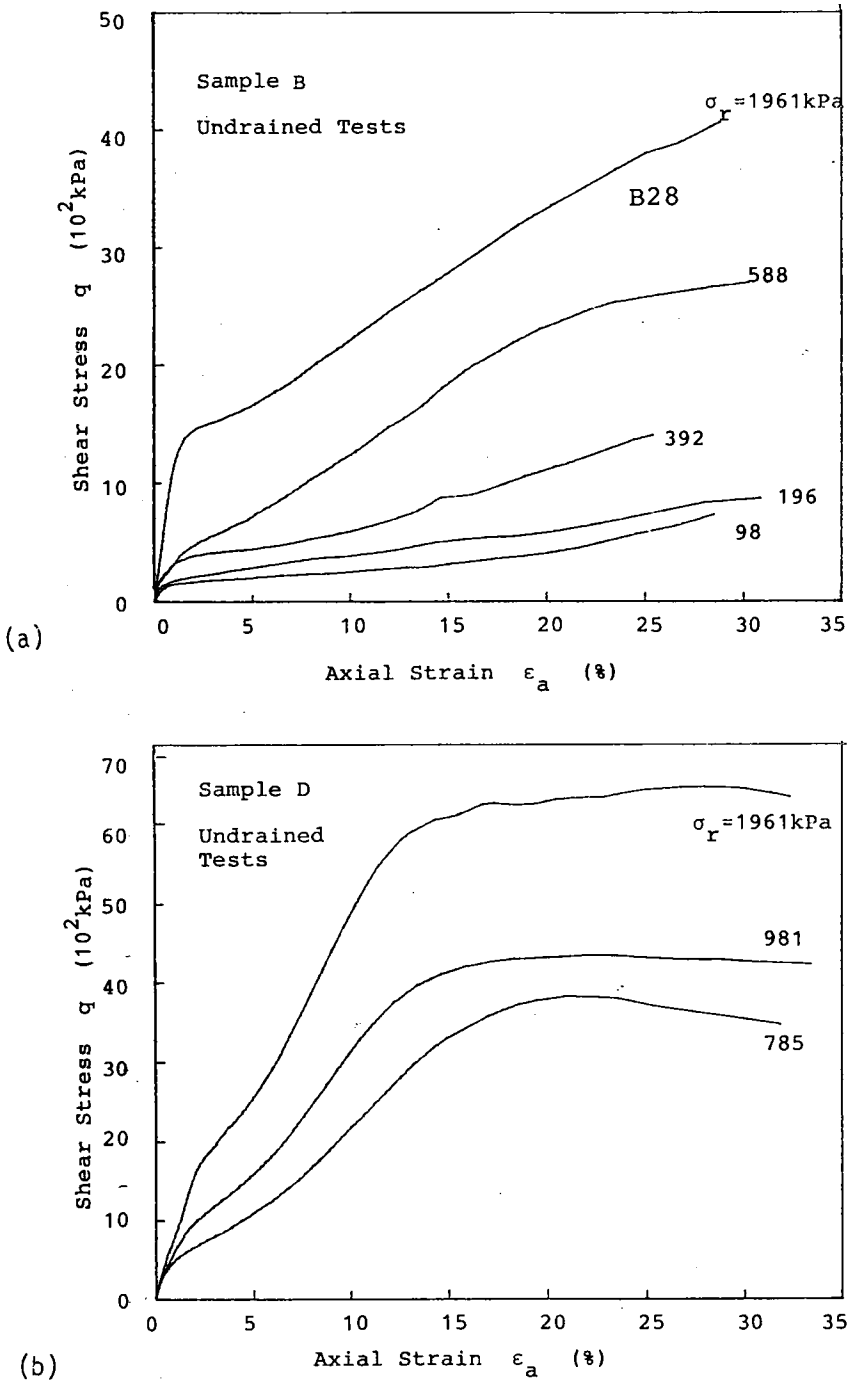

Fig.9.11: Shear stress vs. axial strain (CU tests)
(a) Sample B
(b) Sample D

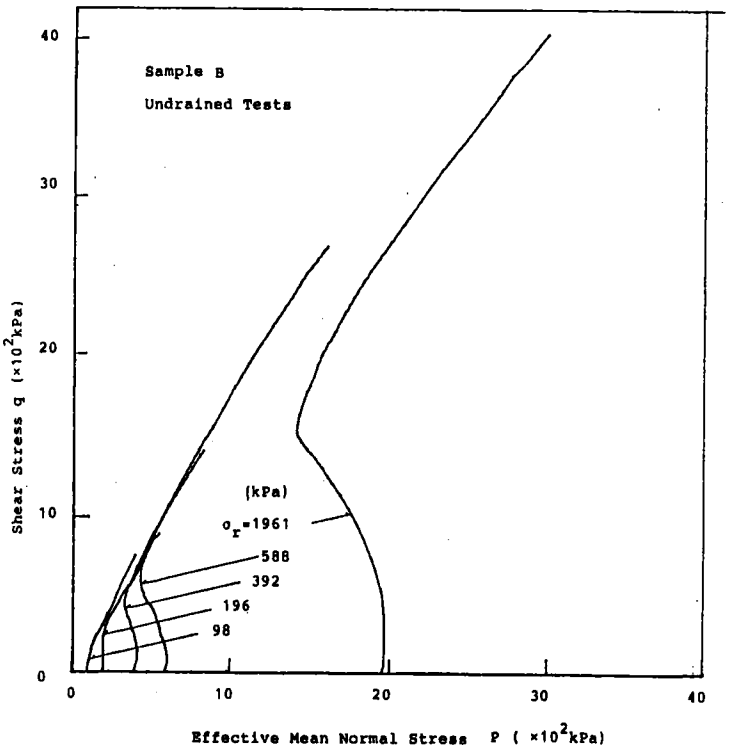

(a)

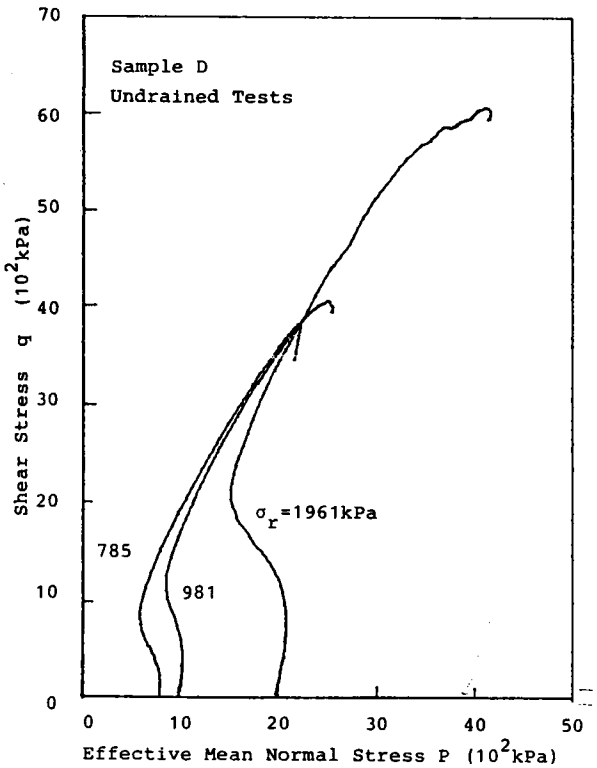

(b)

Fig.9.12:
Effective stress paths:
(a) Sample B; and
(b) Sample D.

of ε_a.

As to the effective stress paths shown in Fig.9.12(a) and (b), the difference between samples is not clearly found, except that,near the end of the test , the effective stress paths for Sample D begins to be curved,while,for Sample B,they continue to rise up to the end of the test linearly. From these figures, the dependency on σ_r is found; at low range of σ_r, effective mean normal stress p does not decrease while at higher range of σ_r, p firstly decreases and subsequently increases. This may be attributed to the dilatancy characteristics.

9.5 CONSIDERATIONS

In this section, particular problems concerned with samples other than Sample A which was already mentioned.

9.5.1 Strength Characteristics

In Fig.9.13, the state of effective stress at failure are plotted for all the tests on Samples B, C and D. As was already pointed out, Sample B had not peak values of q in drained tests, and therefore the final states shown in Fig.9.8(b) were plotted. For all the samples, the cohesion component c' is zero, but the angle of internal friction ϕ' is about 38° for Sample B, and about 48° for Samples C and D. This difference in ϕ' may be attributed to the difference in the internal structure; the joint like discontinuities observed within Sample B might contribute to the decrease of its shear strength.

These values of ϕ' were determined from the linear portion

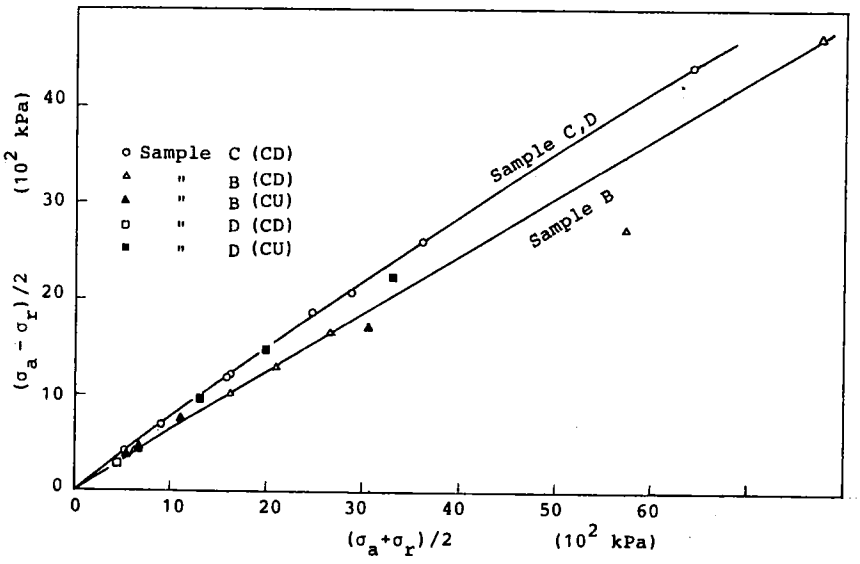

Fig.9.13: Effective stresses at failure.

in the range of $(\sigma'_a + \sigma'_r)/2$ less than 2000 kPa.

Further, in addition to the fact that Sample B has lower ϕ' than Samples C and D, the results of Sample B have more scatters than others. This appears to be attributed to the locality of internal structure within Sample B, i.e., because of non uniformity of the joint like discontinuity the internal structure would be different from specimen to specimen for Sample B.

For example, the strength of Test No.B25 was considerably lower than that of Test No.B37 (see Fig.9.8(b)) although both tests were performed with the same confining stress σ_r=2940 kPa.

According to the observations that a slip surface was obserbed in Test No.B25 while in Test No.B37 the shape of the specimens near the failure was like a cask, it is supposed that any injurious discontineous joint might have been included in Sample B25. As an another example, the results of Test No.B28 (Undrained test) can be cited; this strength was considerably lower than others (see Fig.9.11(a)).

As is clear from the discussions above, it can be stated that the evaluation of shear strength for decomposed granite soils, particularly such as Sample B, is generally difficult and that it is too dangerous to evaluate definitely the strength of soil mass over relatively wide area by using samples from one sampling point.

9.5.2 Volume Change Behaviour

(1) Volume Change Behaviour during Consolidation Drained Tests

In Figs.9.14(a) and (b), the variation of water content with effective mean normal stress p during the isotropic consolidation stage and the subsequent drained shear stage for Sample C. Behaviours for all the tests appear to be the same, and therefore, in Fig.9.15, one representative results of Test No.C27 (σ'_r during shear is 392 kPa) is shown for the detail interpretation of the behaviour.

In this figure, the stage between I and S is isotropic consolidation stage, which precedes the shear stage being denoted by SCDPE. Point S represents the start of shearing,

(a)

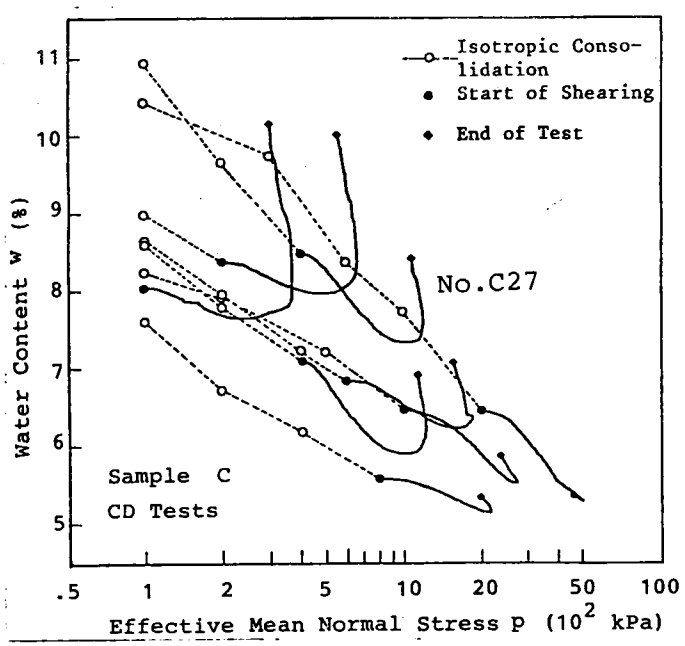

(b)

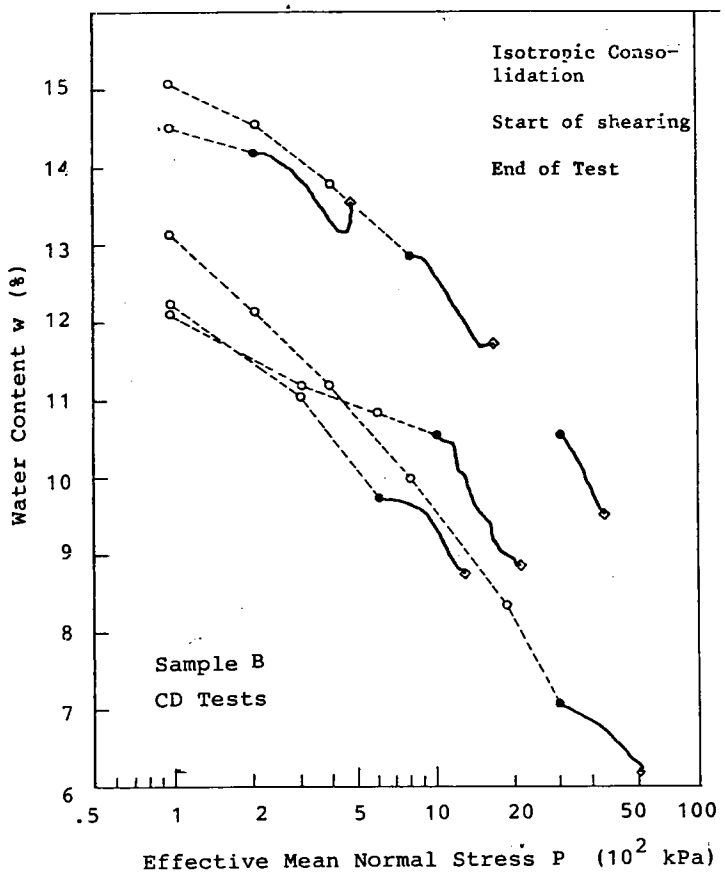

Fig.9.14:
Change in water content during drained triaxial tests
(a) Sample C
(b) Sample B

point P the peak of shear stress, and point E the end of the test. It is observed from this figure that:

i) w~log p relation is linear during the isotropic consolidation stage;

ii) even when shear stress is applied, there exists a linear portion (from C to D) in the w~log p relation;

iii) the decreasing rate of w against log p becomes less and less after passing through the point D, and w begins to increase from a certain point near the failure point P;

iv) after the peak of p or shear stress q, the increasing tendency of w becomes considerable; and

v) over a certain short range from the start of shear, change in w is relatively small comparing to the preceding and following portions

From the observation (i), the change in water content during isotropic compression can be expressed as

$$dw = -\lambda \, d\log p \qquad (9.1)$$

where λ is the slope of the linear relation from I to S. This expression can be also applied to the portion from C to D, where shear stress is applied. Thus, we will be able to assume that the volume change due to the change in isotropic component of stress is expressed by eq.(9.1) and that the component of the volume change due to dilatancy is not included, in other words, dilatancy begins to occur since the point D.

As to the portion between S and C, it seems that the drainage

was not completely allowed because of strain control testing method. By strain control, generally, the sudden increase in q and p cannot be avoided in the beginning of shear. The rate of axial deformation was prescribed by the method proposed in Bishop & Henkel(1965), however, according to this method, the total duration from the beginning to the peak can be determined but the minimum rate required to the complete drainage cannot be determined.

Consequently, we may conclude that dilatancy did not occurred before the point D.

(2) Compressibility due to Isotropic Component of Stress

We may evaluate the volume change due to the change in isotropic component of stress by compressibility index λ in eq. (9.1). In Fig.9.16, λ is plotted against initial void ratio for several specimens. Samples B and C are compared. Since λ would slightly depend on confining stress σ_r, among specimens of Samples B and C, those which were tested with the same σ_r were compared each other. It is seen from this figure that the compressibility of Sample B, which has generally higher initial void ratio, is considerably larger than that of Sample C, The ratio of λ for Sample C to that for Sample C is about three. We can attribute this difference in compressibility to the difference in internal structure mentioned above.

(3) Volume Change due to Dilatancy

The change in water content after the point D includes the

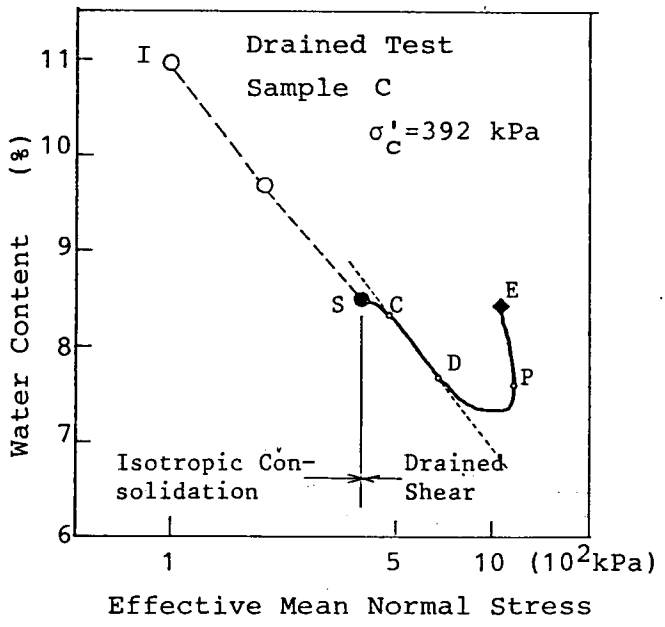

Fig.9.15: Change in water content during a drained test: the results of Test No.C27

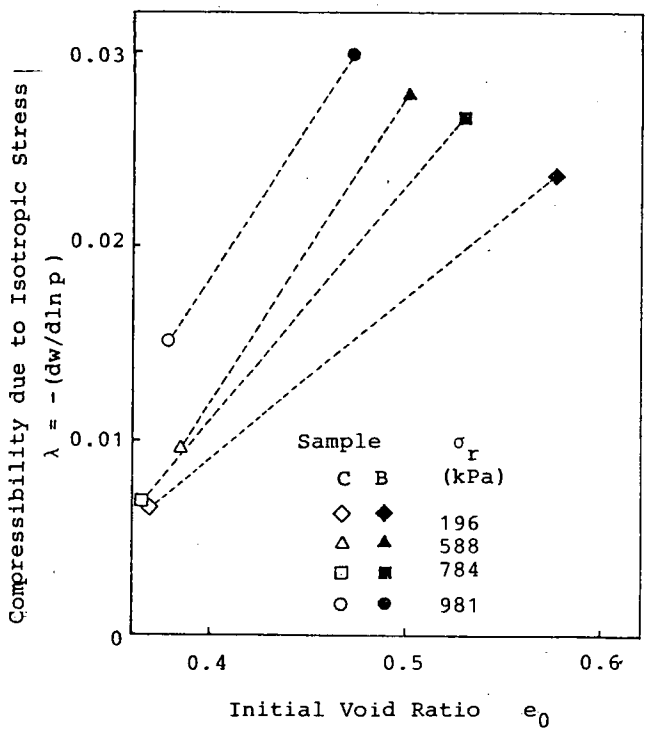

Fig.9.16: Compressibility due to isotropic stress vs. initial void ratio (Sample B and Sample C; Drained tests)

volume change due to dilatancy. In order to separate the volume change due to dilatancy from the observed total volume change, we can use eq.(9.1) when p increases,i.e., before the peak.

$$dw_{dilatancy} = dw_{total} - dw_{eq.(9.1)} \qquad (9.2a)$$

After the peak of shear stress, p decreases. We must know the volume change characteristics when p decreases. Fig.9.17 shows the results of an isotropic consolidation and rebound test. It is clear from this figure that we may neglect the volume change due to change in p when p decreases. In consequence, for the volume change after the peak, we can use the follwing equation

$$dw_{dilatancy} = dw_{total} \qquad \ldots\ldots\ldots\ldots\ldots\ldots (9.2b)$$

Volumetric strain due to dilatancy, denoted by V_D, calculated by the use of eqs.(9.1) and (9.2) are shown in Figs. 9.18 (a) and (b). This figure shows the variation of v_D with shear strain ε. It can be seen in this figure that v_D varies linearly with ε. The slope of $dv_D/d\varepsilon$ can be regarded as a parameter to evaluate the dilatant characteristics. Fig.9.19 shows the variation of this

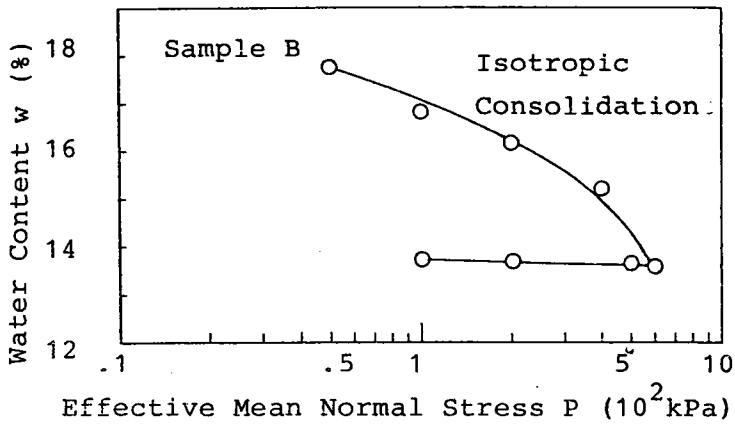

Fig.9.17: Isotropic compression-rebound test.

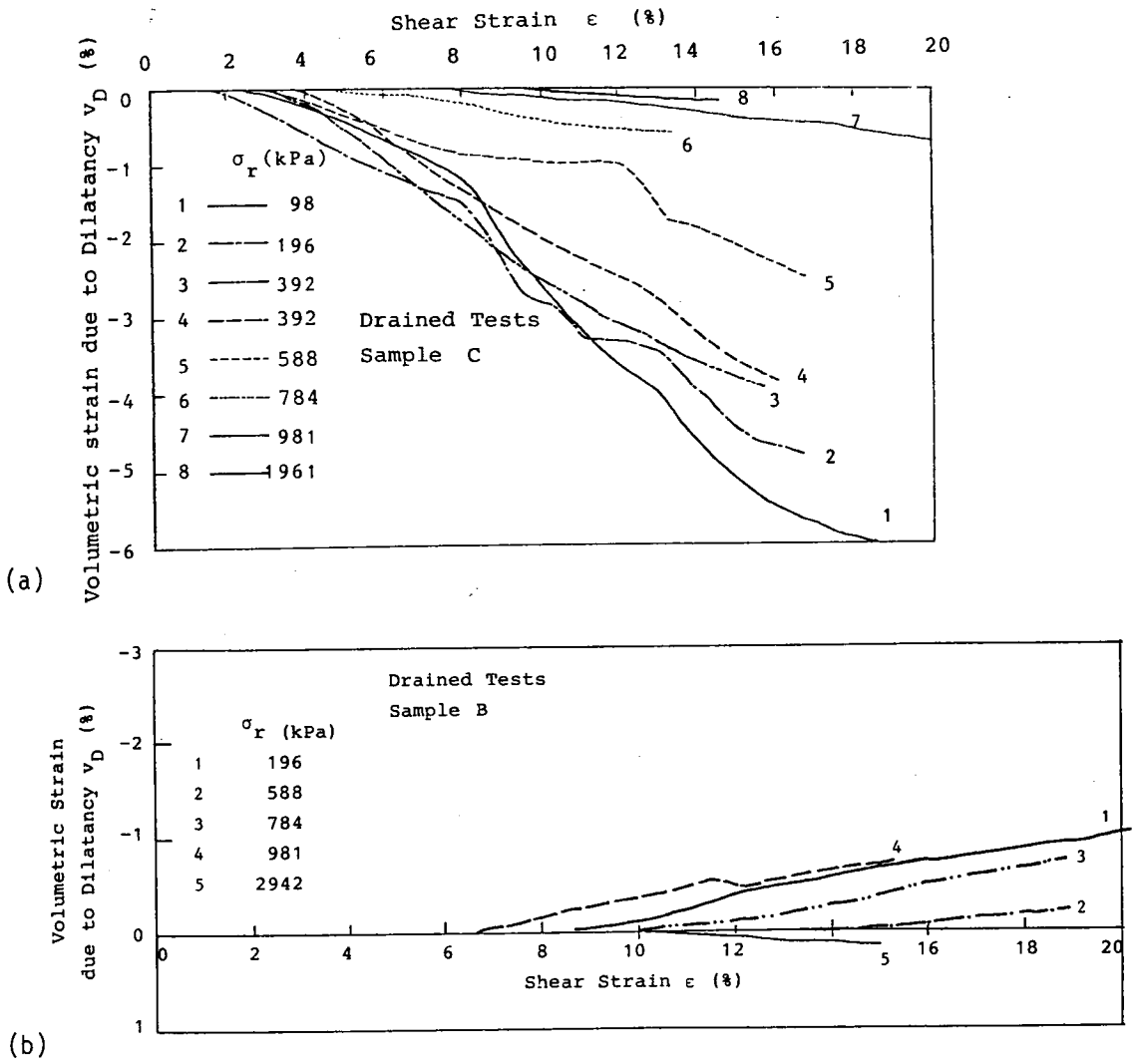

Fig.9.18: Volumetric strain due to dilatancy vs. shear strain
(a) Sample C
(b) Sample B

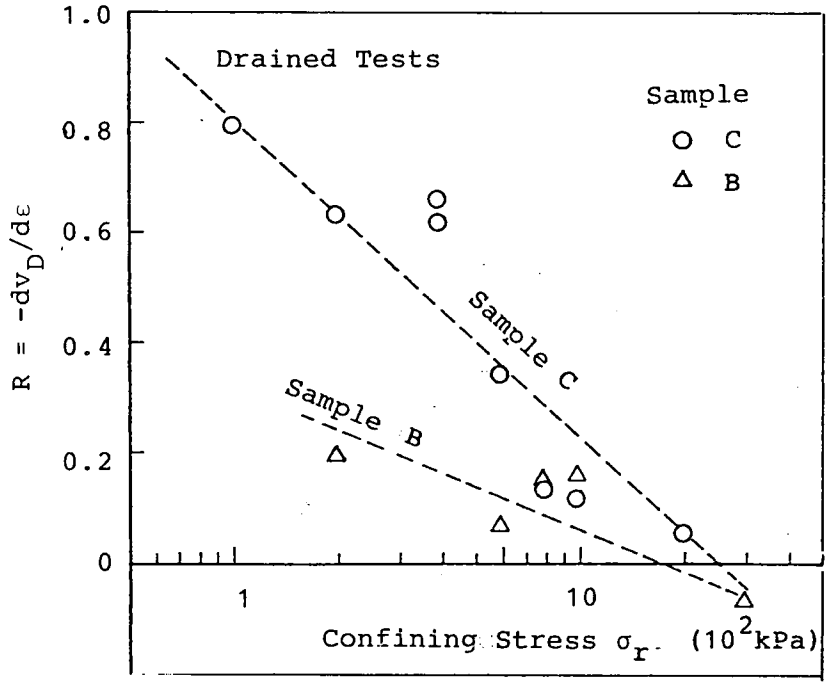

Fig.9.19: Dilatancy rate vs. confining stress (Drained tests).

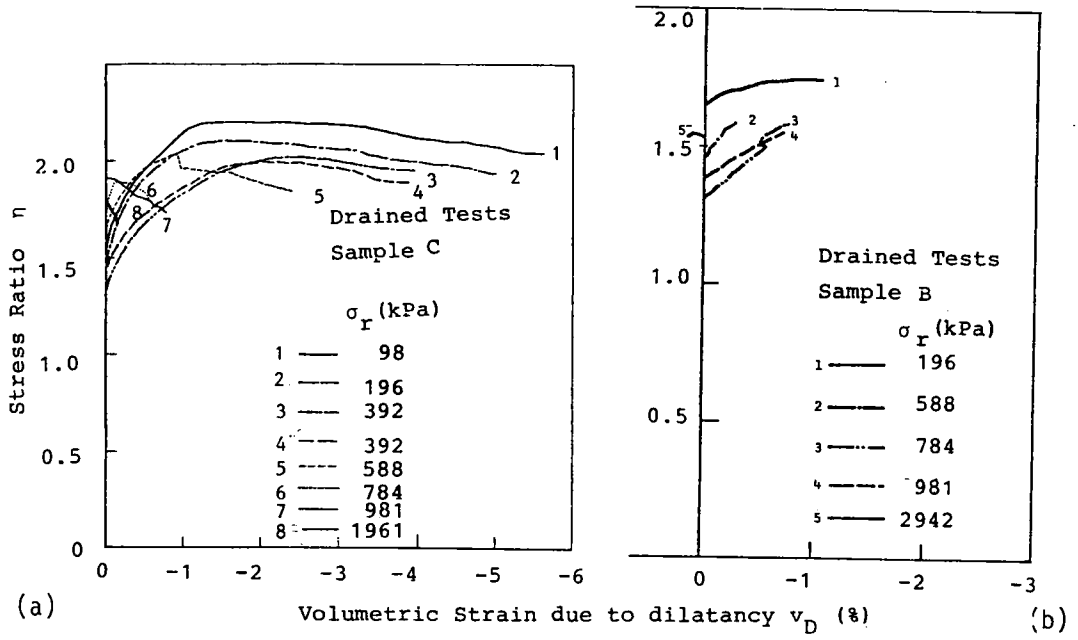

Fig.9.20: Volumetric strain due to dilatancy vs. stress ratio.
(a) Sample C
(b) Sample B

slope $R(=-dv_D/d\varepsilon)$ with the logarithm of confining stress σ_r. Different lines between Sample B and Sample C can be observed in this figure. This indicates that the dilatant tendency of Sample C is stronger than of Sample B. This observation agrees with that for sands or clays. Namely, for a given confining stress, the more is the density, the more considerable is dilatant behaviour.

Figs.9.20(a) and (b) show the relations between v_D and stress ratio $\eta(=q/p)$. At low confining stress, considerable volumetric strain occurs before peak shear stress is molilized, while at high confinig stress, v_D is very small and in the extreme cases of σ_r=1961 kPa or 981 kPa, dilatancy does not occur before peak shear stress. Additionally, it is clear from Figs.9.20(a) and (b) that the curves are ordered by the confining stress. This was not observed for the total volumetric strain (see Fig.9.10)

9.5.3 Shear Modulus

In relations between shear stress q and shear strain ε for drained tests, similar observations to those from Figs.9.8(a) and (b) are also possible. Among them, particular attention will be focused to the linearity of the relations in the beginning of the shear. The slope $\Delta q/3\Delta\varepsilon$ gives shear modulus. Its variation with confining stress is given in Fig.9.21

Thus determined shear modulus cannot necessarily be identical to the elastic modulus. However, if we consider that, at least in the beginning linear portion of the relation $q\sim\varepsilon_1$, no dilatancy

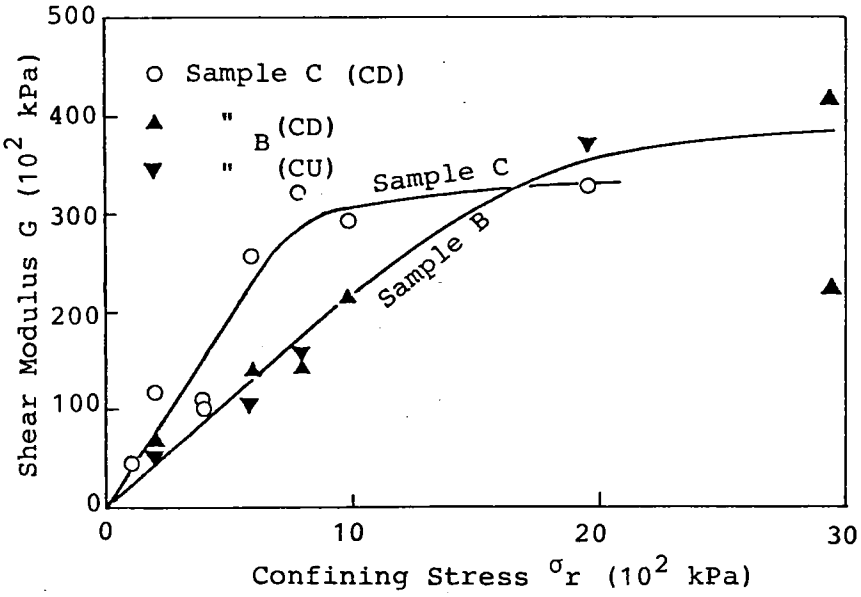

Fig.9.21: Shear modulus G vs. effective confining stress.

occurs as disscussed in the preceding section. And therefore, shear modulus G shown in Fig.9.21 may be regarded as elastic shear modulus.

In this figure, we distinguish two curves, of which each corresponds to Sample B or C. What is observed commonly to both samples is that, in the range of relatively small σ_r, less than 1000 kPa for Sample B and less than 2000 kPa, G increases with increasing σ_r and that G does not continue to increase for higher values of σ_r. This fact that there would be limited value of G was pointed out by Adachi & Ogawa(1979) for a sedimentary rock.

Generally, when σ_r is relatively large, the density of a sample becomes large and it will be expected that G also increases with increasing the density. However, in the case when the density of the sample is considerably large, the increase in the

density would not be expected. In addition, as has been recognized by many researchers, crushing of soil grains is developed due to the increase in σ_r. The crushing may lead to some change in internal structure between soil grains, which contributes to the negative role for increase in rigidity. The effects of the crushing is at present beyond the object of this study and it will have to be studied.

9.6 CONCLUSIONS

In order to investigate the fundamental mechanical characteristics of decomposed granite soil, drained and undrained triaxial conventional triaxial tests were performed on undisturbed samples. Precedingly to the mechanical tests , some basic physical properties were examined to identify the samples used in this study. When considering the results obtained from the mechanical tests, the physical properties were also referred.

Main results obtained can be stated as follows:

i) Heavily weathered granite soil(Sample A) mechanically as well as physically behaves like clays.

ii) As to the less weathered and gravel or sand like samples (Samples B, C and D), the degree of weathering seemed to result in initial void ratio or internal structure. Particularly , within the Sample B, joint like discontinuity of the internal structure which would have occurred because of the preferred decomposition affects the mechanical behaviour,i.e., it reflects on the scatter of the results, on the increase in initial void ratio, consequently, on the decrease in shear strength and the increase in compres-

sibility.

iii) Compressibility dut to the change in isotropic component of stress can be represented by the linear relation between void ratio and log. of the effective mean normal stress.

iv) Volumetric strain due to dilatancy was evaluated by subtracting the volumetric strain due to isotropic stress component from the measured total volumetric strain. Thus separated volumetric strain due to dilatancy correlates well to the confining stress.

v) Shear modulus was determined from the linear portion of the relation between shear stress and shear strain. Shear modulus increases with increasing confining stress but does not continue to increase for higher values of confinig stress. This was attributed to some factor, for example the crusing of soil grains, which contributes to the negative role for increase in rigidity.

REFERENCES FOR CHAPTER 9

Aboshi,H. et al.(1976): "Fundamental study on the prediction of slope failures of decomposed granite soil and the patternization of instable slopes", Research Report of Natural Disaster Science, the Ministry of Education, pp.37-55.

Adachi,T. and Ogawa,T.(1979): "Mechanical characteristics of soft sedimentary rock and its failure criterion", J. JSCE, No.295, pp. 51- 64.

Aoyama,C. et al.(1977): "Structure of decomposed granite soils-the pore distribution", Soils and Foundations, Vol.3, No.4, pp.10-20.

Bishop,A.W. and Henkel,D.J.(1957): The Measurement of Soil Properties in the Triaxial Test, 1st Ed., London, Edward Arnold Ltd., pp.81-82.

JSSMFE(9174): Method for Testing Soils.(in Japanese)

JSSMFE(1979):"Decomposed granite soils", Eng. Properties of Decomposed Granite Soils and Rocks and Their Application, Part II, pp.176-227. (in Japanese)

Lumb,P.(1965): :The properties of decomposed granite", Géotechnique, Vol15, No.2, pp.226-243.

Matsuo,S. and Nishida,K.(1968): "Physical and chemical properties of the decomposed granite soil grains", Soils and Foundations, Vol.3, No.4, pp.10-20.

Nishida,K.(1963): "On the engineering properties of decomposed granite soils", Proc., Annual Regional Conf. of kansai, JSCE, pp.180-184. (in Japanese)

Miura,T. and Yamanouchi,T.(1971): "Drained shear characteristics of Toyoura Sand under high confining stress", J., JSCE, No.193, pp.69-79.(in Japanese)

Nishida,K. and Matsuo,S.(1970): "The properties of decomposed granite soil and their influence on permeability", Soils and Foundations, Vol.10, No.1, pp.93-105.

Onodera,T. et al.(1976): "Shear strength of undisturbed samples of decomposed granite soils", Soils and Foundations, Vol.16, No.1, pp.17-26.

Shono,H. et al.(1975): "On the characteristics of undisturbed samples of decomposed granite soils", Tsuchi To Kiso, J., JSSMFE, Vol.23, No.2, pp.19-24.(in Japanese)

CHAPTER 10 CONCLUSIONS

The main objects of this thesis were as follows:

1) To clarify the effects of overconsolidation to the mechanical behaviour and to construct the stress-strain equations for overconsolidated clays by relating to the experimentally obtained mechanical characteristics to the theory of plasticity.

2) To examine the mechanical characteristics of undisturbed samples of some kinds of soils.

Chpaters 2 to 5 dealt with the first point and the other chpaters were concerned with the second point.

In Chapter 2, the characteristics of dilatancy have been examined experimentally for a saturated clay soil of various OCRs. In order to facilitate the understanding and interpretation of the results, the state paths on normalized state plane (q/p_e,p/p_e) and the relations between stress ratio and strain increment ratio were utilized. Several parameters which serve to specify the dilatancy characteristics were chosen and used. Followings have been obtained:

1) When stress ratio is smaller than an OCR dependent value, state paths are straight, and in the straight portion the dilatancy is negligibly small;

2) Overconsolidated specimens of OCR greater than n*(1.7 for the sample in this study) dilate just from the start of shearing while those of OCR smaller than n* contract.

3) For any degree of overconsolidation, when stress ratio reaches μ which is depend on OCR the stress ratio-strain increment ratio is represented by the equation which is the same as the energy

equation in the original Cam Clay model.

4) State paths in (p,q,w) space reach the state boundary surface at the stress ratio μ, and there seems to exist a unique stress ratio- strain increment ratio relation on the state boundary surface as assumed in the original Cam Clay model;

5)The sign of the strain increment ratio might be always positive for OCR greater than e (the base of the natural logarithm), while it changes from positive to negative for OCR larger than e.

Considering the results in the above, the sign of the dilatancy was classified according to the degree of overconsolidation and the level of shear stress.

Effects of shear stress history on té subsequent shearing deformation and isotropic compression behaviours were investigated in Chapter 3. Shear stress history was given as the cycle of loading-unloading of shear stress in the triaxial compression. Subsequent shearing was performed in the triaxial extension. Some main results are summarized as follows:

1) Dilatancy behaviour in triaxial extension is affected by the level of shear stress history, while corresponding shear deformation behaviour is not so fairly affected by it, particularly when the degree of the history shear stress is relatively low.

2) When the level of the stress history is low, the state of the specimen reaches the state boundary surface(S.B.S.). Once the state reaches the S.B.S., both shear deformation and dilatancy behaviour become similar to those of specimens without the history.

3) When the specimens subjected to the stress history is isotropically compressed, they behaves like overconsolidated specimens.

The value of p at which the v-log p relation coincides with the virgin consolidation line can be well predicted by the Cam Clay model.

4) The applicability of the parameter OCR defined on the basis of the isotropic compression behaviour for explaining the shearing behaviour after the history was examined. OCR for specimens with the stress history was determined by the Cam Clay model. As the results, shearing behaviour and dilatancy characteristics could not be predicted by the OCR.

It was observed that the specimens behaves elastically in the unloading portion in Chapter 3. This fact was reexamined and the variations of the elastic domain developed on the stress plane and of elastic shear modulus with the degree of the shear stress history were investigated in Chapter 4. Main conclusions are summarized as follows:

1) No or little dilatancy occurs while the linearity is observed between shear stress and shear strain after the unloading. Consequently, we can define the elastic range as the linear portion.

2) A parameter which describes the size of the elastic range and another parameter which describes the degree of the deformation history were chosen to examine the effect of the stress stress history on the size of the elastic range (Fig.4.9).A nearly unique relation between these parameters was found independently of the drainage condition or consolidation history.

3) Shear stress history given on the S.B.S. makes a certain domain in which elastic behaviour can be observed after the unloading.

4) Elastic shear modulus G, determined as the slope of the linear

portion of the shear stress-shear strain relation, was not affected by the stress histry but by the change of effective mean normal stress p. Further G-p relation was uniquely determined in spite of the consolidation stress or the way in which p varies for a given sample.

In Chapter 5, a theoretical formulation of stress-strain relationships based on the theory of plasticity was given. The experimental reslts obtained in Chapters 2 to 4 were taken into account in the construction of the concrete equations for over-consolidated clays. The stress-strain relationships developed has the following characteristics:

i) The plastic deformation of soils was assumed to consist of two types of deformation mechanism: one is shearing and another is isotropic compression; two loading variables v_D and v_{co} were chosen (v_D: volumetric strain due to dilatancy; and v_{co}: volumetric strain during isotropic compression) and each of them was related to the increment of stress invariant so that $dv_D=f_D dJ_2$ and $dv_{co}=f_c dI_1$, respectively.

ii) Two loading parameters $\xi_s=\xi_s(v_D, v_{co})$ and $\xi_c=\xi_c(v_{co})$ were incorporated in the corresponding two yielding functions F_s and F_c, respectively.

iii) Initial yield locus of $F_s=0$ was determined as a boundary curve within which no dilatancy occurs, while outside which dilatancy is considerable.

iv) The hardening function H_s was determined from the experimental expression of dilatancy: $dv_D=f_D dJ_2$.

v) Plastic hardening condition associated with consolidation yield

function F_c is always satisfied and associated flow rule was assumed.

vi) Non-associated flow rule was assumed with respect to the plastic shearing strain dv_s^p and $d\varepsilon_s^p$ from the experimental results.

The stress ratio constant tests on a overconsolidated clay was analyzed by the stress-strain equations developed. The strain was estimated reasonably in the case when the stress ratio was so high, but overestimated in the case when the stress ratio was so high.

The comparison between the laboratory vane shear strength and the unconfined compression strength was made on two undisturbed alluvial clays in Chapter 6. It was concluded that the possibility that the difference in strength due to difference in shearing mechanism depends on the type of soils, i.e., the ratio of these two strengths was examined in terms of the plasticity index. It was found that the higher the P.I., the higher the ratio, which had been pointed ou by Shibata(1967),too.

For the purpose to clarify the strength and creep characteristics of clays under tensile axial stress, drained triaxial tests using bone-shaped specimens were performed in Chapter 7.As the results,

1) The method proposed by Bishop & Garga(1969) was found to be available for the determination of the tensile strengths of both undisturbed stiff and remoulded overconsolidated clays although the method has some shortcomings. The measured teansile strengths for both kinds of soils were independent of the confining stress, which indicates that the tensile strength of the soil will be regarded as one of their mechanical properties.

2) Even under tensile normal stress, the empirical creep equation proposed by Mitchell(1976) is available for the transient creep stage. The prediction of the creep rupture by equations by Saito & Uezawa(1961) or Sekiguchi(1972) was also applicable for the tensile creep tests.

Conventional triaxial tests and oedometer tests were performed on stiff diluvial clays in Chapter 8. Main conclusive remarks are given as follows:

1) For a stiff overconsolidated undisturbed clay, of which stress-strain relations are remarkably strain-softening, the tendency of softening is continued during unloading-reloading cycle of shear stress after the peak. When thr stress relaxation-reloading was done, the recovered shear stress became larger than the value before the relaxation for a given strain.This was supposed due to the time hardening effect.

ii) Secondary compression of a stiff overconsolidated clay was ceased about 500 days after the completion of the so-called primary consolidation.

3) For clay used, effects of repeated loading were not clearly noticed, the contineous settlement under repeated loading will be attributed to the effect of secondary or creep comression.

In Chapter 9, the fundamental mechanical cahracteristics of decomposed granite soils were investigated by performing drained and undrained triaxial tests on the undisturbed samples. Precedingly to the mechanical tests, some basis physical properties were examined. Main results obtained are:

1) Heavily weathered granite soil behaves like sedimentary clays mechanically as well as physically.
2) As to the less weathered and gravel or sand like samples, the degree of weathering seemed to result in the initial void ratio or the internal structure. Particularly , joint like discontinuity of the structure affected the mechanical behaviour: i.e., it reflected on the scatter of the test results, on the increase in initial void ratio, on the decrease in shear strength and on the increase in compressibility.
3)Compressibility due to the change in isotropic component of stress can be represented by the linear relation between void ratio and log of p.
4) Volumetric strain due to dilatancy was evaluated by subtracting the volumetric strain due to isotropic stress component from the measured total volumetric strain. Thus separated dilatancy correlated well to the confining stress.
5)Shear modulus, determined from the linear portion of the relation between shear stress and shear strain, increases with incresing confining stress but does not continue to increase for relatively high confining stress. This was attributed to some factor, for example, the crushing of soil grains which contributes the negative role for increase in rigidity.

The Thesis consists of two main parts: one is rather theoretical studies by the use of the remoulded clay as an ideal material: and another is almost purely experimental studies of

the mechanical behaviours of undisturbed soils. It might be ideal to extend the former studies to the explanation of the behaviours clarified in the latter ones. In facts, theoretical considerations given in Chapter has the possibility to be applied to the mechanical behaviou,e.g.,the elasto-plastic behaviour of the stiff overconsolidated clay used in Chapter 8. However this requirement has not been satisfied because the stress-strain equations developed in Chapter 5 include some key parameters, which should be determined by performing some refined experiments.

APPENDIX FACTORS AFFECTING THE MEASUREMENT OF VOLUME CHANGE OF COHESIVE SOILS IN DRAINED TRIAXIAL TESTS*

A.1 INTRODUCTION

In drained triaxial tests on fully saturated soil samples, the volume of water expelled is a direct measure of the volume change and can be measured in a burette. For clayey soils the drainage is facilitated by side drains. A filter paper with a series of drainage strips is recommended to be used as a side drain by Bishop and Henkel(1957). The effect of the permeability of such a filter paper on the consolidation process was analized by Yoshikuni and Nakanodo(1975).

In this note, evaporation of water in a burette and compressibility of filter materials as side drains are examined experimentally among some problems resulting from the procedure above for the measurement of volume change of cohesive soils. It is also investigated and discussed the effect of change in room temperature on the apparent volume change of a saturated cohesive soil.

---

* Shimizu (1981)

A.2 EVAPORATION OF WATER IN BURRETES

In drained triaxial tests on saturated cohesive soils, the water surface in the burette is exposed in the atomosphere in the case without any back pressure. Therefore water evaporation might occur. The amount of water evaporaion will be unnegligible,especially,when long term tests are perfomed. So far there seems to be such two methods as the use of dummy burettes to evaluate the amount of water evaporation (Sekiguchi,1980) and of placing xylen on the water surface to prevent the evaporation itself (Rowe et al.,1963). In this note the results of a simple experiment performed to examine the effectiveness of a similar method to Rowe et al.'s.

Two burettes were prepared and both of them were not connected to a soil specimen. One (denoted by Burette A) was filled with water only and in the other (Burette B) a drop of oil* was placed on the water surface. These were set adjacently to each other in the laboratory where the room temperature was held constant at 20°C, and readings of these burettes were carried out.

In Fig A.1,variations of readings of two burettes are

* : An oil available in the market known as 'TURBINOL 30', a product by GENERAL SEKIYU Co.,Ltd.,was used. Its viscous properties are as follows: kinetic viscosity $=33.10\times10^{-6}m^2/s$ at 37.8 °C; viscosity index=110.

shown as a function of time in days. The liquid surface in Burette B does not vary although that in Burette A falls downwards. This indicates that the evaporation does not occur in Burette B because of the existence of oil on the water. From the results for Burette A, the rate of evaporation e can be evaluated as e=0.0018 ml/d. It should be noted that this value of evaporation rate can not be generalized because it may strongly depend on such conditions as the temperature and humidity in the room, the geometry of burette and so on.

A.3 TEMPERATURE EFFECTS ON THE VOLUME CHANGE OF SAMPLE MESURED BY MEANS OF A BURRETE

An example of volume expansion of water in a burette due to temperature increase can be observed in Fig.3.1. The room temperature was maintained at 20 °C until 14th of July, and it increased by 4.9 °C on 16th of July because of sudden trouble in the air conditioning system. The surface level of water in Burette A had continued to decrease and that of oil in B had been constant until 14th of July. However, sudden changes took place in both burettes on 16th of July, that is, the levels of liquid surface rose. It appears that the water expanded by about 0.01 ml for Burette A and 0.005 ml for B.

Apparent volume change of water in a glass vessel due to change in temperature can be generally given by

$$\Delta V_w = (\beta_w - \beta_g) V_w \Delta T \qquad (A.1)$$

where ΔV_w: apparent volume change of water in the vessel due to temperature change ΔT,

V_w: volume of water in the vessel,

β_w: thermal expansion coefficient of water, and

β_g: thermal expansion coefficient of glass.

By using this equation we can estimate the amount of the volume expansion of water in Burette A and B. Denoting the density of water at T by ρ_T, the thermal expansion coefficient of water is given by

$$\beta_w = (\rho_T/\rho_{T+\Delta T} - 1)/\Delta T \qquad (A.2)$$

For T =20°C and ΔT=4.9°C, we have ρ_T=0.99820 Mg/m^3 and $\rho_{T+\Delta T}$= 0.99707 Mg/m^3 and, therefore, β_w=0.000231°C^{-1} is obtained from eq.(3.2). The volume of water was 9.35 ml in Burette A and 8.57 ml in B. Neglecting the thermal expansion of glass (β_g=0.00002 °C^{-1} << β_w),we can obtain the volume expansion of water ΔV_w as follows: ΔV_w=0.0106 ml for Burette A and 0.0097 ml for B. These values are well close to those shown in Fig.A.1.

Should also be noted ,from the results shown in Fig.3.1, that the volume expansion of water due to temperature increase is followed rapidly by volume contraction due to subsequent temperature decrease.

Another example of volume expansion of water in a test system due to increase in room temperature is discussed hereafter. Fig.3.2 shows a part of the results of a drained triaxial compression test with constant effective mean stress for an

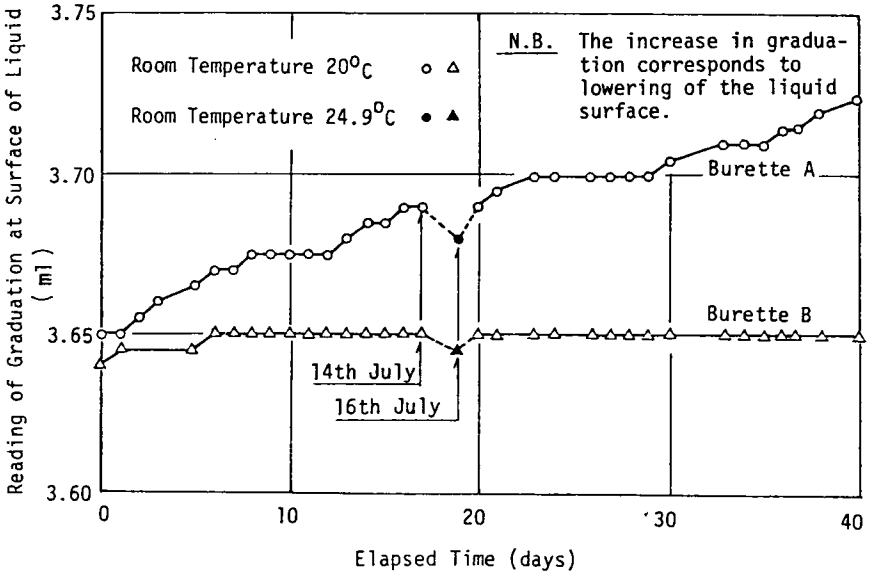

Fig.A.1: Variations of water levels in two burettes; in Burette A there is only water; in B a drop of oil is placed on the water surface.

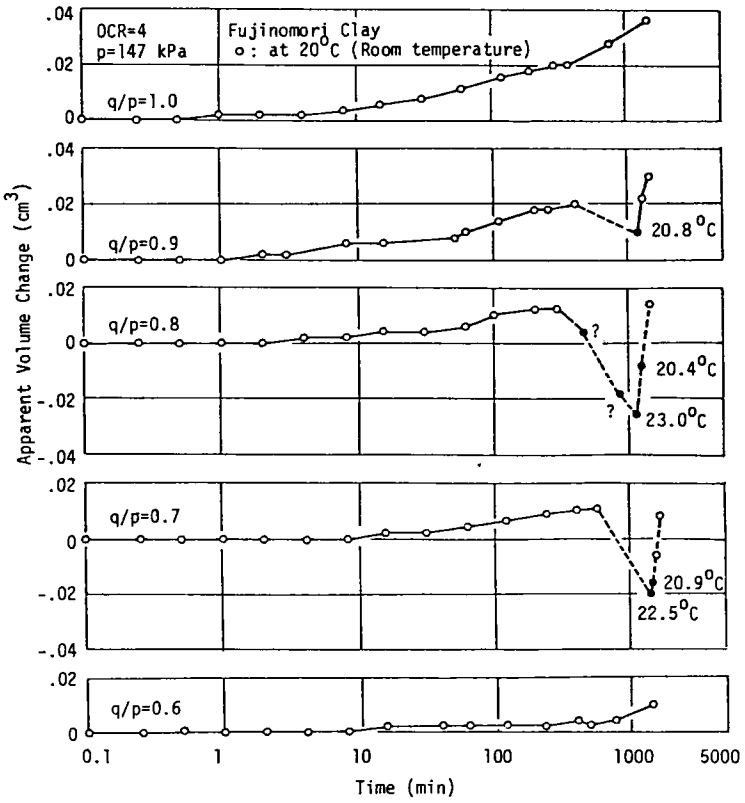

Fig.A.2 Effects of change in room temperature on volume change behavior of an overconsolidated cohesive soil in a drained triaxial test with constant mean effective stress.

overconsolidated cohesive soil. Volume changes of the sample measured directly by using a burette are plotted against the time elapsed after the application of additional shear stress. As can be seen from this figure the apparent volume of the sample has a tendency to increase with time so long as the room temperaure is held constant at 20 °C, but when it becomes higher than 20 °C the apparent volume tends to decrease, i.e.,the water level in the burette becomes higher. It can be seen, too, that the apparent volume which decreased due to temperature rise increases again by the subsequent recovery of the room temperature, i.e.,the water level in the burette returns to the original level. After the recovery of the temperature the subsequent tendency of increasing apparent volume of the sample is observed.

In Fig.3.3 the decrease of the apparent volume of the sample caused by the increase of the room temperature are plotted against the increase in temperature by using data shown in Fig.3.2

It can be observed that the volume of the sample decreases linearly with the degree of temperature rise.

If the temperature is raised and kept at a higher value than an expected or controlled one for time enough to raise not only the temperature of water in a burette but also that of pore water in the sample,the volume of water subjected to thermal expansion, V_w in eq.(A.1), may be considered as the total volume of water in the burette (V_{wB}),in the connection (V_{wC}) and in the sample (V_{wS}).

For the test shown in Fig.A.3, V_{wS} was estimated as 28.53 ml at stress ratio q/p of 0.7 by measuring the water content, the oven-dried weight of the specimen and the specific gravity of soil grains at the end of the test and by assuming the full saturation. The sum of V_{wB} and V_{wC} was about 12 ml. Consequently, from eq.(A.1), the value of $\Delta V_w/\Delta T$ is given as in eq.(A.3)

when it is assumed that the temperature of water both in the specimen, in the burette and in the connection is raised equal to room temperature, and as in eq.(A.4) when it is assumed that the temperature of water in the specimen is not raised equal to room temperature:

$$\Delta V_w/\Delta T = 0.00936 \ (\mathrm{ml/°C}) \tag{A.3}$$

$$\Delta V_w/\Delta T = 0.00277 \ (\mathrm{ml/°C}) \tag{A.4}$$

In the derivation of these equations, β_w was assumed to be $2.31 \times 10^{-4} \mathrm{°C}^{-1}$, which was obtained in the foregoing section.

Relations of eqs.(A.3) and (A.4) are represented in Fig.A.3. Here it must be noted that the increase in V_w corresponds to the decrease in V, which is the apparent total volume of the specimen. In the case shown in Fig.A.3 it is understood that the temperature in the specimen was already raised equal to room temperature, and the difference in the measured total volume change ΔV and the volume change of water due to temperature increase ΔV_w seems to result from the sum of the true total volume change of the soil mass and the thermal expansion of soil minerals due to

temperature change(Mitchel,1976).

In general, when room temperature varies from a controlled value, the measured apparent volume change of the sample includs the volume change due to thermal expansion or contraction of water in the system, the degree of whose effect depends on the duration for which room temperature is held higher or lower than the original controlled temperature.

A.4 COMPRESSIBILITY OF SIDE DRAINS

Some kinds of filter materials are used as side drains in order to facilitate the drainage in drained triaxial tests. For experiments where the volume change of soils may be expected be very small and where cell pressure varies, there may be cases the effects of compressibility of the filter material on the measurement of volume change can not be negligible. Drained compression or extension triaxial tests with constant effective mean stress for heavily overconsolidated cohesive soils may be cited as one of such cases. Compressibilities of two filter materials, a filter paper and a nylon mesh, were examined experimentally.

A.4.1 Compressibility of a filter paper

A filter paper*, whose configuration is such that shown in Bishop and Henkel(1957), and whose dimension and quality

* : Filter paper #2,a product by AZUMI-ROSHI Co.,Ltd.

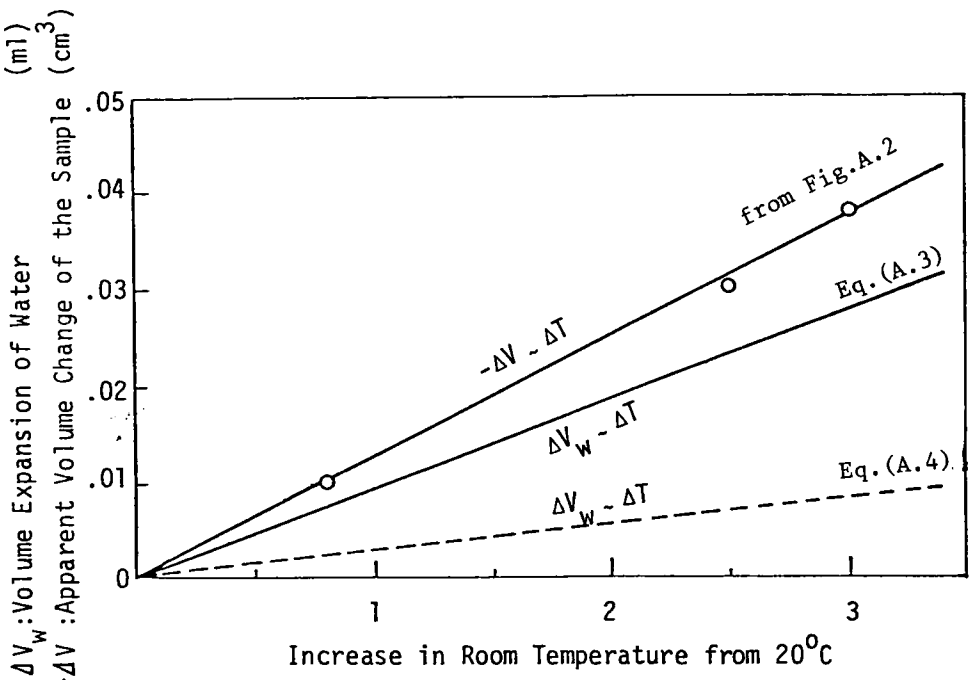

Fig.A.3 Apparent volume change of the sample and calculated volume expansion of water against the increase in room temperature.

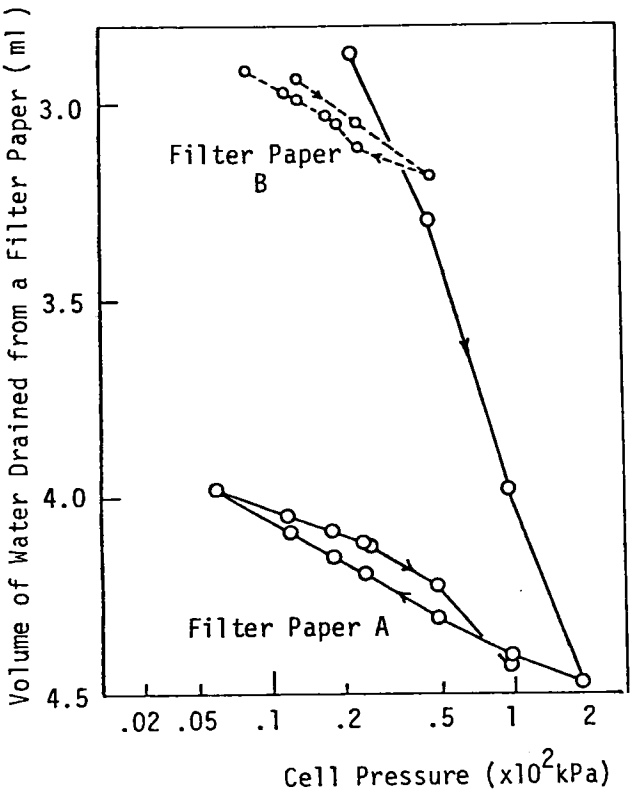

Fig.A.4 Results of compression tests for a filter paper in a triaxial cell.

are the same as those used in triaxial tests for soils, was wrapped round a cylindrical achrylite specimen which has the same dimension as that of a soil specimen,i.e.,36 mm in diameter and 80 mm in height. That prepared specimen was isotropically compressed in a triaxial cell under drained condition by the same procedure as that for soils.

The results are shown in Fig.A.4. Two pieces of filter paper, Paper A and B, were soaked in water. Filter paper B was lightly pressed between two sheets of air-dried filter paper just before being wrapped round the achrylite specimen but filter paper A was not so treated. Therefore water initially contained in Paper A was more than in B. As can be seen in Fig.A.4, in spite of the different initial amount of water,rebound-recompression portion for Paper A and rebound portion for B are represented by straight lines and the slopes of these portions are the same for both A and B. Hence, the compression index of the filter paper for rebound-recompression portion C_{PD} can be defined independently of the initial amount of water as :

$$C_{PD} = \Delta V_{wP} / \Delta log\, \sigma_r \qquad (A.5)$$

, where V_{wP} : volume of water drained from the filter paper, and

σ_r : cell pressure

For the filter paper used here, the volume of C_{PD} can be read as 0.35 ml from Fig.A.4 The value of C_{PD} may depend on the dimension and quality of the filter paper and the duration of each

consolidation stage.

The effect of the last factor will be examined in Fig.A.5, where consolidation curves for another compression test are represented. As can be seen from this figure consolidations corresponding to the virgin compression cease rather rapidly, but rebounds seem to continue, for example, for 10 000 minutes. Also two curves for virgin compression are very close to each other as well as those for rebound. Because the increment of cell pressure is constant in the log scale, and if the duration of each consolidation stage is constant, the relation between the total volume of drained water from the filter paper and log σ_r, as shown already in Fig.A.4, will be straight for both virgin compression and rebound.

A.4.2 Compressibility of a Nylon Mesh

A certain type of nylon mesh is used for drained triaxial tests of soft rocks as a side drain (Adachi and Hayashi, 1980). Fig.A.6 and Fig.A.7, corresponding to Fig.A.4 and Fig.A.5, respectively, show the results of a compression test for a nylon mesh*. From Fig.A.6, the compressibility seems to be defined as the slope of rebound-recompression curve , being denoted by C_{ND}. For this type of nylon mesh, C_{ND} is about 0.1 ml. This value is about 1/3 of C_{PD} obtained for the filter paper discussed above. As can be seen in Fig.A.7, consolidation of the nylon mesh ceases more rapidly than that of the filter paper. The effect of its strength

* : Nylon mesh #270

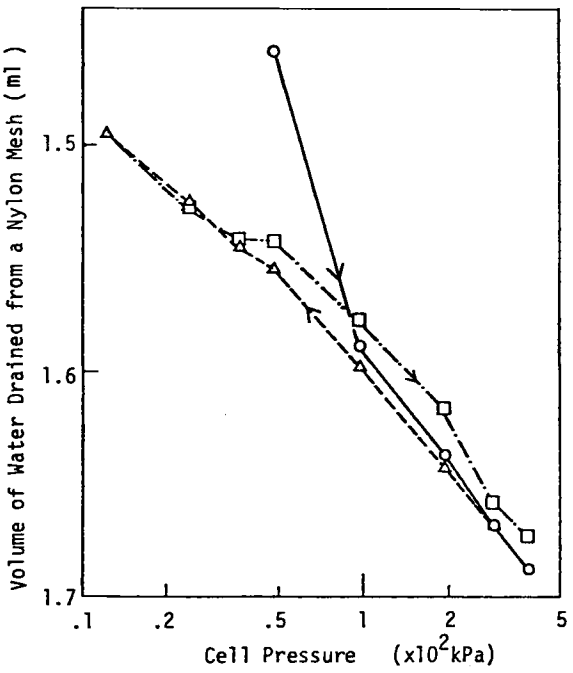

Fig.A.5 Consolidation curves for a nylon mesh.

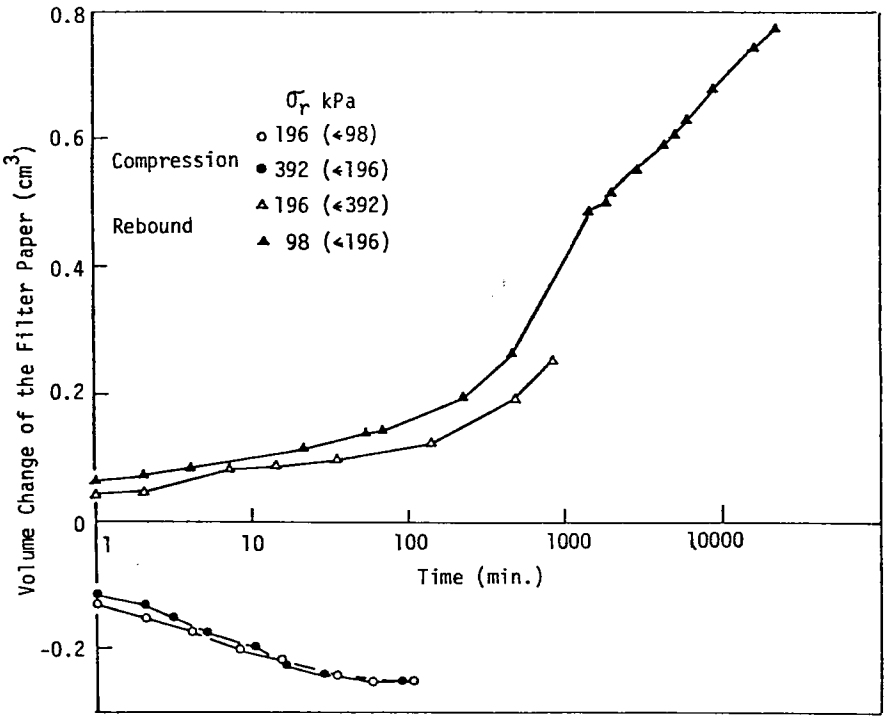

Fig.A.6 Effect of the compressibility on the volume change behavior of an overconsolidated cohesive soil in a drained triaxial test with constant mean effective stress.

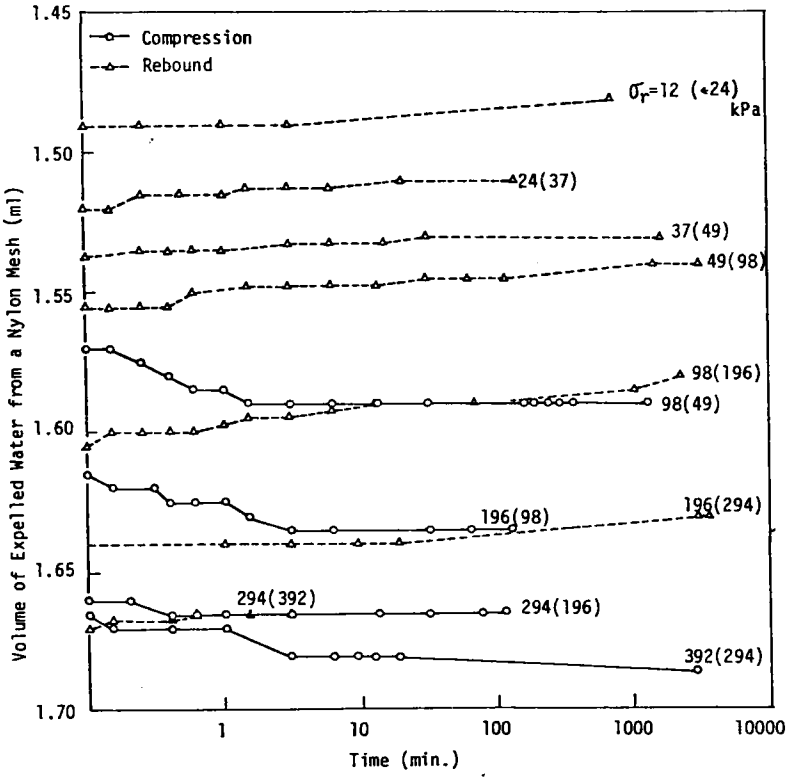

Fig.A.7 Consolidation curves for a filter paper.

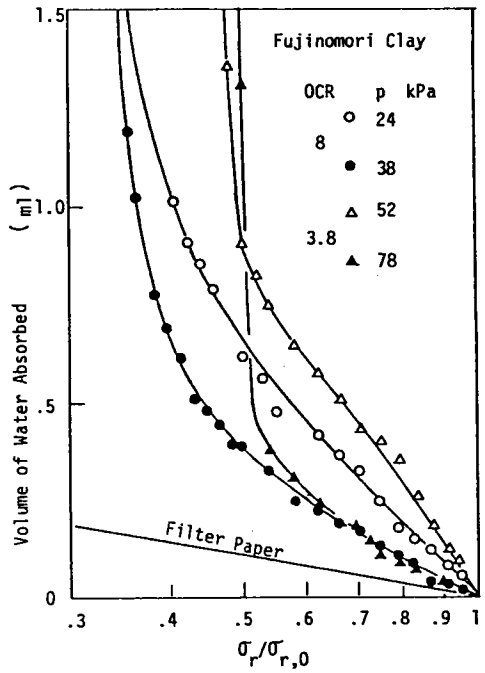

Fig.A.8 Results of compression test for a nylon mesh in a triaxial cell.

on the measured deviator stress is expected to be much larger than that due to filter paper for soft cohesive soils. For this reason the use of any type of nylon mesh as a side drain can not be recommended for cohesive soft soils in spite of its good characteristics of compressibility and permeability.

A.4.3 An Example of the Effect of Compressibility of a filter Paper

Fig.A.8 shows the results of a drained triaxial compression test for an overconsolidated cohesive soil with constant mean effective stress . In such a test, cell pressure decreases with shear and the relation between cell pressure and shear stress is given by

$$\sigma_r/\sigma_{r,0} = 1 - \eta/3 \qquad (A.6)$$

, where $\sigma_{r,0}$: isotropic consolidation stress before shear
i.e.,initial cell pressure,

σ_r : cell pressure during shear, and

η :stress ratio q/p .

By using the compressibility of a filter paper C_{PD} already defined , the volume of water absorbed into the filter paper $(\Delta V)_{PD}$ can be estimated by

$$(\Delta V)_{PD} = -C_{PD} \log(\sigma_r/\sigma_{r,0}) \qquad (A.7)$$

The equation above is shown by the solid straight line in Fig.A.8 where the value of C_{PD} was assumed to be 0.35 ml, which is equal to that obtained from Fig.A.4.

The dilatant behavior of the sample is observed in Fig.A.8,

but, when shear stress is not high enough, measured volume change includes unnegligible quantity due to the expansion of the filter paper by decreasing cell pressure.

A.5 CONCLUSION

There have been discussed the factors which give effects on the volume change behavior measured by means of a burettes. Conclusively, their effects can be summerized as

$$\Delta V = (\Delta V)_E + (\Delta V)_{\Delta T} + (\Delta V)_{PD} + (\Delta V)_m \qquad \text{(A.8)}$$

,where ΔV : apparent volume change of a specimen measured directly from the variation of water level in the burette,

$(\Delta V)_E$: apparent volume change caused by the evaporation of water in the burette ($(\Delta V)_E = e\,\Delta T$,in which ΔT is elapsed time and e the rate of evaporation discussed in section 1),

$(\Delta V)_{\Delta T}$: apparent volume change caused by change in room temperature ΔT ($(\Delta V)_{\Delta T} = -V_w$, in which V_w is given by eq.(A.1)),

$(\Delta V)_{PD}$: apparent volume change caused by compressibility of the filter paper used as a side drain (This may be estimated by eq.(A.7), and

$(\Delta V)_m$: true volume change of the soil mass, eventually including apparent volume change caused by thermal expansion of soil minerals (Mitchell,1976).

Among these factors, the evaporation of water in a burette and a sudden change of room temperature can be controlled, by using a drop of non-volatile oil for the former and by the carefull control of the air conditioning system for the latter. The effect of the compressibility of side drains can, however, not be avoided so far as it is concerned with drained tests with varying cell pressure. In particular, when soils with small compressibility, for example, heavily overconsolidated cohesive soils, are treated, the volume change of filter materials included in the total volume change measured by means of a burette is considerable. Therefore, it seems to be necessary to investigate the effect of compressibility of the filter material used as a side drain on the measurement of volume change of soils when it is concerned with drained triaxial tests during which cell pressure varies.

REFERENCES FOR APPENDIX

Adachi,T . and Hayashi,M.(1980): "Effects of joints on mechanical properties of soft rocks", Proc.JSCE, No.305, pp.97-110.

Bishop,A.W. and Henkel,D.J.(1957): The Measurement of Soil Properties in the Triaxial Test, 1st Ed., Edward Arnold Ltd., London, pp.81-82.

Mitchell,J.K.(1976): Fundamentals of Soil Behaviour, John Willey & Sons, Inc., pp.275-280.

Rowe,P.W. et al.(1963): "The stress dilatancy performance of two clays", ASTM Special Publication No.361, pp.134-143.

Sekiguchi,H.(1980): Personal Communication.

Shimizu,M.(1981): "Factors affecting the measurement of volume change of cohesive soils in drained triaxial tests", Soils and Foundations, Vol.21, No.2, pp.121-128.

Yoshikuni,H. and Nakanodo,H.(1975): "Influences of permeability of filter paper on the consolidation process in triaxial tests of cylindrical specimens", Proc. 20th National Symp. Soil Mech. Found. Eng., pp.121-124.(in Japanese)